SYNCHRONIZATION IN COMPLEX NETWORKS UNDER UNCERTAINTY

Lluís Arola Fernández

UNIVERSITAT ROVIRA i VIRGILI

SYNCHRONIZATION IN COMPLEX NETWORKS UNDER UNCERTAINTY

Lluís Arola Fernández

DOCTORAL THESIS
2022

UNIVERSITAT ROVIRA I VIRGILI
SYNCHRONIZATION IN COMPLEX NETWORKS UNDER UNCERTAINTY
Lluís Arola Fernández

Lluís Arola Fernández

Synchronization in Complex Networks Under Uncertainty

Ph.D. Thesis
Supervised by Dr. Alex Arenas

Departament d'Enginyeria Informàtica i Matemàtiques de la Seguretat

UNIVERSITAT
ROVIRA i VIRGILI
Universitat Rovira i Virgili
Tarragona, Catalonia, Spain

February 2022

Author:
Lluís Arola Fernández

Supervisor:
Dr. Alexandre Arenas Moreno

Universitat Rovira i Virgili

Cover art by: Xavi Bou

UNIVERSITAT ROVIRA i VIRGILI

I STATE that the present study, entitled *Synchronization in Complex Networks Under Uncertainty*, presented by Lluís Arola Fernández for the award of the degree of Doctor, has been carried out under my supervision at the Departament d'Enginyeria Informàtica i Matemàtiques de la Seguretat of this university.

Tarragona, 28th February, 2022

Doctoral Thesis Supervisor,

Dr. Alexandre Arenas Moreno

Als meus pares i a l'Adriana

AGRAÏMENTS

Aquesta tesi no hauria estat possible sense el suport de molts altres. Vull donar les gràcies a les institucions i les persones que m'han ajudat en aquest camí.

Sobretot al meu director, el Dr. Arenas, un visionari imparable amb una personalitat i un cor molt grans. Alex, gràcies per acollir-me a la família, per l'oportunitat d'explorar un problema fascinant i pel continu suport intel·lectual i emocional. Ha sigut un plaer compartir aventures i poder aprendre tant de tu.

Al Benja, per escoltar-me i aguantar-me i per tots els records que hem col·leccionat plegats. Sense dubte, un dels grans descobriments d'aquests anys, divertit i brillant però abans de res un amic excepcional. Gràcies per tot i pel que vindrà! També al Sebas, un altre fora de sèrie, per ensenyar-me tantes matemàtiques, per compartir la passió per la sincro i l'estètica dels resultats analítics i per convidar-me a Hartford.

A tots els membres de l'Alepshys Lab, per fer-me sentir com a casa. A la Clara pels bons consells i la qualitat local. Al Giulio, pel bon gust i el talent, tant en la vida pràctica com en la física teòrica, i al Giacomo per l'enginy i l'oïda per la música dels sistemes complexes. Al Sergio per la moderació i el rigor. Als que ja han volat lluny, com el Joan, el germà gran que es troba a faltar, l'Albert, el Manlio, l'Elisa, l'Eugenio, el Javi, l'Alessio i el Jordi. He après molt de vosaltres. També dels que han arribat fa poc, el Mattia, el Pier i l'Aleix. Estic segur que us ho passareu bé aquí.

Aquests anys he tingut la sort de viatjar molt i conèixer gent fantàstica. Als meus col·laboradors, a l'Albert Díaz i al Dane, per la seva visió amable de la sincro, al Guillem, per compartir l'enfoc, al Sergio, per les bombes construïdes fent zooms en temps difícils. Al Jesús, pel carisma i l'art del descobriment, i al David, un amic i un físic de primera, per tots els moments junts. Als col·legues d'arreu, com l'Alex, l'Oriol, el Jorge, el Francho, el Dima i molts d'altres. Ha estat molt agradable trobar-vos en aquest camí.

No em vull oblidar dels que ja hi eren abans de començar l'aventura. Al Daniel, per presentar-me la incertesa en física i la física a la Jaynes, a l'Eduard per donar-me la primera oportunitat al món real. Al Guim, per mantenir la flama encesa i per ensenyar-me que els grans científics són poetes (i viceversa). Al Berti, pels projectes abandonats que voldria que tornessin i per demostrar-me que la bondat i la virtut van sempre juntes. També al Vasilis, per acollir-me a Grècia i per la seva visió particular del món.

Als meus amics i a la família, que m'heu acompanyat en aquest viatge i m'heu animat sempre. A l'àvia i al Josep per ser al meu costat. Als meus pares, que m'ho heu donat tot, us estimo molt. L'Alfred, el meu referent en les coses importants de la vida, i la Carme, amb tota la tendresa i determinació. Aquesta tesi l'he acabat per ella i gràcies a ella. M'agrada pensar que la mare seria molt feliç llegint-la. A l'Adriana, per ser com és. Per cuidar-me, estimar-me i per sincronitzar-se amb mi quan tot queia. No ho oblidaré mai, i jo també hi vull ser per acompanyar-te en el teu camí. Arribarem tan lluny com vulguis.

PUBLICATIONS

This thesis includes work by the author that has been published or submitted for publication. These publications are the own work of the author of this thesis, and the author has the permission of the publishers to reproduce the contents of these publications for academic purposes. In particular, some data, ideas, opinions and figures presented in this thesis have previously appeared or may appear shortly after the submission of this thesis as follows:

- "Synchronization invariance under network structural transformations", L. Arola-Fernández, A. Díaz-Guilera and A. Arenas, Phys. Rev. E **97**, 060301(R) (2018).
- "Uncertainty propagation in complex networks: From noisy links to critical properties", L. Arola-Fernández, G. Mosquera-Doñate, B. Steinegger and A. Arenas, Chaos **2** 023129 (2020).
- "Geometric unfolding of synchronization dynamics on networks", L. Arola-Fernández, P. S. Skardal and A. Arenas, Chaos **31**, 061105 (2021).
- "Higher-order interactions can better optimize network synchronization", P. S. Skardal, L. Arola-Fernández, D. Taylor and A. Arenas, Phys. Rev. Research **3**, 043193 (2021).
- "Self-organized explosive synchronization in complex networks: Emergence of synchronization bombs", L. Arola-Fernández, S. Faci-Lázaro, P. S. Skardal, E. C. Boghiu, J. Gómez-Gardeñes and A. Arenas, in peer-review at Comm. Phys. (2022).
- "Spectral shortcut to the onset of synchronization in networks", L. Arola-Fernández, B. Steinegger and A. Arenas, in preparation (2022).

CONTENTS

LIST OF FIGURES

ABSTRACT

Synchronization in networks is the music of complex systems. Collective rhythms emerging from many interacting oscillators appear across all scales of nature, from the steady heartbeat and the recurrent patterns in neuronal activity to the decentralized synchrony in power-grids. The mathematics behind these processes are solid and have significantly advanced lately, especially in the mean-field problem, where oscillators are all mutually connected. However, real networks have complex interactions that difficult the analytical treatment. A general framework is missing and most existing results rely on numerical and spectral black-boxes that hinder interpretation. Also, the information obtained from measurements is usually incomplete.

Motivated by these limitations, in this thesis we propose a theoretical study of network-coupled oscillators under uncertainty. We apply error propagation to predict how a complex structure amplifies noise from the link weights to the synchronization onset, study the effect of balancing pair-wise and higher-order interactions in synchrony optimization, and derive weight-tuning schemes to map the synchronization behavior of different structures. Also, we develop a rigorous geometric unfolding of the synchronized state to tackle decentralized scenarios and to discover optimal local rules that induce global abrupt transitions. Last, we suggest spectral shortcuts to predict critical points using linear algebra and network representations with limited information. Overall, we provide analytical tools to deal with oscillator networks under noisy conditions and prove that mechanistic explanations were hidden behind the prevalent assumptions of complete information. Relevant finding include particular networks that maximize the range of behaviors and the successful unfolding of the structure-dynamics interplay from a local perspective.

This thesis advances the quest of a general theory of network synchronization built from mechanistic and geometric principles, a key missing piece in the analysis, design and control of biological and artificial neural networks and complex engineering systems.

1 INTRODUCTION

If physics is the study of symmetries [1], mathematics is the art of drawing them. This interplay has shed the brightest light on the questions we ask the world, either for the sake of curiosity or our desire to progress, and has lead to some of the most remarkable contributions of science in the past. The future is promising too, although some things are changing. In this century, vast computational power, access to large datasets and automatized pattern recognition are challenging the modeling approach by exploiting all the available information and interdependencies at different scales. Whether research is driven by physical reasoning and mathematical modeling; or by lots of data, machine learning and statistical inference (or a combination of both), the scientific community has reached a sort of consensus in the last decades about the benefits of following interdisciplinary approaches, blurring the boundaries between different fields, in an attempt to explain the complexity of the world [1–3].

In this thesis, we focus on some theoretical aspects of a paradigmatic *complex* problem, the synchronization phenomena in networks of coupled oscillators [3–7]. To understand the key role that this particular problem plays in many –apparently unrelated– fields of science, it seems appropriate to begin by exploring a few stories and concepts of complex systems more broadly, and await for the music of synchronization to spontaneously emerge from the interactions between these components.

1.1 THE MUSIC AND MATHEMATICS OF COMPLEX SYSTEMS

If one thinks about systems that display complexity, probably the first that comes to mind is precisely the mind itself [8] –or the nervous system– although it also seems to be the most complicated to understand. It is odd to think about how we think. How can self-consciousness emerge from a remarkably huge wiring mess of 100 billion neurons and 100 trillion chemical and electrical synapses? Are the cognitive functions of the brain completely determined by the complex interplay between its structure and neuronal dynamics? [3]. Evidence points towards an affirmative answer [9–11], although it is not exempt of ethical and philosophical concerns [9, 11]. S. Ramón y Cajal, the precursor of modern neuroscience in the late 19th century and probably an early advocate of the complex system approach, studied and popularized neurons as the elementary building blocks of the nervous system [12], and suggested that “to understand the universe, we have to understand the mind." Since then, this interdisciplinary field has advanced in many fronts to pursue this

quest. We know the physiology of single neurons –cells that can process external signals and communicate with the rest via oscillatory changes in its membrane voltage, called action potentials– and how to model them mathematically, through the pioneer works of A. Hodgkin and A. Huxley [13]. These works opened the door for a computational and theoretical approach to neuroscience. Meanwhile, in the lab, the measurements of brain structural connectivity [10, 14] (see an example of the progress in Fig. 1.1 and its caption) and functional connectivity [11, 15, 16] have significantly improved, leading to many empirical discoveries at different scales. To name a few examples, we learned how activity in single neurons can encode complex concepts [17] and how a few of them behave in a group, extending their axons to wire together and spontaneously reach states of collective firing patterns [16] and sustaining global function after structural damage [18]. It was also found that different cognitive tasks are mostly driven by activity in specific brain regions or lobes, while a correct global functionality requires a coordinated orchestration among the different modules [10, 14]. What seems clear is that the brain is playing a very complex symphony –a neural code [19]– that we are still far from deciphering [10].

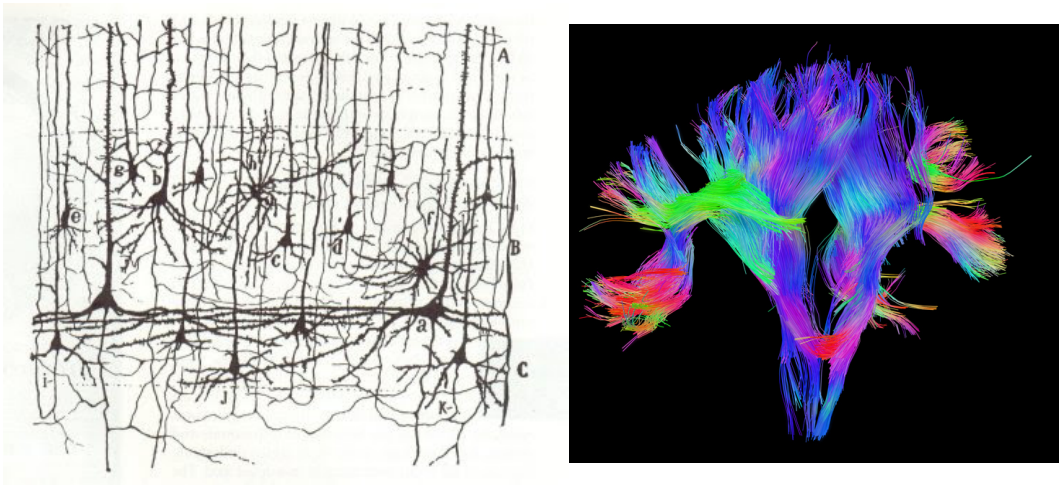

Figure 1.1: Left: Ramón y Cajal's drawing of neurons in layers 5–7 of the 15-day-old human infant visual cortex, using what is known as the Golgi method [12]. Right: White matter fiber architecture of the brain, measured from diffusion spectrum imaging (an advanced magnetic resonance imaging technique). Shown are association and projection fibers, color-coded by different directions, from the human conectome project [10].

Among the myriad of complex tasks, long-term memory and learning are perhaps the ones better understood from physical principles. Much evidence has been collected to support that, what R. Feynman called "this memory thing" is controlled by several mechanisms of synaptic plasticity [20–22], which reinforce and regulate the conductance weights (the coupling) between neurons that fire together in specific patterns of activity, such that these functional patterns can be stored in the structure and reached again in the future, from different external or internal stimuli. These ideas have become much more sophisticated in the experimental realm [11, 23], to the extent of being able to induce fake memories in mice by stimulating a precise population of neurons in the hippocampus region [23], to name but one striking result. On another successful and applied path, engineers have been

inspired by these memory models, and also by neuronal circuits in the visual cortex, to build artificial neural networks. Since the perceptron model that F. Rosenblatt introduced in 1958 [24], these algorithms with input, hidden and output layers of connected units are able to learn patterns from data and make predictions by tuning the connection weights in a clever way such that the model fits the data. It eventually turned out that, when using a very deep number of parameters and particular structures (like convolutional or recurrent neural networks), they can classify almost everything [25] and even outperform humans in very complex decision-making problems dealing with both complete or incomplete information (as in the game of chess [26] or, more recently, poker [27]) and also solve long-standing biological problems like protein unfolding [28], by predicting the spatial shape of proteins from its DNA sequence with high accuracy.

From a theoretical standpoint, the main issue with these powerful algorithms is that they are black-boxes. The captured relations are difficult to understand and to generalize to broader contexts, and, in practice, each problem is tackled somewhat differently, using brute force, rules of thumb and heuristics, rather than following a minimal model [25]. Something similar occurs with the brain, as the largest and most complicated black-box of all [10]. Indeed, a pure theoretician would propose another view, and ask: if the brain is the most *complex* complex system, which is the simplest one that keeps the minimal complex ingredients, and, what do we understand about it? The concept of emergence, states of matter and many-body systems have been in the physics community for a while, and it was precisely in this context where key models of neural networks that could store and process information were proposed. One might wonder if other cognitive abilities such as complex decision-making, creativity, and ultimately the emergence of the mind could be explained by simple physical models? At least from a historical perspective, here we are tempted to be somewhat optimistic [1, 8].

We go back in time to the birth of thermodynamics in the 17th century, where the notion of heat and the arrow of time were explained with the idea of a physical system, which evolved to thermal equilibrium by minimizing its free energy and increasing its entropy [8, 29]. Phase-transitions, as the one observed in neuronal activity when anesthesia induces an unconscious state [30] or in an epileptic seizure [31], were described back then in a phenomenological manner, as abrupt changes in the observable state of a system (like water boiling or ice melting) when a controllable parameter, for instance temperature or pressure, was smoothly varied. However, it was not really understood from microscopic principles. While thermodynamics was a fully consistent theory on its own that made accurate predictions on the macroscopic properties of matter, it was statistical mechanics, [29, 32], a more mathematically-driven theory culminated in the 19th century by J.W. Gibbs and L. Boltzmann among others, that provided a more satisfying picture of the whole system. The theory bridged the probabilistic counting of the accessible configurations of particles with the macroscopic properties that one can actually measure, in a crucial step towards the acceptance of the atomic theory [8, 32].

Under these statistical lenses, temperature and pressure are now well understood as macroscopic properties that emerge from the interactions between molecules and the physics

behind critical phenomena can be explained using idealized models of interacting spins. These spin models started with the work of E. Ising in 1920 [29] to describe, using a binary variable, the magnetic moment of atoms (more precisely, of its electrons) placed in a lattice. This abstraction was made in an attempt to explain the microscopic origin of phase-transitions and to understand why ferromagnetic materials had a net macroscopic magnetic field. In the first model, the ingredients were minimal: a chain of spins, where configurations that are aligned in the same direction (where adjacent spins take the same value) have lower energy, and a temperature parameter that controls the strength of fluctuations. Ising showed that a phase transition did not occur in one dimension, but eventually L. Onsager in 1944 [33] analytically proved[1] that, for two or more dimensions, a phase transition from a disordered to an ordered state occurred when lowering the temperature below a critical threshold. Spontaneous symmetry breaking [1, 29] appeared to be the mechanism responsible for the transitions between phases with distinct order and the anomalous properties of measurable quantities, as heat capacity or susceptibility, around the critical points [29]. Advancing in the understanding of spin-models, spin-glasses with random interaction strengths in the lattice were introduced [34–36], and by combining these spin systems with the ideas of associative learning [20] and synaptic plasticity in the brain, models as acclaimed as J. Hopfield's in 1982 [37] provided a physical explanation of computation.

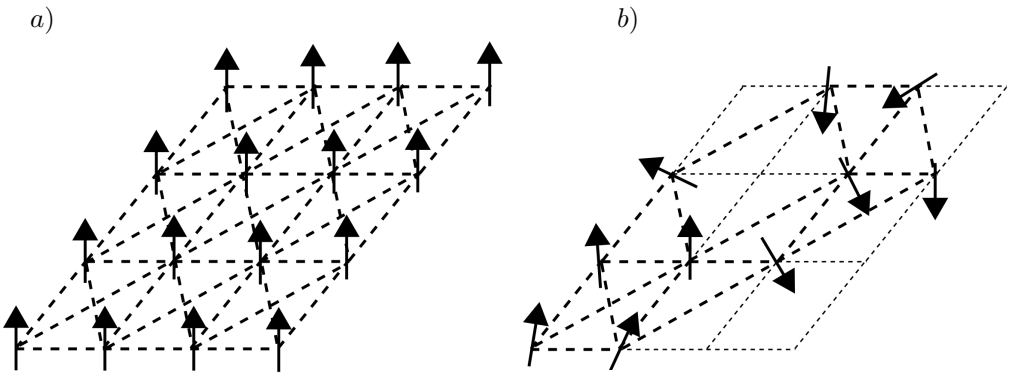

Figure 1.2: a) Illustrative sketch of the Ising model in a lattice with all spins aligned in up position (value $+1$) b) Illustrative sketch of a spin-glass with random interactions and disordered spins, here represented as vectors with three components.

Importantly, the idea of combining broken symmetries and disordered systems was at the core of the early paradigm of complexity and its applications rapidly increased in different directions, far beyond these toy models of memory and computation. In fact, the usage of the complex system terminology arises in P. W. Anderson's 1972 paper, "More is Different" [1] when discussing decreasing symmetry and increasing complexity in some condensed matter problems (the field studying the properties of many atoms under strong interactions), but also in particle physics, biophysics and even in the social sciences. It seems pertinent to quote P.W. Anderson here [1], on a particularly visionary line of further research, at least to our interests. "Keeping on with the attempt to characterize types of

1 Lars Onsager won the 1958 Nobel in Chemistry, in part thanks to this result.

broken symmetry which occur in living things, I find that at least one further phenomenon seems to be identifiable and either universal or remarkably common, namely, ordering (regularity or periodicity) in the time dimension. A number of theories of life processes have appeared in which regular pulsing in time plays an important role."

To describe time well, we have to shift our perspective from a statistical to a more kinetic and dynamical description of a complex system. Coupled systems of non-linear differential equations describe the temporal evolution of a set of variables in a phase-space, where non-linearity simply means that the outputs of the equations are not proportional to the inputs [38]. These equations can be deterministic or stochastic (with or without noise), ordinary or partial (with dependencies on only one or more variables), and have revealed to be the best way to describe the dynamical behavior of many interacting units. Most classical and quantum systems [8, 29, 38], the forecasting of weather or epidemics [39–42], reaction-diffusion processes of chemical substances [38], food-web relations in ecological systems [43], the dynamics of the power-grid between electricity generators and consumers [44, 45], the aforementioned neuronal dynamics [7, 13, 46, 47], and even the turbulence of a fire flame[2] [38] can be modeled as non-linear dynamical systems. Under this framework, phase transitions are seen as bifurcations in the equilibrium of low-dimensional order parameters in the phase-space when parameters of the equations are tuned. The appealing concept of chaos also emerged in this context, in the works of H. Poincaré at the end of the 19th century on the prediction problem of three-body systems in celestial mechanics [48], and was popularized by E. Lorenz and O. Rössler and their strange attractors [49, 50]. We learned that very simple models could lead to very complicated dynamics [51], and that the strong sensibility to initial conditions limit the predictive power of our models beyond a certain, and rather short, time horizon. Interestingly, even under the pessimist view of unpredictability, we also started to unveil ways to control this chaos [52, 53].

A key feature of most complex systems is that they are discrete, made of a countable number of units (like neurons, spins, power-generators or people), which can interact with each other in different ways. An abstract representation to capture these interactions is a network or a graph, consisting of a set of vertices (nodes) joined by edges (links) [2]. Graph theory is the branch of discrete mathematics that studies these objects, and was largely decoupled from the analysis of dynamical systems in the last century, where mean-field (all-to-all interactions), random models or regular lattices of different dimensions were taken as the underlying medium of interactions, imposing the symmetries of ordinary matter [2, 5, 6]. As we will see, at the end of the 20th century physicists learned an important lesson. Most of the interaction patterns in nature are complex and irregular (far away from lattices or random graphs), and the complex interaction patterns dramatically affect the dynamical behavior [54–56]. The study of these complex structures and the dynamical processes running on top of them, gave birth to the interdisciplinary field of complex networks [2, 6, 57, 58], which brought many tools from statistical, non-linear physics and graph theory. but also required new methods and models to handle the network complexity.

2 A central name in our work, Y. Kuramoto, also has a great model for the dynamics of a fire flame, known as the Kuramoto-Sivashinksy equation [38].

Overall, non-linearity, complex interaction patterns and interdependencies, emergent properties like collective behaviors, but also chaos and unpredictability, are some of the features that many complex systems share, ranging from the brain to the power-grid and society. An open question that persists throughout different fields is to understand the rich interplay between structure and dynamics, yet one may feel overwhelmed by the large variety of existing theoretical perspectives and also by the accurate predictions of integrated, multiscale and data-driven approaches. Listening to the emergent music of synchronization, the striking phenomena of interacting oscillators that synchronize their rhythms in a spontaneous manner, sounds just great. In fact, its study has already provided key answers into the origins of temporal order in complex systems, and we are *almost* at the beginning of the way. In the words of S. H. Strogatz, "sync is grounded in rigorous mathematical ideas; it has passed the test of experiment; and it describes and unifies a remarkably wide range of cooperative behavior in living and non-living matter" [3]. Mathematics and music have been related since Pythagoras [59], who discovered that simple ratios in the frequencies of a single vibrating string produced a pleasant sensation to the ear, now known as intervals in music theory, and understood from harmonic analysis of sound waves [59]. Interestingly, the phenomena of synchronization produces a similar pleasant sensation. In American popular culture, this feeling is captured by the expression "playing in the pocket", referring to two or more musicians that play together and are perfectly on-beat, never missing a note or going off tempo in any way[3].

Figure 1.3: Emergent collective behavior in a flock of birds, captured with an ornitography, by Xavi Bou. Reprinted by permission of the author.

It is evident that musicians are not simple oscillators, but analogies are powerful in mathematics and physics. We will see that treating the interactions of units of very diverse kinds (neurons, crickets or humans) as a network of coupled phase-oscillators, where oscillators are described by a single variable, its phase in a circle, has proven tremendously

3 From www.urbandictionary.com.

useful to explain empirical phenomena across all scales and disciplines, both qualitatively and quantitatively [3, 5, 6]. This approach captures the key point: the competition between the internal rhythms of the units and the coupling with the network leads to distinct collective behaviors, as incoherence or synchrony, but also waves and chaos, and these states are transited via critical points! A single mechanism appears to be behind the coherent motion of cardiac pacemaker cells [60], responsible for the heart beat, the simultaneous flashing of fireflies in Malaysian forests [61], the correct functionality of the decentralized power-grid [44], and the hypnotic coordination of a flock of birds or a human crowd, like in the synchrony of applause from the audience after a good concert [5]. Collective rhythms are difficult to capture in static pictures, by definition. The beautiful work of photographer Xavi Bou challenges this idea with the concept of ornitographies[4], as shown in Fig. 1.3.

As mentioned, the theory behind the phenomena of network synchronization is the main topic of this dissertation. For this reason, we will not spend more time explaining the vast number of applications that this framework can tackle, and refer the reader to the fascinating book by Strogatz and to some great reviews on the field [5–7, 62]. Nevertheless, we have to once again mention the brain, where there is large empirical evidence that phase-synchronization can describe the physics behind memory processes [63], the dynamical coordination of modules in different cognitive tasks [10], and also that many models of pulse-coupled neurons can be mapped into models of phase-oscillators [7, 64, 65]. Paraphrasing Ramón y Cajal, it seems that to understand the mind we have to understand synchronization. Or, in the more eloquent words of Strogatz, “For if consciousness is the by-product of some sort of neural sync, then just thinking about sync involves a stupendous act of sync itself" [3]. In fact, the attraction some researchers feel towards synchronization theory may be explained by this self-consistent argument. Perhaps just as a coincidence, the Kuramoto model –a celebrated mathematical description of synchronization phenomena and the starting point of our research– was initially solved, in the mean-field case, by employing also a beautiful and ingenious self-consistent argument [4].

In the previous paragraphs, we have attempted to present a broad overview of several theoretical approaches to complex systems, and to explain how the paradigm of synchronization in complex networks fits in the whole picture. We do not want to give the false impression that our work attempts to answer general questions of complex systems, quite the contrary: we tackle a few specific and technical problems in idealized models of coupled oscillators, focusing on the largely unexplored roles that network uncertainty and partial information have in the prediction aspects of the system and in the interpretation of these predictions. An underlying assumption of this dissertation is that synchronization in networks is sufficiently ubiquitous and general such that the findings obtained in our particular toy models may find validation and application in more realistic scenarios. Before getting into the main questions of our research and into the technicalities of our results, we introduce a brief review of previous works on the theory of coupled oscillators and complex networks, which will uncover some of the most relevant discoveries and also introduce important concepts to our work.

4 A gallery of ornitographies is displayed on the artist website: www.xavibou.com.

1.2 IN SYNC: COMPLEX NETWORKS AND THE KURAMOTO MODEL

Synchronization and networks, or graphs, are so ubiquitous in nature that they have probably been around the curious minds since ancient times[5]. However, maybe the imperceptible interactions that caused sync and the volume of its music were too subtle compared to all the phenomena we could directly observe from everyday experience. We had to wait until the end of the scientific revolution to witness the first contributions to synchronization and graph theory, and then to the beginning of the current century to unveil the real potential of combining both fields.

C. Huygens, a Dutch scientist who contributed to the early foundations of probability theory and optics, to name a few examples, was also an excellent engineer obsessed with measurement [3]. Huygens invented many kinds of telescopes and also the first pendulum clock, a significative achievement at the time that increased the precise measure of time and promised applications in navigability problems, in particular in the estimation of the longitudinal coordinate on earth from temporal measurements. In 1665 [6], when testing two of his pendulum clocks, Huygens described that an "odd kind of sympathy" occurred when both clocks were hanging from the same physical support. Huygens realized that, if the clocks were sufficiently close to each other, and started to swing at different angles and speeds, they would completely synchronize their motion after some time, usually in anti-phase (meaning that the pendulums ended up swinging at the same speed but in opposite directions), but if the clocks were too far from each other, then synchronization would never occur. Huygens had discovered the phenomena of synchronization (also known now as entrainment or collective rhythms) of coupled oscillators. In his case, the oscillators were pendulum clocks, coupled via a mechanical interaction through the medium, possibly wood. This mechanism was actually not great for Huygens' initial interest, regarding his idea of using two or more clocks to measure time during navigation (because the synchronization effect would reduce the precision of individual clocks). However, his finding turned out to be of great importance for many branches of science.

Quite a few years later, in 1736, the Swiss mathematician L. Euler[6], studied the possibility of taking a walk that crosses the seven bridges in the Russian city of Königsberg and returns to the initial point by crossing each bridge only once. By abstractly representing the bridges as lines connecting dots (thus creating a network), Euler realized that for that particular case the answer was negative (by noting that the intermediate vertices in the path needed to have an even number of links, which was not the case, as can be seen in Fig. 1.4), proving the first theorem of graph theory [2]. Although research on collective oscillations, i.e. synchronization processes, and the study of networks and graphs was largely decoupled for several centuries, it is fun to note that some connections were already present in the beginning of the path. Euler admired and supported Huygens' work on the oscillatory theory of light, which defied Newton's crepuscular view and ended up being the accepted paradigm until the later establishment of quantum mechanics [3]. In the end,

5 The etymology of both terms come from classical Greek, from sync "together" and khronos "time" and from the suffix grapho, meaning "to scratch, to scrape, to graze", from www.wordreference.com

6 Modestly known in popular terms as the king of mathematics.

both were fascinated by oscillatory phenomena, and in the case of synchronization in networks, we will see how this connection is shared among other researchers. Insisting in Euler, his most beautiful formula in the history of mathematics[7], will actually play a key role in the Kuramoto model, probably the most elegant mathematical description of sync and the theoretical framework on which this thesis is based.

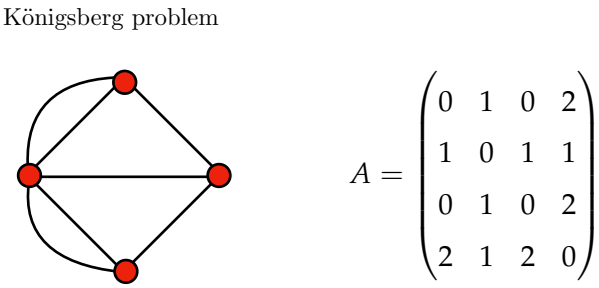

Figure 1.4: Königsberg network, assumed symmetric, and its representation in the adjacency matrix. Node indices are labelled clock-wise, starting from the top node, and multi-edges are captured by entries with a value of two.

It is important to think of networks as matrices. For instance, the representation of the Königsberg network using the adjacency matrix A is given in Fig. 1.4, where zero entries represents an absent connection, $a_{ij} = 1$ represents an unweighted connection from j-node to i-node and $a_{ij} = 2$ captures a double edge. In this notation, the degree (or strength for weighted networks) is simply $k_i = \sum_{j=1}^{N} a_{ij}$, i.e. the sum of incoming links or weights, but if the network was directed we should consider both in and out-degree. Throughout this thesis we will work with several types of representations (Laplacian, normalized adjacency) and different network conditions, which will be presented at the specific sections.

It is worth introducing the network spectra due to its key role in the dynamics. We say that A is diagonalizable if it can be written as $A = P^{-1}\Lambda P$, where Λ is a diagonal matrix containing the eigenvalues of A and P is a matrix with the eigenvectors as columns. If one thinks of a matrix as an operator that acts on a vector, then the eigenvectors define the directions where the matrix only acts by stretching (with magnitudes given by the eigenvalues), without rotating [2, 66]. The spectra of networks is known only in some particular cases, and in general, it is a challenging problem [2, 6, 66–68]. Luckily, there are some important theorems available. For instance, the Perron-Frobenious theorem [2] tells us that if a matrix A is square (here $\mathcal{R}^{4\times4}$) with positive entries, then the largest eigenvalue is real and unique, and from the Gerschgorin circle theorem [69], we know that the eigenvalues of A will be inside N circles with centers at a_{ii} and radius $r_i = \sum_j |a_{ij}|$, thus bounded in $(-4, 4)$. A numerical method is used to compute the spectra of the previous matrix, where the eigenvalues (the diagonal entries of Λ) are given by $\lambda_1 \approx 3.63$, $\lambda_2 = 0$, $\lambda_3 \approx -0.77$, $\lambda_4 \approx -2.87$, which obviously satisfy the two mentioned theorems. In this thesis, we will use some more tools from these fields, which will be described in the specific chapters. After this technical detour, we can return to our timeline of sync.

7 In words of R. P. Feynman [8].

Since Huygens, synchronization in the natural realm kept fascinating researchers in several unrelated fields, as in the contemplation of simultaneous flashing of fireflies in Malaysian forests [61], or the observation of chemical periodic waves and entrainment of menstrual cycles among women [3]. However, the emergence of periodic collective phenomena was poorly understood by physical principles (in terms of how and why it happened) and was given very little attention compared to many other branches of physics [3]. It was in the biological context of neural oscillations (the so-called brain waves), where the first quantitative leap in terms of mathematical modeling was achieved. Mathematician N. Wiener, most known for his contributions to stochastic processes[8], claimed in 1958 [70] to have measured, with EEG technics, the spectrum of alpha waves (one type of brain waves with a frequency between 8 and 12 Hz) with an astonishing accuracy at the time, and published the qualitative distribution of this spectrum, as shown in Fig. 1.5.a), which had a surprising peak in the center and then two additional peaks after a dip shallow.

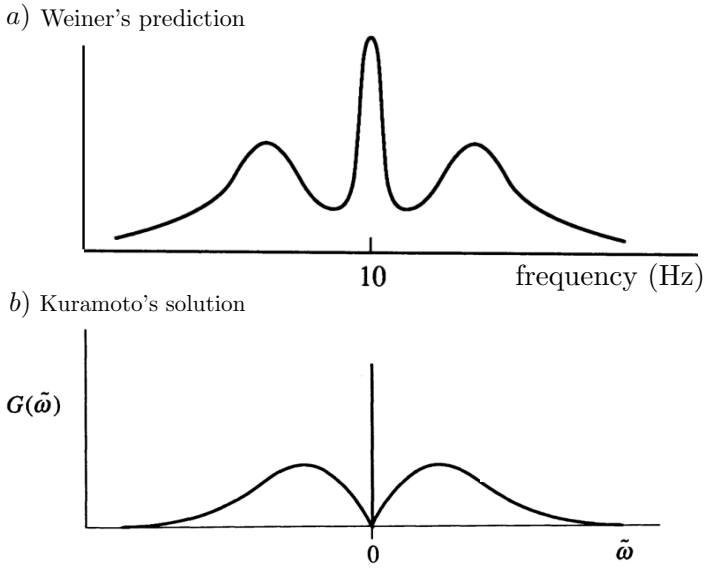

Figure 1.5: a) Qualitative results of the distribution of α-wave frequencies in the brain, by N. Wiener and b) Distribution of effective frequencies in the Kuramoto model. Note that in b), the entrained oscillators have an effective frequency of zero, meaning that some oscillators have synchronized their frequency completely.

Wiener conjectured that this spectrum was the consequence of synchronization in the collective spiking rhythms of neurons, otherwise it would be distributed normally. The peak of the center would correspond to the neurons or groups of neurons with similar internal rhythms, that are able to synchronize their pace at the mean effective frequency, approximately, and then the rest of neurons would not be synchronized, thus having an effective frequency in the tails of the distribution. This data was never revised in detail [3] and Wiener did not successfully model his prediction either, but a few years later, in 1975, Y. Kuramoto [4], a young Japanese statistical physicist, inspired by the work of A. Winfree [71], proposed and solved a model of globally-coupled phase-oscillators that

8 The differential equations with uncorrelated noise on the position and velocity take his name [38].

displayed a phase transition from disorder to order at a given critical coupling strength and whose effective distribution of frequencies, after the transition, resembled very much the spectrum hypothesized by Wiener, as observed in Fig. 1.5.b).

The Kuramoto model in Eq. (1.1) was the beginning of some promising and novel lines of research in complex systems,

$$\dot{\theta}_i = \omega_i + K \sum_{j=1}^{N} \sin(\theta_j - \theta_i), \ \forall \ i \in 1, \ldots, N, \tag{1.1}$$

where θ_i is the phase (angle) of the i-th oscillator, $\dot{\theta}_i$ its time derivative, ω_i the internal frequency, drawn from some distribution $g(\omega)$ and K is the coupling strength. In this thesis, we will follow the mathematical approach proposed by Kuramoto, and the details on his celebrated model and its self-consistent analysis are presented with more care in 2.1. This model became a paradigmatic framework in the community of statistical and non-linear physics studying large systems of phase oscillators [5], and many relevant results were obtained in the last two decades of the 20th century, considering a mean-field, all-to-all network, or lattices of different dimensions. Mathematical success was achieved by taking the thermodynamic limit of the model (large size) and using several techniques, as the Fokker-Planck formalism including white noise in the process. Also, many interesting variations of the problem were studied, introducing delay (a finite velocity in the interactions), inertial effects (considering the variation in speed, not only in phase), external random fields [72] or frustrated coupling strengths [73]. Important connections between the Kuramoto and the Hopfield Model were made, in an important step to explain the physics behind computation and memory processes [74]. We refer the reader to the excellent review of [5] on more details on the Kuramoto model and all its variants in the mean-field case or in lattices of different dimensions. In this dissertation, we are interested in another source of complexity, the underlying network of interactions.

Before diving into the nuances of complex networks, it is important to mention here that other approaches have been considered to model synchronization processes beyond phase models. Pulse-coupled systems, where the oscillators have a charging voltage until they cross a threshold and only then they fire (integrate-and-fire) are another way of describing many types of oscillators, like pacemaker cells [60] or neurons [7, 75, 76]. Interestingly, some of these models can be mapped into phase-models [7, 65], and also non-linear types of limit-cycle oscillators can be described, in first approximation, by its phase [77–79]. Another direction was to use the master stability function, a framework to analyze the stability of the fully-synchronized state of identical oscillators [6, 80]. In this context, synchronization of identical coupled chaotic systems was discovered [53]; a phenomenon that at first glance seemed counterintuitive, because these systems were able to completely synchronize their trajectories, which were chaotic in isolation, even starting from different initial conditions. This finding promised applications in cryptography for some time [3]. In any case, the key role of complex networks and its ubiquity in nature was disregarded in most of these theoretical approaches during the last century, probably because empirical data was scarce and the mathematics of networks were still at an early stage.

The study of networks followed its own pace during the 20th century. We must comment on three lines relevant to our research. Random graphs were introduced by P. Erdös and A. Rényi in 1959 [81] and described networks where a certain number of links are placed at random (or similarly, each pair of nodes has a probability p of being connected). In this model, the degrees of the nodes (the sum of connections to their neighbors) are distributed in a binomial form, with

$$P(k) = \binom{N-1}{k} p^k (1-p)^{N-1-k}, \tag{1.2}$$

where k is the degree, N the number of nodes and p the parameter of the model [2]. In the large size limit, this distribution is well approximated by a Poisson,

$$P(k) = \frac{(pN)^k e^{-pN}}{k!}, \tag{1.3}$$

centered at $pN \approx \langle k \rangle$, and being bell-shaped for a wide range of p. Random models found applicability in the study of percolation [82] (adding or removing nodes or links), as we will discuss in more detail in chapter 5. The other lines are spectral graph theory [67, 68, 83] and random matrix theory [84], the latter being introduced by E. Wigner in physics to study the energy spectrum of heavy atomic nucleus in terms of the spectra of a random a matrix [85]. These matrices have played a key role in many problems of theoretical physics and condensed matter [84, 86], and also found applications in large complex systems, as in the study of the stability of ecological food-webs [43, 87]. Overall, the advance of graph theory in these lines was key to the study of dynamical processes in future years. For instance, M. Fiedler in the seventies found important results relating the spectra of the Laplacian matrix of the graph $L = D - A$ (where D is the diagonal matrix of degrees) to the problem of graph partitioning [88], i.e. finding the minimal cuts to split the graph in disconnected components, which found many applications in network synchronization and community detection later on. However, it was thanks to applied works of sociologists as S. Milgram and H. A. Simon that complex networks entered the modeling game.

It was around 1998 when D. Watts and S. H. Strogatz wondered about synchronization on top of small-world networks [54], a concept introduced by the famous experiment of Milgram about the six degrees of separation in the world [89], which showed that social networks had very short network paths. The key idea behind the model of Watts and Strogatz (WS) was to consider both a regular (a ring) and a random network as the two limiting cases, with interpolation parameter p, as shown in Fig. 1.6.a). Small-world networks would lie in between, displaying both clustering (your neighbors are also neighbors between them, as in a ring or a lattice) and short average path lengths (as in the random case), both being relevant features of real networks. An important property that was missing in the WS model, and observed in the web, mail or acting networks, and many more examples, was scaling [55] –the signature of phase-transitions [58]– meaning that the degree distributions in these networks were found to approximately follow a power-law $p(k) \sim k^{-\gamma}$, with many empirical networks with low values of exponent, between 2 and 4, thus being very heterogeneous in degree. Power-law distributions span several orders of

magnitude, and they do not have a well-defined scale (that is why they are called scale-free networks) [2, 66]. In the infinite size, the variance (and higher-moments) of the degree distribution diverge, because of the long tails of the distribution, meaning that it is not easy to quantify and predict rare events. In networks, this effect translate into the concept of hubs, super well-connected nodes (another way of having short network paths) that produce the paradox of friendship[9] and many other very noticeable effects in economy. Hubs are found in the brain and also in social and infrastructure networks, to name some examples, and are crucial to global function [2, 90]. Several models, as the well-known preferential attachment [55, 90] and some modifications to control the exponent or the clustering in the scale-free network [91–93], were proposed to generate these networks by exploiting the mechanism of cumulative advantage [90], meaning that rich nodes, with more connections, get richer, a concept that already modelled by H.A. Simon in the sixties and D.J.S. Price in the seventies [2]). Examples of small WS and SF networks are shown in Fig. 1.6.

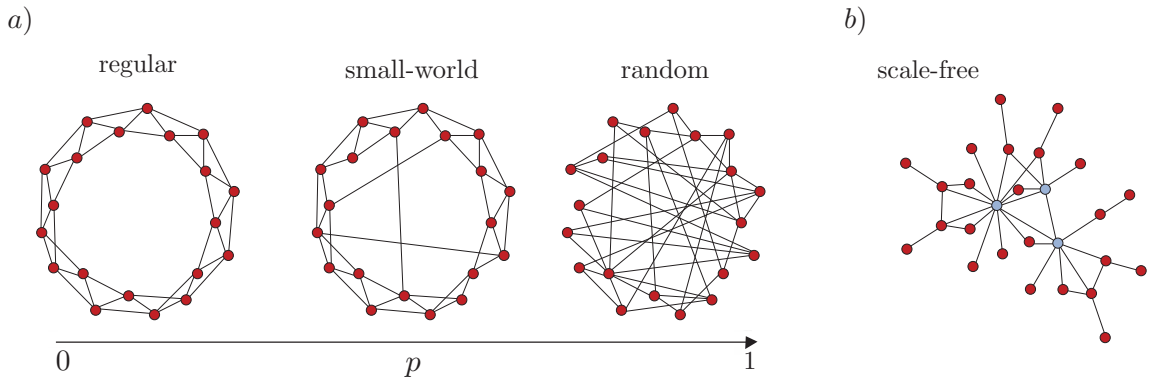

Figure 1.6: Toy examples of a) the Watts-Strogatz model interpolating between a ring and a random network and, b) a scale-free network where hubs are represented as gray dots. Note that for networks to have a true power-law distribution in the degrees, the size of the network should be much larger such that the degrees can reach several orders of magnitude.

With the aforementioned works, we entered the current century and the foundations of complex networks (and the dynamics on top of them) were rapidly established [2, 6, 56–58]. Null models were proposed to compare against empirical networks and analyze the significance of its properties. The configuration model [94] (random networks with a fixed degree distribution) and, more generally, exponential random graphs [95] (imposing any kind of constraints in a statistical mechanics formalism) are good examples. The stochastic block model [2, 96] has been used also to deal with communities, another prominent feature of complex networks where different modules are defined by having more connections inside than between them [2, 97]. Modularity maximization is the challenging optimization problem that attempts to find these communities. It has received a huge amount of attention due to applications in graph partitioning [98], in neuroscience [14] and social network analysis [99], to name a few examples. In the opposite limit of modular networks, we have bipartite networks, that connect nodes of different type and are of high

9 Due to the presence of hubs (celebrities, influencers), on average, your friends have more friends than you [2].

relevance in many biological and technological systems [2]. All these network features, the relevant algorithms and different networks models, are excellently reviewed in the book of M. Newman [2].

In parallel, the properties of complex networks were studied in systems of Kuramoto oscillators, first with numerical simulations, but rapidly by analytical means [6, 62]. We learned that small-world networks synchronize faster than rings (because long-range interactions facilitate the emergence of global synchrony) [54, 100], and also that heterogeneous networks anticipate the onset of synchronization with respect to homogeneous ones and follow different synchronization routes [101], as observed in Fig. 1.7.a). Approximations for the synchronization onset in networks were obtained [102–104], and many new phenomena were discovered [6, 62]. Breathing and standing chimeras [105, 106] (populations of identical oscillators where only a part of them synchronize, due to the effects of the network), remote synchronization [107] (where nodes can be synchronized even if they are not connected, due to network symmetries), explosive transitions [108, 109] and chaos [110] (due to correlations between the structure and the frequencies) and other optimal and counter-intuitive properties, [111] as the benefits of directed and weighted networks [112–114] or noise [110, 115]. Importantly, the role that the spectra of network matrices plays on synchronization dynamics has become more understood [116–118] and in turn, this spectral view of sync allowed to gain insight from the underlying networks, finding topological scales [116] as observed in Fig. 1.7.b), dynamical communities [119] and ideas for coarse-graining techniques [120].

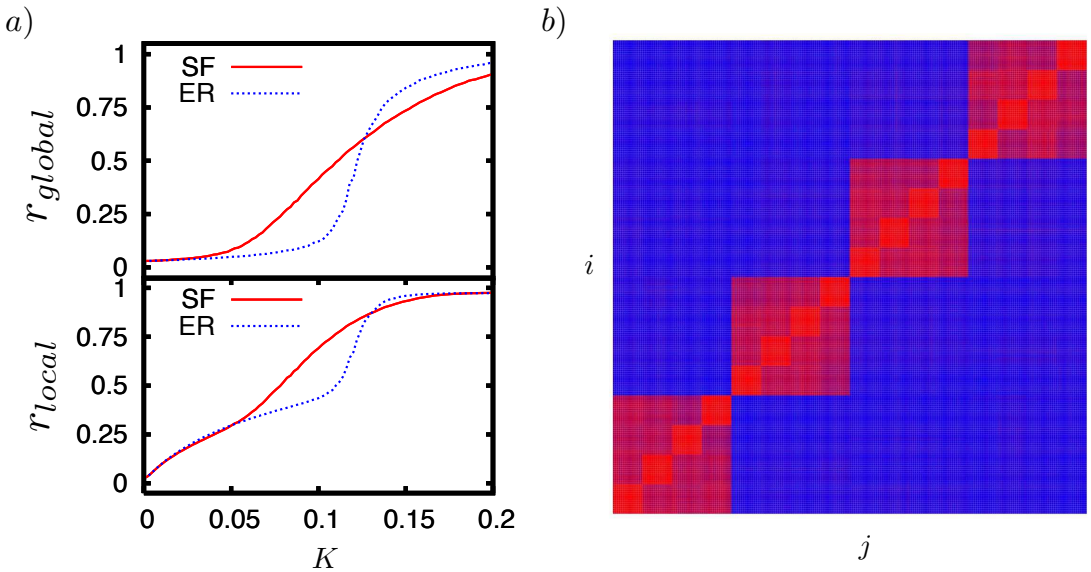

Figure 1.7: a) Global (top) and local (bottom) degree of synchronization depending on coupling in random (ER) and scale-free (SF) networks of the same size, which follow different routes towards full synchrony ($r \approx 1$). The order parameter $r \in (0,1)$ will be introduced in detail in the next chapter. Reprinted by permission of [121]. b) Average phase similarity (from blue to red) between pairs of oscillators in a hierarchical network of three groups. This well-known result unveiled that the communities of the network can be recovered from the synchronization properties between nodes. Reprinted by permission of [116].

An important breakthrough in the infinitely large, mean-field case was made by E. Ott and M. Antonsen in 2008 [122] (OA), when they found an exact dimensional reduction into a few coupled differential equations, where bifurcations can be more *easily* studied. We will introduce in more details the OA ansatz in the following chapter, in section 2.4.1, but it is worth to mention that it was indeed a remarkable achievement for the globally coupled problem (i.e. without considering a complex network). Closed solutions can only be obtained under some conditions [7, 123–126], but its usage has led to many new discoveries and techniques [7, 127] and empirical validation in biological experiments [7, 128].

In complex networks, research on synchronization during the last decade has gradually shifted from a more descriptive and exploratory approach of the system to more concrete problems, in different lines. One focus of concern has been control and optimization [69, 118, 129–131], driven by the applications in the power-grid [44, 132, 133] and in network neuroscience [10, 134, 135]. The second has been an increase in both structural complexity, either going to multilayer networks [136] or consider higher-order (beyond pair-wise) interactions [79, 125, 137–140], and dynamical complexity, by coupling the synchronization dynamics to other processes as diffusion or epidemics [141–143] and proposing new models displaying even richer phenomena, for instance the versatile system of *Janus* oscillators studied in [126, 144]. The third branch has focused on mathematical aspects of the basic models, looking for dimensional reductions and algebraic approaches [145–147], generalizations in higher-dimensional spaces [127, 148] or going back to unsolved problems in rings of identical oscillators [149–151]. In Fig. 1.8 we show two examples of striking discoveries that are recently being made in the minimal Kuramoto model with identical oscillators.

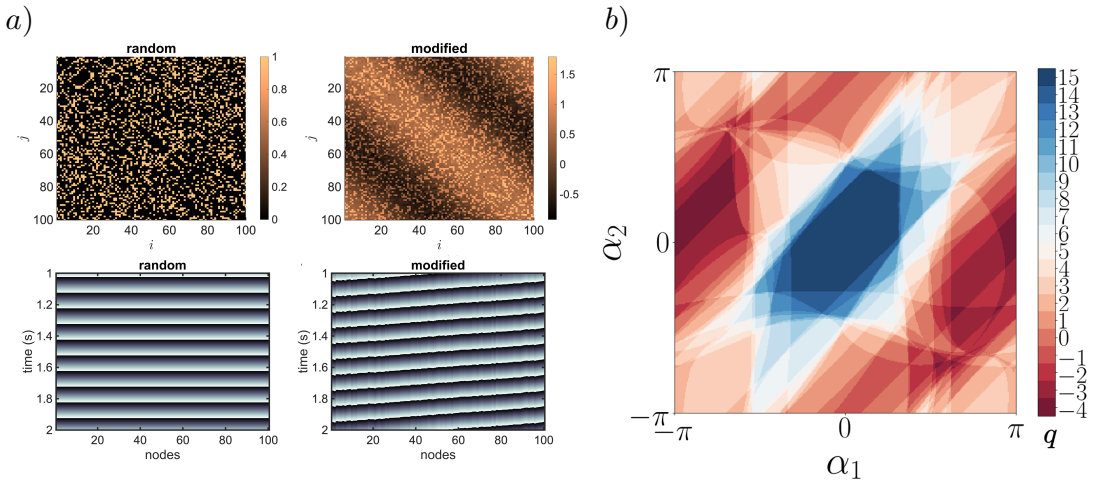

Figure 1.8: a) Design of a twisted (almost synchronized state) by Nguyen et al. [151] in a random network by modifying the adjacency matrix following the algebraic solution of a linear limit of the Kuramoto model (KM) for identical oscillators [147] (we refer the reader to chapter 6 for more details), and b) Basins of attraction (how many initial conditions end up at a given equilibrium point) in the KM on a ring network. The basins turned out to be octopus-like instead of the expected hypercubes. The *tentacles* can be observed by measuring the probability of ending at a given equilibrium when applying perturbations in different α-directions. Reprinted by permission of [149, 151].

Our thesis builds upon some of the aforementioned results, ranging from the approximations of the synchronization onset to the optimization of synchrony in both pair-wise and higher-order networks or the interplay between synchronization and percolation processes. The novel insight of our approach is to introduce uncertainty into the network description, dealing with oscillator networks only with partial knowledge, with the aim of revealing new phenomena and finding clear mechanistic explanations that were hidden behind the more prevalent, albeit unrealistic assumptions of complete information.

1.3 UNEXPLORED ROLES OF NETWORK UNCERTAINTY

Research on network synchronization has arrived quite far, but at the same time it feels that we have only scratched the surface and there is much more to learn and discover in this field. It is hard to negate the myriad of situations and observed collective phenomena that the physics of synchronization can explain and how the minimal model of Kuramoto naturally emerges from different places, ranging from its original derivation in the context of self-sustained biological oscillators [4], to its equivalence with neuronal models [7, 64, 65, 152], its direct usage in power-grid modeling [44, 45, 133] and the recent connections with quantum systems of correlated particles showing entanglement [153, 154]. In this sense, this model is a quite general, *effective* theory to explain the emergence of temporal order in the universe [3]. When one combines this observation with the evidence that complex networks are all around us, it turns out that studying the physics dictated by the Kuramoto model in complex networks is a fundamental problem, very specifically defined in mathematical terms but with broad physical implications and straightforward applications. Even in its simplest form, there are still open questions to answer and important questions to ask. Therefore, staying in the idealized realm seems an equally or even more promising line of research than adding more layers of complexity into the description.

If we consider the physics of Kuramoto oscillators in complex networks as a minimal *ground truth* of systems with many interacting oscillators, then we end up with a combination of just two ingredients: heterogeneity in the frequencies of the oscillators and diversity of interaction patterns, and we aim to understand how this interplay affects global function. We already know that this combination can lead into a variety of phenomena [6, 62], like different kinds of phase transitions and macroscopic states, but a general theory is still missing [7, 143]. Some general questions about the interplay of structure and dynamics, both for theoretical and practical reasons are: how many non-trivial macroscopic behaviors can occur in this system?; and, can we predict, control and optimize them in an arbitrary network? What does observing the structure of a network tell us about the possible dynamics that we can measure? And also in the opposite direction, when observing the macroscopic dynamics: what can we say about the underlying network and the distribution of frequencies? These types of questions are understood in the infinite size of globally coupled systems thanks to the Ott-Antonsen ansatz [7, 122]. However, when one considers a complex network of interactions and a large but finite size –which are definitively the most usual empirical conditions– things quickly get messier, but also richer.

There are some analytical results that we can use to tackle our problems of interest. However, a general framework to classify, predict and control the range of collective behaviors is not known, due to the large irregularities of the network domain which presumably hinder symmetries [7, 143], and one has to figure out the most fitting technique for the specific problem at hand. Most existing results are obtained in terms of the eigenvalues of network matrices and the interplay of the frequencies with their eigenvectors, which are all global properties and which computation relies on numerical methods that can be seen as black-boxes [118, 129, 130, 135]. These spectral black-boxes make the interpretation of results difficult and hinder direct control and extrapolation of findings. Also, their global nature raises the question of how complex biological systems can evolve towards non-trivial macroscopic states, when they usually navigate in the optimization space exploiting only local information and are subjected to noise, as occurs in the brain [16, 155–157]. Which are the microscopic rules between structure and nodal dynamics that lead to different macroscopic properties, such as optimal synchronization [118], chaos [110] or an explosive transition [108, 143], beyond particular cases? The answer up to the moment is also incomplete. Related features that are only partially understood in the networked case is how noise or uncertainty in the structure propagates into the macroscopic properties or into the critical points [158–160], or to which extent networks with different interaction patterns (heterogeneous or homogeneous, modular or bipartite) and types of interactions (pair-wise or higher-order, multilayer or monolayer) can be tuned to reach a targeted dynamical behavior [69, 135, 161, 162]. We know several stories in this line, for instance that random networks with a given degree sequence can behave as an all-to-all network with weights representing the product of degrees [6, 102] and also that networks with two clusters can be mapped into an all-to-all network with bimodal distribution [163], to name a few, but a complete picture is still missing.

In this thesis, we will try to advance in the understanding of network synchronization by studying the unexplored roles that structural uncertainty have on the collective dynamics of coupled-oscillators. What do we mean by uncertainty here? Essentially a lack of information, when we only have partial information from the system at hand, and we still aim at predicting and controlling things. In this sense, the problems we study are also inspired by realistic scenarios, where usually data from measurements is noisy or incomplete [115, 164–166], we do not know the specific details of the system at hand [118, 164, 165], and the large size of the system make spectral computations and numerical optimization very costly [130]. Working under uncertainty is the norm in most applied disciplines, but has only lately become relevant in our field, once we have started gaining access to more data [128, 133, 135], and we have been able to start validating the theories from the last decades. However, there is a clear lack of theoretical works dealing with incomplete information in the modeling, prediction and control of network synchronization [6, 7, 62, 143, 165].

Looking back, treating uncertainty as information has been a key concept in our successful description of the world and in quantifying how well and efficiently we can measure its properties. Under the light of C. Shannon's seminal works on information theory [167], in 1957 E.T. Jaynes showed [32] that the core principles of statistical mechanics can be

derived by imposing a maximum entropy principle on our probabilistic descriptor of a system, when subject to known constraints from the physics at hand. These ideas are behind the success of state-of-art Bayesian inference and maximum likelihood methods in community detection [42, 96, 168–170] and statistical calibration of model parameters [39], and also in the foundations of null-models for networks exploiting only structural information (using the so-called exponential random graphs) [2, 95, 171, 172]. However, this line of thought has not percolated much into the study of phase-oscillatory dynamics on networks, the modelling of which usually treated uncertainty as noise, incorporated directly into the microscopic dynamics [5, 62, 72, 160, 173] or in the coupling of interactions [62, 73, 158]. An important exception are inference methods [164, 168, 174, 175], where stable oscillatory dynamics have been indeed useful to predict structures that are compatible with the observed behavior, although numerical black-boxes tend to appear again in the obtained solutions, hindering interpretation. There are also works where uncertainty is introduced as difficulties in empirical measurements of power-grids [166, 176] or brain networks [177]. More similar to our approach are the seminal works of Arenas et al. and Gómez-Gardeñes et al. [116, 121] that show how networks can display particular synchronization paths, and the more recent work of Skardal et al. [165], where the linearized synchronization dynamics are studied by considering uncertainty on the frequency allocation, which reveals the underlying effect of the structure, smoothing out the role of frequencies. Other recent works that may have resemblances to ours are models that study how a network non-trivially amplifies the output signal when noise is added to the system [115, 159]. We have learned the benefits of noise in optimization [111], robustness to collective phenomena as explosive synchronization [178], or the possibility to use oscillator networks as noise-cancelling filters [159]. Can we gain novel and more general analytical insight by dealing with partial, incomplete information from the oscillator network?

1.4 THESIS CONTRIBUTIONS AND OUTLINE

Overall, the main focus of this research is to explore the synchronization dynamics of coupled oscillators in the presence of different sources of uncertainty in the complex network of interactions. We will borrow some ideas from classical physics and its mathematics (error propagation, Lagrange optimization, truncated expansions, stability analysis, etc...) and combine them with numerical simulations and several techniques suitable to model coupled oscillators (network generative models and spectral graph theory, dimensional reductions and also mean-field, perturbative and algebraic approaches, to name a few examples). The aim is to find quantitative predictions, but there is a bias towards the search for mechanistic explanations that deepen our understanding of the global problem, i.e. the interplay between the structure and the dynamics in networks of coupled oscillators. The most relevant contributions and finding of this thesis are included in the following list.

- An error propagation analysis to unveil how a complex network can non-linearly amplify noise in the weights towards the macroscopic onset of synchronization.

- A composite Laplacian framework applied to the study of optimal synchronization in networks that can balance pair-wise and higher-order interactions.
- An extended mean-field approach to approximate functionally invariant dynamics by weight-tuning networks with different degree distributions.
- An exact geometric unfolding of the synchronized state to unveil the mechanistic interplay between structure and dynamics and to tackle decentralized systems.
- A model of a synchronization bomb, where abrupt synchronization transitions emerge by adding or removing single links following an optimal local rule.
- An explicit connection between the recent algebraic solution of a linear complex-valued oscillator system and the heuristic origin of the Kuramoto model, which leads to a direct estimation of the onset of synchronization in complex networks.

The reader will find that the novel results are a mixture of analytical methods and predictions of different phenomena in several idealized problems of coupled oscillators, which are motivated by empirical problems in neuroscience and engineering, but mainly driven by theoretical curiosity. The remainder of this dissertation is organized as follows:

Chapter 2 reviews several well-known mathematical techniques suitable to deal with network-coupled phase-oscillators. We go through the classical solution of the Kuramoto model, the well-known approximations of the onset of synchronization and the tools to deal with optimization problems. We also introduce the Ott-Antonsen and the Collective Coordinate model reductions. All the methods reviewed here are used in the next chapters.

Chapter 3 focuses on the question: how do structural constraints in the complex network affect the range of possible synchronization behaviors? We consider fixed structures and allow fine-tuning or fluctuations in the link weights to explain how network properties as degree heterogeneity and higher-order interactions affect the dynamical range. Some of these heuristic approaches pave the way for further works, including our next results.

Chapter 4 presents the results on the geometric expansion of the synchronized state and the associated proofs. We discuss its implications in our problems and related ones. We perform a convergence analysis and derive a local approximation of synchrony to explain several features that were only understood numerically. In this context, we also predict the Braess' Paradox (the effect of links removals that improve synchrony) in directed networks exploiting only decentralized information.

Chapter 5 introduces a model of a synchronization bomb, where explosive transitions are induced by perturbations of single links. The framework is a competitive percolation process driven by a local rule, derived using the machinery introduced in chapter 4. We find that phenomena hold in models of chaotic oscillators and cardiac pacemakers, and we provide an analytical characterization in the Kuramoto case. We

also discuss the benefits of noise in this decentralized process and the link between explosive synchronization, percolation and optimization in complex networks.

Chapter 6 shows an explicit connection between an algebraic approach to the Kuramoto model, proposed by Muller et al. [147], and the heuristic derivation of Kuramoto starting from a coupled system of complex oscillators in 1975 [4]. These results point towards the potential of using a matrix, complex-valued formalism in several open problems of network synchronization, as the prediction of the critical threshold. As a first step in this line, a novel derivation of the mean-field synchronization onset is presented using a linear algebra framework and a rank-reduction of the complex network.

Chapter 7 concludes this thesis. First, we briefly summarize our work and discuss our results in the broad context of the theory of network synchronization. We highlight some limitations and interesting points that we did not cover, and we suggest a particularly promising line of further work.

2

THEORETICAL BACKGROUND

Hello everyone, I'm Kuramoto, I'm sending a message from Tokyo. This workshop, especially its title, makes me realize how far I have come and how old I'm getting.

Prof. Yoshiki Kuramoto[1]

In this dissertation, we focus on the interplay that emerges between the complex network and the dynamics of coupled oscillators described by the Kuramoto model (KM). After almost fifty years of theoretical research on this model, there are many important mathematical results that we can exploit in our problems of interest. Overall, we will leverage some key results that provide simple, closed-form expressions relating dynamical properties of the system with structural ones, and use them to understand how different sources of uncertainty in the structure can affect the dynamical predictions and the functionality of the oscillator network.

Accordingly, this chapter introduces the technical results available in the literature that are more relevant to our purposes. In section 2.1, we introduce the original solution derived by Kuramoto for his mean-field model of weakly-coupled phase oscillators [4, 38]. In section 2.2 we introduce several known approximations of the synchronization onset in complex networks, in particular the closed-form expressions obtained by Restrepo et al. [103] and Ichiminoya [102]. In section 2.3 we present the Synchrony Alignment Framework introduced by Skardal et al. in [118] to study optimal synchronization in networks, and we discuss its relation with the formula for the critical loss of phase-locking predicted by Dörfler et al. [44]. Finally, in section 2.4 we present two model reduction techniques of the KM, that decrease the dimensionality of the system for further analysis: in section 2.4.1 we introduce the exact mean-field reduction for the infinite size, globally-coupled network derived from the celebrated Ott-Antonsen ansatz [122], and in section 2.4.2 we present a more recent technique to deal with finite systems and complex structures, based on the collective coordinates ansatz introduced by Gottwald in the globally-coupled case [145] and extended to complex networks by Hancock and Gottwald in [146].

Before diving into these technical results in detail, we suggest that the reader takes a look at Kuramoto's speech, transcribed in the appendix of this thesis, which tells a brief story on the origins of the KM, in the words of Y. Kuramoto himself. This speech begins

1 In a video message to the international conference "Dynamics of coupled oscillators: 40 years of the Kuramoto model", organized by A. Pikovsky, A. Politi and M. Rosenblum, held at Max Planck Institute of Complex System, Dresden, Germany, on 27th July 2015. The full speech is transcribed in the appendix.

with the sentence at the head of the chapter and explains a fascinating, and quite recent chapter in the history of science. We found it interesting to learn about the birth and fate of this key model and also to know where we come from, and to appreciate some of the difficulties and uncertainties that most novel research lines have to face.

2.1 CLASSICAL RESULTS

Inspired by several problems in biology, A. Winfree was the first in proposing a system of interacting non-identical, limit-cycle oscillators to model synchronization phenomena [71]. The minimal assumptions of his model were that oscillators had to be heterogeneous and self-sustained. Self-sustained means that each oscillator has a stable limit cycle with a constant amplitude (a circular trajectory in the phase-space which is attracting to surrounding trajectories), and oscillators are able to sustain their motion in absence of external forcing and return to their limit-cycle after a perturbation is applied (known as non-conservative systems), unlike systems of mechanical oscillators studied in many-body physics [5, 38, 179]. If the interactions between the oscillators are sufficiently weak (compared to their intrinsic frequencies), the oscillators are said to be weakly-coupled and then their dynamical state can be well described by a single variable, its phase in a circle. Our starting point here are phase-models, which can be simply understood as systems of oscillators that rotate in a circle, and we will focus in more detail in chapter 6 on how to connect systems of non-linear limit-cycle oscillators to one-dimensional phase-models. In his original model, Winfree proposed to use

$$\dot{\theta}_i = \omega_i + \left(\sum_{j=1}^{N} x(\theta_j) \right) Z(\theta_i) \; \forall \; i \in 1, \ldots, N, \tag{2.1}$$

where θ_i is the phase of the i-th oscillator at a given time, $\dot{\theta}_i$ its time derivative and ω_i its internal frequency. $x(\theta)$ and $Z(\theta)$ are the stimulus and sensitive functions mentioned by Kuramoto in its speech, which capture the interaction of neighboring oscillators and the dependence on the internal phase, respectively. Using some numerical simulations and analytical approximations, Winfree was able to show that the system displayed a phase-transition from disorder to order depending on the relation between the internal frequencies and the coupling [71], but the model appeared at that moment to be analytically intractable (a solution was later found by J. T. Ariaratman and S. H. Strogatz [76]).

In 1975, Y. Kuramoto proposed his celebrated model of sinusoidal coupling instead of using a product of two functions. In his original work, he derived his model from a system of non-linear limit-cycle oscillators, the Ginzburg-Landau equations [4] (as we will see in chapter 6), although his main interest was in solving the resulting dynamical system

$$\dot{\theta}_i = \omega_i + \frac{K}{N} \sum_{j=1}^{N} \sin(\theta_j - \theta_i), \; \forall \; i \in 1, \ldots, N, \tag{2.2}$$

where $K \geq 0$ is the coupling strength the natural frequencies ω_i are drawn from a probability distribution $g(\omega)$, which is assumed unimodal and symmetric about a mean ω_0, that can be set without loss of generality $\omega_0 = 0$, by going to a co-rotating frame at the speed given by the mean frequency, and shifting the phases by $\theta_i + \omega_0 t$. The sinusoidal coupling captures the simplest non-linear 2π-periodic function of the phase differences, and represents a force that tends to synchronize (by pushing or pulling) the oscillator speeds $\dot{\theta}_i$ if the phases are not exactly equal ($\theta_i = \theta_j$) or in complete anti-phase ($\theta_i = \theta_j + \pi$). A mean-field coupling (all-to-all) is considered, and the normalization of the size N is chosen to ensure a non-trivial behavior in the thermodynamic limit $N \to \infty$.

Kuramoto proposed to use a complex order parameter to measure the degree of phase-synchrony in the system, given by the centroid of the phases in the complex circle

$$r(t)e^{i\Psi(t)} = \frac{1}{N}\sum_{j=1}^{N} e^{i\theta_j(t)}, \tag{2.3}$$

where the modulus r measures the degree of synchrony between $r \approx 0$ (incoherence or complete splay) and $r = 1$ (complete synchronization) and $\Psi(t)$ the average phase of the system, as shown in Fig. 2.1.a). By setting the average phase $\Psi(t) = 0$ by an appropriate choice of the origin in the co-rotating frame, multiplying both sides of the order parameter by $e^{-i\theta_i}$, using Euler's formula $e^{ix} = \cos x + i \sin x$ and equating the imaginary parts of both sides, the coupling terms in Eq. (2.2) vanish and one can write the evolution for the phases depending only on the mean-field parameter r as

$$\dot{\theta}_i = \omega_i - Kr(t)\sin(\theta_i), \ \forall\ i \in 1, \ldots, N, \tag{2.4}$$

To find a solution, Kuramoto assumed that r was constant and looked for long-term solutions of his self-consistent system (note that the evolution of the phases depends on the mean-field r, which in turn depends on the value of the phases). The fixed points –the stationary states– of the system are obtained by setting $\dot{\theta}_i = 0$, finding that oscillators with sufficient small frequency $|\omega_i| < Kr$ will lock their frequency to the mean frequency, following

$$\omega_i = Kr\sin\theta_i, \tag{2.5}$$

with its phase locked at $\theta_i \leq \pi/2$. The oscillators with $|\omega_i| > Kr$ are not locked to the mean pace, instead they are drifting on the circle, with a time-varying frequency. In order to satisfy the assumption that r was constant, Kuramoto required the drifting oscillators to be distributed in a stationary manner in the whole circle, with a distribution

$$\rho(\theta, \omega) = \frac{C}{|\omega - Kr\sin\theta|}, \tag{2.6}$$

assuming that the density of oscillators is inversely proportional to the speed (oscillators would aggregate at slow paces and splay out at fast places). The normalization condition is just determined by the integral $\int_{-\pi}^{\pi} \rho(\theta,\omega)d\omega$, leading to

$$C = \frac{1}{2\pi}\sqrt{\omega^2 - (Kr)^2}. \tag{2.7}$$

Here comes a key step of the derivation, by invoking the self-consistent condition that the order parameter defined in Eq. (2.3) must be constant and equal to the sum of contributions of locked and drift oscillators $r = \langle e^{i\theta}\rangle_{lock} + \langle e^{i\theta}\rangle_{drift}$ where the angular brackets mean population averages. In the case of the locked oscillators, we have that

$$\langle e^{i\theta}\rangle_{lock} = \int_{-Kr}^{Kr} \cos\theta(\omega)g(\omega)d\omega + i\int_{-Kr}^{Kr} \sin\theta(\omega)g(\omega)d\omega. \tag{2.8}$$

Note that the phases θ have the explicit dependence on the frequency, as dictated by the fixed point relation of Eq. (2.5). The imaginary part of the integral in Eq. (2.8) vanishes because of the symmetry of $g(\omega)$ and the fact that $\sin()$ is an odd function. A direct change of variables from ω to θ leads to

$$\langle e^{i\theta}_{lock}\rangle = Kr\int_{-\frac{\pi}{2}}^{\frac{\pi}{2}} \cos^2\theta g(Kr\sin\theta)d\theta. \tag{2.9}$$

The contribution of the drifting oscillator also vanish, in this case because of the symmetry of $g(\omega) = g(-\omega)$ and $\rho(\theta+\pi,-\omega) = \rho(\theta+\omega)$. Under these considerations, the self-consistent condition reduces to

$$r = Kr\int_{-\frac{\pi}{2}}^{\frac{\pi}{2}} \cos^2\theta g(Kr\sin\theta)d\theta. \tag{2.10}$$

The trivial solution $r = 0$ is always a solution, and corresponds to the incoherent state with $\rho(\theta,\omega) = 1/(2\pi)$. Kuramoto showed that another branch of solutions (corresponding to partial synchrony of the locked oscillators) exists and bifurcates continuously from $r = 0$ at a critical value $K = K_c$, obtained by cancelling r in both sides of Eq. (2.10), letting $r \to 0^+$ and integrating. Then, Kuramoto had then arrived at his famous result,

$$K_c = \frac{2}{\pi g(0)}, \tag{2.11}$$

the exact formula for the onset of synchronization in the mean-field model of infinite size.

Kuramoto also found that the amplitude of the order parameter around the onset obeys a square-root scaling law (the usual scaling for a mean-field model [58]), and, for the case of a Lorentzian, or Cauchy distribution with

$$g(\omega) = \frac{\gamma}{\pi(\gamma^2+\omega^2)}, \tag{2.12}$$

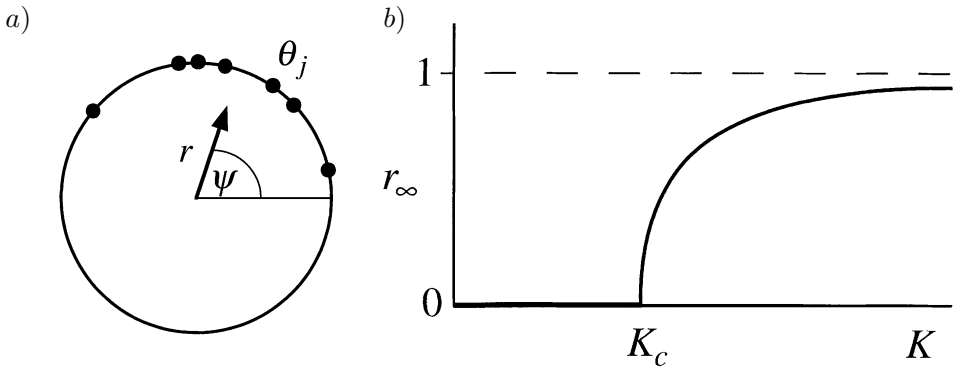

Figure 2.1: a) Order parameter proposed by Kuramoto. The modulus r measures the degree of synchrony and the phase Ψ indicates the average phase of the system (here it is displayed a system of only 7 oscillators). b) Synchronization curve given by the time-averaged modulus of the order parameter, depending on the coupling strength K, with $g(\omega)$ Lorentzian. A second order-phase transition emerges at the critical coupling K_c, where $r > 0$ and $r \to 1$ only when $K \to \infty$, due to the heterogeneity in the internal frequencies.

he could integrate exactly Eq. (2.10), leading to the remarkable result

$$r = \sqrt{1 - K_c/K}, \tag{2.13}$$

which was shown to match accurately numerical simulations [179]. Kuramoto had just solved his mean-field model of synchronization, which showed the emergence of a smooth, second-order phase transition at a critical strength K_c, as shown in Fig. 2.1.b).

In the next years, many important results on this mean-field model were obtained, including the solution of the local stability problem at the onset mentioned by Kuramoto in his speech. Strogatz and Mirollo managed to show that the incoherent solution was marginally stable before the transition and become unstable afterwards [179]). The model was also extended in many directions [5], including noise, delays or considering regular lattices of different dimensions, but here we are particularly interested in the complexity and irregularities of the interaction patterns. The first analytical results tackling the onset of synchronization in arbitrary complex networks beyond the all-to-all case or regular lattices were obtained at the beginning of the current century, and from now on, we will focus more on this modified KM, which goes beyond the original model by including the adjacency matrix A of the complex network into the description.

2.2 THRESHOLD APPROXIMATIONS IN NETWORKS

It was around 2005, in the agitated early times of the study of complex networks, when Ichinomiya [102] and Restrepo and colleagues [103, 104] found several approximations for the onset of synchronization in complex networks. Here, we will follow the work of [103] since the results of [102] also emerge from the same derivation.

The authors considered the KM of Eq. (2.2) but allowing for an arbitrary network of interactions. The KM in complex networks reads as

$$\dot{\theta}_i = \omega_i + \frac{K}{N}\sum_{j=1}^{N} a_{ij}\sin(\theta_j - \theta_i),\ \forall\ i \in 1,\dots,N, \tag{2.14}$$

where a_{ij} are the elements of the adjacency matrix that capture the presence and intensity of the connections. We allow the coupling matrix A to be non-symmetric and weighted, in general. A local order parameter is defined in a straightforward manner

$$r_i e^{i\Psi_i} = \sum_{j=1}^{N} a_{ij}\langle e^{i\theta_j}\rangle. \tag{2.15}$$

Then, the equations of motion can be uncoupled as

$$\dot{\theta}_i = \omega_i + Kr_i\sin(\Psi_i - \theta_i),\ \forall\ i \in N. \tag{2.16}$$

One impose equilibrium solutions by fixing $\dot{\theta}_i = 0$, i.e.

$$\sin(\Psi_i - \theta_i) = \frac{\omega_i}{Kr_i}. \tag{2.17}$$

Now we consider that only the locked oscillators (the ones that can satisfy Eq. (2.17)) contribute to the order parameter r_i, and crucially assume that the solutions (r_i, θ_i) are independent of the intrinsic frequency w_i (a strong assumption which turn out to be valid for dense enough networks). Then, we can write

$$r_i = \sum_{|\omega_j|\leq Kr_j} a_{ij}e^{i(\theta_j - \Psi_i)} = \sum_{|\omega_j|\leq Kr_j} a_{ij}e^{i(\theta_j - \Psi_j)}e^{i(\Psi_j - \Psi_i)}. \tag{2.18}$$

By taking only the real part of Eq. (2.18) and using Eq. (2.17), we obtain

$$r_i = \sum_{|\omega_j|\leq Kr_j} \cos(\Psi_j - \Psi_i)\sqrt{1 - (\frac{w_j}{Kr_j})^2}. \tag{2.19}$$

It can be argued that the smallest critical coupling is obtained when $\cos(\Psi_j - \Psi_i) = 1$. Eq. (2.19) can be solved numerically if the full vector of frequencies is known. Furthermore, if we assume again that the network is dense enough and if the frequencies are randomly allocated, then the frequencies of the neighbors $\{w_j\}$ can be approximated by the distribution $g(w)$. Using this idea, one obtains

$$r_i = K\sum_{j=1}^{N} a_{ij}r_j\int_{-1}^{1} g(xKr_j)\sqrt{1 - x^2}dx. \tag{2.20}$$

The critical point can be determined by letting $r_j \to 0^+$. At first order, $g(xKr_j) \simeq g(0)$, and we obtain

$$r_i^0 = \frac{K}{K_0} \sum_{j=1}^{N} a_{ij} r_j^0, \tag{2.21}$$

where $K_0 = 2/(\pi g(0))$ is the critical coupling derived for the all-to-all network, as obtained in the previous section. Eq. (2.21) is an eigenvalue equation (i.e. $Ar = \lambda r$). Since we are interested in finding the smallest K satisfying Eq. (2.21), thus the critical value can be determined by the largest eigenvalue λ_* of the adjacency matrix A, obtaining

$$K_c = \frac{K_0}{\lambda_*}. \tag{2.22}$$

For the all-to-all network, $\lambda_* = N - 1$, and Eq. (2.22) recovers the critical coupling derived by Kuramoto in his original work. Eq. (2.22) is known in [103] as the perturbative approximation of the threshold, but it has been also called the quenched approximation because it exploits information of the fixed structure, given by the largest eigenvalue of the adjacency matrix $\lambda_*(A)$. We remark that this result does not use the information on the frequency vector, equivalent to assuming a random allocation of frequencies in the nodes in a sufficiently large and dense network.

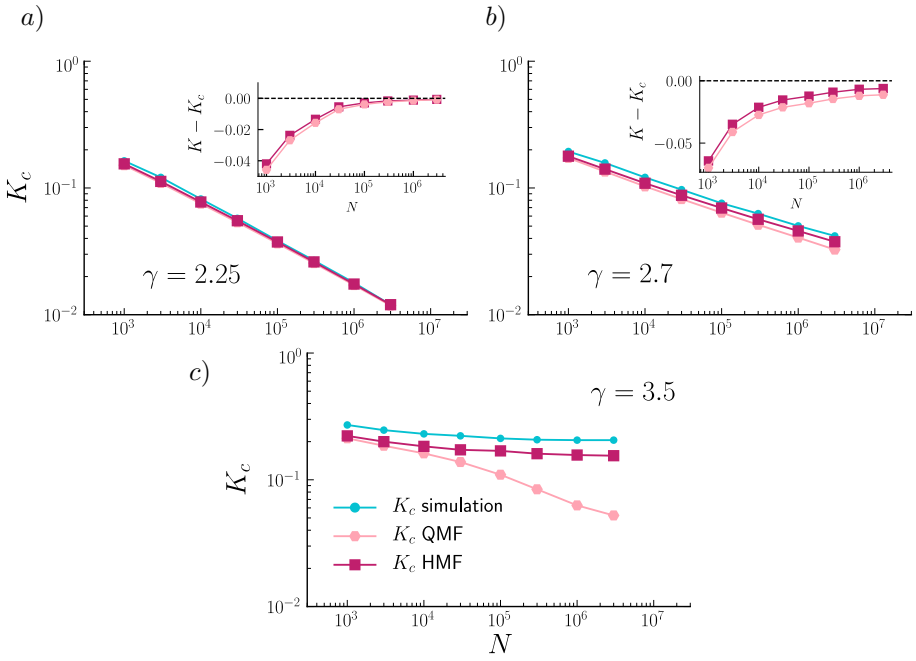

Figure 2.2: Numerical estimations of the critical threshold (blue) via direct integration of Eq. (2.14) and using susceptibility measurements, against the predictions of the QMF (light pink) and HMF (dark pink) approximations, for different exponents of a scale-free network, where it is confirmed that the critical threshold vanishes in the infinite size if the exponent is $\gamma \leq 3$, similarly to the epidemic onset in the SIS model [40]. Reprinted by permission of [180].

A further approximation of K_c can be obtained by using a mean-field approach in the derivation [102]. The main assumption here is to consider that the local order parameter r_i

is proportional to the global r, weighted by the incoming strength of the node (or simply the degree for unweighted networks), i.e.

$$r_i = s_i r, \tag{2.23}$$

where $s_i = \sum_{j=1}^{N} a_{ij}$ and $r = 1/N|\ \sum_j e^{i\theta_j}$. By inserting Eq. (2.23) into Eq. (2.21), and summing over all i, one directly obtains

$$K_c = K_0 \frac{\langle s \rangle}{\langle s^2 \rangle}, \tag{2.24}$$

where $\langle \cdot \rangle$ are the moments of the strength (or degree) distribution. We will call this approximation the Heterogeneous Mean-Field (HMF) because it exploits the information of the strength (or degree) sequence, which can be potentially heterogeneous, and to distinguish against the Quenched Mean-Field (QMF) introduced before. Also, worth to note, the HMF approximation has been recovered recently using another technique, a Gaussian ansatz for the phase distribution [7], and the validity of both approximations has been revisited by Peron et al. in [180], where it is shown (see Fig. 2.2 for details) that the HFM works slightly better than the QMF, specially for scale-free networks with large exponent (thus, towards homogeneous networks). Lastly, we note that Eq. (2.24) can be further extended to the case of directed networks [103], where one has to distinguish between input and output strengths, i.e. $s_i^{in} = \sum_j a_{ij}$ and $s_i^{out} = \sum_i a_{ij}$. The ansatz in this case is simply given by

$$r_i = s_i^{in} r. \tag{2.25}$$

By inserting again Eq. (2.25) into Eq. (2.21), summing over all nodes and taking into account the asymmetry of the network, one obtains

$$K_c = K_0 \frac{\langle s^{in} \rangle}{\langle s^{in} s^{out} \rangle}. \tag{2.26}$$

In this thesis, we will use some of the aforementioned results. In particular, in section 3.2 of the following chapter, when relating the structural constraints posed by the network and the critical range of synchronization onsets in the presence of noisy weights in the network, and in section 3.4, to motivate and justify our extended mean-field approach to tackle the mapping problem between different networks via weight-tuning schemes.

2.3 SYNCHRONY ALIGNMENT FRAMEWORK

An important problem in network synchronization is optimization, i.e. how should one arrange the structure and frequencies such that the degree of phase synchrony is maximized? A relevant result in this thesis is the work of Skardal et al. in 2014 [118], which triggered a series of further works [79, 129, 130, 165], on the study of optimal synchronization in

the strongly-synchronized regime using the so-called Synchrony Alignment Framework. In this approach, one considers a quite general system for the oscillator dynamics

$$\dot{\theta}_i = \omega_i + \sigma \sum_{j=1}^{N} a_{ij} H(\theta_j - \theta_i) \; \forall \; i \in 1, \ldots, N, \tag{2.27}$$

where $H(\theta_j - \theta_i)$ is an arbitrary 2π-periodic non-linear coupling function of the state differences of pairs of connected oscillators. While the particular choice of $H(\theta)$ depends on the application at hand, notable choices $H(\theta) = \sin(\theta)$ and $H(\theta) = \sin(\theta - \alpha)$, where $\alpha \in [-\pi/2, \pi/2]$, yield the network Kuramoto and Sakaguchi-KMs, respectively [118]. Invoking maximum synchronization, one is concerned with the strongly synchronized regime, where a phase-locked state becomes attainable (all the oscillators rotate at the same frequency and there are fixed phase differences between them). To reach this regime, we have to assume that $|H(0)| \ll 1$, so that for a strongly synchronized state where $|\theta_j - \theta_i|$ we have that $H(\theta_j - \theta_i) \approx H(0) + H'(0)(\theta_j - \theta_i)$ [118]. We note here that for the classical KM we have $H(0) = 0$ and $H'(0) = 1$. Now, by defining the effective frequency $\hat{\omega}_i = \omega_i + \sigma H(0) k_i^{in}$ and entering a suitable rotating frame, the synchronized state is then described by the fixed point satisfying $\dot{\theta} = 0$. After the linearization, the synchronized state then satisfies the following equation,

$$\hat{\omega} = \sigma H'(0) L \theta, \tag{2.28}$$

where $L = D - A$ is the Laplacian of the network, and D is a diagonal matrix with the in-degrees or in-strengths of the nodes, i.e. $D_{ii} = k_i = \sum_{j=1}^{N} a_{ij}$. Since the matrix L has zero row sum, it has a trivial eigenvalue $\lambda_1 = 0$ with a constant associated eigenvector $v_1 \propto 1$, and therefore it is singular and not invertible [118, 181]. Moreover, this spectral property reveals an important physical characteristic of the system, namely that the dynamics are invariant to a constant shift to the phases, i.e., translation along the synchronization manifold defined as the span of the trivial eigenvector v_1. Thus, while solutions to Eq. (2.28) are not unique, that which minimizes the norm $||\theta||$ is likely the most useful and is given by

$$\theta^* = \frac{L^\dagger \hat{\omega}}{\sigma H'(0)}, \tag{2.29}$$

where $L^\dagger$ is the Moore-Penrose pseudo-inverse of the Laplacian matrix [181]. Importantly, to write down the exact pseudo-inverse we require a full spectral decomposition of the Laplacian matrix (i.e., global information of the network) if the network is undirected. In the general case, i.e. for a possibly directed network, the pseudo-inverse can be computed via the singular value decomposition of L as

$$L^\dagger = \sum_{n=2}^{N} \frac{v_n u_n^T}{\mu_n}, \tag{2.30}$$

where $0 < \mu_2 \leq ... \leq \mu_N$ are the $N-1$ singular values of L and $\{v_n\}$ and $\{u_n\}$ are the set of right and left singular vectors. Note that for the particular case of undirected networks

the singular values are given by the eigenvalues of L and the left and right singular vectors are given by the eigenvectors of L, so $L^\dagger$ is defined by its eigenvalue decomposition.

Eq. (2.29) gives precisely the linearized synchronized state and therefore is critical to understand the interplay between structure and synchronization dynamics in tasks involving the fully synchronized state, and for this reason there is a myriad variety of phenomena and applications involving it [6, 44, 62, 118, 165]. In the context of optimization, one aims at minimizing the norm $||\theta||$, because this makes the degree of synchrony to increase. To see this, we linearize the order parameter in Eq. (2.3) to first order (valid for sufficiently small phases, as occurs here) and find that $r \sim 1 - ||\theta||^2$. In order to minimize the norm of the phases, and according to Eq. (2.30), the frequency vector should be aligned with the eigenvector associated with the largest eigenvalue (or singular value) of L. Alignments of ω with different eigenvectors of L are shown in Fig. 2.3.a), where it is observed that the maximum synchronization (for any value of the coupling K) is obtained by the alignment with the eigenvector v_{1000} associated here to the largest eigenvalue in a scale-free network of $N = 1000$ nodes. This optimal alignment can be also approximately reached by starting with a random configuration and performing a process of links rewiring such that the optimal alignment increases, as shown in Fig. 2.3.b), where the initial network is random with a Gaussian distribution of frequencies, also randomly allocated. After the rewiring, the network evolves towards a configuration with non-trivial microscopic correlations between the structure and the dynamics, as observed in Fig. 2.3.c), where nodes with larger positive (blue) or negative (red) frequencies accumulate more links, and the connections are usually between nodes with large frequency differences. Importantly, these correlations could be only studied a posteriori, from the outcome of numerical optimizations of the spectral black box.

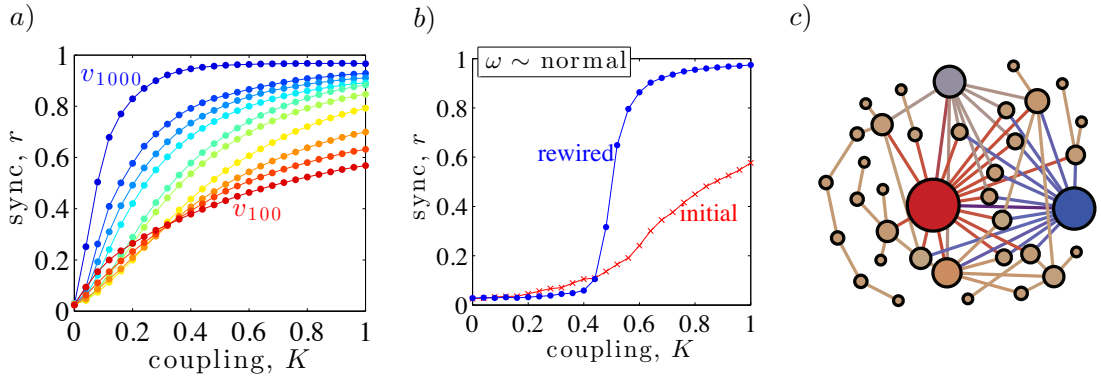

Figure 2.3: a) Synchronization curves $r(K)$ for different allocations of ω (different alignments with the eigenvectors of L) in a scale-free network with $N = 1000$, minimum degree $k_{min} = 2$ and exponent $\gamma = 3$. b) Synchronization curves for the initial and rewired (near-optimal) configurations of links, in a random network with Gaussian frequencies. c) Visualization of a toy network of $N = 40$ after the link rewiring to maximize the optimal alignment. Color-coding represents the frequency of the node (ranging from blue to red) and the size is proportional to the degree. Reprinted by permission of [118].

In this thesis, we will use this framework in several places. In section 3.3 of the following chapter, we will extend this formalism to study optimal synchronization in networks with

both pair-wise and higher-order interactions, finding the benefits of higher-order interactions in both optimizing synchronization and maximizing the range of synchronized states in a fixed structure. Furthermore, in chapter 4, we will see how this spectral optimization can be decomposed in small pieces of information ranging from local terms to more global neighborhoods of the nodes, which turns out to be a very suitable technique when dealing with decentralized optimization procedures (where the global information contained in the spectra is not available). A particular example of this decentralized approach is the model of a self-organized synchronization bomb, which we introduce in chapter 5.

Before closing this section, it is worthy to mention that the Synchrony Alignment Framework, given by the interplay between the Moore-Penrose Laplacian pseudo-inverse object and the frequency vector in Eq. (2.29) emerges in many other problems beyond the optimization of phase synchrony [44, 133, 159, 182]. A particularly interesting example is the result of Dörfler et al. [44], where a critical condition for the loss of global phase-locking in the KM in a complex network is given by $||L^{\dagger}\omega||_{\epsilon,\infty} < 1$ where the sub-index indicates that the condition is given by the maximum difference in the entries of the $L^{\dagger}\omega$ vector among connected nodes (where $a_{ij} = 1$). In this sense, this spectral object provides another prediction of the synchronization onset, here meaning the lower value of the coupling strength K that sustains a state of global phase-locking (frequency synchronization) in the network.

2.4 MODEL REDUCTION TECHNIQUES

The goal of model reduction techniques is to reduce the dimensionality of a system of network-coupled oscillators, from the large (or infinite) set of coupled equations to a system of one or few variables, which becomes much more tractable, both analytically and numerically. In the following, we consider two of these techniques (the ones that we use in our work), but it is important to remark that there are a few more available for different purposes [7]. In particular, here we introduce the Ott-Antonsen (OA) model reduction [122], based on the OA ansatz, which is an exact reduction valid for globally coupled oscillators in the infinite size, and also a model reduction for finite size systems, based on a collective coordinates (CC) ansatz and studied both in the globally coupled case by Gottwald [145] in 2015 and in the complex network case later by Hancock and Gottwald [146] in 2018. In this thesis, we will apply both techniques in chapter 5, in order to analytically predict the transition points in our model of a synchronization bomb. It is important to remark that, beyond its practical usage in many specific problems, this kind of model reductions of coupled oscillators are next-generation techniques, which allow understanding the dynamics of a high-dimensional and non-linear system by studying the behavior of a few macroscopic variables, sometimes in an exact manner, without having to rely on heuristics or strong approximations [7]. However, the complex network case poses more difficulties than the globally-coupled one, and we still lack a reduction approach that captures the rich repertoire of behaviors emerging from the oscillator dynamics and the complex structure [7, 146].

2.4.1 *Ott-Antonsen ansatz*

The Ott-Antonsen ansatz is the particular form that the authors guessed for the coefficients in a specific a Fourier expansion, as we will see, but the whole method is now known as the Ott-Antonsen model reduction [7]. This method applies to the mean-field limit (globally-coupled oscillators in the infinite size) of several models of coupled phase oscillators. The KM is our problem of interest, although it is important to remark that this technique can be extended to variations of the original model and to more realistic descriptions of neuronal dynamics [7].

In the following, we will restrict to the KM with a single population, thus being equivalent to the system studied by Kuramoto in his original work. In the thermodynamic limit, a distribution for the phases $\rho(\theta, \omega, t)$ can be defined, and due to the conservation of the number of oscillators, this distribution has to satisfy the transport equation[2]

$$\frac{\partial \rho}{\partial t} + \frac{\partial}{\partial \theta}(\dot{\theta}\rho) = 0, \tag{2.31}$$

where $\dot{\theta}$ is the velocity dictated by the KM, which can be written as

$$\dot{\theta} = \omega + Im[KZ(t)e^{-i\theta}], \tag{2.32}$$

where $Im[x]$ is the imaginary part (corresponding to the sinusoidal term), i is the imaginary unit and Z(t) is the standard Kuramoto order parameter. Eq. (2.32) can be easily rewritten as

$$\dot{\theta} = \omega + \frac{K}{2i}[Ze^{-i\theta} + Z^* e^{i\theta}], \tag{2.33}$$

with Z^* the complex conjugate. In this continuous description, the order parameter $Z(t)$ is given by

$$Z(t) = \int_{-\infty}^{\infty} \int_{-\pi}^{\pi} \rho(\theta, \omega, t) e^{i\theta} d\theta d\omega. \tag{2.34}$$

Thanks to the periodicity of the phases, the density function $\rho(\theta, \omega, t)$ can be expanded in a Fourier series in the variable θ, in the form

$$\rho(\theta, \omega, t) = \frac{g(\omega)}{2\pi} \sum_{n=-\infty}^{\infty} \alpha_n(\omega, t) e^{in\theta}, \tag{2.35}$$

with $\alpha_0 = 1$, and $\alpha_{-n} = \alpha_n^*$. In this form, the order parameter given by Eq. (2.34) reads as

$$Z(t) = \int_{-\infty}^{\infty} \int_{-\pi}^{\pi} \frac{g(\omega)}{2\pi} \sum_{n=-\infty}^{\infty} \alpha_n(\omega, t) e^{i(n+1)\theta} d\theta d\omega. \tag{2.36}$$

Here, it is important to note that $e^{i(n+1)\theta}$ is an odd function, meaning that the integral from $(-\pi, \pi)$ will vanish for all n except $n = -1$, when the exponential becomes one and

2 Note that the transport equation in Eq. (2.31) just ensures that the number of oscillators is fixed, in the same way as in an incompressible fluid the mass density is conserved.

the integral over the phases is simply $\int_{-\pi}^{\pi} d\theta = 2\pi$. Therefore, the order parameter only depends on the coefficient $\alpha_{-1} = \alpha_1^*$ as

$$Z(t) = \int_{-\infty}^{\infty} \alpha_1^*(\omega, t) g(\omega) d\omega. \tag{2.37}$$

On the other hand, by plugging the expressions for the density function, Eq. (2.35) and the velocity, Eq. (2.33), into the continuity equation, Eq. (2.31) and taking the derivatives, it is straightforward to show that each coefficient $\alpha_n(\omega, t)$ in the expansion evolves following the differential equation

$$\dot{\alpha}_n = -in\omega\alpha_n + \frac{K}{2}(n\alpha_{n-1}Z^* - n\alpha_{n+1}Z) \;\forall\; n = -\infty, \ldots, \infty. \tag{2.38}$$

We still have to deal with an infinite system of coupled differential equations. The miracle of the Ott-Antonsen ansatz (OA) is to assume a special form for the coefficients. In particular, the OA ansatz guesses that the coefficients are just powers of the first coefficient $\alpha_1(\omega, t)$, i.e.

$$\alpha_n(\omega, t) = \alpha_1(\omega, t)^n. \tag{2.39}$$

Using this ansatz in Eq. (2.38), one rapidly sees that the equations for all n become identical, collapsing into a single differential equation for the first coefficient as

$$\dot{\alpha}_1 = -i\omega\alpha_1 + \frac{K}{2}(Z^* - \alpha_1^2 Z), \tag{2.40}$$

where Z is given by Eq. (2.37). To proceed further, it is important to note that the integral in Eq. (2.37) can be analytically studied with the residue theorem of complex analysis if $\alpha(\omega, t)$ satisfies some conditions [7, 122]. In particular, let us consider a Lorentzian distribution $g(\omega)$ with mean ω_0 and width γ, given by

$$g(\omega) = \frac{\gamma}{\pi} \frac{1}{(\omega - \omega_0)^2 + \gamma^2}, \tag{2.41}$$

which has two poles in the complex plane at $\omega = \omega_0 \pm i\gamma$. In this case, the order parameter can be directly written as

$$Z(t) = \frac{\gamma}{\pi} \int_{-\infty}^{\infty} \frac{\alpha_1^*(\omega, t)/(\omega - \omega_0 - i\gamma)}{\omega - \omega_0 + i\gamma} d\omega. \tag{2.42}$$

By Cauchy's integral formula, we know that if a complex integral can be written as a contour integral in a path Γ enclosing a pole, then the integral is given by

$$\oint_\Gamma \frac{f(z)}{z - z_0} = 2\pi i f(z_0), \tag{2.43}$$

where z_0 is the pole. From Eq. (2.42), we identify $z_0 = \omega_0 + i\gamma$ and $f(z) = \alpha_1^*(\omega, t)/(\omega - \omega_0 - i\gamma)$, therefore, the order parameter is given by $Z(t) = \alpha_*(\omega_0 - i\gamma, t)$. Finally, by plugging this last result into Eq. (2.40) and using $\omega = \omega_0 - i\gamma$, one arrives at

$$\dot{Z} = (-\gamma + i\omega_0)Z + \frac{K}{2}Z(1 - |Z|^2), \tag{2.44}$$

where $|Z|$ is the modulus of the complex order parameter Z. Remarkably, we end up with a two-dimensional system (since Z is complex-valued), which is quite surprising considering that we started with an infinitely-coupled one. Now, by writing the order parameter in polar coordinates $Z = re^{i\Psi}$, and separating real and imaginary parts, one obtains a two-dimensional system

$$\dot{r} = \left(-\Delta + \frac{K}{2} - \frac{K}{2}r^2\right) r \tag{2.45}$$

$$\dot{\Psi} = \omega_0. \tag{2.46}$$

Since the equation for the mean phase Ψ is completely uncoupled ($\Psi(t) = \omega_0 t + C$), we only need to solve the first equation. By doing a straightforward calculation of the fixed points, we find that $r = 0$ is stable for $K < K_c = 2\gamma$ and loses the stability where the solution $r = \sqrt{1 - K_c/K}$ becomes stable, recovering the exact same solution obtained by Kuramoto in his original derivation.

2.4.2 *Collective-Coordinates ansatz*

The OA technique is very powerful, but it is usually valid in the thermodynamic limit of globally coupled populations of oscillators. In the following, we introduce another technique, based on collective coordinates, that is suitable for finite size systems and allows introducing the complex network into the description. Let us focus on the scenario of a single synchronizing cluster in a complex network, introduced in [146], which generalizes the results of [145] for the all-to-all case. Interestingly, in [146], the technique is extended to several synchronizing clusters, but we will restrict to the single cluster because it is the scenario that we will face when solving the synchronization bomb, in chapter 5.

The key idea of the CC method is to consider that in the phase-locking, synchronized regime, the phases of the oscillators can be described with the ansatz

$$\theta_i(t) = \alpha(t)\frac{N}{K}L^\dagger\omega, \tag{2.47}$$

assuming that the phase of the i-th oscillator (which is synchronized to the cluster) is proportional to the phase in the linearized regime. As we have seen in section 2.3, the solution in the linearized regime is given by the product of the pseudo-inverse Laplacian and the frequency vector, i.e. $L^\dagger\omega$, thus, it is reasonable to assume that for a sufficiently large coupling K, the dynamics of the fully non-linear KM in a complex network, given by Eq. (2.14) will approach its linearized limit. The variable $\alpha(t)$ is the collective coordinate,

and it is the scaling that controls how far the non-linear solution of the phases departs from the linearized version. The goal of this approach is to write the coupled system of N equations as a single equation for the evolution of the collective coordinate $\alpha(t)$.

The first step is to insert the ansatz given by Eq. (2.47) into Eq. (2.14), obtaining the error made by the ansatz in the full dynamics as

$$\epsilon_i = \dot{\alpha}\Phi_i - \omega_i - \frac{K}{N}\sum_j a_{ij}\sin(\alpha(\Phi_j - \Phi_i), \tag{2.48}$$

where we have defined the vector $\Phi = (N/K)L^{\dagger}\omega$. One wants to minimize the error ϵ, which is achieved by imposing that the error has to be orthogonal to Φ, i.e. $\sum_i \epsilon_i\Phi_i = 0$. Imposing this constraint, one obtains an equation for the evolution of the collective coordinate as

$$\dot{\alpha} = \frac{K}{N}\frac{\Phi^T L\Phi}{\Phi^T\Phi} + \frac{K}{N\Phi^T L\Phi}\sum_i\sum_j \Phi_i a_{ij}\sin(\alpha(\Phi_j - \Phi_i). \tag{2.49}$$

After an appropriate rescaling of time, one ends up with

$$\dot{\alpha} = 1 + \frac{1}{\Phi^T L\Phi}\sum_i\sum_j \Phi_i a_{ij}\sin(\alpha(\Phi_j - \Phi_i). \tag{2.50}$$

Remarkably, this is a single differential equation on α. The equilibrium solution can be found implicitly by setting $\dot{\alpha} = 0$ and finding $\alpha(K)$, and then the phases can be obtained by substituting this solution into Eq. (2.47). In [146], numerical simulations confirm the validity of the ansatz for the dynamics of the KM in the phase-locking regime, where all the oscillators rotate at the same frequency and are phase-locked to their neighbors. In this sense, this ansatz also extends the validity of the SAF results in previous section 2.3 to the non-linear regime.

The CC method can be heuristically extended to find the value of the phases for the oscillators that are synchronized even if the system is not in the phase-locking regime. This occurs when K is lowered, and some oscillators desynchronize from the cluster, while the rest remain synchronized. If K is further lowered below the critical threshold, all the oscillators break synchrony and the incoherent state is recovered. In the partially synchronized state, thus between the incoherent and full phase-locking regimes, the ansatz in Eq. (2.47) still applies, but only to the largest subset of nodes C_m that can synchronize. In order to find this subset of nodes, in [146] the authors propose a dynamical criterion based on linearizing the dynamics of the KM around an equilibrium solution α^*, and finding numerically the spectra of the Jacobian matrix (the matrix of derivatives evaluated at the equilibrium point). The set of nodes to be excluded from the synchronized cluster (where the ansatz still applies) is selected from the largest components of the eigenvector associated with the positive eigenvalues, because positive eigenvalues of the Jacobian matrix indicate unstable modes of the dynamics.

We will use the Jacobian matrix to determine the stability of the non-linear system in section 5.3.2, in order to find the critical point of our synchronization bomb. For more details

on the method used to extend the collective coordinates ansatz to the partially synchronized state, we refer the reader to [146], but it is important to note that this method becomes computationally prohibitive as one approaches the critical coupling strength, where many small subsets of nodes compete to become the giant synchronized cluster. In this sense, this ansatz requires using numerical methods which can be as costly as simulating the full dynamics around the critical point, and does not provide a reduction in terms of order parameters where bifurcations can be studied, as occurs with the OA method. Nevertheless, this CC technique becomes very useful to unveil the interplay between the microscopic dynamics and the complex structure in the phase-locking regime [146].

Having introduced the CC method, we close the chapter dedicated to expose several techniques that we found appropriate for our problems of interest. It is time to move to the chapters where we actually apply them in novel problems.

3

ON STRUCTURAL CONSTRAINTS AND DYNAMICAL RANGE

3.1 INTRODUCTION

The range of collective dynamical behaviors that a complex, interconnected system can show is clearly bounded by the specific network of interactions between its microscopic constituents. Paradigmatic examples include biological [15, 21, 22, 31, 63, 183, 184] and artificial neuronal circuits [24, 25, 37]. In the brain, the networked architecture of neurons and synapses [15, 184], coupled with the adaptation mechanism of synaptic plasticity [21, 22], constrain the number of functional patterns and associated tasks that can be achieved [31, 63, 183]. In artificial neural models, ranging from the classical three-layer perceptron [24], to the Hopfield model for memory storage [37] and state-of-art predictive algorithms such as deep neural networks [25], the topology of the network is a leading factor affecting the processing, storing and learning capacities of the system. In complex ecological systems like food-webs, the structure of predator-pray interactions between species controls the stability of an equilibrium state against external perturbations or intrinsic fluctuations [43, 87]. Furthermore, in infrastructure networks, the spatial distribution and capacity of the existing transmission lines and roads determine the operational range of stable power-grids [44, 133, 166] and the potential effects of congestion in traffic flows [185–187].

The previous examples illustrate a ubiquitous feature in most complex systems, i.e. the structure critically constrains the dynamical range, and they serve also to highlight a common feature that is present across problems in the different mentioned fields. In many realistic circumstances, biological, ecological and engineered systems need to change or adapt their configurations to achieve a target dynamical response, but this process is usually limited by the constraints posed by the underlying structure, such as a fixed number of specific connections that are inevitably present or absent. It is therefore natural to wonder to which extent a system of interacting units on top of a fixed structure can display a range of macroscopic dynamical behaviors. In other words, what are the accessible dynamical states that can be reached from a given set of structural constraints? These types of questions play a central role in the theory of statistical mechanics, which, in its most elegant derivation [32], gives the less-biased statistical, macroscopic description of a physical system when subject to constraints on the accessible configurations. This framework has proven tremendously useful in classical [29] and quantum mechanics [188], condensed matter and biophysics [189, 190] and in pioneer works studying disordered systems [34–

36], and the foundations of complex network models [90, 95, 171]. However, the technical requirements of the theory rapidly become very challenging or even unfeasible as we increase the complexity in the dynamics or in the structural patterns of the model at hand. Nevertheless, the important and, perhaps, counterintuitive idea that introducing uncertainty and probabilistic arguments on the microscopic –kinetic– description can enhance the comprehension of macroscopic properties is persistent in the successful modeling of many network dynamics [57, 58, 99, 191].

In this chapter, we leverage the concept of uncertainty to unveil the relation between structural constraints and dynamical range within the framework of the Kuramoto model. We focus on three specific problems: In section 3.2 we study how small uncertainty or noise in the weights of the interactions (noisy links) affect the location and range of the critical threshold at which we predict the standard phase-transition from incoherence to partial synchrony. Using error propagation techniques in a mean-field approximation of the threshold, we derive analytical results for the critical range depending on the underlying connectivity patterns, unveiling interesting noise-amplyfing properties of the network. Results of this section are based on the published work [192]:

- "Uncertainty propagation in complex networks: From noisy links to critical properties", L. Arola-Fernández, G. Mosquera-Doñate, B. Steinegger and A. Arenas, Chaos **2** 023129 (2020).

In section 3.3, we move from the critical regime to the strongly phase-locking state, and study the dynamical range of synchrony in the presence of different interaction mechanisms, balancing between pair-wise and higher-order interactions in a fixed structure. By imposing explicit uncertainty on the frequencies and analyzing the spectral properties of the Laplacian, we reveal how higher-order interactions can improve optimal synchrony and also increase the dynamical range without altering the structure. Results of this section are based on the published work [79]:

- "Higher-order interactions can better optimize network synchronization", P. S. Skardal, L. Arola-Fernández, D. Taylor and A. Arenas, PRR **3** 043193 (2021).

In section 3.4, we focus on a generalization of previous set-ups, by considering the problem of predicting the dynamical range within different synchronization regimes (i.e. from the critical threshold to the linear regime). By using information-theoretic optimization tools and an extended mean-field approach, we derive weight-tuning schemes that illustrate the fact that a fixed network can map a wide range of behaviors, but this mapping is limited by local structural constraints. Results of this section are based on the published work [162]:

- "Synchronization invariance under network structural transformations", L. Arola-Fernández, A. Díaz-Guilera and A. Arenas, Phys. Rev. E **97**, 060301(R) (2018).

Finally, in section 3.5 we give a summary of the main findings presented in the chapter and explain the limitations and unsolved issues of the proposed approaches, paving the way for new analysis to come. Highlighting the *continuist spirit* of the thesis, in chapter 4, we will introduce the geometric unfolding of the synchronized state, a technique that turns out very useful to tackle the problems we discuss here and many more to come.

3.2 UNCERTAINTY PROPAGATION: FROM NOISY LINKS TO CRITICAL PROPERTIES

3.2.1 *A measurement problem*

We begin our journey on the study of structural constraints and dynamical range by focusing on the critical regime of the system. The critical point (or threshold) refers to the minimum value of a tuning parameter that triggers a phase transition in a dynamical process [5, 58]. In the context of networks of coupled oscillators, the critical threshold refers to the precise value of the interaction strength at which the system transits from incoherence to partially coherent dynamics. This point is known as the synchronization onset and its prediction is of upmost importance to control and analyze oscillatory dynamics like the brain or power-grids [6]. We have seen in section 2.2 that the available approximations are obtained in terms of the spectral or degree properties of the network, and interestingly, they are equivalent to the results found for other dynamical processes, including percolation [2, 143] epidemic spreading [40, 193–195] and spin dynamics [58], which highlight the universal properties of phase-transitions of dynamical processes on networks.

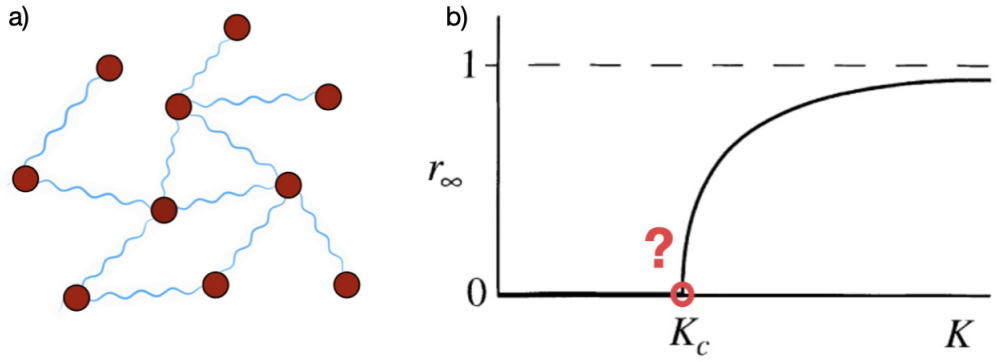

Figure 3.1: a) Illustrative sketch of a network with noisy links, with small quenched disorder, represented by curved links propagate to the value of the global coupling strength that predicts the onset of synchronization, b). This propagation of uncertainty in a fixed structure induces a distribution of critical onsets, which serves as a proxy of the dynamical range of the network in the critical regime.

Beyond the realm of theoretical models, empirical data is never free of errors and the measurement of interaction strengths, or links' weights of real networks is not an exception. The increasing data collected from empirical settings present experimental errors, induced for example by device accuracy, sampling biases, or mistakes in data entry [196, 197]. Interestingly, the literature on network science usually dismisses these error sources, and produces results that are only valid if data is error free, without providing any confidence intervals (error-bars) on the estimation of macroscopic properties. Some authors have concentrated their attention on inference of missing data in networks [96, 170, 196–198] and to incorporate the effect of external fluctuations or noise in the modeling side [5, 6, 159, 160, 165]. However, to the best of our knowledge, less attention has been paid to the propagation of uncertainty from the structure to the properties of dynamical processes running on

top of it. The reasons behind the lack of works devoted to the analysis of error propagation from structural to dynamical properties may be that many studies considered, for the sake of simplicity, networks to be unweighted, where a link is a binary variable denoting its existence or not [2]. However, the vast majority of empirical networks are weighted, i.e. the existence or not is valued by its intensity [199]. In practice, the accurate determination of the weight is unlikely, and therefore, the error in their numerical values will influence any particular measurement of the network properties. Moreover, the weights of the links may fluctuate intrinsically [22, 41] and usually these variations in the weights occur at faster scales than changes of links [2, 22, 31]. These scenarios highlight the importance of studying a fixed structure of links affected by small noise in their weights.

In this section, we present a study of error propagation in networks where fixed links are subject to uncertainty in their weights, and we wonder about the effect that this uncertainty, amplified by the complex network, will have in the determination of the critical threshold. We consider synchronization to illustrate the effects, but our results find validity for a wider class of processes where the threshold is determined by the inverse of the largest eigenvalue of the adjacency matrix. Motivated by an inaccurate measurement problem, our findings here will attempt to answer the question raised on the relation between structural constraints and dynamical range, at least in the interesting critical regime of the system.

3.2.2 *A mean-field trick*

We start by considering the classical Kuramoto model on top of a complex network [5, 6, 62]. For the sake of clarity, we recall here that the dynamics of the system are described by the following set of coupled differential equations

$$\dot{\theta}_i = \omega_i + K \sum_{j=1}^{N} w_{ij} a_{ij} \sin(\theta_j - \theta_i), \ \forall \ i \in 1, \ldots, N, \tag{3.1}$$

where we have introduced small quenched noise in the weights of the links, given here by the entries w_{ij}. For the sake of simplicity, we assume Gaussian and uncorrelated noise, meaning that each weight is independently drawn from a normal distribution $\mathcal{N}(\mu, \sigma^2)$, being $\mu > 0$ the average weight and σ^2 its variance. Nevertheless, the proposed analysis can be extended to other distributions of noise, either theoretical or obtained through empirical measurements, if the covariance matrix of the noise is known (we refer the reader to the method presented below for more details on the covariance matrix of the noise). Importantly, our restriction $\mu > 0$ implies that we are not considering a model with disorder in the classical sense [73, 158], where negative fluctuations can induce frustration and the standard transition may disappear.

The degree of phase synchrony in the system is captured, as will be common praxis during the course of this thesis, by the modulus of the complex order parameter $r(t) = (1/N) \left| \sum_{j=1}^{N} e^{i\theta_j(t)} \right|$ which gives a value of $r \approx 0$ in the incoherent regime (with fluctuations of order $N^{-1/2}$) and $r \approx 1$ in the fully-synchronized regime. The synchronization onset is given by the critical value of the coupling strength K_c at which the order parameter

transits from zero to some $r > 0$ [5, 6, 62]. In section 2.2 we saw that for a unimodal and symmetric distribution $g(\omega)$ and a sufficiently well-connected network with only positive interactions, one expects to observe the standard second-order transition from incoherence to partial synchrony [6, 62]. After neglecting small time-fluctuations and assuming a random allocation of the frequencies (i.e. without strong dynamical correlations) the critical threshold K_c is well approximated by the inverse of the largest eigenvalue λ_{max} of the network connectivity matrix C whose values represent the weighted structure of the network and in our case have entries $c_{ij} = w_{ij}a_{ij}$, i.e.

$$K_c \approx \frac{K_0}{\lambda_{max}(C)}, \tag{3.2}$$

where K_c is a constant that depends on the specific details of the process. In the classical Kuramoto, $K_0 = 2/(\pi g(0))$, i.e. the critical coupling of the all-to-all network [5, 38]. Without loss of generality, we fix $K_0 = 1$ here because Eq. (3.2) acts as our starting point in the problem and a constant scaling will not alter our results. The main goal of this section is to understand, by analytical means, how small noise in the entries of the matrix C affects the statistical properties of the macroscopic threshold in the context of the Kuramoto model, but the ubiquity of Eq. (3.2) allows our findings to be extended to the other dynamical processes [2, 40, 99, 194].

In order to study the exact statistics of K_c in Eq. (3.2) induced by the presence of noise, one should take into account the powerful machinery of Random Matrix Theory [84, 85] and Spectral Graph Theory [67, 68]. However, we rapidly found that it becomes very challenging to study noisy sparse networks with arbitrary degree distributions in these frameworks. We proposed a shortcut, a *mean-field trick* to analytically approximate the value of K_c and then apply well established error propagation techniques to the approximated expression of K_c. This chain of approximations will obviously restrict the validity range of the analysis, however, the results are found to be very accurate in some scenarios and, more importantly, they provide clear analytical insight on how the uncertainty in the structure affects the determination of the critical threshold. In other words, we honestly compromise the expected range of validity of our results to gain analytical insights and a better understanding of the phenomenology at hand, i.e. the prediction of the critical range in our system. The proposed trick is based on the weighted mean-field approximation of Eq. (3.2), which, under the conditions of small noise and undirected (symmetric) interactions, reads as [103, 180, 200, 201]

$$K_c \approx \frac{\langle s \rangle}{\langle s^2 \rangle}, \tag{3.3}$$

where $\langle s^n \rangle$ is the n-moment of the strength distribution (the strength of a node is the sum of incoming weights). As we have seen in the theoretical background section 2.2, Eq. (3.3) can also be obtained directly from the equations of motion of the dynamical process by assuming that the local field in a node is proportional to the global field weighted by the in-strength of the node [102], (i.e. $r_i \sim s_i r$). For the remaining of the section, we will refer to Eq. (3.3) as the Mean-Field approximation (MFA).

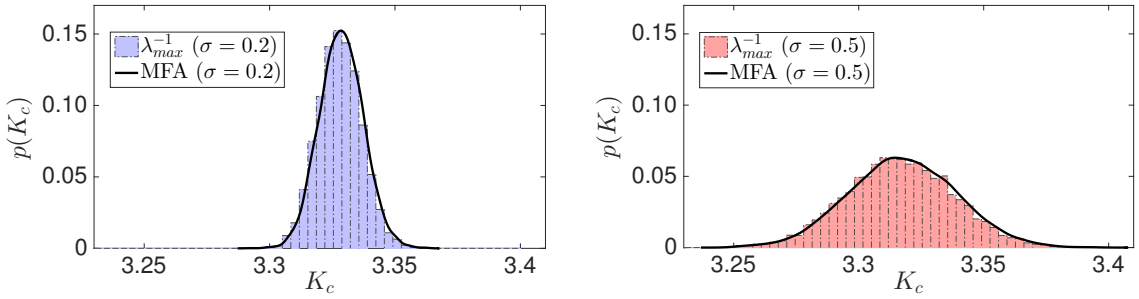

Figure 3.2: Empirical distribution of the critical point K_c governed by the exact Eq. (3.2) (boxes) and MFA Eq. (3.3) (solid lines) in an Erdös-Rényi, random network with $N = 200$, $p = 0.3$, $K_0 = 1$, $\mu = 1$ for two different noise intensities ($\sigma = 0.2$ gray and $\sigma = 0.5$ red). The distribution corresponds to 10^4 independent realizations of the noise. Reprinted by permission of [192].

Before going into the details of our method, we test the accuracy of the critical threshold in the MFA, Eq. (3.3), by comparing it to Eq. (3.2), in Erdös-Rényi, random networks with explicit uncertainty in the positive weights. In Fig. 3.2 we plot the threshold distribution for two different values of the intensity of the uncertainty σ. We observe that the MFA accurately determines the distribution, and we also can see that the values of the expected critical threshold K_c and its variance are clearly dependent on σ. In general, we expect our results to be accurate in the cases in which the approximation of Eq. (3.3) remains valid, and we refer the reader to the references [103, 201] where the range of validity of the mean-field approach is discussed. We would like to remark that in our current mean-field approach, we are only using the information contained on the strength (or degree) distribution, assuming that the networks are drawn from a random configuration model [2]. This means that we are neglecting by assumption the effects of clustering, modularity and other non-trivial interaction patterns in the networks and focusing on the non-trivial role of degree heterogeneity.

3.2.3 *Error propagation in the critical threshold: Main results*

Let us introduce our error propagation method. First, we compute the mean value of the critical threshold in the presence of small noise in the weights of the links under the MFA. To do so, we write the degrees and strengths in terms of the binary connections ($a_{ij} = 0$ or 1) and weights ($w_{ij} \in R$) of the connectivity matrix C, i.e. $k_i = \sum_{j=1}^{N} a_{ij}$ and $s_i = \sum_{j=1}^{N} a_{ij} w_{ij}$. For the average strength $\langle s \rangle$, we have

$$\langle s \rangle = \frac{1}{N} \sum_{i=1}^{N} (\sum_{j=1}^{N} a_{ij} w_{ij}). \tag{3.4}$$

Note that we can write Eq. (3.4) equivalently as $\langle s \rangle = (1/N) \sum_i \mu_i k_i$, where μ_i is the average weight of node i. For a sufficiently large degree ($k_i \gg 1$), one can approximate $\mu_i = \mu$, and therefore $\langle s \rangle = \mu \langle k \rangle$. However, in general, it is important to keep the contribution of each

node because each μ_i has a specific uncertainty depending on the degree of node i, and this affects the overall uncertainty on K_c. For the second moment $\langle s^2 \rangle$, we have

$$\begin{aligned} \langle s^2 \rangle &= \frac{1}{N} \sum_{i=1}^{N} (\sum_{j=1}^{N} a_{ij} w_{ij})^2 \\ &= \frac{1}{N} \sum_{i=1}^{N} (\sum_{j=1}^{N} a_{ij} w_{ij}^2 + \sum_{j \neq k}^{N} a_{ij} a_{ik} w_{ij} w_{ik}). \end{aligned} \tag{3.5}$$

We note that $\sum_{j \neq k} a_{ij} a_{ik} = k_i^2 - k_i$, to get

$$\langle s^2 \rangle = \frac{1}{N} [\sum_{i=1}^{N} \mu_i^2 (k_i^2 - k_i) + \sum_{i=1}^{N} \langle w^2 \rangle_i k_i], \tag{3.6}$$

where $\langle w^2 \rangle_i$ is the average second moment of the i-node. Plugging Eq. (3.4) and Eq. (3.6) into the critical approximation of Eq. (3.3), one obtains

$$K_c \approx \frac{\sum_{i=1}^{N} \mu_i k_i}{\sum_{i=1}^{N} \mu_i^2 (k_i^2 - k_i) + \sum_{i=1}^{N} \langle w^2 \rangle_i k_i}, \tag{3.7}$$

where μ_i is the average weight of a node i, and $\langle w^2 \rangle_i$ the average second moment of the weight distribution for node i. Note that there are $2N$ random variables (two for each node) and interestingly, for sufficiently large degree ($k_i \gg 1$), we can approximate $\mu_i = \mu$, and $\langle w^2 \rangle_i = \sigma^2 + \mu^2$ in Eq. (3.7). This approximation allows writing down a simple relation between the mean of the critical threshold and the uncertainty of the network as

$$\langle K_c \rangle \approx \frac{\mu \langle k \rangle}{\mu^2 \langle k^2 \rangle + \sigma^2 \langle k \rangle}. \tag{3.8}$$

The simple approximation of Eq. (3.8) already tell us that the critical threshold decreases as the noise intensity σ increases. This can be understood because the noise in the weights is another source that can increase the structural heterogeneity of the network, and heterogeneity tends to make the critical threshold to vanish [6, 40, 193]. Note that for $\mu = 1$ and $\sigma = 0$, we recover the usual threshold for unweighted, undirected networks [201], given by $K_c = \langle k \rangle / \langle k^2 \rangle$.

Having computed the expected mean of the threshold, $\langle K_c \rangle$, we proceed now to estimate confidence intervals (i.e. error bars) for the uncertainty of K_c, that is the standard deviation named here δK_c (or the variance $(\delta K_c)^2$). For this purpose, we use a well-known method of experimental physics, the error propagation [202] technique, that quantifies how the error in the microscopic variables of a system (the $2N$ random variables in our nodal description) propagate through a macroscopic quantity (the critical threshold K_c). The propagation of uncertainty of a non-linear function of the random variables as Eq. (3.3) requires using a truncated Taylor expansion [202]. Up to second-order, the approximate variance of the function is given by

$$(\delta K_c)^2 \approx J_0^T V J_0 + \frac{1}{2} Tr[(H_0 V)^2], \tag{3.9}$$

where $J_0 \in R^{2N}$ is the Jacobian vector evaluated at the mean values of the random variables $\vec{\mu}$ and $\langle \vec{w^2} \rangle$, $V \in R^{2N \times 2N}$ is the covariance matrix, which depends on the full connectivity matrix C and H_0 is the Hessian (squared) matrix, which entries evaluated again at the mean values of the random variables $\vec{\mu}$ and $\langle \vec{w^2} \rangle$.

The Jacobian of the system in Eq. (3.7) is given by

$$J = (\frac{\partial K_c}{\partial \mu_1}, ..., \frac{\partial K_c}{\partial \mu_N}, \frac{\partial K_c}{\partial \langle w^2 \rangle_1}, ..., \frac{\partial K_c}{\partial \langle w^2 \rangle_N}). \tag{3.10}$$

First, we compute the partial derivatives in Eq. (3.10) explicitly from Eq. (3.7), obtaining

$$\begin{aligned} \frac{\partial K_c}{\partial \mu_i} &\approx \frac{1}{N} \frac{k_i(\mu^2 \langle k^2 \rangle + \sigma^2 \langle k \rangle) - 2\mu^2 (k_i^2 - k_i)\langle k \rangle}{(\mu^2 \langle k^2 \rangle + \sigma^2 \langle k \rangle)^2}, \\ \frac{\partial K_c}{\partial \langle w^2 \rangle_i} &\approx -\frac{1}{N} \frac{k_i \mu \langle k \rangle}{(\mu^2 \langle k^2 \rangle + \sigma^2 \langle k \rangle)^2}, \end{aligned} \tag{3.11}$$

where the sign $\approx$ stands for assuming, in good approximation, that the input parameters μ and σ^2 are the actual mean values of the random variables $\vec{\mu}$ and $\vec{\sigma^2} = \langle \vec{w^2} \rangle - \vec{\mu}^2$.

The Hessian matrix, the square matrix of the second-order partial derivatives of the function in Eq. (3.7) can be directly obtained by taking derivates from Eq. (3.11). After some algebra, and defining $Q = \mu^2 \langle k^2 \rangle + \sigma^2 \langle k \rangle$, we obtain

$$\begin{aligned} \frac{\partial^2 K_c}{\partial \mu_i \partial \mu_j} \approx & \frac{1}{N^2 Q^3} [Q(2\mu(k_j^2 - k_j)k_i - (2 + 2\delta_{ij}\mu(k_i^2 - k_i)k_j)) \\ & - (k_i - 8\mu^3 \langle k \rangle (k_i^2 - k_i)(k_j^2 - k_j)). \end{aligned} \tag{3.12}$$

The Hessian matrix of our system is symmetric, such that $\partial^2 K_c / \partial \mu_i \partial \langle w^2 \rangle_j = \partial^2 K_c / \partial \langle w^2 \rangle_i \partial \mu_j$. We obtain

$$\frac{\partial^2 K_c}{\partial \mu_i \partial \langle w^2 \rangle_j} \approx \frac{1}{N^2 Q^3} [-Q k_i k_j + 4\mu^2 \langle k \rangle k_j (k_i^2 - k_i)], \tag{3.13}$$

and for the last term we have

$$\frac{\partial K_c}{\partial \langle w^2 \rangle_i \partial \langle w^2 \rangle_j} \approx \frac{2\mu k_i k_j \langle k \rangle}{N^2 Q^3}. \tag{3.14}$$

For the covariance matrix, we can obtain explicit expression for the entries V_{ij} when the noise in the weights is assumed Gaussian and uncorrelated. By assumption, the network is symmetric and so it will be the covariance matrix, which can be written in block form as

$$V = \left(\begin{array}{c|c} v_{\mu}{}^2 & v_{\mu, \langle w^2 \rangle} \\ \hline v_{\mu, \langle w^2 \rangle} & v_{\langle w^2 \rangle}{}^2 \end{array} \right),$$

where ${v_\mu}^2$, $v_{\mu,\langle w^2\rangle}$ and ${v_{\langle w^2\rangle}}^2$ are symmetric matrices in $\mathcal{R}^{N\times N}$ that capture each covariance term between the two random variables $(\mu_i, \langle w^2\rangle_i)$ of all nodes. Explicitly,

$$({v_\mu}^2)_{ij} = \frac{\sigma^2}{k_i}(\delta_{ij} + \frac{a_{ij}}{k_j}), \tag{3.15}$$

$$(v_{\mu,\langle w^2\rangle})_{ij} = \frac{2\mu\sigma^2}{k_i}(\delta_{ij} + \frac{a_{ij}}{k_j}), \tag{3.16}$$

$$({v_{\langle w^2\rangle}}^2)_{ij} = \frac{2\sigma^2(2\mu^2+\sigma^2)}{k_i}(\delta_{ij} + \frac{a_{ij}}{k_j}). \tag{3.17}$$

The first term in the sums is the contribution of the diagonal entries. The Gaussian variances (σ^2 and $2\sigma^2(2\mu^2+\sigma^2)$) and covariance ($2\mu\sigma^2$) of a single weight w_{ij} drawn from (μ,σ^2) are divided by the number of elements (the degree k_i) involved in computing the averages μ_i and $\langle w^2\rangle_i$. The second term accounts for the non-diagonal entries. If two nodes (i,j) are neighbors ($a_{ij}=1$), then we have to add another correlation due to the presence of the shared weight, which is divided by the product of their degrees (k_i and k_j).

Let us now consider only the first order expansion (neglecting the Hessian term in Eq. (3.9)). Then, we can compute explicitly $(\delta K_c)^2$ in terms of the noise parameters (μ,σ) and the moments of the degree distribution. Then, we can write Eq. (3.9) as

$$\begin{aligned}(\delta K_c)^2 \approx \sum_{i=1}^{N}\sum_{j=1}^{N}[(\frac{\partial K_c}{\partial \mu_i})(\frac{\partial K_c}{\partial \mu_j})({v_\mu}^2)_{ij},\\ +(\frac{\partial K_c}{\partial \langle w^2\rangle_i})(\frac{\partial K_c}{\partial \langle w^2\rangle_j})({v_{\langle w^2\rangle}}^2)_{ij} + 2(\frac{\partial K_c}{\partial \mu_i})(\frac{\partial K_c}{\partial \langle w^2\rangle_j})(v_{\mu,\langle w^2\rangle})_{ij}],\end{aligned} \tag{3.18}$$

and after some algebra, we obtain

$$\begin{aligned}(\delta K_c)^2 \approx \frac{2\sigma^2\langle k\rangle}{NQ^4}[Q^2 - 4\mu^2\langle k^2\rangle Q + 2\mu^2(2\mu^2+\sigma^2)\langle k\rangle^2\\ +2\mu^4(\langle k\rangle\langle k^3\rangle + \langle k^2\rangle(\langle k^2\rangle - 4\langle k\rangle) + 2\langle k\rangle^2) + 8\mu^4\langle k\rangle(\langle k^2\rangle - \langle k\rangle)],\end{aligned} \tag{3.19}$$

where we have used that $\sum_i\sum_j a_{ij}k_ik_j = N\langle k^2\rangle^2/\langle k\rangle$. Simplifying further, we get

$$(\delta K_c)^2 \approx a[\mu^4(2\langle k\rangle\langle k^3\rangle\langle k^2\rangle^2) - 2\mu^2\sigma^2(\langle k\rangle\langle k^2\rangle - \langle k\rangle^2) + \sigma^4\langle k\rangle^2], \tag{3.20}$$

with $a = 2\sigma^2\langle k\rangle/[N(\mu^2\langle k^2\rangle + \sigma^2\langle k\rangle)^4]$.

Eq. (3.20) shows that, beyond the non-linear dependence on the network and noise parameters, the uncertainty in the threshold is a finite-size effect, and decays with $N^{-1/2}$. To compare networks of different sizes, we will scale the threshold by the size N in the current analysis. In Fig. 3.3.a), we show the accuracy of the derived analytical expressions for an Erdös-Rényi network, confirming the validity of the approach, at least for small noise and homogeneous and random structures.

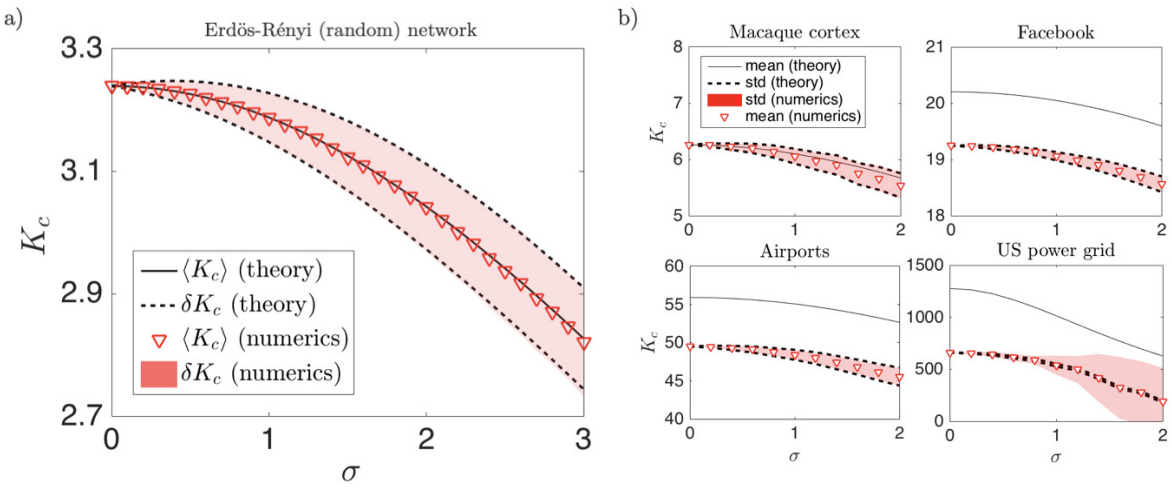

Figure 3.3: Numerics (Eq. (3.2)) vs theory (Eq. (3.7) and Eq. (3.20)): mean and standard deviation of the threshold K_c depending on the noise intensity σ for a) a single, fixed Erdös-Rényi network with $N = 200$, $p = 0.3$, $\mu = 1$, and 5000 independent realizations for each value of the noise intensity σ. For this random network, analytical results show a good agreement with numerical simulations. In b) we show the results applied to four empirical networks with different size, density and patterns of interactions, namely the brain network of the Macaque cortex ($N = 242$, $\langle k \rangle \approx 33$), the Facebook network of the trinity college ($N = 2613$, $\langle k \rangle \approx 85$), the Airport network ($N = 3154$, $\langle k \rangle \approx 12$) and the US power-grid network ($N = 4914$, $\langle k \rangle \approx 2$). Network data is obtained from the online repository *www.network-repository.com*, except for the Airports network (see below for more details). Panel a) is reprinted by permission of [192].

Before discussing in more details the accuracy of our estimation in the empirical networks shown in Fig. 3.3.b), we remark here that, in terms solely of the error propagation technique, the linear approximation used in Eq. (3.9) is valid as far as [202]

$$J_0^T V J_0 \gg \frac{1}{2} Tr[(H_0 V)^2]. \tag{3.21}$$

Both terms in Eq. (3.21) depend implicitly on the value of the noise, so the scaling of each term with σ will determine the range of validity of Eq. (3.20). We numerically examine the goodness of both the linear, Eq. (3.20) and the second-order approximation for the uncertainty δK_c of Eq. (3.9) against the numerical results obtained for the Erdös-Rényi network analyzed before, and also for a real world network with large size and heterogeneous connectivity patterns (the worldwide air transportation network). This empirical air transportation network was constructed using data from the website openflights.org, which has information about the traffic between airports updated to 2012, data available from [41]. This network accounts for the largest connected component, with 3154 nodes and 18,592 edges.

From Fig. 3.4, one can extract several important facts. First, the figure shows that the first and second order solutions are practically indistinguishable for small noise, therefore validating the result in Eq. (3.20) in this regime. Second, the significative difference in the magnitude of the fluctuations for both networks occurs for the difference in size N

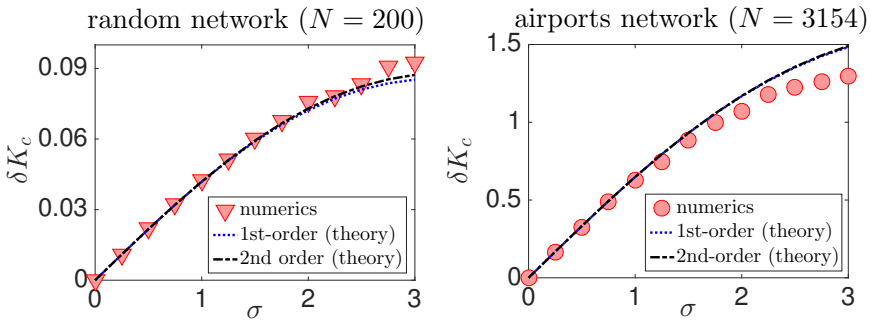

Figure 3.4: Numerics vs theory: standard deviation of the critical threshold δK_c depending on the noise intensity σ with $\mu = 1$ for a (left) fixed Erdös-Rényi network ($N = 200$, $\langle k \rangle = 60$, $p = 0.3$) and (right) the empirical network of airports ($N = 3154$, $\langle k \rangle \approx 12$) for 2000 independent realizations for each value of the noise. Results have been rescaled by N. Reprinted with permission from [192].

and density L/N^2. The mean value of the threshold is highly affected by the density [58], decreasing with the mean degree, and the same occurs for the fluctuations, as predicted by Eq. (3.20). Third, the deviation of the theory from the actual values in some empirical networks (right plots in both Fig. 3.3 and Fig. 3.4) points towards another direction: the goodness of the MFA itself. Basically, the theory is expected to be accurate for networks that deviate from a random structure as long as the MFA in Eq. (3.3) holds. As mentioned before, it is not our main goal here to convey an exhaustive verification of the theory for particular networks. Interestingly, as observed in the right plots in both Fig. 3.3 and Fig. 3.4, for the particular example of the airports network (and also the Facebook network), even if the mean value of the threshold is not well predicted by the mean-field approach, its dependence with noise is still well captured by the theory, and more importantly, the precise value of the fluctuations remains accurate for sufficiently small noise.

Moreover, it is important to remark that even if the MFA holds, the method of error propagation (at any order) can only be applied in our problem when the mean of the signal μ is sufficiently large compared to the noise. For $\sigma \gg \mu$, many negative weights appear and, the eigenvalues of the adjacency matrix become strongly correlated random variables and the statistics of K_c cannot be estimated using approaches based on normality assumptions [67, 203] as the one we are using here. Furthermore, the usual transition from incoherence to partial synchrony may disappear in the presence of many negative interactions, due to frustration effects that can hinder the appearance of a giant synchronized cluster [204], and therefore our initial goal to infer the uncertainty in the synchronization onset losses its meaning. While being the scenario of large noise a definitely interesting venue of research (especially in the context of the brain, which presents a combination of excitatory and inhibitory interactions [205], and also in ecological networks, where negative interactions may capture a competitive relation between species [43]) here we restricted the analysis to systems dominated by the mean of the signal ($\mu > \sigma$), where mostly positive weights appear in the entries of the adjacency matrix.

3.2.4 *The role of network heterogeneity*

The mathematical machinery has been presented, and we are in a position to answer some questions raised in the introduction of this section regarding the dynamical range in the critical threshold, the so-called critical range. As one can see already from the highly non-linear dependencies in Eq. (3.20), the network structure will play an important role in the uncertainty range of K_c. Interestingly, the dependence of δK_c on the heterogeneity and density of the network leads to a rich phenomenology that is worth studying in more detail. The effect of density can be already observed in Fig. 3.3.b) and Fig. 3.4: basically, the denser the network, the smaller will be the fluctuations of the threshold. Regarding heterogeneity in the degree distribution, some interesting questions arise: does the heterogeneity induce an increase of the critical fluctuations with respect to a homogeneous network? Is the behavior of (δK_c) monotonous with the moments of the degree distribution of the network? If not, is there any particular structure that maximizes the uncertainty of the critical point induced by noise in the weights?

To answer these questions, we consider the regime where networks are sufficiently large and $\sigma \ll \mu$. Then, we can approximate Eq. (3.20) by its leading term, neglecting terms in σ larger than $\mathcal{O}(\sigma^2)$

$$(\delta K_c)^2 \approx 2\sigma^2 \frac{2\langle k\rangle\langle k^3\rangle - \langle k^2\rangle^2}{N\langle k\rangle^3}\langle K_c\rangle^4. \tag{3.22}$$

Note that Eq. (3.22) we can also be written as

$$(\delta K_c) \approx \sigma f(C)\langle K_c\rangle^2, \tag{3.23}$$

where $f(C) = \sqrt{\frac{2\langle k\rangle\langle k^3\rangle - \langle k^2\rangle^2}{N\langle k\rangle^3}}$ encapsulates the structural dependence on the critical range. Quite surprisingly, one can note that δK_c increases linearly with the noise intensity and scales with $\langle K_c\rangle^2$. We know that $\langle K_c\rangle^2$ is reduced by the heterogeneity of the degree distribution [6, 40, 193], and therefore one would expect δK_c to follow the same trend. However, the nonlinear dependence on the moments of the degree distribution is counterintuitive. In particular, due to the correcting structural factor $f(C)$, some networks may show the contrary effect, meaning that even if the mean value of the critical threshold is smaller, the uncertainty in δK_c can be still be larger. To understand this effect, we choose first a homogeneous (regular) network as a reference, where $k_i = k, \forall\ i$. We can compute K_c and δK_c for a regular network in a straightforward manner from the previous results, obtaining

$$\langle K_c\rangle_{\text{reg}} \approx \frac{1}{\mu k},\ (\delta K_c)^2_{\text{reg}} \approx \frac{2\sigma^2}{N\mu^4 k^3}. \tag{3.24}$$

We propose to compare $(\delta K_c)^2$ with $(\delta K_c)^2_{\text{reg}}$ for networks with the same size and average degree, and for the same noise parameters μ and σ. After some straightforward algebra, the condition for a network to display higher uncertainty in K_c than a random regular one reads

$$\langle k^3\rangle > \frac{\langle k^2\rangle^2}{2\langle k\rangle}\left(1 + \frac{\langle k^2\rangle^2}{\langle k\rangle^4}\right). \tag{3.25}$$

Now, we can use the resulting Eq. (3.25) to evaluate the role of heterogeneity. In particular, let us consider a power-law distribution $p(k) \approx k^{-\gamma}$, where the exponent γ controls the tail of the distribution. For the value $\gamma = 3$, one recovers the well-know scale-free network that emerges from preferential attachment [55]. For lower (higher) values of γ, the network becomes more (less) heterogeneous. It is well understood that, for a finite power-law network, the moments of the degree distribution [2] are given by

$$\langle k^n \rangle = \frac{(-\gamma+1)(k_{\max}^{n-\gamma+1} - k_{\min}^{n-\gamma+1})}{(n-\gamma+1)(k_{\max}^{\gamma+1} - k_{\min}^{\gamma+1})}. \tag{3.26}$$

By fixing the value of $k_{\min}$, we can explore the space of networks with a given $(\gamma, k_{\max})$, thus revealing the effect of heterogeneity and size. To simplify the visualization, we define

$$q = \log\left[\frac{2\langle k\rangle\langle k^3\rangle}{\langle k^2\rangle^2\left(1+\frac{\langle k^2\rangle^2}{\langle k\rangle^4}\right)}\right]. \tag{3.27}$$

This way, when $q = 0$, the uncertainty of the critical threshold of a network will be the same as that of the regular one, and for positive (negative) values of q, we are measuring an increase (decrease) of δK with respect to the homogeneous network. In Fig. 3.5 we show the theoretical results obtained for the q value of networks in the space $(\gamma, k_{\max})$.

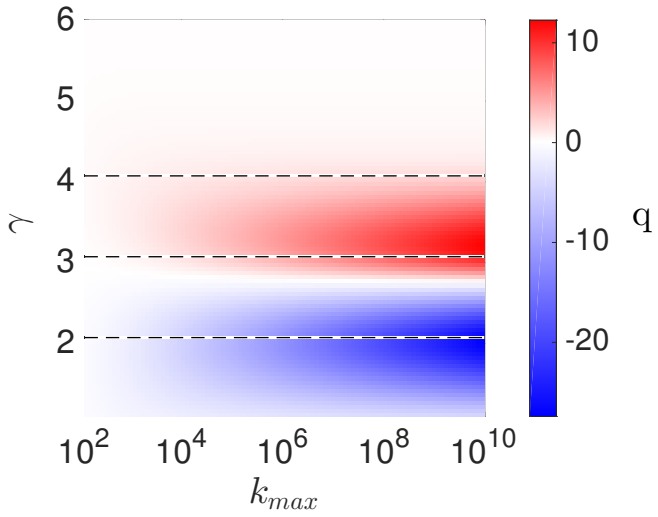

Figure 3.5: Colormap showing the theoretical dependence of q on the exponent γ and the maximum degree of the network $k_{\max}$. The value of $k_{\min}$ is fixed to $k_{\min} = 5$ and the resolution of the map is 100x100. White color represents equal fluctuations than a homogeneous network, while red (blue) colors capture higher (lower) fluctuations. Reprinted by permission of [192].

The reader should note that the three horizontal lines correspond to the cases where the network has an integer exponent of 2, 3 or 4. In there, the first, second or third moments diverge [2, 55]. It is also important to remark that, below $\gamma = 2$, it is not feasible to generate networks with a pure power-law distribution [2]. Besides that, we observe what we believe to be a very interesting result. As expected, for large values of the exponent γ,

the networks show similar uncertainty to that of a regular network (towards white color). However, for $\gamma < 4$, uncertainty significantly increases, reaching a maximum as the exponent approaches $\gamma = 3$, before decreasing again. In other words, when approaching the value of $\gamma = 3$, the network maximizes the third moment of the degree distribution (while minimizing its second moment), and therefore emerges as the optimal uncorrelated structure amplifying the uncertainty in the threshold. On the other hand, our theory estimates that uncertainty is minimal for maximally heterogeneous networks corresponding to an exponent $\gamma \approx 2$. Furthermore, the non-monotonous dependence on γ is amplified as we increase the size of the system (in terms of its maximum degree). In other words, the theory predicts the existence of a region of uncorrelated networks where the structures satisfy the condition in Eq. (3.25) and therefore show higher fluctuations than a regular network with the same average degree. This occurs for networks that are very heterogeneous in the degree distribution, but up to some extent. When approaching the famous value of $\gamma = 3$, the network is able to maximize the third moment while minimizing the second moment of the degree distribution (if the network has a finite size), and therefore emerges as the optimal uncorrelated structure to amplify the critical range (i.e. the uncertainty in the threshold).

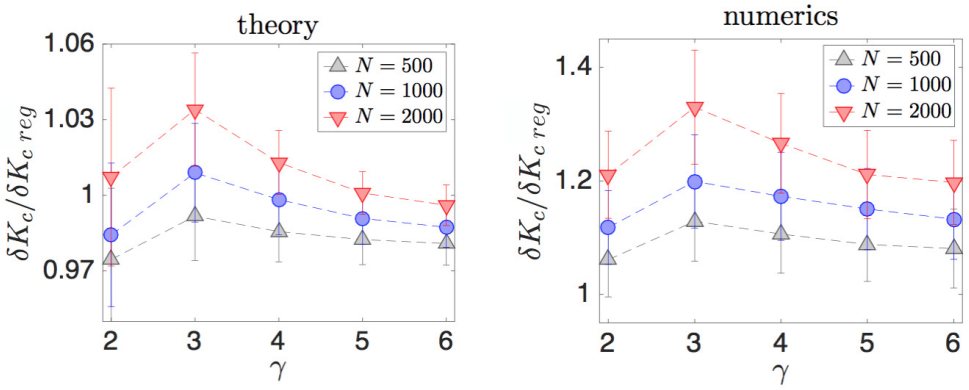

Figure 3.6: Relative value of the theoretical (left) and numerical (right) uncertainty δK_c for scale-free networks in the range $\gamma \in [2, 6]$ of sizes $N = 500$, 1000 and 2000, $\mu = 1$, $\sigma = 0.05$ and minimum degree fixed at $k_{\min} = 5$ compared to regular networks with the same average degree, and the same characteristics of the noise. The results are obtained with 200 realizations of the noise for each network and then averaging with 200 networks for each configuration of the modified preferential attachment algorithm. The high variance at each point shows that the results are very sensitive to the particular structure of the network, although the general trend is captured. Reprinted by permission of [192].

To validate the previous theoretical prediction, we generate synthetic power-law networks using the modified preferential attachment algorithm with an attractiveness parameter that control the exponent, introduced by Dorogovtsev in [91]. Fixing the value of the minimum degree $k_{\min}$, and tuning the exponent and the size of the network, we are able to detect a maximum in the uncertainty δK_c for the exponent $\gamma = 3$, as shown in Fig. 3.6, thus confirming the prediction of the theory. We observe good qualitative agreement for the non-monotonous dependency on the heterogeneity, and also that system size reinforces this dependency. We suspect that the slight mismatch, in the form of a shift, may

be originated by the fact that, for scale-free networks with $\gamma > 5/2$, the critical threshold is better approximated by $K_c \approx 1/\sqrt{k_{max}}$ than by the ratio of moments proposed in our approach [103, 193, 200, 201]. Furthermore, the small sizes that are considered in the numerical analysis produce significant degree correlations (not captured by the MFA) which may contribute to the mismatch. Despite these flaws, the mean-field approach captures well the dependence on the exponent and size of these networks.

Our results here point towards the difficulty to accurately determine the critical threshold of scale-free networks, with exponent $\gamma \approx 3$, since δK_c is maximized in the presence of noisy weights for these networks. Conversely, the scale-free network with exponent $\gamma \approx 3$ can be seen as the one that has a larger critical range due to noisy links in a fixed structure, and in this sense, it becomes the most versatile configuration in terms of maximizing the critical dynamical range when there are structural constraints on the presence (and absence) of links. We will give a summary and a more detailed discussion of these results in the conclusive section 3.5 of this chapter, connecting these findings with the results that are presented in the following lines. Before moving to the next problem, we introduce some more results using our error propagation method, here in a simple network, the star-graph.

3.2.5 *Exact results for the star graph*

In the star-graph, the exact statistics of the largest eigenvalue can be analytically computed using the error propagation technique, without requiring to use the *mean-field trick*. Importantly, the following results are not useful to predict the synchronization onset and its uncertainty (because in a star-graph, the values of the frequencies in the hub and the leaves strongly determines the location of the threshold [108]) but to show that the error propagation technique can be used to estimate the fluctuations in the global spectral properties from the microscopic, noisy variables of the network.

The star-graph is a simple network of only two type of nodes, the so-called hub and leaves, the hub being connected to all the leaves (we assume here that connections are symmetric) that has been used in the literature to illustrate the role of large hubs and to understand the properties of very heterogeneous networks as the scale-free ones [108]. For the sake of analytical consistency with previous shown results, we keep using the notation $K_c = 1/\lambda_{max}$ although we remark that in the star-graph, the statistics of the inverse of the largest eigenvalue do not necessarily translate into the statistics of the synchronization onset.

We consider noisy undirected weights in the star-graph as illustrated in Fig. 3.7.a) and we wonder how this microscopic noise propagates to the global uncertainty of the inverse of the largest eigenvalue K_c. For this simple and deterministic network, the exact expression for the largest eigenvalue (and therefore for its inverse K_c) is known [68] and it can be easily computed by induction starting from smaller sizes where diagonalization can

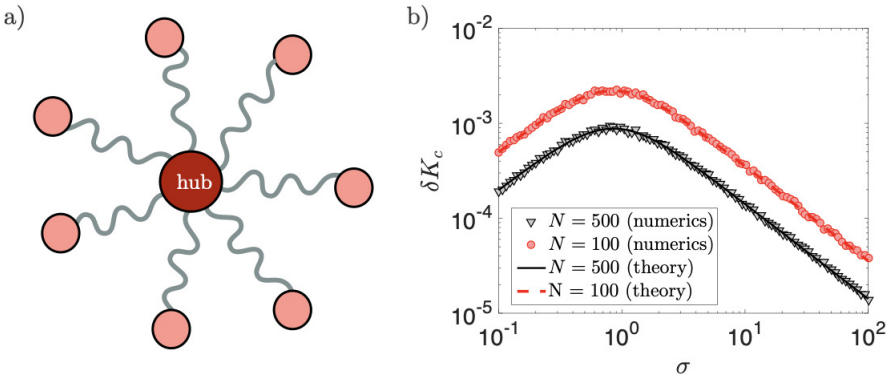

Figure 3.7: a) Illustrative sketch of a small star network with noisy weights, where the central node is referred to as the hub. b) Standard deviation of the inverse of the largest eigenvalue (named here K_c) depending on the noise intensity in a log-log plot for a star network with $\mu = 1$, and two network sizes. We observe a perfect agreement between numerical results and the theory and the non-monotonous behavior of δK_c for large noise.

be done by analytical means and then one can set N arbitrarily large. The inverse of the largest eigenvalue for the weighted, symmetric star is given by

$$K_c = \frac{1}{\sqrt{\sum_{l=1}^{N} w_{hl}^2}}, \tag{3.28}$$

where w_{hl} is the symmetric weight between the hub to the l-th leaf. Using the tools of 3.2.3, it is straightforward to obtain the mean and standard deviation of K_c up to first-order approximation. After some simple algebra, omitted here for the sake of clarity, one gets

$$\langle K_c \rangle \approx \frac{1}{\sqrt{(N-1)(\mu^2+\sigma^2)}}, \tag{3.29}$$

$$(\delta K_c)^2 \approx \frac{\sigma^2(2\mu^2+\sigma^2)}{2(N-1)^2(\mu^2+\sigma^2)^3}. \tag{3.30}$$

From Eq. (3.29), we can see that the dependence of the mean value of K_c is monotonous with size N and the intensity of noise σ, decreasing to zero as size or noise increases. Regarding the fluctuations δK_c, Eq. (3.30) tell us that the dependencies become highly non-linear. In Fig. 3.7.b), we plot the comparison between theory and numerics for δK_c, showing a perfect match. We observe a non-monotonous behavior of the spectral fluctuations with noise, which can be explained as a competition between two terms in Eq. (3.30). Fluctuations grow linearly with σ, $\delta K_c \sim \sigma$ for $\sigma \ll \mu$, and decays with σ^{-2} for $\sigma \gg \mu$. In between, a maximum appears for which a specific value of the noise maximizes the fluctuations of the threshold. For instance, when $\mu = 1$, the critical value of the noise in the star graph is independent of N and reduces to $\sigma = 1$, which corresponds to the peak in Fig. 3.7.b). These technical results proving the validity of error propagation on the spectra of a star graph conclude the section. It is time to dive into our second problem of the chapter.

3.3 SYNCHRONY OPTIMIZATION: FROM PAIR-WISE TO HIGHER-ORDER INTERACTIONS

3.3.1 *A balance problem*

We have seen the effect that uncertainty in the network weights has on the fluctuations of the synchronization onset. As we increase the coupling strength between the oscillator units well beyond this synchronization onset, more and more oscillators become entrained to a mean pace, entering the giant synchronization cluster until all of them rotate with the same effective frequency and the phase difference between the oscillators remains locked in time [6, 38, 62]. This dynamical regime is known as the phase-locking state, the so-called synchronized state, and it is one of the most paradigmatic examples of collective behavior emerging from local interactions among the microscopic constituents, which in our case are the heterogeneous phase oscillators.

The optimization of collective behaviors as the phase-locked, synchronized state is a key problem for predictive and control purposes in a variety of empirical network-coupled systems, ranging from brain dynamics, where strong phase synchronization is a recurrently observed state, to engineered systems like the power grid [44, 45, 133], where the critical condition for having spontaneous synchrony and stable phase-locked dynamics is directly controlled by the phase differences in the synchronized state [44]. In section 2.3 we saw that the optimization of strong synchrony in networked systems of heterogeneous oscillators coupled with standard, pair-wise interactions, is well understood in terms of the Synchrony Alignment Framework (SAF). As occurred in the prediction of the synchronization onset, the spectra of several network matrices show up as the key global properties that determine the dynamical behavior of the system, a result that persists among many dynamical processes on top of networks [2, 6, 57, 58].

Interestingly, recent works point toward the presence of higher-order (triadic, beyond pair-wise/dyadic) interactions in brain networks [138, 206, 207] and generic limit-cycle oscillator systems with phase and amplitude variables [77, 78]. The presence of these higher-order interactions can be encoded in mathematical objects that generalize the concept of networks to higher dimensions. These objects are known as simplicial complex or hypergraphs [139, 208, 209] and, in the recent years, many tools have been developed to characterize them and to understand the effect of higher-order interactions on the collective dynamics of networked systems [139]. In the realm of heterogeneous oscillators, the higher-order paradigm has led to the discovery of a variety of regimes such as multistability and abrupt desynchronization [125, 137, 140], and new forms of chaos [210], or explosive transitions [211] to name a few examples. Nevertheless, as also occurred in most of the seminal works on theoretical models of synchronization dealing with standard, pair-wise networks, the former studies have focused on the analysis of random configurations or globally coupled systems under the usage of global mean-field assumptions. Furthermore, the possibility to combine several interaction mechanisms (including both pair-wise and higher-order interactions) in the optimization problem has not been explored in the

past, neither the analysis of the accessible dynamical configurations that can be reached by a network structure by leveraging these different types of interactions. Considering the increasing evidence on the presence of both pair-wise and higher-order interactions in several empirical systems, it sounds relevant to study the relation between the structural constraints posed by a fixed network structure and the variety of collective regimes that can be reached by balancing both pair-wise and higher-order interactions.

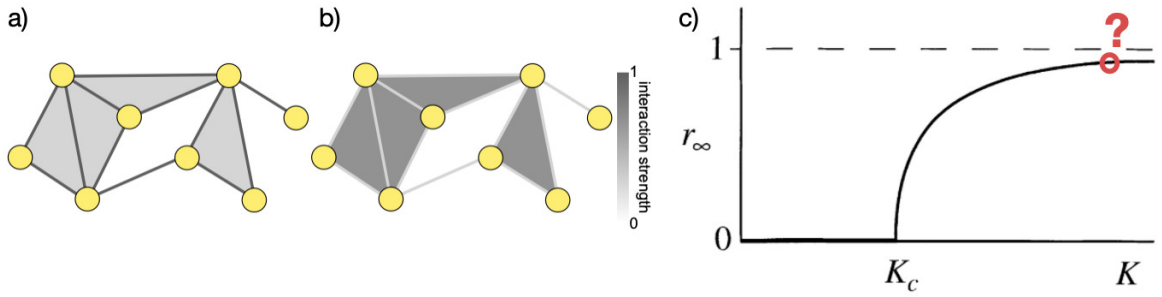

Figure 3.8: An illustration of a small network with a) 1-simplex (pair-wise) vs b) 2-simplex (higher-order) dominated coupling. Shading indicates the relative strength of each type. In c) we point at the synchronized regime of the system (far beyond the synchronization onset K_c),and the question mark illustrates the idea of studying the dynamical range of r when balancing the coupling strength between pair-wise and higher-order (triangles here) interactions. Reprinted by permission of [79].

In this section, we address this problem by introducing a composite Laplacian matrix that encodes the interactions at multiple orders in a weighted simplicial complex, and we generalize the SAF to account for these new type of interactions. The reader should note that, while the problem and settings here are quite different from results in the previous section, there is a natural continuation that relates the structural constraints (in terms of a fixed structure of links) and the range of accessible collective behaviors. Before, we studied how noisy weights affect the range of the synchronization onset, and now we will look at how different interaction mechanisms (interpolating pair-wise and higher-order ones) affect the range of the synchronized state. From noisy links to higher-order interactions, we keep attempting to prove that the dynamical range of an oscillator network can be explored within an approach based on network uncertainty.

3.3.2 *The composite Laplacian framework*

We begin by introducing the generalization of the Kuramoto model of coupled phase-oscillators [38] that includes higher-order (here three-body) interactions as described in [140]. The N heterogeneous oscillators with phases θ_i evolve following

$$\dot{\theta}_i = \omega_i \frac{K_1}{\langle k^{(1)} \rangle} \sum_{j=1}^{N} A_{ij} \sin\left(\theta_j - \theta_i\right) + \frac{K_2}{2\langle k^{(2)} \rangle} \sum_{j=1}^{N} \sum_{l=1}^{N} B_{ijl} \sin(2\theta_j - \theta_l - \theta_i), \tag{3.31}$$

where ω_i represents, as usual, the natural frequency of the i-th oscillator and K_1 and K_2 are coupling strengths that are associated with 1- and 2-simplex interactions, respectively

(namely pair-wise and three-body interactions). In this setting, A is the standard adjacency matrix, and B is a 2-simplex adjacency tensor. We assume the network to be unweighted and undirected so that the entries $a_{ij} = a_{ji} = 1$ if a link exists between oscillators i and j, and $b_{ijl} = b_{ilj} = b_{jil} = b_{jli} = b_{lij} = b_{lji} = 1$ if and only if a triadic interaction (a triangle) exists between oscillators i, j and l. An additional assumption here is that our system is a simplicial complex, meaning that the existence of a three-body interaction (i,j,l) requires the presence of dyadic connections (i,j), (j,l) and (l,i). In general, the 1- and 2-simplex coupling topologies may be uncorrelated for a general hypergraph [139]. Furthermore, we restrict our analysis to the so-called 'clique complexes' [212], where all triangles existing in the network give rise to 2-simplices. In this case, the 3-tensor B can be completely determined by the adjacency matrix as $B_{ijl} = A_{ij}A_{jl}A_{li}$.

The coupling strengths K_1 and K_2 in Eq. (3.31) are scaled by the 1- and 2-simplex mean degrees $\langle k^{(1)}\rangle$ and $\langle k^{(2)}\rangle$, which are just the pair-wise and three-way degree averages $k_i^{(1)} = \sum_{j=1}^{N} A_{ij}$ and $k_i^{(2)} = \frac{1}{2}\sum_{j=1}^{N}\sum_{l=1}^{N} B_{ijl}$. This scaling ensures that the overall connectivity is maintained when balancing, and the factor $1/2$ ensures that we are not counting triangles twice. In other words, we are conserving the sum $K = K_1 + K_2$, fixing the overall amount of coupling strength available in the network, regardless of the specific topologies encoded in A and B. In this context, we introduce a new *bias parameter* $\alpha \in [0,1]$, defined via $K_1 = (1-\alpha)K$ and $K_2 = \alpha K$, so that $\alpha \approx 0$ corresponds to a system where 1-simplex interactions are stronger (as displayed in the toy network of Fig. 3.8.a)) than 2-simplex interactions and vice-versa if $\alpha \approx 1$ (as displayed in Fig. 3.8.b)). The parameter α essentially controls the balance between both type of couplings. We also note that other higher-order interaction terms may exist in alternative formulations of a higher-order Kuramoto model [77, 78]. In this section, we will focus our attention on the particular configuration given by Eq. (3.31). As shown in [79], other type of higher-order interaction terms would yield similar results to the ones presented in the following.

Once we have introduced our dynamical model, we can shift our focus towards the optimization of phase synchrony. We consider the strongly synchronized regime where $|\theta_j - \theta_i| \ll 1$, allowing us to linearize Eq. (3.31) to

$$\begin{aligned}\dot{\theta}_i \approx \omega_i - K\Bigg[&(1-\alpha)\left(k_i^{(1)}\theta_i - \sum_{j=1}^{N} A_{ij}\theta_j\right)/\langle k^{(1)}\rangle \\ &+\alpha\left(k_i^{(2)}\theta_i - \sum_{j=1}^{N} A_{ij}\left(\sum_{l=1}^{N} A_{jl}A_{li}\right)\theta_j + \frac{1}{2}\sum_{j=1}^{N} A_{ji}\left(\sum_{l=1}^{N} A_{il}A_{lj}\right)\theta_j\right)/\langle k^{(2)}\rangle\Bigg],\end{aligned} \tag{3.32}$$

which in vector form can be written simply as,

$$\dot{\theta} = \omega - KL\theta, \tag{3.33}$$

where $L = (1-\alpha)L^{(1)} + \alpha L^{(2)}$ is a composite Laplacian, defined as a weighted average of the first and second-order Laplacian. In particular, $L^{(1)} = (D^{(1)} - A^{(1)})/\langle k^{(1)}\rangle$ and $L^{(2)} = (D^{(2)} - \left(A^{(2)} - A^{(2)T}/2\right))/\langle k^{(2)}\rangle$. The matrix $L^{(1)}$ is simply a scaled version of the typical

combinatorial Laplacian with $D^{(1)} = \text{diag}(k_1^{(1)}, \dots, k_N^{(1)})$ and $A^{(1)} = A$, while $L^{(2)}$ encodes the 2-simplex interactions with $D^{(2)} = \text{diag}(k_1^{(2)}, \dots, k_N^{(2)})$ and $A^{(2)} = A * (A^2)^T$, where $*$ represents the Hadamard (i.e., element-wise) product.

The reader should note that Eq. (3.33) already showed up in the context of the Synchrony Alignment Function introduced in section 2.3, where the optimization of strong synchrony in pair-wise, networks, takes the same form, but using the standard Laplacian matrix of the network, here $L^{(1)}$. We will not delve into the details of the SAF results here, just recall that the stationary solution of Eq. (3.33) is given by

$$\theta^* = \frac{L^\dagger \omega}{K}. \tag{3.34}$$

where $L^\dagger$ here is the Moore-Penrose pseudoinverse of the composite Laplacian, which can be constructed as usual from their eigenvalues and eigenvectors. For optimization purposes, where one wants to have as higher phase synchrony as possible (meaning that phases are very close to one another), the magnitude r of the Kuramoto order parameter $z = re^{i\psi} = N^{-1}\sum_{j=1}^{N} e^{i\theta_j}$ can be linearized to first order as $r \approx 1 - \|\theta^*\|^2/2N$. Key to our interest here, the usage of the composite Laplacian framework allows us to encapsulate the effect of both pair-wise and three-body interactions in a unique Laplacian matrix, and the dynamics of our system can be understood from the interplay between the spectra of this composite Laplacian and the vector ω capturing frequencies of the oscillators. In particular, optimal synchrony can be still achieved by aligning the frequency vector ω with the eigenvalue associated with the largest eigenvalue of L. We remark that, with respect to section 3.2 where the synchronization onset was estimated by assuming a random allocation of frequencies, here we are dealing with the explicit interplay between the structure and the oscillator dynamics. The case of random frequency allocation can still be recovered and in this case we can extract results solely in terms of the structure. Overall, the picture in the linearized regime in the presence of higher-order interactions can be richer. Before focusing on the spectral analysis of the composite Laplacian, we find worthy to introduce first some numerical results on synthetic geometric networks.

3.3.3 *Results for noisy geometric networks: random vs optimal cases*

In our first experiment, we consider a class of random geometric networks [2] that contain both geometrically (spatial) constrained and unconstrained edges between nodes uniformly placed on the unit disc in $\mathbb{R}^2$. In these spatial networks, triangles (2-simplexes) arise from the geometrically constrained edges. We can tune the number of triadic interactions using a probability $p \in [0, 1]$: (i) with probability p each of the total $M = N\langle k^{(1)}\rangle/2$ edges is placed between the two closest nodes that are not yet connected and (ii) with probability $(1 - p)$ each edge is placed randomly, where $\langle k^{(1)}\rangle$ is the target mean 1-simplex degree. In the limit $p \to 1$, the network is purely geometric (spatial), and many triangles exist, while in the limit $p \to 0$ the network is Erdős-Rényi [81, 82]. The choice of this geometric

model for the network design is motivated here by the evidence pointing at the existence of simplicial complexes in physically embedded networks as the brain [138, 139].

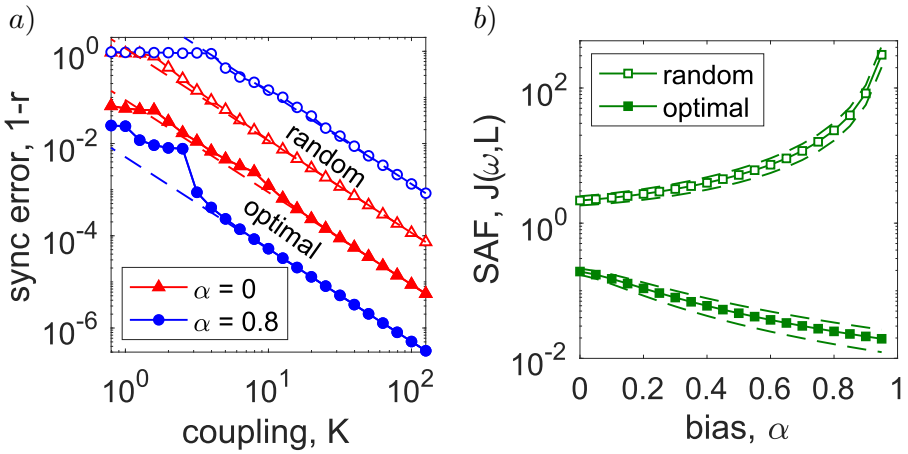

Figure 3.9: a) We plot the synchronization error $1-r$ vs K for random (open symbols) and optimal (closed symbols) frequencies for two choices of the bias parameter: $\alpha = 0$ (red triangles) and 0.8 (blue circles), for cases where interactions are exclusively defined by 1-simplexes and dominated by 2-simplexes, respectively, for a random geometric network (see text). b) The Synchrony Alignment Function (SAF) $J(\omega, L)$ as a function of α for randomly-allocated (open squares) and optimal (closed squares) frequencies averages over 10^3 networks. Reprinted by permission of [79].

Using the geometric model, we generate one network of size $N = 500$ with mean degree $\langle k^{(1)} \rangle = 10$ and $p = 0.25$. In Fig. 3.9a), we plot the synchronization error $1-r$ from direct integration of Eq. (3.31) as a function of coupling strength K for four cases (explained as follows), all under the constraint that the natural frequency vector has unit variance, $\sigma^2(\omega) = 1$. All simulations of Eq. (3.31) are done using Heun's method with a time step of $\Delta t = 0.02$, integrating over a transient of 5×10^3 time-steps and then averaged over a steady state of 2×10^3 time steps. We also plot the predicted synchronization error, given by $J(\omega, L)/2K^2$ for each case in dashed curves, where the SAF function is given by $J(\omega, L) = (1/N)\sum_j \langle v^j, \omega \rangle / \lambda_j^2$ (minimizing the SAF is therefore equivalent to maximize synchrony), which accurately capture the dynamics for sufficiently large coupling.

First, let us consider the fully 1-simplex (pair-wise) dominated case, i.e., $\alpha = 0$ so that coupling is purely dyadic, and plot the results for random (uncertain) and optimal (via alignment of $\omega \sim v^N$) choices of natural frequencies in open and closed red triangles, respectively. Note that the optimal alignment outperforms the random case, given by a set of natural frequencies drawn from the standard normal distribution, by about an order of magnitude, and for all range of K. Next, we set $\alpha = 0.8$, thus strengthening higher-order interactions at the expense of pair-wise ones, and plot the results for random (open blue) and optimal (closed blue) choices of natural frequencies. Focusing on the optimal case, the presence of higher-order interactions *improves* the optimal collective behavior supported by the system. Moreover, the more 2-simplex dominated a network is (i.e., the larger α is), the better the optimal states become. This is illustrated in Fig. 3.9b), where we plot the value of the SAF as a function of the bias parameter α for randomly chosen frequencies

and the optimal choice in open and closed squares, respectively. We see that as α increases, thus making the network more 2-simplex dominated, the optimal state improves while the random states worsen. Thus, strengthening higher-order interactions not only improves the optimal states, but also widens the range of possible synchronized states that are supported by the underlying network, which we remark has a fixed structure of links (constraints) regardless of the value of the bias parameter α.

3.3.4 *Spectral analysis and the variance proxy*

Now we explore the spectral properties of the composite Laplacian $L = (1-\alpha)L^{(1)} + \alpha L^{(2)}$ to explain the improvement that occurs in the optimization of synchrony in the presence of higher-order interactions. From the definition of the SAF and the analysis shown in section 2.3, one can see that the eigenvectors of L, their alignment with ω, and the eigenvalues of L affect the range of possible states. In fact, the optimal choice of ω occurs when $\omega = \sigma\sqrt{N}v^N$, thus aligning with the largest eigenvector, and synchrony is $r = 1 - 1/(2NK^2\lambda_N^2)$. Complementary, the decrease that would lead to the worst-case optimization is obtained by setting the frequency vector proportional to the first non-trivial (the smallest) eigenvector, $\omega \propto v^2$. Furthermore, in the case of random (uncertain) allocation, using the eigenvector basis of L one can write $\omega = \sum_{j=2}^{N} c_j v^j$, with $\sum_{j=2}^{N} c_j^2 = N\sigma^2$ (where the variance σ^2 is fixed to one for simplicity). When frequencies are random and independent of network structure, the expected value of each coefficient is $E[c_j] = \pm\sqrt{N/(N-1)}$ and therefore the expected value of r is given by

$$\langle r \rangle \approx 1 - \frac{1}{2K^2}\langle \lambda^{-2} \rangle, \tag{3.35}$$

where the average is taken over all eigenvalues except for the trivial eigenvalue $\lambda_1 = 0$.

Now we attempt to provide analytical insight on the previous effects by using a variance trick. As given by Eq. (3.35), in the random scenario, the range of r is controlled by the distribution of λ^{-2}. It seems difficult to unfold this distribution in terms of the properties of the network (degree, clustering, etc., ...), but we can find other spectral statistics, and then relate these statistics to the ones of its inverse. We acknowledge here that Prof. P. S. Skardal performed the following calculations involved in the variance trick. First, due to the conservation of the overall weighting of $L^{(1)}$ and $L^{(2)}$, the mean is always conserved to one: $\langle \lambda \rangle = N^{-1}\mathrm{Tr}(L) = N^{-1}[(1-\alpha)\sum_i k_i^{(1)}/\langle k^{(1)} \rangle + \alpha \sum_i k_i^{(2)}/\langle k^{(2)} \rangle] = 1$. Then, the variance of the spectra of L can be written as

$$\mathrm{Var}(\lambda) = \langle \lambda^2 \rangle - \langle \lambda \rangle^2 = N^{-1}\mathrm{Tr}(L^2) - 1. \tag{3.36}$$

Our focus turns to the quantity $\mathrm{Tr}(L^2)$. First, using the fact that the network is undirected, and therefore $A^{(2)} = A^{(2)T}$ we write

$$L^2 = \left[(1-\alpha)\frac{D^{(1)} - A^{(1)}}{\langle k^{(1)} \rangle} + \alpha \frac{D^{(2)} - A^{(2)}/2}{\langle k^{(2)} \rangle} \right]^2, \tag{3.37}$$

By expanding the terms in the binomial, one finds

$$\begin{aligned} L^2 = (1-\alpha)^2 &\frac{D^{(1)2} - D^{(1)}A^{(1)} - A^{(1)}D^{(1)} + A^{(1)2}}{\langle k^{(1)}\rangle^2} \\ &+ \alpha(1-\alpha)\frac{D^{(1)}D^{(2)} - D^{(1)}A^{(2)}/2 - A^{(1)}D^{(2)} + A^{(1)}A^{(2)}/2}{\langle k^{(1)}\rangle\langle k^{(2)}\rangle} \\ &+ \alpha(1-\alpha)\frac{D^{(2)}D^{(1)} - D^{(2)}A^{(1)} - A^{(2)}D^{(1)}/2 + A^{(2)}A^{(1)}/2}{\langle k^{(1)}\rangle\langle k^{(2)}\rangle} \\ &+ \alpha^2\frac{D^{(2)2} - D^{(2)}A^{(2)}/2 - A^{(2)}D^{(2)}/2 + A^{(2)2}/4}{\langle k^{(2)}\rangle^2}. \end{aligned} \tag{3.38}$$

By the properties of the trace, one can compute it as the sum of traces for each term in Eq. (3.38). Noting that, since no self-links exist and triangles only exist between three distinct nodes, we have that $A^{(1)}_{ii} = A^{(2)}_{ii} = 0$ for $i = 1,\dots,N$, so that $\mathrm{Tr}(D^{(1,2)}A^{(1,2)}) = \sum_{i=1}^N D^{(1,2)}_i A^{(1,2)}_{ii} = 0$, and all mixed terms vanish. After rearranging the whole expression, one obtains

$$\begin{aligned} \mathrm{Tr}(L^2) = &\frac{(1-\alpha)^2}{\langle k^{(1)}\rangle^2}\left[\mathrm{Tr}(D^{(1)2}) + \mathrm{Tr}(A^{(1)2})\right] \\ &+ \frac{2\alpha(1-\alpha)}{\langle k^{(1)}\rangle\langle k^{(2)}\rangle}\left[\mathrm{Tr}(D^{(1)}D^{(2)}) + \mathrm{Tr}(A^{(1)}A^{(2)})/2\right] + \frac{\alpha^2}{\langle k^{(2)}\rangle^2}\left[\mathrm{Tr}(D^{(2)2}) + \mathrm{Tr}(A^{(2)2})/4\right]. \end{aligned} \tag{3.39}$$

The traces of each of the matrices $D^{(1)2}$, $D^{(1)}D^{(2)}$, and $D^{(2)2}$ are given simply by $\mathrm{Tr}(D^{(1)2}) = \sum_{i=1}^N k_i^{(1)2}$, $\mathrm{Tr}(D^{(1)}D^{(2)}) = \sum_{i=1}^N k_i^{(1)}k_i^{(2)}$ and $\mathrm{Tr}(D^{(2)2}) = \sum_{i=1}^N k_i^{(2)2}$, while the traces of each of the matrices $A^{(1)2}$, $A^{(1)}A^{(2)}$, and $A^{(2)2}$ are given by

$$\mathrm{Tr}(A^{(1)2}) = \sum_{i=1}^N\left(\sum_{j=1}^N A^{(1)}_{ij}A^{(1)}_{ji}\right) = \sum_{i=1}^N k_i^{(1)} \tag{3.40}$$

$$\mathrm{Tr}(A^{(1)}A^{(2)}) = \sum_{i=1}^N\left(\sum_{j=1}^N A^{(1)}_{ij}A^{(2)}_{ji}\right) = \sum_{i=1}^N k_i^{(2)} \tag{3.41}$$

$$\mathrm{Tr}(A^{(2)2}) = \sum_{i=1}^N\left(\sum_{j=1}^N A^{(2)}_{ij}A^{(2)}_{ji}\right) = \sum_{i=1}^N q_i. \tag{3.42}$$

We have used that $A^{(1)}$ and $A^{(2)}$ are undirected, $A^{(1)}$ is unweighted, and $q_i = \sum_{j=1}^N A^{(2)2}_{ij}$. Finally, inserting the expressions for the traces into Eq. (3.39), dividing by N and using the relation given by Eq. (3.36), yields

$$\begin{aligned} \mathrm{Var}(\lambda) = (1-\alpha)^2&\left(\frac{\langle k^{(1)2}\rangle}{\langle k^{(1)}\rangle^2} + \frac{1}{\langle k^{(1)}\rangle}\right) \\ &+ 2\alpha(1-\alpha)\left(\frac{\langle k^{(1)}k^{(2)}\rangle}{\langle k^{(1)}\rangle\langle k^{(2)}\rangle} + \frac{1}{2\langle k^{(1)}\rangle}\right) + \alpha^2\left(\frac{\langle k^{(2)2}\rangle}{\langle k^{(2)}\rangle^2} + \frac{\langle q\rangle}{4\langle k^{(2)}\rangle^2}\right) - 1, \end{aligned} \tag{3.43}$$

where $q_i = \sum_{j=1}^{N} A_{ij}^{(2)2}$. Eq. (3.43) tell us that varying α interpolates the variance between $\langle k^{(1)2}\rangle / \langle k^{(1)}\rangle^2 + 1/\langle k^{(1)}\rangle - 1$ and $\langle k^{(2)2}\rangle / \langle k^{(2)}\rangle^2 + \langle q\rangle / (4\langle k^{(2)}\rangle^2) - 1$ in the extremes where connections are completely dominated by 1-simplex (pair-wise) and 2-simplex (three-way) coupling, respectively. The variance trick relates the statistics and of λ with the statistics of λ^{-2}, and also the behavior of the extreme eigenvalues. One can see that when $\alpha = 0$ (only pair-wise interactions), the variance is only controlled by degree heterogeneity, indicating that heterogeneous networks have broader Laplacian spectra [68, 165], which translate into a broader range of synchronized states than in homogeneous networks. Interestingly, the role of clustering, modularity, and other types of structural correlations is absent in the dependence with the variance of λ, which lies in contrast to the effect of these network properties on the second eigenvalue of the Laplacian matrix [2, 6]. By switching on $\alpha > 0$, we can also examine the effect of higher-order interactions. From Eq. (3.43), we expect that, when the ratio of moments in the 2-simplex degree (the 'triangles') is larger than in the 1-simplex case, variance increases, occurring when the 2-simplex degree distribution is more heterogeneous than the traditional 1-simplex degree distribution.

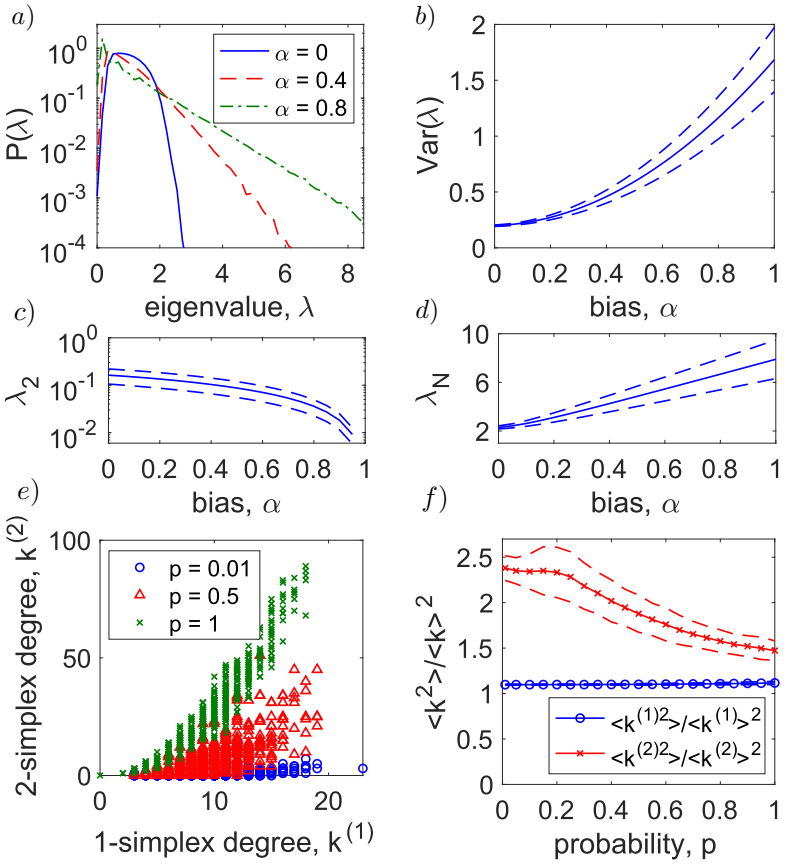

Figure 3.10: a) The eigenvalue spectrum $P(\lambda)$ of the composite Laplacian L for $\alpha = 0$ (solid blue), 0.4 (dashed red), and 0.8 (dot-dashed green) obtained from 10^3 networks of size $N = 500$ with mean degree $\langle k\rangle = 10$ and $p = 0.25$. b) The spectral variance and the extreme eigenvalues, c) λ_2 and d) λ_N from the same ensemble. e) 2-simplex degrees $k^{(2)}$ vs 1-simplex degrees $k^{(1)}$ for a single network realization and f) the quantities $\langle k^{(1)2}\rangle / \langle k^{(1)}\rangle^2$ and $\langle k^{(2)2}\rangle / \langle k^{(2)}\rangle^2$ (blue circles and red crosses) obtained from 10^3 networks as a function of the parameter p. Reprinted by permission of [79].

We validate the analytical results in Fig. 3.10. In Fig. 3.10.a), we plot the eigenvalue spectrum of L averaged across 10^3 networks of size $N = 500$ and built using the model described above with mean degree $\langle k^{(1)} \rangle = 10$ and $p = 0.25$ for $\alpha = 0$ (solid blue), 0.4 (dashed red), and 0.8 (dot-dashed green). Note that as the higher-order interactions strengthen at the expense of pairwise interactions (larger α), the eigenvalue spectrum becomes broader. In Fig. 3.10.b), we plot the mean variance of the spectral density as a function of α which we calculated from the same ensemble as in panel a) (one standard deviation is represented with dashed curves). We observe a monotonic increase in the variance of the eigenvalue spectrum as higher-order interactions are strengthened, which is consistent with the broadening shown in panel a). As shown in Fig. 3.10.c)-.d), the extreme eigenvalues λ_2 and λ_N follow the same trend, decreasing and increasing, respectively, for increasing α. We have also checked that the effect is sustained over a large range of networks. In Fig. 3.10e) we show results for networks ranging from completely random to strongly geometric (interpolating with parameter p). We can see that the 2-simplex degree distribution is more heterogeneous than the 1-simplex one for all values of p, which translates into the broadening of the spectra. This property is captured by the concave form in each of the three curves of panel e), and in panel f), where the ratios of the degree distributions in pair-wise and three-body interactions (in blue circles and red crosses, respectively) across a full range of the parameter p of the geometric network model, ranging from random networks ($p \approx 0$) to completely spatial ones ($p \approx 1$). All points in panels e) and f) are obtained from averaging over an ensemble of 10^3 networks. These results support the predicted role of higher-order couplings, namely the broadening of the synchronized range and the improvement of optimal states. We have also check that these results hold for networks drawn from different degree distributions (as Poisson or power-laws) and empirical ones. However, there may be particular, although we believe rare, cases where the increases in the variance predicted in Eq. (3.43) does not hold. In this section, we restricted to geometrically-embeded networks due to its practical relevance in biological and engineered systems where higher-order interactions presumably play a role [139, 140].

3.3.5 *Optimization in constrained scenarios*

To close this section, we consider a more realistic optimization scenario where optimal alignment may not be possible (due to structural constraints). The following results also bridge the random and optimal allocation methods under the same framework.

We assume an initial random allocation of frequencies, and allow some perturbations to optimize synchronization. We denote this perturbation by $\delta\omega = \omega_{\text{new}} - \omega$, and constrain the relative size $\|\delta\omega\|/\|\omega\|$ while fixing the variance of ω. The perturbation can be optimally chosen in terms of the eigenvector expansion $\omega = \sum_{j=2}^{N} c_j v^j$ by orthogonalizing away from the eigenvectors with smallest associated eigenvalues in order to eliminate the largest contributions to the SAF. To do this, one lets $\delta\omega = \sum_{j=2}^{N} \beta_j v^j$ and, for as large k as possible, let $\beta_j = -c_j$ for $j = 2, \ldots, k$, $\beta_j = c_j$ for $j = k+1, \ldots, N-1$, and $\beta_N = c_N(\sqrt{1 + \sum_{j=2}^{k} c_j^2/c_N^2} - 1)$, resulting in $\omega_{new} = \sum_{j=2}^{N} \gamma_j v^j$ with $\gamma_j = 0$ for $j = 2, \ldots, k$,

$\gamma_j = c_j$ for $j = k+1, \ldots, N-2$, and $\gamma_N = c_N \sqrt{1 + \sum_{j=2}^{k} c_j^2 / c_N^2}$. Note that this both orthogonalizes ω_{new} against the eigenvectors with the smallest eigenvalues while increasing the alignment with v_N in order to conserve the variance of ω. This method can be further improved by applying a permutation to the initially random vector ω. We do so with an accept-reject algorithm that interchanges chosen pairs of frequencies if the exchange improves the degree of strong synchrony (in terms of the SAF).

Now we explore the results of these two methods. In Fig. 3.11.a), we plot the resulting SAF $J(\omega, L)$ averaged over 10^2 networks using the same parameters as before, after imposing perturbations of sizes $\|\delta\omega\| / \|\omega\| = 0$, 0.4, 0.8, and 1.2 (blue circles, red triangles, green crosses, and black squares) in a random frequency vector normally distributed. Note that the maximum possible perturbation that conserves the standard deviation of the frequencies is $\|\delta\omega\| / \|\omega\| = 2$, obtained by $\omega_{new} = -\omega$. In Fig. 3.11.b), we observe that the method with a preliminary permutation of frequencies minimizes better the SAF (increasing synchrony). One sees that there is often an ideal balance of dyadic to triadic interactions, i.e., a critical optimal α that lies between zero and one, for a given perturbation size.

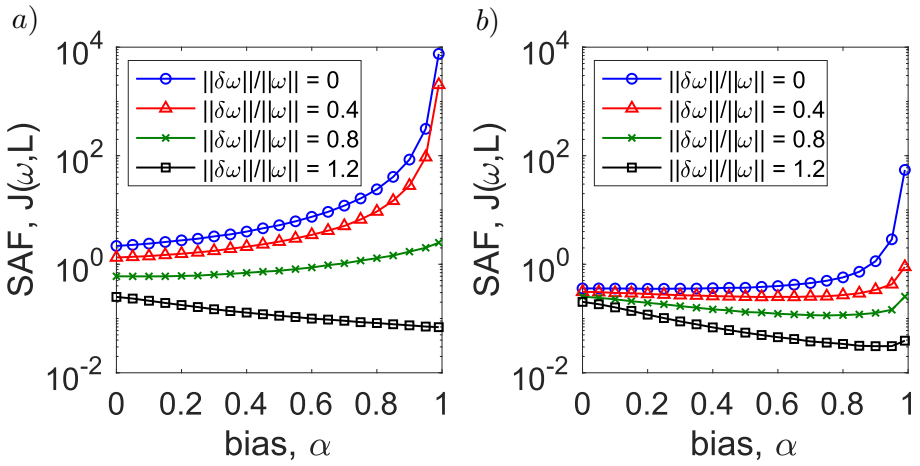

Figure 3.11: The SAF $J(\omega, L)$ as a function of α obtained after optimal perturbations of sizes $\|\delta\omega\| / \|\omega\| = 0$ (blue circles), 0.4 (red triangles), 0.8 (green crosses), and 1.2 (black squares) are applied to a randomly drawn vector of frequencies a) without and b) with preprocessing the frequency vector using a (near) optimal permutation. Results are obtained from an ensemble of 10^2 networks of size $N = 100$ with mean degree $\langle k^{(1)} \rangle = 10$ and $p = 0.25$. Reprinted by permission of [79].

This last experiment connects the random allocation of frequencies, where higher-order interactions decrease collective coherence, and optimal (unconstrained) allocation, where higher-order interactions improve collective behavior. Specifically, constraints in the optimization allow higher-order interactions to improve the optimal state, but only to some extent, since the frequency vector cannot be precisely aligned with the eigenvector vector v^N. With these findings, we conclude the section and move on to the third problem of the chapter, where we heuristically study a more general problem joining the critical point and the strong synchronized regime. We leave a summary of the previous findings and a discussion of some limitations and open problems for the final section 3.5.

3.4 DYNAMICAL INVARIANCE UNDER NETWORK TRANSFORMATIONS

3.4.1 *A mapping problem*

Up to now, we have explored the role of network uncertainty in the critical and the linearized regime of our oscillatory system separately, but we lack a holistic view on the full dynamics. This broader picture is still missing even for the most simple form of the Kuramoto model (with pair-wise, undirected connections, positive weights, etc ...) in arbitrary complex networks, due to the irregularities in the specific network patterns. We attempt to contribute to this research direction by introducing a novel mapping problem that tackles an apparently simple question: can different network structures, when tuned appropriately, achieve the same range of functionality? Which are the constraints that limit the possible mapping of behaviors? In the literature of network synchronization, it is well understood that different interaction structures can give rise to a common functionality, usually in terms of a macroscopic observable as the order parameter r. This idea of multivaluation has been explored in the context of network inference [164, 168], prediction [177, 213, 214] and control [44, 69], but, to our knowledge, the particular ranges of synchrony for different type of structures have not been studied in the past. Considering the intricate patterns of real world networks [2] and the ubiquity of synchronization phenomena [3, 6], improving the understanding of the relation between network structure and potential range of behaviors seems of upmost relevance to the field.

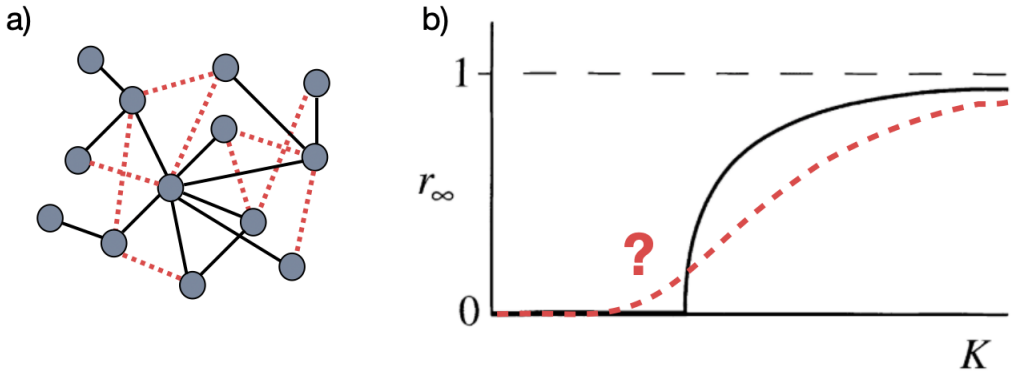

Figure 3.12: a) Illustrative sketch of a network with two configurations of links (black solid and red dashed, respectively), inducing in b) two different synchronization curves. Can we map the dynamical behavior of both networks for all range of coupling K by tuning the weights in one of the structures?

In this section, we address this problem driven again by the pace of uncertainty. The information we can obtain from the network is usually incomplete, because of experimental errors, lack of resolution, or, as shown before, due to noisy weights, random frequencies or diverse interaction mechanisms. Moreover, the non-linearities in the dynamics and the complex network patterns difficult the analytical treatment even in possession of complete information of the system. An example of this limitation, is how the spectra of the adjacency A and the Laplacian L matrices show up in the critical and linearized regimes of

the Kuramoto model, but there is no available theory that relates both regimes or spectral objects by analytical means. Motivated by these uncertain conditions, we study the mapping between different structures, wondering how can one transform the interactions in one of the networks such that the collective behavior remains invariant in both. Such transformation must adjust the weights of the interactions in the targeted configuration to achieve the goal, if possible, of having an equivalent steady-state functionality to the original structure. In Fig. 3.12 we show an illustrative sketch on the mapping problem.

Inspired by the derivation of statistical mechanics from information theory as a particular case of statistical inference [32], we propose to tackle the mapping problem as an optimization problem for the unknown weights subject to structural constraints on the networks that capture our prior, incomplete knowledge on the system. Our constraints will rely on an extended mean-field approach, exploiting different scales of structural information, from local to further-neighborhoods. The proposed method is heuristic, and we show results only for the standard Kuramoto model. We impose several strong assumptions: namely random networks drawn from a known degree distribution, uncertain allocation of frequencies, and we allow only positive weights on the interactions. Despite the limitations of our experiment, we will unveil that the mapping of homogeneous networks into heterogeneous ones is usually less accurate and requires more –costly– microscopic information than the reverse process, which points to *symmetry-unbalance* phenomenon that emerges from the partial impossibility of preserving the local structural constraints of hubs. While certainly not the definitive answer to the ambitious mapping problem, the following results anticipated some further works, which improve our capacity to control and predict the relation between structure and dynamical range in oscillator networks, but usually rely on global, complete information and numerical methods that treat networks as black-boxes [44, 129, 135, 162]. The results of this chapter rely on negating this complete information, and this section is not an exception. Hopefully, the proposed heuristics can be useful to enhance our mechanistic comprehension of the system and to pave the way to more rigorous findings. In fact, the results presented in the next chapter will somehow confirm that the uncertain and intuitive route followed in these initial steps was heading towards the good direction.

3.4.2 *Heuristic extension of mean-field constraints*

As it is a common praxis in the course of the thesis, we focus on the well-known Kuramoto model (KM) to study a novel problem. Here, we use it to motivate our method to generate functionally invariant networks. To this purpose, we return to the standard version of the KM [5, 6, 38, 62], considering the dynamical system

$$\dot{\theta}_i = \omega_i + K \sum_{j=1}^{N} a_{ij} \sin(\theta_j - \theta_i), \ \forall \ i \ \in 1, \dots, N. \tag{3.44}$$

It is well understood that, when the frequencies are randomly allocated and one neglects the effect of structural correlations (thus working in the random ensemble of the config-

uration model), particular unweighted instances drawn from the same degree distribution will produce the desired invariant collective behavior [2, 6, 58]. Here we wonder if the former invariance can be achieved for weighted networks drawn from different degree distributions, preserving the number of nodes N. To tackle this problem, we consider a reference network $\mathcal{A}$ with a given coupling matrix A, which might be non-symmetric and directed with fixed entries a_{ij}, and a candidate network B, with a different coupling matrix B. We look for transformations of B in the form $B' = W \circ B$, with entries $w_{ij}b_{ij}$, where w_{ij} are the parameters to find and b_{ij} are the binary entries of B. Then, our condition for having synchronization invariance can be written as

$$\langle r^2(\omega, K, A)\rangle = \langle r^2(\omega, K, B')\rangle, \ \forall \ K > 0, \tag{3.45}$$

where the measurements are in the steady-state, the average refers to different initial conditions and frequency allocations, accounting for fluctuations of order $1/\sqrt{N}$. The invariance condition of Eq. (3.45) is written in terms of the usual KM complex order parameter $re^{i\Psi(t)} = (1/N)\sum_{j=1}^{N} e^{i\theta_j}$. We assume that the macroscopic order parameter r is the only available observable from measurements (in fact we use r^2 to better capture the differences in both networks for small values of r around the synchronization onset, which does not alter the results) and we look for network transformations (via weight tuning of the entries of W) that keep this observable invariant, for any value of the control parameter K.

To the best of our knowledge, a method appropriate to solve the mapping problem, as defined above for the Kuramoto model, is not available in the literature. The multivaluation of synchronization dynamics [164] and the vast number of network configurations and frequency choices that can possibly generate invariant dynamics in Eq. (3.44) [6, 62, 135, 149, 163], highlight the difficulty of finding solutions to the weight tuning problem in general. Furthermore, we know, from results presented in previous sections, that the preservation of the adjacency and Laplacian spectra and the precise alignment of the frequencies play a crucial role in generating the invariant transformations, but we do not know yet which spectrum nor alignment has to be preserved and how a spectral invariance would translate into actual network modifications (such as weight adjustments of fixed links). Considering these limitations, we decide to tackle the mapping problem guided by physical intuition and uncertainty assumptions.

We propose a heuristic approach based on exploiting decentralized structural information, extending a detailed balance, in terms of the mean-field constraints of the nodes, from local to higher-orders. With this idea in mind, we treat the mapping as an optimization problem for the unknown weights subject to the structural constraints (the proposed mean-field balances) posed on the network. In particular, the key assumption is to achieve Eq. (3.45) by imposing a local detailed balance for the main structural properties of the nodes: the overall coupling intensities –the sum of incoming weights– received from neighbors (or input strengths [2]). For each node, we define the zero-order input strength as $s_i^{(0)} = \sum_j a_{ij}$, the first-order as $s_i^{(1)} = \sum_j a_{ij}(\sum_k a_{jk})$ and so on. For a fixed order M, the

detailed balance is given by a set of $N(M+1)$ equations for the $s_i^{(m)}$. If we let q be the N-vector of ones $q = (1, 1, ..., 1)$, we can write

$$A^{m+1}q = B'A^m q, \ \forall \ 0 \leq m \leq M, \tag{3.46}$$

where $(A^{m+1}q)_i = s_i^{(m)}$ are the node structural bounds in the optimization of the weights in B'. The local constraint ($m = 0$) can be written explicitly as

$$\sum_{j=1}^{N} a_{ij} = \sum_{j=1}^{N} w_{ij} b_{ij}, \ \forall \ i \ \in 1, \ldots, N, \tag{3.47}$$

which ensures to preserve the overall coupling in the transformation ($\sum_i \sum_j a_{ij} = \sum_i \sum_j w_{ij} b_{ij}$). Eq. (3.47) can be seen as a local mean-field *ansatz* that relies on the weighted annealed approximation [215, 216], assuming statistical similarity among nodes with the same $s_i^{(0)}$. This weighted description is known to be valid in the linear regimes of the diffusion of random walkers [216] and the Master Stability Function (MSF) [80, 161]. In the context of the Kuramoto model, Eq. (3.47) appears in an implicit manner when relating the local order parameter of Eq.(3.44), $r_i = |(1/N) \sum_j a_{ij} e^{i\theta_j}|$, with the global order parameter r via the in-strength $s_i^{(0)}$ of the nodes as $r_i \approx s_i^{(0)} r$ [103, 104]. In section 3.2 we showed an application of this weighted mean-field description when computing the synchronization onset in the presence of noisy weights, and we confirmed its validity by numerical means, at least in the context of random networks with small noise on weights. Furthermore, we note that within the mathematical tool presented in the following chapter 4, the validity of the local ansatz will also be recovered by the first-order (local) truncation of the geometric expansion of the linearized synchronized state.

The previous arguments point that the local mean-field constraint given by Eq. (3.47) can be a reasonable choice to impose in the mapping problem, at least for networks drawn from the configuration model (in absence of strong clustering or modular structures), with small variations of weights among the existing links. Our additional guess is that higher order constraints ($m > 0$) might be required when the non-linearity of Eq. (3.44) plays a crucial role, or the connectivity patterns of the units become highly non-trivial (as a large heterogeneity of degrees). Importantly, we remark that the proposed constraints only exploit structural information of the system (the M-order input strengths) but neglect information about the frequencies, given by the vector ω in Eq. (3.44). Thus, we are working with uncertain information of the nodal dynamics, and structural transformations proposed here should be taken into account only for very large systems with random frequencies, or ensembles of systems with frequencies randomly drawn from a given distribution $g(\omega)$. Furthermore, we allow the unknown weights in the matrix W to be non-negative, restricting our problem to finding positive solutions for the interaction strengths. This last assumption is motivated by empirical oscillatory systems where negative weights are not allowed (as in excitatory networks or power-grids [6, 135]) and it constrains even more the space of configurations. Overall, the intuition behind the mean-field ansatz is that the dynamical mapping can be achieved for different networks by tuning the interaction weights in

one network such that the distribution of (generalized) input strengths become invariant (assuming a random allocation of frequencies), even if the initial distribution of links is different between two networks (for instance, a different degree distribution). The hypothesis that we are testing is if we can generate functionally invariant networks by satisfying these structural constraints.

3.4.3 *Analytical solutions of maximal entropy*

To solve the mapping problem under the chosen constraints, we take advantage of information theory [167], to define an appropriate objective function to optimize the unknown weights. In an uncertainty scenario, the best we can do is to rely on the maximum entropy principle [32]. It states that, subject to the available data (i.e. the constraints in Eq. (3.46)), the probability distribution which best captures our lack of information is the one that maximizes the entropy. Here, we can interpret the weights' distribution in probabilistic terms, where the input strength $s_i^{(0)}$ is the normalization condition, and define the entropy [167] of a node S_i as a sum of weights over the accessible states, i.e. where $b_{ij} = 1$,

$$S_i = -\sum_{j=1}^{N} w_{ij} \log w_{ij}, \ \forall \ i \in N, \tag{3.48}$$

where the normalization constant has been neglected for simplicity, and it is assumed that $w_{ij} \geq 0$. Now we use the method of Lagrange multipliers [32] to solve this optimization problem. The Lagrangian function reads as

$$\mathcal{L} = \sum_{i=1}^{N} (S_i - \sum_{m=0}^{M} \beta_i^{(m)} [(A^{m+1} q)_i - (B' A^m q)_i]), \tag{3.49}$$

where $\beta_i^{(m)}$ is the m-order Lagrange multiplier of i-node. By optimizing Eq. (3.49) with respect to the unknown weights and finding the values of the multipliers, we can derive analytical expressions for the entries of B'. For the zero-order case ($M = 0$), we obtain

$$w_{ij}^{(0)} = \frac{\sum_{k=1}^{N} a_{ik}}{\sum_{k=1}^{N} b_{ik}}, \ \forall \ i, j \in N, \tag{3.50}$$

that can be written as $w_{ij}^{(0)} = s_i^{(0)} / k_i^B$, where k_i^B is the degree of node i in $\mathcal{B}$. This solution is very *intuitive*, since it homogeneously allocates the input strength of a node into the available links. The weights are therefore equal for all the incoming links of a node (w_{ij} is independent of the node j), implying usually a non-symmetric coupling. The solution in Eq. (3.50) is precisely the scheme used in [80, 161] to transform a network topology into a purely homogenous one to optimize the stability of the synchronized state in the scope of the MSF. That means that the solution should be valid in the linear regime, close to the synchronization attractor. However, this solution is yet to be validated in the fully non-linear regime of Eq. (3.44).

To validate the naive, zero-order solution of Eq. (3.50), we simulate the dynamics of $N = 2000$ oscillators following Eq. (3.44) with fixed $g(\omega) \in (-\pi, \pi)$, measuring $\langle r^2 \rangle$ in a quasi-static process controlled by the control parameter $K \in [0, 0.5/N]$. We try to map pairs of uncorrelated networks drawn from different degree distributions, that range from homogeneous in degree, Erdös-Rényi networks, to power-law in degree (SF) networks, which are initially unweighted and symmetric. We interpolate between both degree distributions with a single parameter α, using the model proposed in [121]. For $\alpha = 0$ we have pure power-law (SF) distributions $p(k) \sim k^{-\gamma}$ with exponent $\gamma = 3$ while for $\alpha = 1$ we obtain homogeneous (ER) random networks, keeping the average degree fixed, in our case $\langle k \rangle = 10$. In practice, we fix the binary links of a network $\mathcal{A}$ drawn from the model for a certain value α, i.e. the target network $\mathcal{A}_\alpha$, and the candidate network $\mathcal{B}_{\alpha'}$ drawn for another value α'. Then, we compute the weights, using Eq. (3.50), and transform the weights of the candidate network to map the behavior of the original one, obtaining the resulting matrices $T_0(\mathcal{B}_{\alpha'}|\mathcal{A}_\alpha)$, where the sub-index of T means that the method exploits only zero-order information (the local constraint of Eq.(3.47)).

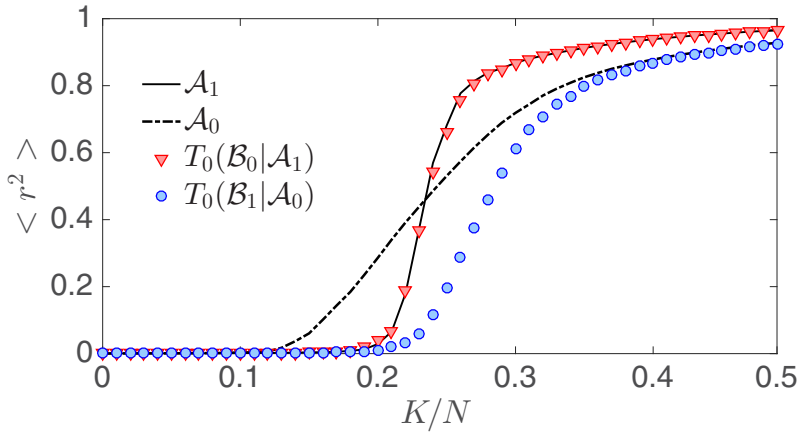

Figure 3.13: We plot r^2 as a function of the coupling strength K of the Kuramoto model, with $\Delta(K/N) = 0.01$ simulated with a 4th-order Runge-Kutta method with $\Delta t = 0.01$, for one instance of $\mathcal{A}_1$ (ER) and $\mathcal{A}_0$ (SF) networks and their respective transformations using Eq. (3.50), averaged over 50 realizations with $\theta_0 \in [-\pi, \pi]$ (standard deviations are smaller than the size of the symbols). Reprinted by permission of [162].

In Fig. 3.13 we present the results of the transformation for the extreme cases $T_0(\mathcal{B}_0|\mathcal{A}_1)$ and $T_0(\mathcal{B}_1|\mathcal{A}_0)$. These results show that the dynamical invariance is attained in the linear regime ($K \gg K_c$) in both directions of the transformations, as expected. However, there is a clear discrepancy in the transformation $T_0(\mathcal{B}_1|\mathcal{A}_0)$, i.e. from a homogeneous in degree network towards a heterogeneous, power-law, network. This discrepancy shows that, when Eq. (3.50) is applied, homogeneous networks are not able to capture the role of heterogeneous connectivity patterns. In other words, when trying to map a very heterogeneous network, a reallocation of the weights preserving the heterogeneous (zero-order) input strength is not sufficient to fully map the synchronization behavior, thus invalidating the local ansatz of Eq. (3.47) beyond the linear regime of the system.

Following our theory, to improve the accuracy of the T_0 method in the mapping, one should include higher-order constraints in the optimization problem. We extend the detailed balance to first order ($M = 1$) by imposing that, for each node, the transformation must also preserve the first-order input strengths $s_i^{(1)}$, i.e.

$$\sum_{j=1}^{N} a_{ij} s_j^{(0)} = \sum_{j=1}^{N} w_{ij} b_{ij} s_j^{(0)}, \ \forall \ i \in 1, \dots, N. \tag{3.51}$$

Note that $s_j^{(0)}$ is the same at both ends of Eq. (3.51) because we still retain the constraint presented in Eq. (3.47). We aim to maximize Eq. (3.48) subject to Eq. (3.47) and Eq. (3.51). The Lagrangian in Eq. (3.49) can be written explicitly as

$$\mathcal{L} = \sum_{i=1}^{N} [- \sum_{j=1}^{N} w_{ij} \log w_{ij} - \beta_i^{(0)} (s_i^{(0)} - \sum_{j=1}^{N} w_{ij} b_{ij}) - \beta_i^{(1)} (\sum_{j=1}^{N} \lambda_{ij}^{A} s_j^{(0)} - \sum_{j=1}^{N} w_{ij} b_{ij} s_j^{(0)})]. \tag{3.52}$$

By imposing $d\mathcal{L}/dw_{ij} = 0$ and isolating the unknown weight w_{ij}, we obtain the implicit expression

$$w_{ij}^{(1)}(\beta_i) = \frac{s_i^{(0)} e^{-\beta_i s_j^{(0)}}}{\sum_{k=1}^{N} b_{ik} e^{-\beta_i s_k^{(0)}}}, \ \forall \ i, j \in N. \tag{3.53}$$

The values of the multipliers β_i are found by substituting Eq. (3.53) back in Eq. (3.51) and numerically solving the resulting system. However, the existence of real and non-negative solutions cannot be ensured a priori. Indeed, the structural bounds can be estimated by considering the worst-case scenarios, i.e.

$$s_i^{(0)} \times \min_{\forall j \in N} (b_{ij} s_j^{(0)}) \leq s_i^{(1)} \leq s_i^{(0)} \times \max_{\forall j \in N} (b_{ij} s_j^{(0)}), \ \forall \ i \in N. \tag{3.54}$$

The inequality in Eq. (3.54) turns out to be unfeasible for most nodes if the reference network is very heterogeneous in local input strength. This effect is consistent with the loss of accuracy found in mean-field approaches [217], which depends on the degrees of first neighbors of the nodes. In a very heterogeneous network, the hubs have a very large number of links, thus connect to other hubs in the network with high probability. In a homogeneous network, even if we tune the incoming weights of a given node to satisfy the input strength of a given hub at local order, the preservation of first-orders strengths will not be usually possible to achieve since the neighbors of the 'transformed' hub do not necessarily have a large input strength. Intuitively, one cannot fake the structural importance of hubs simply by tuning the weights in homogeneous networks. On the other hand, Eq. (3.50) is recovered from Eq. (3.53) only when $s_i^{(0)} \simeq \langle s^{(0)} \rangle$, $\forall \ i \in N$, i.e. when A is very homogeneous in local input strength, regardless of the topology of B. This last observation explains why the mapping from heterogeneous to homogeneous ones was already working in the initial transformation shown in Fig. 3.13.

The previous reasoning unfolds the *symmetry-unbalance* between homogeneous and heterogeneous networks observed in Fig. 3.13 and suggests that the mapping can indeed be enhanced, although it is strongly limited by the structural bounds. To provide an analytical

transformation that improves the performance of Eq. (3.50) while still preserving $w_{ij} \geq 0$, we expand Eq. (3.53) to first order around its average value, i.e.

$$w_{ij}^{(1)}(\beta_i) \simeq \frac{s_i^{(0)}[1-\beta_i(s_j-\langle s\rangle)]}{\sum_{k=1}^{N} b_{ik}[1-\beta_i(s_k-\langle s\rangle)]},\ \forall\ i,j \in 1,\dots,N, \tag{3.55}$$

where $\langle s\rangle = (1/k_i^B)\sum_j b_{ij}s_j^{(0)}$. We insert Eq. (3.55) into Eq. (3.51) to obtain an approximate value $\beta_i^* \simeq \beta_i$ as

$$\beta_i^* = \frac{1}{s_i^{(0)}}\left(\frac{s_i^{(0)}\langle s\rangle - s_i^{(1)}}{\langle s^2\rangle - \langle s\rangle^2}\right),\ \forall\ i \in N. \tag{3.56}$$

The approximate first-order solution is finally obtained by direct substitution of Eq. (3.56) into Eq. (3.53), and we denote this transformation $T_1(\mathcal{B}_{\alpha'}|\mathcal{A}_\alpha)$. Note that T_1 does not provide uniform weighting for each node anymore, but depends explicitly on the balance between input strengths and heterogeneity in each node.

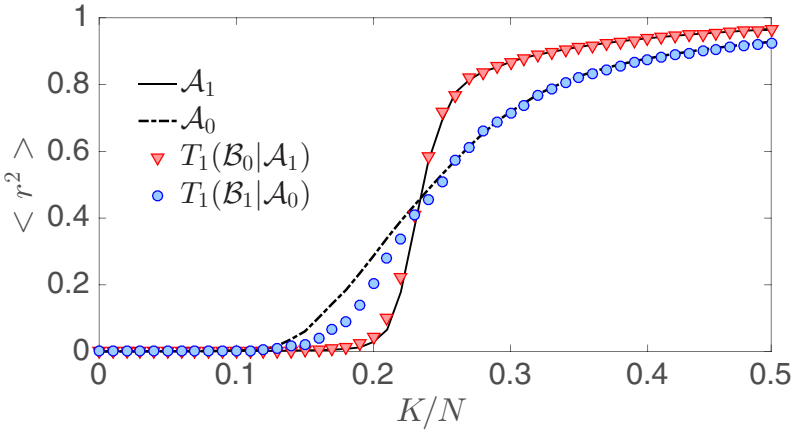

Figure 3.14: We plot r^2 as a function of K, for one instance of $\mathcal{A}_1$ and $\mathcal{A}_0$ networks and transformations $T_1(\mathcal{B}_0|\mathcal{A}_1)$ and $T_1(\mathcal{B}_1|\mathcal{A}_0)$ using Eqs.(3.55,3.56), averaged over 50 realizations with $\theta_0 \in [-\pi,\pi]$. The mapping is significantly improved with respect to Fig. (3.13). Reprinted by permission of [162].

Now we can test the performance of the T_1 in the mapping and compare it to the previous T_0 case. In Fig. 3.14 we present the synchronization diagram for the extreme cases $T_1(\mathcal{B}_0|\mathcal{A}_1)$ and $T_1(\mathcal{B}_1|\mathcal{A}_0)$ in the same set-up as before ($N = 2000$). We can observe a remarkable improvement in the transformation $T_1(\mathcal{B}_1|\mathcal{A}_0)$ with respect to the zero-order method in Fig. 3.13, although there still are non-vanishing errors around the critical point, which we attribute to the unfeasible structural bounds of Eq. (3.54).

To qualitatively validate these last findings, we define, for each transformation, the dynamical error

$$\sigma_d = N^{-1}\int_0^{K_\infty}[\langle r^2(\vec{\omega},K,\mathbf{A})\rangle - \langle r^2(\vec{\omega},K,\mathbf{B}')\rangle]^2 dK, \tag{3.57}$$

as a measure of the total difference in the synchronization diagrams between the reference and transformed networks, and we define the structural error

$$\sigma_s = N^{-1}\sum_i^N[\sum_j^N(a_{ij}s_j^{(0)} - w_{ij}b_{ij}s_j^{(0)})]^2, \tag{3.58}$$

as a measure of the total difference in the first-order local structure. In Fig. 3.15, we plot a) the dynamical σ_d and b) structural σ_s errors for different values of the parameter α in $T(\mathcal{B}_\alpha|\mathcal{A}_{1-\alpha})$. Note how the accuracy of the transformations is enhanced by T_1 for any value of α, and it is associated to a decrease in the structural error, thus validating the main assumptions of our approach.

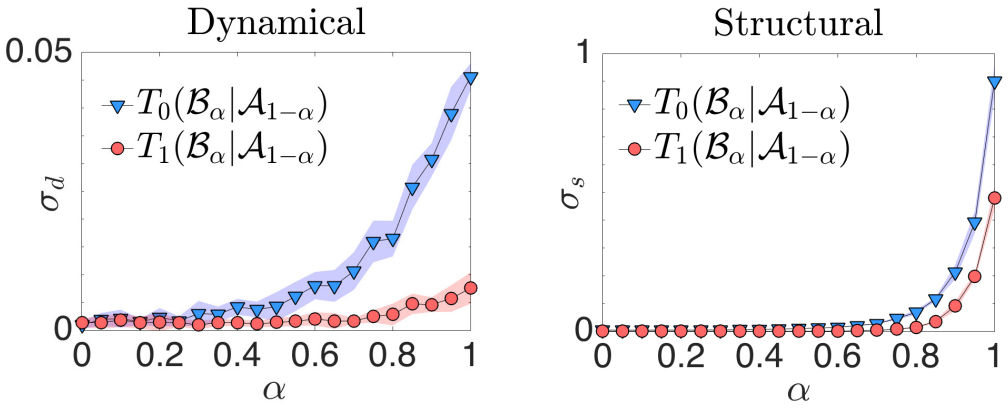

Figure 3.15: a) Dynamical (left) error curves for $T_0(\mathcal{B}_\alpha|\mathcal{A}_{1-\alpha})$ and $T_1(\mathcal{B}_\alpha|\mathcal{A}_{1-\alpha})$, averaged over 100 independent network instances for each α (standard deviations fall in the shaded region). In b) right, associated structural error curves (standard deviations are of the size of the symbols and the values of σ_s are properly normalized). Reprinted by permission of [162].

Last, we further support these results using an analytical argument. Our extended mean-field ansatz is equivalent to consider that the ratio between the local and global order parameters is not simply given by the zero-order input strength (or degree) as in [102, 103] but by a more general property of the node, that is a function of M-orders of input strengths, where each term is weighted by an unknown coefficient α_k. Explicitly,

$$r_i \approx (\sum_{k=0}^{M}\alpha_k s_i^{(k)})r, \tag{3.59}$$

where $s_i^{(k)}$ is the input strength of order k, defined as $s_i^{(0)} = \sum_j a_{ij}$, $s_i^{(1)} = \sum_j a_{ij}s_j^{(0)}$ and so on, and the α_k are unknown coefficients. Note that if $\alpha_0 = 1$ and all the rest are zero, we recover the previous mean-field solution. The only condition that we impose is that $\alpha_k s_i^(k) \gg \alpha_{k+1}s_i^{(k+1)}$, i.e. it is a decreasing function of the order k. By using this ansatz and following the results presented in 2.2, one obtains

$$\lambda_c \approx K_c\frac{\sum_{k=0}^N \alpha_k\langle s^{(k)}\rangle}{\sum_{k=0}^N \alpha_k\langle s^{(k+1)}\rangle}, \tag{3.60}$$

where $K_c = 2/(\pi g(0))$. We can compute the difference in the critical strength $\Delta\lambda_c$ among networks A and B as

$$\Delta\lambda_c \approx K_c \frac{\sum_n \sum_m \alpha_n \alpha_m (\langle s_A^{(n)} \rangle \langle s_B^{(m+1)} \rangle - \langle s_A^{(n+1)} \rangle \langle s_B^{(m)} \rangle)}{\sum_n \sum_m \alpha_n \alpha_m \langle s_A^{(n+1)} \rangle \langle s_B^{(m+1)} \rangle}. \tag{3.61}$$

Assuming that $\alpha_k s_i^{(k)} \gg \alpha_{k+1} s_i^{(k+1)}$ we can approximate this expression by keeping only the dominant terms, i.e. the ones with α_0^2. Imposing also that the zero-order constraint is fixed in both networks, $\langle s_A^{(0)} \rangle = \langle s_B^{(0)} \rangle$, we obtain

$$\Delta\lambda_c \approx K_c \frac{\langle s^{(0)} \rangle}{\langle s_A^{(1)} \rangle \langle s_B^{(1)} \rangle} (\langle s_B^{(1)} \rangle - \langle s_A^{(1)} \rangle). \tag{3.62}$$

At first approximation, the resulting expression shows that the error in the critical threshold scales with the differences of average first-order strength, thus confirming the origin of the inaccurate mapping from homogeneous networks to heterogeneous ones. We have checked that this expression approximately matches the error between the curves around the observed in Fig. (3.13) and in Fig. (3.14), but we leave the analysis of its validity for further work.

In any case, the proposed approach to the mapping problem is by no means the definitive solution. In the current setting, there are several ways to improve the method, for instance *i)* by considering higher-order constraints ($M > 1$), but then the system would become coupled, and it should be solved simultaneously for all nodes, *ii)* allowing the presence of negative interactions or indistinguishable units (without labelling the nodes in the transformation), and also *iii)* imposing global constraints instead of local ones, which may require costly numerical methods and global objective functions [42]). However, our results indicate the need for better constraints that exploit both the structural and dynamical information from the system (the network and the frequencies of the oscillators). In the following pages, we will comment on some interesting directions that can lead to an improvement of the previous results, including our geometric unfolding of the synchronized state, a novel technique that it is introduced in the next chapter.

3.5 SUMMARY AND DISCUSSION

In this chapter, we have studied three theoretical problems on oscillator networks that allowed us to introduce different sources of uncertainty in the network structure and to predict the range of collective behaviors induced by these noisy sources. Besides the applicability of our results in realistic scenarios of imperfect information, the methods developed in this chapter have enhanced our fundamental understanding of the interplay between structure and dynamics in oscillator networks. A brief summary and discussion of the main results are given as follows.

In section 3.2 we have wondered about the critical range in the presence of uncertainty on the coupling weights of the network. By means of novel developments of error propaga-

tion techniques for network dynamics, we have characterized the non-linear amplification of noise from the microscopic interactions to the macroscopic properties of the system as the synchronization onset (which is controlled by the inverse of the largest eigenvalue of the adjacency matrix). Analytical, closed form results have been derived for the critical statistics of random heterogeneous networks, and we have shown that particular structures, such as scale-free networks with a scaling exponent of three, are able to maximize the critical range. These results are relevant to problems of adaptation and evolution in biological systems [218–220], specially considering the ubiquity of scale-free networks [2, 55, 66] and the well established hypothesis that brain networks are operating near critical points [6, 15, 183, 221]. From the methodological side, this formalism represents a first step towards the analysis of error propagation in network dynamics, which we conjecture will receive more attention in the future due to the increasing amount of data (not free of errors), that is being collected for a large variety of systems.

In section 3.3 we have switched our focus from noisy weights to higher-order interactions, and from the critical to the strongly synchronized regime. We have wondered about the effect that different interaction patterns (pair-wise vs. three-body) have on the dynamical range and the optimization of synchrony in spatially embedded and random networks. By means of a composite Laplacian framework and a detailed spectral analysis, we have revealed that both optimal synchronization and dynamical range can be enhanced by the presence of higher-order interactions. This phenomenon stems from the broadening of the Laplacian spectra as three-body interactions are strengthened. The self-regulatory mechanism of interaction strengths described in this section is relevant to the analysis of adaptive biological systems like the brain, where there is an increasing evidence that interactions beyond pair-wise ones and the concept of dynamical range [183, 219] play an important role in memory and other cognitive processes [138, 206, 207]. From a theoretical standpoint, these results represent a first step on the analysis of optimal synchronization in the emergent field of dynamics on hyper-graphs or simplicial complexes [139].

Finally, in section 3.4 we have considered a functional mapping of networks via weight-tuning transformations. We have shown that different structures can have an invariant dynamical response and that this invariance can be approximately achieved by exploiting the structure at the surroundings of the nodes, in a decentralized manner. In particular, we have solved the weight-tuning optimization using a maximum entropy principle under extended mean-field constraints, deriving analytical expressions for the transformed weights depending on the amount of accessible information from the network. We have found that heterogeneous networks, as scale-free ones, are more difficult to map than homogeneous ones, specially around the critical point, due to the impossibility to satisfy the structural constraints posed by the hubs. This result connects with the findings of section 3.2, confirming that scale-free networks have a larger dynamical range with respect to random, homogeneous, ones. Overall, we showed that by locally tuning the weights, networked systems can adapt to different configurations and show distinct behaviors, including a shift in the synchronization onset or a change in the synchronization profile, although the range of behaviors is critically bounded by the structural constraints of the network. These

results may be of interest when designing or controlling artificial and biological neural systems, where the mechanisms of back-propagation [25] and synaptic plasticity [21, 22] are specific weight-tuning transformations that allow the neuronal circuits to learn and to adapt their response to a changing environment. However, a more relevant result has been to unveil the potential of exploiting local information to navigate in global optimization problems.

There are several limitations faced by the proposed methods of the chapter. As explained, the three problems are tackled with heuristic and approximate tools that rely on several mean-field and spectral tricks. In the problem of critical range, the current methodology should be improved by taking into account correlations in the structure, such as clustering and modularity [2]. Also, the presence of large amount of noise and negative weights should be studied in detail, since these are prevalent conditions in brain networks [43, 205]. In the end, the critical range depends on the fluctuations of the largest eigenvalue of the adjacency matrix, and more sophisticated tools are required to describe these spectral fluctuations by exact means. Up to date, the spectral theory of complex networks is still at its infancy [203, 222–224] and many key results await to be found. Similarly, in the higher-order problem, the spectra of the Laplacian determines the dynamical range, but it is not well understood how particular network constraints or local perturbations affect these spectral properties [118, 130], and consequently the dynamics of the system. Additionally, current results should be extended by optimizing other collective regimes beyond the strongly synchronized one and by considering a variety of networks wider than random and geometric ones. Finally, in the mapping problem, the heuristic method should be improved by imposing more informed constraints [32], i.e. prior guesses based also on dynamical information (as the oscillator frequencies), or more ideally, exact objective functions. In fact, some further works that explore this mapping problem by more rigorous means have showed up recently, when working in reaction diffusion systems [225] or in the same Kuramoto case using convex optimization black-boxes [135]. These works confirm some of our results, as the presence of structural constraints that bound the mapping in positive-weighted networks, in a research line that attempts to advance towards a general theory of functional control in complex networks [44, 69, 131, 135, 162, 226].

Overall, the results presented in this chapter illustrate that the addition of uncertainty on the structure can induce non-trivial effects on the dynamical range of the system at hand. We have explained some of these effects using several mean-field shortcuts that allowed us to analytically solve (sometimes under strong approximations) quite ambitious problems that require global information contained in the network spectra and the usage of numerical methods and black-boxes that are difficult to interpret. In the following chapter, we are able to present a novel mathematical tool, the geometric unfolding of the synchronized state, that, fortunately, will allow us to approach these types of problems under a more rigorous framework and to explicitly work with partial, incomplete information. The lack of information captures a key feature of many biological and engineered systems: the fact that units operate using only decentralized information and are subjected to noise.

4

ON THE GEOMETRY OF THE SYNCHRONIZED STATE

4.1 INTRODUCTION

The solution to the phase-locking, synchronized state in a network of coupled heterogeneous oscillators is an excellent framework to study the interplay between structure and dynamics in a complex system. In section 2.3 we already introduced the derivation in the context of the synchrony alignment framework, and in section 3.3, we exploited its properties to explain the role of higher-order interactions in optimal synchronization. This framework finds applications in a broader variety of synchronization problems, including the prediction of phase-locking loss [44], the control of specific dynamical patterns [69] and the inference of the unknown structure from the observed stationary response [164]. The synchronized state also shows up beyond the realm of coupled oscillators, in the context of consensus dynamics [99] or the theory of electric circuits [182], and in problems of signal processing on network domains [227], where the synchronized state can be seen as the output of a filtering process. The network acts as a diffusive filter that transforms the input signal of the nodes (the microscopic dynamics or frequencies of the oscillators, in our context) into the observed stable response (our synchronized state).

The standard way to solve the strong phase-locking problem in an arbitrary network is by using the spectral properties of the network, via the singular value decomposition of the Laplacian pseudo-inverse object [118, 181]. This decomposition requires the usage of numerical methods, which for large networks can translate into high computational costs. Also, the analysis of the subtle interplay between the structure and dynamics and the interesting properties that emerge in optimal configurations can only be observed *a posteriori*, from the outcome of these numerical schemes that are usually treated as black-boxes [118, 135, 159, 225]. In other words, to compute and interpret the synchronized state one usually exploits global information of the network, which is not available at the level of the nodes. In fact, having access to partial –incomplete– information from the structure is a common constraint in both artificial and biological neuronal circuits and in the decentralized power-grid, as discussed in the introduction of this thesis. It remains unsolved how the synchronized state can be estimated in these conditions of network uncertainty, and how the global –spectral– information contained in the synchronized state can be decomposed into smaller pieces of partial or local information.

Motivated by the previous limitations, in this chapter we propose an alternative, geometric approach to compute the synchronized state in arbitrary networks of heterogeneous oscillators, without exploiting the spectral information of the system. More concretely, we will see that the steady-state solution of the linearized synchronization dynamics may be written as a geometric series whose subsequent terms represent different spatial scales of the network. In particular, each addition term in the proposed expansion incorporates contributions from wider network neighborhoods, providing a spatial and multi-resolution description of the state. This analytical tool will be used to obtain a decentralized, fast and accurate computation of the synchronized state up to a desired degree of accuracy (or amount of available information) and to unveil interesting analytical insights that deepen our understanding of the interplay between structure and dynamics in network synchronization problems and beyond. Results presented in this chapter are mainly based on the published work:

- "Geometric unfolding of synchronization dynamics on networks", L. Arola-Fernández, P. S. Skardal and A. Arenas, Chaos 31, 061105 (2021).

In the paper, the mathematical results were introduced in a rigorous manner, but the exploration of the potential usages of the proposed machinery was rather concise. In this thesis, we take the opportunity to explore the nuances of the geometric unfolding of network synchrony, justifying the relevance and implications of our results in related problems, as the ones introduced in the previous chapter, and the potential applications in more depth. The reader will have to wait until the next chapter to find a last proof of concept that demonstrates the utility of this novel geometric approach.

4.2 GEOMETRIC UNFOLDING OF SYNCHRONIZATION DYNAMICS

We recall that the strong synchronized state is the solution to the linearized dynamics of a system of coupled phase-oscillators, captured by a coupled forced-diffusion system with the set of equations

$$\dot{\theta}_i = \omega_i + K \sum_{j=1}^{N} a_{ij}(\theta_j - \theta_i). \tag{4.1}$$

After some considerations discussed in detail in section 2.3, one ends up with a simple linear system, that in matrix form reads as

$$\omega = L\theta. \tag{4.2}$$

Eq. (4.2) expresses the stationary relation between the microscopic dynamics of the units (the frequencies in the ω vector) and the actual phases (the θ vector) via the Laplacian matrix of the network, $L = D - A$, where D is a diagonal matrix with the in-degrees or in-strengths of the nodes, i.e. $D_{ii} = k_i = \sum_{j=1}^{N} a_{ij}$. We recall here that, since the matrix L has zero row sum, it has a trivial eigenvalue $\lambda_1 = 0$ with a constant associated eigenvector $v_1 \propto 1$, and therefore it is singular and not invertible [2, 118]. Moreover, this spectral property reveals an important physical characteristic of the system, namely that the dynamics

are invariant to a constant shift to the phases, i.e., translation along the synchronization manifold defined as the span of the trivial eigenvector v_1. Thus, while solutions to the underdetermined system of Eq. (4.2) are not unique, that which minimizes the norm $||\theta||$ is likely the most useful and is given by

$$\theta^* = L^\dagger \omega, \tag{4.3}$$

where $L^\dagger$ is the Moore-Penrose pseudo-inverse of the Laplacian matrix [181] introduced also in more detail in Section 2.3. Importantly here, the reader should note that to write down the exact pseudo-inverse, one requires a full spectral or singular value decomposition of the Laplacian matrix (i.e., global information of the network). For the general case of a directed network, the pseudo-inverse can be computed via the singular value decomposition of L as [129]

$$L^\dagger = \sum_{n=2}^{N} \frac{v_n u_n^T}{\mu_n}, \tag{4.4}$$

where $0 < \mu_2 \leq ... \leq \mu_N$ are the $N-1$ singular values of L and $\{v_n\}$ and $\{u_n\}$ are the set of right and left singular vectors. Note that for the particular case of undirected networks, the singular values are given by the eigenvalues of L and the left and right singular vectors are given by the eigenvectors of L, so $L^\dagger$ is defined by its eigenvalue decomposition.

Our main goal here is to solve Eq. (4.2) without using the Moore-Penrose pseudo-inverse, or equivalently without exploiting the global –spectral– information of the system. To achieve this goal, it is better to focus our attention more directly on L. First, using $L = D - A$, we write

$$L = D(I - D^{-1}A). \tag{4.5}$$

While D is invertible (assuming that the network is connected and thus each node has some positive degree), $(I - D^{-1}A)$ is not. This can be seen by noting that $D^{-1}A$ is a stochastic, row-sum matrix, and therefore has a leading eigenvalue $\lambda_1 = 1$. Then $I - D^{-1}A$ has a zero eigenvalue, making it singular. However, replacing $D^{-1}A$ with matrix X that yields $(I - X)$ invertible, we have that

$$[D(I - X)]^{-1} = (I - X)^{-1}D^{-1}. \tag{4.6}$$

Moreover, the matrix $(I - X)^{-1}$ may be expanded in the geometric series

$$(I - X)^{-1} = \sum_{m=0}^{\infty} X^m. \tag{4.7}$$

The issue now arises that X cannot be replaced by $D^{-1}A$, or more specifically, we have that

$$[D(I - D^{-1}A)]^{-1} \neq \sum_{m=0}^{\infty} (D^{-1}A)^m D^{-1}, \tag{4.8}$$

namely, on the left-hand side the inverse is ill-posed, and this is reflected by the fact that the series on the right-hand side diverges. However, this does not rule out the possibility

of the right-hand side converging when it is applied to a vector of particular form. In fact, under the relatively mild conditions of the network having a primitive adjacency matrix, when the series is applied to an appropriately shifted frequency vector ω, the right-hand-side does converge and yields a solution to Eq. (4.2), which leads to the formulation of our first main result for undirected networks.

Theorem 1 (Convergence of the geometric series for undirected networks) *Consider an undirected network with primitive adjacency matrix A and a frequency vector ω with zero mean, i.e., $\langle \omega \rangle = 0$. Then, the infinite series*

$$\phi = \sum_{m=0}^{\infty} (D^{-1}A)^m D^{-1}\omega, \tag{4.9}$$

converges.

Proof 1 *We begin by denoting the symmetric normalized adjacency matrix as $B = D^{-1/2}AD^{-1/2}$. Since A is symmetric, so is B, and therefore its normalized eigenvectors $\{v_j\}_{j=1}^{N}$ form an orthonormal basis for $\mathcal{R}^N$. Moreover, since A is primitive, that is, there exists some integer $M > 0$ such that A^M is strictly positive (note that this is equivalent to A being both irreducible and aperiodic), so is B. The Perron-Frobenius theorem [2] then implies that B has a single largest eigenvalue λ_1 that is real and larger in magnitude than all other eigenvalues, i.e., $\lambda_1 > |\lambda_j|$ for $j = 2, \ldots, N$. Moreover, since B is normalized, we have $\lambda_1 = 1$ and $|\lambda_j| < 1$ for $j = 2, \ldots, N$. Finally, the leading eigenvector associated with the leading eigenvalue $\lambda_1 = 1$ has entries that are proportional to the square root of the degrees of the respective nodes, i.e., $v_1 \propto k^{1/2}$.*

Next, it is useful to define

$$\phi_m = D^{-\frac{1}{2}} B^m D^{-\frac{1}{2}} \omega, \tag{4.10}$$

so that the right-hand-side of Eq. (4.9) is given by $\sum_{m=0}^{\infty} \phi_m$. Defining the vector $x = D^{-\frac{1}{2}}\omega$, we now expand x via the orthonormal basis of eigenvectors of B, namely,

$$x = \alpha_1 k^{\frac{1}{2}} + \alpha_2 v_2 + \ldots + \alpha_N v_N, \tag{4.11}$$

where $\alpha_i = \langle x_i, v_i \rangle$ are the coefficients given by projections of X onto the different eigenvector directions and we assume that the eigenvector $v_1 = k^{1/2}$ is also appropriately normalized. Inserting Eq. (4.11) into Eq. (4.10) yields

$$\begin{aligned} D^{\frac{1}{2}}\phi_m &= B^m x \\ &= \alpha_1 \lambda_1^m k^{\frac{1}{2}} + \alpha_2 \lambda_2^m v_2 + \ldots + \alpha_n \lambda_n^m v_n. \end{aligned} \tag{4.12}$$

Note now that for terms $j = 2, \ldots, N$, λ_j^m decays geometrically while $\lambda_1^m = 1$. However, we now show that the coefficient α_1 must be zero. To see this, recall that the natural frequency vector has mean zero, or in other words, ω is orthogonal to the constant vector 1, i.e., $\langle 1, \omega \rangle = 0$. This is equivalent to $\langle D^{1/2}1, D^{-1/2}\omega \rangle$, or more simply, $\langle k^{1/2}, x \rangle = 0$, which is precisely α_1. Thus,

$$D^{\frac{1}{2}}\phi_m = \alpha_2 \lambda_2^m v_2 + \ldots + \alpha_n \lambda_n^m v_n. \tag{4.13}$$

The convergence of the right-hand-side of Eq. (4.9) now follows quite easily: since each of the finitely-many series $\sum_{m=0}^{\infty} \alpha_j \lambda_j^m v_j$ converges to $\alpha_j v_j / (1 - \lambda_j)$ for $j = 2, \ldots, N$, we have that the full series converges to

$$\begin{aligned} \phi &= D^{-1/2} \sum_{m=0}^{\infty} D^{1/2} \phi_m \\ &= D^{-1/2} \sum_{m=0}^{\infty} \sum_{j=2}^{N} \alpha_j \lambda_j^m v_j \\ &= D^{-1/2} \sum_{j=2}^{N} \frac{\alpha_j v_j}{1 - \lambda_j}, \end{aligned} \tag{4.14}$$

which concludes the proof.

The reader should note that we have only proved convergence of the proposed expansion, but we have not proved that the expansion converges to the solution of the synchronized state. We provide here an additional argument to support the fact that the expansion converges to the synchronized state. First, since we are considering undirected networks here and the Laplacian L is symmetric and $L1 = 0$. Then, we can apply a standard rank-one correction to the Laplacian matrix and write the pseudo-inverse in the form

$$L^{\dagger} = (L + \tau J)^{-1} - \frac{1}{\tau N^2} J, \tag{4.15}$$

where $J = 11^T$ is a rank-one matrix of all ones and τ is a real parameter that can take an arbitrary value different from 0. By defining the modified matrix $A' = A - \tau J$ and rearranging the first term, we can write

$$L^{\dagger} = (I - D^{-1} A')^{-1} D^{-1} - \frac{1}{\tau N^2} J. \tag{4.16}$$

When τ is set small and positive, the spectral radius (and the norm) of $D^{-1}A'$ is smaller than one. This can be proved by applying first-order perturbation theory to the leading eigenvalue of $D^{-1}A$, showing that, when $\tau > 0$, the perturbed eigenvalue always decreases. We will omit this calculation here for the sake of simplicity, but assuming that $\rho(D^{-1}A') < 1$, Eq. (4.9) admits a geometric expansion in terms of a convergent series. Using the definition of the series, we can write

$$L^{\dagger} = \sum_{m=0}^{\infty} (D^{-1} A')^m D^{-1} - \frac{1}{\tau N^2} J. \tag{4.17}$$

We are interested in Eq. (4.3), where the matrix $L^{\dagger}$ is applied to the vector ω, which has zero mean. Since J is the matrix of all ones, the product $(1/\tau N^2) J\omega = 0$ for any value of τ and we can already neglect this term. On the other hand, the value of τ can be set arbitrary small and, in the limit of $\tau \to 0^+$, we can finally approximate Eq. (4.3) as

$$\theta \approx \sum_{m=0}^{\infty} (D^{-1} A)^m D^{-1} \omega. \tag{4.18}$$

Eq. (4.18) shows how the proposed expansion converges to a solution of the linear system Eq. (4.2). However, even if the infinite series applied to the zero-mean vector ω converges to a solution of our system, it does not necessarily converge to the minimum norm solution given by Eq. (4.3), which turns out to be the zero-mean solution obtained by the Moore-Penrose pseudo-inverse approach. This can be seen, for instance, by noting that at initial truncation of the geometric series we have that $\langle \phi_0 \rangle = \langle \omega / k \rangle$, which is not necessarily zero. However, this issue can be fixed by simply applying a constant shift to the resulting vector to ensure that it is orthogonal to the constant eigenvector v_1 and the solution converges to the one with minimal norm. This correction leads us to a generalization of our main result, which importantly applies to both undirected and directed networks.

Theorem 2 (Convergence of the geometric series: General case) *Consider a network with primitive adjacency matrix A. Then, the infinite series*

$$\phi = \sum_{m=0}^{\infty} \left(\phi_m - \langle \phi_m \rangle \right), \tag{4.19}$$

where

$$\phi_m = (D^{-1}A)^m D^{-1}\omega, \tag{4.20}$$

converges.

Proof 2 *Rather than making use of the symmetric normalized adjacency matrix, as in the Proof of Theorem 1, here we use the more classically stochastic matrix $D^{-1}A$. However, this matrix shares similar properties with its symmetric counterpart, namely, because A is primitive, then so is $D^{-1}A$, and the Peron-Frobenius theorem guarantees similar eigenvalue properties, namely there is a single largest eigenvalue λ_1 that is real and larger in magnitude than all other eigenvalues, i.e., $\lambda_1 > |\lambda_j|$ for $j = 2, \ldots, N$. Also, since $D^{-1}A$ is stochastic, $\lambda_1 = 1$ and $|\lambda_j| < 1$ for $j = 2, \ldots, N$. On the other hand, the leading eigenvector is now given by the constant vector $v_1 \propto 1$. Importantly, since $D^{-1}A$ is not symmetric (even if A is), the eigenvectors are not orthogonal to one another and cannot be used to form an orthonormal basis for $\mathbb{R}^N$. Nonetheless, we may use these eigenvalues as a (non-orthogonal) basis for $\mathbb{R}^N$ and uniquely expand the vector $x = D^{-1}\omega$ using this basis, specifically*

$$x = \sum_{j=1}^{N} \alpha_j v_j. \tag{4.21}$$

We then look at each eigenmode $j = 1, \ldots, N$ of the term ϕ_m, namely $\phi_m^{(j)} = \alpha_j (D^{-1}A)^m v_j$ so that $\phi_m = \sum_{j=1}^{N} \phi_M^{(j)}$. In terms of the full expression for ϕ, we then have that

$$\begin{aligned} \phi &= \sum_{m=0}^{\infty} \sum_{j=1}^{N} \left(\phi_m^{(j)} - \langle \phi_m^{(j)} \rangle \right) \\ &= \sum_{j=1}^{N} \sum_{m=0}^{\infty} \left(\phi_m^{(j)} - \langle \phi_m^{(j)} \rangle \right). \end{aligned} \tag{4.22}$$

We now treat the contribution of each eigenmode separately. We begin with the eigenmodes $j \geq 2$ for which $|\lambda_j| < 1$. First, we have that

$$\phi_m^{(j)} = \alpha_j (D^{-1}A)^m v_j = \alpha_j \lambda_j^m v_j, \tag{4.23}$$

and

$$\langle \phi_m^{(j)} \rangle = \langle \alpha_j \lambda_j^m v_j \rangle = \alpha_j \lambda_j^m \langle v_j \rangle, \tag{4.24}$$

so together we have that

$$\begin{aligned} \sum_{m=0}^{\infty} \left(\phi_m^{(j)} - \langle \phi_m^{(j)} \rangle \right) &= \sum_{m=0}^{\infty} \alpha_j \lambda_j^m \left(v_j - \langle v_j \rangle \right) \\ &= \frac{\alpha_j}{1-\lambda_j} \left(v_j - \langle v_j \rangle \right), \end{aligned} \tag{4.25}$$

i.e., each component converges for $j \geq 2$.

To complete the proof, we now show that the $j = 1$ eigenmode, for which $\lambda_1 = 1$, converges. In fact, it turns out that this component has no contribution due to the shift of the mean. As in Eqs. (4.23) and (4.24), we have that

$$\phi_m^{(1)} = \alpha_1 (D^{-1}A)^m v_1 = \alpha_1 \lambda_1^m v_1 = \alpha_1 v_1, \tag{4.26}$$

and

$$\langle \phi_m^{(1)} \rangle = \langle \alpha_1 \lambda_1^m v_1 \rangle = \alpha_1 \lambda_1^m \langle v_1 \rangle = \alpha_1 \langle v_1 \rangle, \tag{4.27}$$

so

$$\phi_m^{(1)} - \langle \phi_m^{(1)} \rangle = \alpha_1 \left(v_1 - \langle v_1 \rangle \right), \tag{4.28}$$

but since $v_1 \propto 1$, i.e., it's constant, we have that $v_1 = \langle v_1 \rangle$ and each term $\phi_1^{(m)} - \langle \phi_1^{(m)} \rangle$ vanishes, which completes the proof.

Before proceeding to discuss the implications and applications of the proposed expansions, we remark that Theorem 2 includes no zero mean condition on the frequency vector nor is it restricted to undirected networks, thus it has a potential usage that is wider than Theorem 1. In Fig. 4.1 we illustrate the goodness of the more general case given by Eqs. (4.19) and (4.20) when applied to random Erdös-Rényi and Scale-Free networks with random allocated frequencies. We truncate the expansion at different neighborhood orders M and compare the approximated solution against the exact one given by Eq. (4.3), showing that, for these network configurations, the approximation is accurate even for small M, and also that the larger dispersion of SF networks with respect to ER ones is well captured by the truncated approximations.

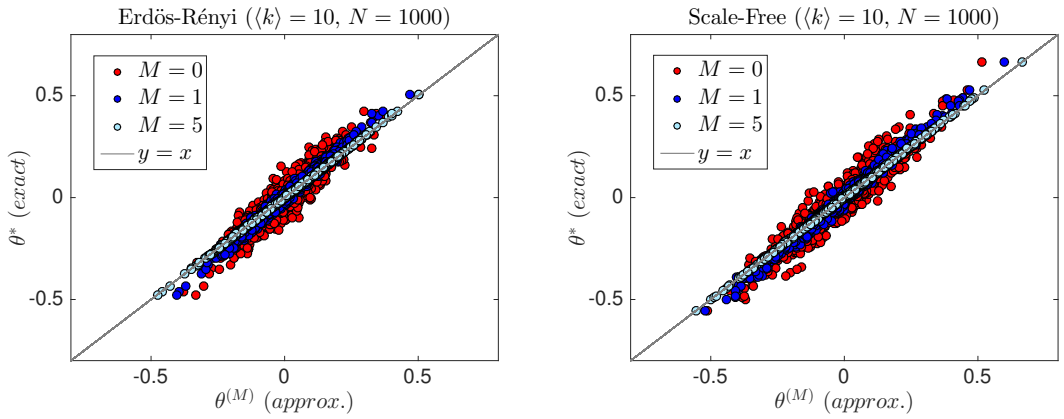

Figure 4.1: Scatter-plot of the exact Eq. (4.3) vs the truncated Eq. (4.19) approximation of the stationary phases in a fixed Erdös-Rényi networks of size $N = 1000$, mean degree $\langle k \rangle = 10$ with a normal distribution of frequencies $\mathcal{N}(0, 1)$ for three different truncation orders.

4.2.1 *Implications of main results*

Now we investigate more deeply the implications of our main results described in Eq. (4.9) and Eqs. (4.19) and (4.20). First, we note that the geometric expansion expresses the solution of the linear system as a sum of contributions of terms $\sim \omega/k$ coming from increasingly further neighborhoods of the nodes. In particular, by explicitly writing the entries of Eq. (4.9) (where we have chosen the undirected case for simplicity here) for the initial truncation orders, we have that

$$\theta_i = \frac{\omega_i}{k_i} + \frac{1}{k_i}\sum_{j=1}^{N} a_{ij}\frac{\omega_j}{k_j} + \frac{1}{k_i}\sum_{j=1}^{N}\frac{a_{ij}}{k_j}\sum_{k=1}^{N} a_{jk}\frac{\omega_k}{k_k} + \ldots \;\; \forall\, i \in 1, \ldots, N. \tag{4.29}$$

From Eq. (4.29), it is clear that the matrix expansion in Eq. (4.9) expresses the steady-state solution of a node in terms of its local properties (the intrinsic frequency ω_i and the input degree or strength k_i), the properties of the first neighbors, second neighbors and so on, with the contributions usually decaying faster as we move further from a node. That is, the m^{th} order term consists of terms ω_j/k_j corresponding to oscillators located precisely m-hops away from a given oscillator. Thus, the series represents the Taylor expansion of the solution expanded around each oscillator, with higher-orders corresponding to larger network neighborhoods. In this sense, it constructs the exact solution by adding infinitely many incremental pieces of local information in a polynomial basis that is not necessarily orthogonal. Interestingly, this differs from the spectral decomposition used for $L^\dagger$ in Eq. (4.3). In the latter, the solution is constructed by adding $N-1$ pieces of global information (i.e. rank-one matrices for each non-zero eigenvalue and its associated eigenvector), analogously to a Fourier expansion that expresses the solution in the basis of orthogonal eigenmodes with its associated eigenfrequencies (which carry global information on the original function, see for instance the works of [117, 227]).

There are several more connections between our method and key results from stochastic processes and network science. First, in the context of Markov chains for random walks in

discrete domains as networks [228], the transition matrix of probabilities P for the random walk is given by the normalized matrix $P = D^{-1}A$ (or AD^{-1}, depending on the definition of the random walk), and the stationary distribution, if it exists, as the vector π, such that $\pi P = \pi$. If the Markov chain is irreducible and aperiodic (the same requirements we had here for our networks to converge), then there is a unique stationary distribution reached as $\lim_{m\to\infty} P^m = 1\pi$. Here $D^{-1}A$ appears in the geometric series because the solution is expressed in terms of "in-neighborhoods" of radius zero, one, two, three, etc., and convergence of the expansion implies that eventually these neighborhoods must include the whole network, i.e. each node must be reachable from each node in a manner that is eventually well-mixed, hence the need for the network adjacency matrix to be irreducible and aperiodic, i.e. primitive [228]. Consider, as a counterexample, a bipartite network such as a star-graph or a one-dimensional ring. These networks are periodic and therefore the Markov chain does not converge to a unique stationary distribution, but oscillates between two possible states because of the presence of a group of nodes connecting only to the other group of nodes, meaning that all nodes cannot be reached at a given iteration of the Markov process (or at a given truncation order of our expansion), which hinders convergence.

Furthermore, the spectral density of the adjacency matrix A can also be expressed in terms of a series expansion of closed walks of order M [229]. In particular, the spectral density $\rho(z)$ is given by

$$\rho(z) = -\frac{1}{n\pi z}\sum_{m=0}^{\infty}\frac{Tr[A^r]}{z^r}, \tag{4.30}$$

where n is the number of nodes (rows or columns) in A. The quantity $Tr[A^r]$ counts the number of walks at a given m-hop, and thus computing the spectral density is equivalent to count number of closed walks returning to the nodes. These calculations can get complicated pretty fast [229], but luckily in our case, the product of the m-neighborhoods matrix powers with the frequency vector (which has zero mean, or the mean is appropriately shifted) make higher-order terms to decay faster to zero compared to initial terms and allow an early truncation of the expansions to be accurate (as we will prove in the following lines). We note that similar expressions to Eq. (4.30) show up when computing network properties as the Katz or Betweenness centrality [2, 230], but to the best of our knowledge, our results are the first ones that exploit the geometric properties of the linear Laplacian system of Eq. (4.2) and apply them to the context of synchronization dynamics of coupled heterogeneous oscillators.

Lastly, it is worthy to remark here that one could tackle the problems relating structural constraints and dynamical range (presented in the previous chapter) by means of truncated expressions of the synchronized state, providing a mechanistic shortcut to spectral *black-boxes*. Particular examples include the possibility to extend the error propagation technique to the phase-locking regime by propagating the error in the weights, which explicitly appear in the geometric series of the synchronized state. Also, the mapping problem could be tackled by using improved, more rigorous constraints, based on the truncation of the expansion at different orders, as the ones given by Eq. (4.29) (thus exploiting dynamical

information in terms of the frequencies, not only structural one as we did in our heuristic approach) and the geometric technique would allow us analyzing the effect of higher-orders from a decentralized perspective. Finally, we note that our results can be extended to the non-linear phase-locked regime by leveraging the Collective Coordinate method (CC) [145, 146], introduced in section 2.4.2. We can combine these results with our proposed geometric expansion, to write an equation that reduces the fully non-linear coupled system of the Kuramoto Model to a single differential equation in terms of collective coordinate parameter α_M, approximated at any resolution level M of available information from the network as

$$\dot{\alpha}_M \approx 1 + \frac{1}{\theta^{(M)T} L \theta^{(M)}} \sum_{i,j} [\theta^{(M)}]_i \sin(\alpha_M([\theta^{(M)}]_j - [\theta^{(M)}]_i)), \tag{4.31}$$

where $\theta^{(M)} = \sum_{m=0}^{M} (D^{-1}A)^m D^{-1}\omega$ is the truncated expansion in the undirected case. For instance, when truncating at the local order $M = 0$, Eq. (4.31) reduces to

$$\dot{\alpha}_0 \approx \frac{\sum_{i,j} \frac{\omega_i}{k_i} \sin(\alpha_0(\frac{\omega_j}{k_j} - \frac{\omega_i}{k_i}))}{\sum_{i,j} a_{ij}(\frac{\omega_i}{k_i} - \frac{\omega_j}{k_j})^2} + 1, \tag{4.32}$$

By setting $\dot{\alpha}_0 = 0$, solving for α_0 and using our local version of the CC ansatz, which states that the phases $\theta_i \approx \alpha_0 K^{-1}\omega_i/k_i$, one can obtain the solution of the phases in the non-linear phase-locking regime at any value of the coupling strength K (which is set to $K = 1$ for simplicity in the rest of this chapter). This shows that the geometric approach can be used to gain analytical insight beyond the linearized regime of synchronization dynamics when dealing with partial, incomplete information from the network structure.

We expect some of the aforementioned problems to be addressed in future work and, now we move to more practical questions regarding the geometric expansions.

4.3 CONVERGENCE ANALYSIS

4.3.1 *Error scaling*

It is time to address a more computationally practical question related to our expansions. We return to the safer realm of the linearized regime controlled by Eq. (4.1) to investigate the rate of convergence of this expansion, to understand how fast can we truncate the expansion to get a desired degree of accuracy in the approximation.

We consider again the case of undirected networks with a frequency vector of zero mean, such that we can use results of Theorem 1. We recall that the M-order approximation defined as $\theta^{(M)} = \sum_{m=0}^{M} (D^{-1}A)^m D^{-1}\omega$. Using Eq. (4.12), the error is given by

$$\begin{aligned} D^{\frac{1}{2}}(\theta^* - \theta^{(M)}) &= \sum_{m=M+1}^{\infty} (\alpha_2 \lambda_2^m v_2 + \cdots + \alpha_n \lambda_n^m v_n) \\ &= \frac{\alpha_2 v_2}{1-\lambda_2}\lambda_2^{M+1} + \cdots + \frac{\alpha_N v_N}{1-\lambda_N}\lambda_N^{M+1}. \end{aligned} \tag{4.33}$$

As the order M of the approximation increases, the dominant term in Eq. (4.33) is that which corresponds to the second largest (in magnitude) eigenvalue λ_2 of the normalized adjacency matrix B (recall that the largest of eigenvalue of B is $\lambda_2 = 1$). If we discard the unlikely scenario where $x = D^{-1/2}\omega$ is exactly orthogonal to v_2 (in which case α_2 vanishes) then for large enough M the mean square error will scale geometrically with the magnitude of this second-largest eigenvalue, i.e.,

$$||\theta^* - \theta^{(M)}|| \sim |\lambda_2|^{M+1}. \tag{4.34}$$

Therefore, the smaller $|\lambda_2|$ is, the quicker the approximation will converge. On the other hand, convergence will be slower for sparse networks with either strong modularity or clustering as well as strong bipartite structure, in which cases λ_2 tend to be close to 1 and -1, respectively [2, 228] and a larger number of terms are needed to obtain a desired level of accuracy. In Fig. (4.2) we plot the error of the truncated approximation depending on the truncation order for different values of the network density, modularity, clustering coefficient and small-worldness and compare against the theoretical scaling predicted by Eq. (4.34) observing a perfect agreement for sufficiently large order M in all the cases.

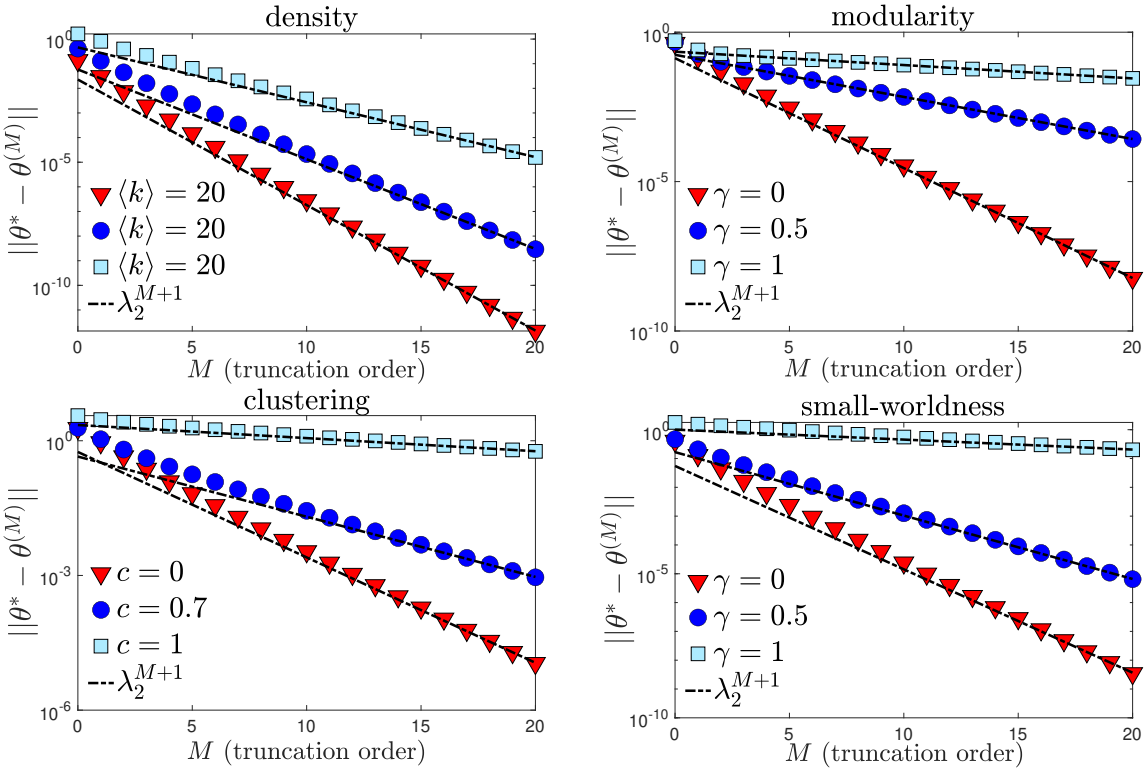

Figure 4.2: Error of the approximation depending on the truncation order for several interpolating network models, with fixed size $N = 1000$. We study the effect of density (varying the average degree), modularity (interpolating from a random network to a 2-modules), clustering (using the algorithm [92] to generate SF networks with controllable clustering) and the small-world model to interpolate between a ring and a random network [54]. In all the scenarios, we observe that, for sufficiently high truncation order M, the error is dominated by λ_2, the second-largest eigenvalue of the normalized adjacency matrix B. λ_2 increases with sparsity, modularity, and clustering as expected. From [231].

The prediction of Eq. (4.34) is clearly accurate for large truncation order M. However, it tells us nothing about the error at lower orders (when taking only a few terms in the expansion) and this situation is very much relevant in contexts of decentralized information, when the information is available only at the surrounding of the nodes. To overcome this issue, in the following lines, we explicitly introduce uncertainty in the allocation of frequencies to obtain closed-form expressions for the error at any truncation order. Interestingly, these expressions will reduce to very short formulas (with a clear interpretation) when considering the local truncation case.

4.3.2 *Closed forms for uncertain dynamics*

Let us introduce a well-known theorem from Probability Theory for Quadratic Forms [165]. Given an operator X and random vector y with mean μ and covariance matrix Σ, the expected value of the quadratic form $y^T X y$ is

$$\langle y^T X y \rangle = Tr[X\Sigma] + \mu^T X \mu. \tag{4.35}$$

This theorem was applied in [165] to compute the squared norm of the exact solution, and from there the linearized synchronization order parameter since $r \approx 1 - ||\theta^*||^2/(2K^2N^2)$. From the exact solution of Eq. (4.3), one can write

$$||\theta^*||^2 = \omega^T (L^\dagger)^T L^\dagger \omega. \tag{4.36}$$

From the spectral decomposition of $L^\dagger$, we have that $L^\dagger = VSV^T$, where S is a diagonal matrix with entries $s_{ii} = \lambda_i^{-1}$ for $2 \leq i \leq N$ and $s_{11} = 0$. V is the matrix with the eigenvectors of L in columns and V^T is its transpose. Plugging it Eq. (4.36), one can write

$$||\theta^*||^2 = \omega^T V S^2 V^T \omega. \tag{4.37}$$

Then, applying Eq. (4.35) with $X = VS^2V^T$, noting that the second term in Eq. (4.35) gets cancelled because $\mu = 0$, and setting $\Sigma = \sigma^2 I$ (valid when the components of ω are drawn independently from the same distribution), one obtains [165]

$$\langle ||\theta^*||^2 \rangle = \sigma^2 N \langle \lambda^{-2} \rangle, \tag{4.38}$$

where $N\langle \lambda^{-2} \rangle = Tr[X]$. Eq. (4.38) tell us that the expected value of the exaction solution increases with the variance of the distribution of ω and with the spectral heterogeneity of the underlying network. The reader should note that we already derived Eq. (4.38) by different means in Eq. (3.35) of the previous chapter. We remark that we have assumed that the entries of ω are independent random variables drawn from a known distribution. This is equivalent to a scenario with uncertainty where we have knowledge on $g(\omega)$ but the specific ω_i are not accessible [165]. Here we consider this scenario and work with expected quantities, thus removing the dependence on the choice of the ω vector.

Having introduced the mathematical machinery, we proceed to apply it to compute the expected error made by the geometric approximations. We define $\phi^M = \langle ||\theta^* - \theta_g^M||^2 \rangle$, as the averaged mean square error between the exact solution θ^* and the truncated one θ^M. In the following, we omit the bracket notation in ϕ^M for simplicity, since we work only with expected errors due to the random frequency allocation. First, we express the error in terms of the spectrum of the normalized adjacency matrix B. From Eq. (4.33), note that we can write

$$\theta^* - \theta_g^M = \sum_{m=M+1}^{\infty} D^{-\frac{1}{2}} B^m D^{-\frac{1}{2}} \omega, \tag{4.39}$$

where B^m is the m-th power of the normalized adjacency matrix defined before. By defining the vector $z = D^{-\frac{1}{2}}\omega$, we can write

$$\theta^* - \theta_g^M = D^{-\frac{1}{2}} (\sum_{m=M+1}^{\infty} B^m) z. \tag{4.40}$$

Again, we write the squared norm of $(\theta^* - \theta_g^M)$ as a quadratic form. Noting that the random vector z has mean $\mu = 0$ and covariance $\Sigma = \sigma^2 D^{-1}$, and applying Eq. (4.35), we have that

$$\phi^M = Tr[(D^{-\frac{1}{2}} \sum_{m=M+1}^{\infty} B^m)^T (D^{-\frac{1}{2}} \sum_{m=M+1}^{\infty} B^m) \sigma^2 D^{-1}]. \tag{4.41}$$

Now, we apply the property of the trace of symmetric matrices $Tr[A, B] = Tr[B, A]$ and use the spectral decomposition $\sum_{m=M+1}^{\infty} B^m = \sum_{m=M+1}^{\infty} U H^m U^T$, with H a diagonal matrix containing the eigenvalues of the normalized adjacency matrix B, i.e. $H_{ii} = \mu_i$, and U is the matrix with the columns populated by its orthogonal eigenvectors. Since z is orthogonal to the leading eigenvector u^N of B because $\langle \omega \rangle = 0$, see [231], this mode will not contribute to the error, and we can set $\mu_N = 0$ for the remaining of the analysis. Then, we can write

$$\phi^M = \sigma^2 Tr[D^{-2} \sum_{m=M+1}^{\infty} (U H^m U^T)^2]. \tag{4.42}$$

Expanding the squares of the sum using the binomial theorem, we get

$$\phi^M = \sigma^2 Tr[D^{-2} U \sum_{m=M+1}^{\infty} m H^{m+1} U^T]. \tag{4.43}$$

Eq. (4.43) is exact but requires computing an infinite sum. Luckily, we can exploit the convergence of the series

$$\sum_{M+1}^{\infty} m \mu_i^{m+1} = (\frac{\mu_i}{\mu_i - 1})^2 [2 - \mu_i^M (M\mu_i - M + 1), \tag{4.44}$$

valid when $|\mu_i| < 1$, as in our case. Defining the diagonal matrix X^M with entries $x_{ij}^M = \delta_{ij} (\frac{\mu_i}{\mu_i - 1})^2 [2 - \mu_i^M (M\mu_i - M + 1)$, we finally obtain

$$\phi^M = \sigma^2 Tr[D^{-2} U X^M U^T]. \tag{4.45}$$

Eq. (4.45) is an exact, analytical expression for the geometric error ϕ^M in terms only of the degrees in D^{-2} and the spectra of B. Note that in the 0-order approximation (local truncation), the entries of the diagonal matrix are simply $x^0_{ij} = \delta_{ij}(\frac{\mu_i}{\mu_i - 1})^2$. From here, it is worth distinguishing between the regular and the heterogeneous degree distribution.

In the regular case $D^{-2} = k^{-2}$, i.e. a constant, and we can write ϕ^0 as a very simple formula given by

$$\phi^0 = \sigma^2 k^{-2} \sum_{i=1}^{N-1} (\frac{\mu_i}{\mu_i - 1})^2. \tag{4.46}$$

Using the affine transformation $\mu_i = 1 - \lambda_i/k$ [117], we can express the result also in terms of the more familiar spectra of L. Explicitly

$$\phi^0 = \sigma^2 k^{-2} \sum_{i=1}^{N-1} (\frac{k}{\lambda_i} - 1)^2. \tag{4.47}$$

Expanding the previous expression, we get the clean result

$$\phi^0 = \sigma^2 N(\langle \lambda^{-2} \rangle + k^{-2} - 2k^{-1}\langle \lambda^{-1} \rangle), \tag{4.48}$$

which can be further approximated by

$$\phi^0 \approx \sigma^2 N[\langle \lambda^{-1} \rangle - k^{-1}]^2. \tag{4.49}$$

Both Eq. (4.48) and Eq. (4.49), and also the more compact expression of Eq. (4.47) tell us that, for networks with homogeneous degree distributions, the local accuracy of the expansion is controlled by the whole spectra of L and not only by a single eigenvalue. In other words, as the eigenvalue spectra broadens with respect to the degree k, the error grows, a result that confirms that random dense networks or, for instance, the all-to-all one (where the eigenvalues are all peaked at $k = N - 1$ [2]) are very *local*, meaning that a low truncation of the expansion will provide accurate results for the synchronized state (in the case of the all-to-all, the local truncation is just exact). Instead, if the whole spectra broadens (and not only one eigenvalue), the accuracy gets reduced, and gradually more global information is required.

For the non-regular case (heterogeneous degree distribution), one cannot explicitly compute the trace $Tr[D^{-2}UX^MU^T]$ in general. Several approaches can be used at this point to approximate this object in an algebraic manner. The straightforward choice is to expand the matrix D^{-2} in a power series, which is valid for small heterogeneity in the degrees. We have that

$$(D^{-2})_{ij} = \delta_{ij} \frac{1}{(\langle k \rangle + \epsilon_i)^2}, \tag{4.50}$$

with $\epsilon_i = k_i - \langle k \rangle$. Then, expanding $D^{-2}(\epsilon)$ around $\epsilon = 0$, we get

$$D^{-2}(\epsilon) \approx \langle k \rangle^{-2} I - 2\langle k \rangle^{-3} \epsilon I + 6\langle k \rangle^{-4} \epsilon^2 I - O(\epsilon^3) + \dots, \tag{4.51}$$

where I is the identity matrix. Now, plugging Eq. (4.51) into Eq. (4.45), decomposing the resulting expression as a sum of traces and approximating the smaller (higher-order) terms by its expectation value $Tr[\epsilon^m X] \approx \langle Tr[\epsilon^m X]\rangle = \langle \epsilon^m \rangle Tr[X]$ (assuming that the components of ϵ^m are random variables), one obtains

$$\phi^0 \approx \sigma^2 N \sum_{n=0}^{\infty} \frac{(-1)^n (n+1)! \sigma_n^2}{\langle k \rangle^{n+2}} [\sum_{i=1}^{N-1} (\frac{\mu_i}{\mu_i - 1})^2], \tag{4.52}$$

where $\sigma_n^2 = \frac{1}{N}\sum_i (k_i - \langle k \rangle)^n$ is the n-th central moment of the degree distribution. Note that $\sigma_0^2 = 1/N$, $\sigma_1^2 = 0$ and σ_2^2 is the variance of the degree distribution. Explicit approximations could be obtained by truncating Eq. (4.54) at a given n.

An alternative approach is to directly approximate the matrix D^{-2} by its average (i.e. approximating the trace in Eq. (4.45) by its expected value), obtaining

$$\phi^0 \approx \sigma^2 N \langle k^{-2} \rangle [\sum_{i=1}^{N-1} (\frac{\mu_i}{\mu_i - 1})^2], \tag{4.53}$$

and then apply the affine transformation $\mu_i \leq 1 - \lambda_i / \langle k \rangle$ to obtain a tight upper-bound. Expanding the resulting expression, one finally obtains

$$\phi^0 \approx \sigma^2 N \langle k^{-2} \rangle (\langle k \rangle^2 \langle \lambda^{-2} \rangle - 2 \langle k \rangle \langle \lambda^{-1} \rangle + 1). \tag{4.54}$$

In the absence of heterogeneity, $\langle k^{-2} \rangle = k^{-2}$ and one recovers Eq. (4.48). Interestingly, we can further approximate Eq. (4.54) assuming small heterogeneity in spectra and degree, which leads to

$$\phi^0 \approx \sigma^2 N [\langle \lambda^{-1} \rangle - \langle k^{-1} \rangle]^2. \tag{4.55}$$

This last result shows how the error in the local truncation is controlled by both the moments of the spectral and degree distributions. Note that, if instead of computing the mean square error of the phases in the local truncation case, we compute the error between the squared modulus (which is equivalent to compute the error in synchrony because $\Delta r^{(M)} \sim ||\theta^*||^2 - ||\theta^M||^2$), following the same tools as before, we obtain that

$$|||\theta^*||^2 - ||\theta^0||^2| = \sigma^2 N |\langle \lambda^{-2} \rangle - \langle k^{-2} \rangle|, \tag{4.56}$$

which tells us that, when the second inverse moment is the same for both the spectra and degrees, the local error is zero. Interestingly, if the degree distribution becomes heterogeneous at the same rate as the spectral one, the local error will still be small, and this is indeed what occurs to random scale-free networks, that have both large heterogeneity in degree and spectra [68], but not to clustered scale-free networks, for which the spectra heterogeneity increases (due to small eigenvalues approaching zero [68, 92]) and in this case the local error grows. A more pronounced effect occurs for homogeneous networks with communities, where the degree of heterogeneity is small, but the spectral broadening is large, and the local error will be even larger, as predicted by Eq. (4.54) and Eq. (4.55).

4.3.3 *Damped harmonic oscillatory decays*

We consider a final point regarding the convergence of the expansions. In particular, we unveil an interesting analogy between the convergence paths of the proposed series and the type of decays in a classical damped harmonic oscillator. This analogy will provide a key insight into the range of microscopic configurations that can be reached by a given structure, therefore advancing in the understanding of structural constraints and dynamical regimes in oscillator networks.

Let us consider first the scenario where frequencies are randomly allocated on the nodes. This means that, in average, there will not be any amount of frequency-frequency correlations among connected nodes, and it is equivalent to say that ω does not have a preferred direction, i.e. it is not aligned with any eigenvector of B in particular while still being orthogonal to the constant eigenvector (due to the constraint $\langle\omega\rangle = 0$). Then, when the truncation order of the expansion is sufficiently large, $(m \gg 0)$, we have that the m-term of the expansion, $\psi^m = (D^{-1}A)^m D^{-1}\omega$ is well approximated by

$$\psi^m \approx D^{-\frac{1}{2}}(\alpha_* \lambda_*^m v_*), \tag{4.57}$$

where again the subscript $*$ accounts for the largest eigenvalue in absolute value (which can be positive or negative). The rest of terms in Eq. (4.33) decay much faster for large m so they can be neglected. The entries of ψ^m can change their sign if $\lambda_* = \lambda_{min} < 0$, because, in this case, $\lambda_*^m > 0$ for odd values of m and $\lambda_*^m > 0$ for even values of m.

The previous observation indicates that, if we study the error in the modulus of the phases (which is a proxy of the synchronization error) insteand of using the mean square error of the vector as in the previous sections, then the convergence path can follow different routes. To see this effect, note that the modulus of the exact solution can be written as $||\phi|| = ||\sum_m^\infty \Psi^m||$. Truncating at a large m, we have that

$$||\phi^m|| = ||\phi^{m-1} + \psi^m||. \tag{4.58}$$

From Eq. (4.57), we see that the difference in modulus $||\phi^m|| - ||\phi^{m-1}||$ can change sign in alternating powers of m (if $\lambda_* < 0$) while decreasing to zero. In other words, the difference in the modulus between the exact solution and the m-order approximation, i.e. $\Delta||\phi||^m = ||\phi^*|| - ||\phi^m||$ can follow different paths of convergence for large m depending on the sign of the largest eigenvalue λ_* (in magnitude).

We can classify the paths between convergent and divergent ones. In the first class, we can distinguish between *i)* the underdamped regime $(-1 < \lambda_* < 0)$, where $\Delta||\phi||^m$ converges to 0 in an oscillatory way (oscillatory decay), *ii*) the overdamped regime $(0 < \lambda_* < 1)$, where $\Delta||\phi||^m$ converges to 0 exponentially, without oscillators (exponential decay) and *iii)* the critically damped regime $\lambda_* \to 0$, where $\Delta||\phi||^m$ converges to 0 as fast as possible (optimal decay). Furthermore, there are two cases where the expansion does not converge: *iv*) the undamped regime $(\lambda_* = -1)$, when the network is completely bipartite (it can be separated in two groups of nodes that connect only to the other group). In this

case, the solution never converges and $\Delta||\phi||^m$ oscillates around 0 indefinitely, and finally *v*) the infinitely damped regime ($\lambda_* = 1$), when the network is completely disconnected in modules. The solution never converges but grows indefinitely due to the mode associated to λ_*, which never decays.

The aforementioned regimes are therefore equivalent to the solutions of the differential equation for a damped harmonic oscillator [8], which universal form is given by

$$\frac{d^2q}{d\tau^2} + 2\zeta\frac{dq}{d\tau} + q = 0. \tag{4.59}$$

Here, the leading eigenvalue of the normalized adjacency matrix λ_* plays the role of the damping ratio ζ, the error in the approximation $\Delta||\psi||^m$ is our q and instead of differentiating over time, here we do it over increasingly further neighborhoods m. We have explained that for a large truncation order, λ_* will determine the type of decay of the system if frequencies are randomly allocated. However, if λ_* is not very close to one in magnitude or if the frequency vector is not specifically aligned with its associated eigenvector v_*, then convergence will be very fast ('critically-damped') for most configurations and its decay will be determined by the combination of the eigenmodes in Eq. (4.33). The system will only show the fingerprint of strongly exponential or oscillatory decay for lower truncation order M when $\alpha_*\lambda_*$ is sufficiently large in magnitude compared to the rest of terms in Eq. (4.33), so depending both on the structure (via λ_*) and on how the frequencies are allocated (via the coefficient α_*).

The previous observation is of a technical nature, although the classification of microscopic configurations using the signature given by its convergence path in the geometric domain seems a promising line of thought. In fact, we can exploit this idea by noting that the spectral gap $\Delta\lambda_* = \lambda_{max} - \lambda_{min}$ –if the eigenvalue $\lambda_N = 1$ is not considered– constrains the possible range of decays that a given system can show. Furthermore, depending on how the frequencies are allocated (so depending on the specific values of the coefficients α), one can go from the maximal oscillatory to the maximal exponential decay that are permitted by the spectral gap of the underlying structure. This effect, in turn, translates into a constrained range of synchronized behaviors. To see this, one returns to the local construction given by the geometric expansion in Eq. (4.29), and realizes that having an oscillatory (exponential) decay in the real space is equivalent to having negative (positive) frequency correlations among connected neighbors. Since the type of decay is constrained by the spectral gap $\Delta\lambda_*$ of the underlying structure, the range of dynamical correlations (frequency-frequency correlations among neighbors) is also constrained by the same spectral gap. In other words, the spectra of the normalized adjacency matrix, and the magnitude of the largest negative and positive eigenvalues determine the range of convergence paths, which in turn bound the amount of dynamical correlations among neighboring nodes in an oscillator network, and this effect also determines the range of synchronized states. Overall, the previous connection shows how the shape of the network bounds the range of phase-locking states, in terms of some spectral properties, and the well-known types of decay in a classical damped oscillator provide a geometric interpretation, and a classification of these results.

In order to clarify the reasoning above, we choose a particularly simple network model. We consider a stochastic block model with two groups, where connections inside the groups are assigned with probability p_+ and connections between the groups with probability p_-. The random network model [81, 82] is recovered when $p_+ = p_- = p$, and the all to all is reached in the limit of $p = 1$. A modular-like network (bipartite-like) is obtained when $p_+ > p_-$ ($p_- > p_+$), leading to a disconnected network of two groups if $p_- = 0$ and a purely bipartite if $p_+ = 0$. We also introduce a measure to capture the dynamical correlations in the system. A straightforward choice is to use the smoothness of the network [227], given by the positive-semi-definite quadratic form $S = \omega^T L \omega$ which can be explicitly written as

$$S = \sum_i \sum_j a_{ij}(\omega_j - \omega_i)^2. \tag{4.60}$$

If we normalize S by the number of links $\sum_i \sum_j a_{ij}$, such that $\hat{S} = S/(N\langle k \rangle)$, we have that $\hat{S} = \langle \Delta\omega^2 \rangle$ is just the average squared difference of frequencies among connected nodes. If the frequencies ω are drawn from a normal distribution, $\hat{S}$ for the all-to-all network or in absence of frequency correlations is the mean of a chi-squared variable with one degree of freedom, so $\hat{S}_0 = 1$. If a given system has $1/\hat{S} > 1$, we have positive correlations and $1/\hat{S} < 1$ means negative correlations. Note that if the original distribution of frequencies is not normal (and even not unimodal or symmetric), we can always compare a given amount of dynamical correlations against its random counterpart.

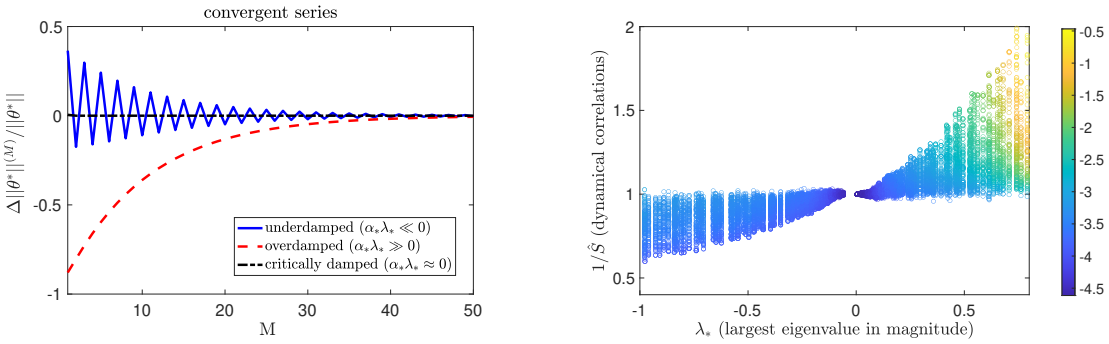

Figure 4.3: Left: relative error of the modulus depending on the truncation order M in three networks generated from our model: an extremely bipartite one with negative frequency negative correlations –underdamped– ($p_+ = 0.1, p_- = 0.9, \omega \sim v_1$), an extremely modular one with frequency positive correlations –overdamped– ($p_+ = 0.9, p_- = 0.1, \omega \sim v_N$), and a random network without frequency correlations –critically damped– ($p_+ = 0.5, p_- = 0.5, \omega \sim \mathcal{N}(0,1)$). Right: dynamical correlations depending on the largest eigenvalue of B, λ_* for frequency allocations ranging from $\omega \sim v_*$ to $\omega \in \mathcal{N}(0,1)$, thus interpolating from maximal correlations to no correlations, preserving the variance σ^2, for 10^3 networks generated with different $p_+, p_- \in (0,1)$. The center ($\lambda_* = 0$) is the all-to-all network, where no correlations are possible regardless of the particular alignment of ω. The color indicates the logarithm of the squared norm of the phases of the system, such that higher (lower) synchronization is captured with blue (yellow) colors.

In Fig. (4.3)-left, we can see the three examples of convergent paths depending on the underlying network and the frequency allocation (see caption). In the right figure, we can observe that, for the particular block-model that we considered, the region of accessible

dynamical correlations is clearly bounded by the spectra of the network, and in turn, the degree of synchronization is affected by both axis. In this sense, the synchronization of the system is determined by an effective geometry that emerges from the constrained interplay between the structure and the frequencies. In the following, we discuss these results by going through several well-known network examples.

First, the all-to-all network has the smallest spectral gap $\Delta\lambda_* = 0$ [2]. In this case, the decay will be always optimal (critically damped). In our theory, this means that it is not possible to induce any kind of positive or negative correlations, since every node is connected to the rest. Equivalently, the same synchronized behavior is reached by any rearrangement of the frequencies, as observed in the phase-space of Fig. (4.3)-right, where all configurations in this network collapse to a single point –the origin–, where synchronization is maximal. Second, a random (ER) network has a larger $\Delta\lambda_*$ than the all-to-all case, which increases for smaller density, but it is still quite localized around 0 and symmetric for large p [68, 94, 165]. In this networks one can induce the three different type of decays and some amount of positive and negative dynamical correlations but up to some extent. Third, it is well-known that a scale-free (SF) network has a triangular, symmetric shape of the spectra [68] and a larger $\Delta\lambda_*$ than the random network with the same average degree. From our theory, we can predict that the SF will have a broader dynamical range than the random one. More positive and negative correlations can be generated and the range of synchronized states will also be larger. In this sense, the SF network can be seen as slightly more modular than the random one, and also slightly more bipartite. In general, when some eigenvalues are large in magnitude and of a preferred sign, then the symmetry of the system is "broken" and the network becomes more modular (if $\Delta\lambda_* \gg 0$) or more bipartite (if $\Delta\lambda_* \ll 0$). In these limits, the network will have a tendency to show one specific type of decay. For modular-like networks, the convergence of the geometric expansion will be usually exponential and slow and only positive to random frequency-frequency correlations can be induced. For bipartite-like networks, the convergence will be usually oscillatory and fast and only negative to random frequency-frequency correlations can be induced. These effects can also be observed in (4.3)-right, in terms of the effective cone where the networks can fall in. As a fifth example, we consider spatial embedded networks such as rings, low-dimensional lattices or grids, where the spectral distribution is broad and λ_{min} and λ_{max} are large in magnitude, so $\Delta\lambda_* \approx 2$ [68, 100]. In this case, maximal oscillatory and exponential decay can occur, and equivalently, one can induce maximal positive and negative dynamical correlations among the nodes. For instance, imagine a ring where the frequencies can be placed in alternating order (negative correlations) or smoothly (positive correlations). Intuitively, the network is at the same time modular and bipartite and this can be shown by the fact that the ring has an eigenvalue $\lambda_{min} = -1$ (so it is completely bipartite) and $\lambda_{max} \to 1$ for large size (so it is also extremely modular).

Overall, the results introduced in this section suggest a promising view to analyze oscillator networks in the synchronized state. We presented some introductory points emerging from our convergence analysis, and we expect to follow this line of though in further

works. Now we shift our focus towards more practical applications of the geometric unfolding technique, in the context of decentralized systems.

4.4 THE LOCAL APPROXIMATION OF SYNCHRONY AND ITS APPLICATIONS

In this last section of results, we generate a local approximation from the geometric expansion presented above to describe the degree of synchronization of a system given by the Kuramoto order parameter [38], $re^{i\psi} = N^{-1}\sum_j e^{i\theta_j}$. First, after the linearizing about a strongly synchronized state where all $|\theta_i| \ll 1$ (note that an appropriate shift in initial conditions allows us to set the mean phase $\psi = 0$) one obtains [118] $r \approx 1 - \frac{1}{2K^2N^2}||\theta^*||^2$. Note that the degree of synchronization increases, i.e., tends towards one, as the dispersion in the phases is reduced. By truncating Eq. (4.9) at the first-order term and neglecting the contribution of the shift to the mean, an approximation which is accurate for locally tree-like networks for which $|\lambda_j| \ll 1$ for $j = 2, \ldots, N$, we have that

$$\theta_i \approx \frac{\omega_i}{k_i} + \left\langle \frac{\omega}{k} \right\rangle_i^{(1)}, \tag{4.61}$$

with $\langle \frac{\omega}{k} \rangle_i^{(1)} = \frac{1}{k_i}\sum_{j=1}^{N} a_{ij}\frac{\omega_j}{k_j}$ being the average contribution of the first neighbors arriving at node i. We can then directly write the order parameter as

$$r \approx 1 - \frac{1}{2K^2N^2}\sum_{i=1}^{N}\left(\frac{\omega_i}{k_i} + \left\langle \frac{\omega}{k} \right\rangle_i^{(1)}\right)^2. \tag{4.62}$$

The local unfolding of synchronization dynamics from the geometric expansion that we use to write Eq. (4.62) allows us to gain analytical insight into the interplay between topology and dynamics that improves synchronization as well as understand several features that to date have only been investigated numerically [118, 129, 130, 132, 232, 233].

4.4.1 *Insights on the interplay topology vs dynamics*

We give several observations in this line, included in the following list.

- Degree-frequency correlations. For uncorrelated and sufficiently dense networks, $\theta_i \sim \omega_i/k_i$, thus higher frequencies must be placed in the nodes of higher degree in order to decrease the absolute value of the phases and therefore increase synchronization [108, 129, 232].
- Frequency-frequency correlations. Negative frequency-frequency correlations between connected neighbors tends to make the first order term of opposite sign (but smaller) to the local term, and this reduces the dispersion (increasing synchronization) [118, 129].
- Weight localization. At first-order $\theta_i \approx \omega_i/k_i + \sum a_{ij}(\omega_j/k_j)/k_i$, thus, the sum of the contributions of the neighbors are divided by the node's degree. For denser and

uncorrelated networks, the number of neighbors is higher, and therefore the sum approaches faster to 0, leading, in average, to smaller values of the phases and therefore to a higher synchrony [165].

- Homogeneity vs heterogeneity. Using the local approximation, one can show that $r \approx \langle s^{-2} \rangle$ in the linearized regime, where s are the strengths (or degrees of the nodes). The inverse second moment is larger for homogeneous networks, thus homogeneity promotes synchronization in the linearized regime. This is opposite to what occurs in the critical threshold, where $K_c \sim \langle s \rangle / \langle s^2 \rangle$ [6, 165].

The interpretability of these effects emerge naturally from the local description of synchrony, and although the particularities of each phenomenon may require further analysis, the geometric unfolding allows unveiling the underlying mechanistic rules that control the interplay of structure and dynamics in synchronization.

4.4.2 *Quantifying the impact of link perturbations*

Using the local approximation of synchrony derived in the previous lines, we aim at quantifying the impact of link perturbations (additions and removals) using only local information, this is information available at the first –immediate– neighborhood of the nodes.

We want to study how modifications to the network structure affect the degree of synchronization in the system. This problem has already been tackled in [133] by studying the linear stability of the system in the context of power-grids, and more precisely in [130] by applying a perturbative expansion on the Laplacian eigenvectors. For a removal $(-)$ or addition $(+)$ of a specific edge (p, q), the authors in [130] obtain

$$\Delta r \approx \pm \epsilon Q_{pq} + O(\epsilon^2), \tag{4.63}$$

where ϵ is the intensity of the perturbation (usually $\epsilon = 1$ for unweighted networks) and Q_{pq} is

$$Q_{pq} = \frac{2}{N} \sum_{n=2}^{N} \left(\frac{\omega^T v^{(n)}}{\lambda_n^3} \right) \left(\sum_{m=1}^{N} \frac{[\omega^T v^{(n)}](v_p^{(m)} - v_q^{(m)})(v_p^{(n)} - v_q^{(n)})}{(1 - \lambda_m/\lambda_n) - \delta_{nm}} \right). \tag{4.64}$$

The first-order perturbation result in Eq. (4.64) is found to be very accurate when applied to a wide variety of networks, and it is significantly faster than re-computing Eq. (4.3) exactly after a single removal or addition of link. However, the impact of the perturbation is explicitly given by the products of differences in eigenvector components (p, q) among all eigenvectors pairs, which complicates the understanding on the effect that specific perturbations have on the system and still requires global information on the whole network structure.

Here we propose to tackle the problem of finding an analytical expression for Δr that provides a more physical interpretation on how the parameters affect the system, beyond the intriguing interplay between the eigenvectors of L and the frequencies in Eq. (4.64), while still being accurate when applied to real networks. We will consider the case of perturbations in the form of link removals and additions, distinguishing between directed

perturbations (where only one direction is affected) and undirected scenarios (where the perturbation affects both directions). In the strongly synchronized regime, we have that

$$\Delta r_{pq} \approx \frac{1}{2N}\sum_{i=1}^{N}(\theta_i^2 - \theta_i'|_{pq}^2), \tag{4.65}$$

where $\theta_i \equiv \theta_i^*$ is the unperturbed phase of the i-th oscillator (we neglect the superscript $*$ in the following) and θ_i' is the phase in the new steady-state after the removal of link (directed or undirected) (p,q). Writing the perturbed phase as $\theta_i'|_{pq} = \theta_i + \delta\theta_i|_{pq}$, we have that

$$\Delta r_{pq} \approx \frac{1}{2N}\sum_{i=1}^{N}(-2\theta_i\delta\theta_i|_{pq} + \delta\theta_i|_{pq}^2). \tag{4.66}$$

Instead of using the spectral decomposition of $L^\dagger$ to quantify the response to a perturbation as in [130], we exploit here the spatial expansion of Eq. (4.3) in terms of increasing neighborhoods. We recall that, at first-order expansion, which is approximately valid for sufficiently large and uncorrelated networks, we have that $\theta_i \approx \frac{1}{k_i}(\omega_i + z_i)$, where $z_i = \sum_{j=1}^{N} a_{ij}\frac{\omega_j}{k_j}$ is the term accounting for the influence of first-neighbours connected to the i-th node.

We will quantify the response to perturbations only in the surroundings of the link that is being removed, and therefore we are estimating the local impact of the perturbation in the global value of Δr_{pq}, neglecting non-local effects. As we will see, this approximation works sufficiently well in many situations, which means that it is possible to estimate the impact that a single link has in the overall synchrony of the system by using only local information. This mechanism is presumed to occur in many empirical decentralized systems, where the units do not have access to global information on the system but still they are able to optimize the collective performance in a very efficient way.

Directed links: We focus first on the problem of removing or adding a directed link (p,q), this is a link received at p-node by an incoming q-neighbor. Under the local approximation of Eq. (4.61), the removal or addition of the link will affect only the phases of the p-node and the neighboring nodes that received an input from p, leaving all the rest of phases unchanged. After some algebra, we can write

$$\delta\theta_i|_{pq} \approx \pm\delta_{pi}[\frac{\theta_i - \theta_q^0}{k_i \mp 1}] \pm a_{ip}[\frac{\theta_p^0}{k_i(k_i \mp 1)}], \tag{4.67}$$

where the upper (lower) operator accounts for a removal (addition) of the directed link (p,q) and $\theta_q^0 = \omega_q/k_q$ is the approximation of Eq. (4.61) without the contribution of first-neighbours ($z_q = 0$). Substituting Eq. (4.67) back into Eq. (4.66), performing the sum, and noting that in the crossed term of the binomial we have that $d_{pi}a_{ip} = 0$ in absence of self-loops, we explicitly obtain

$$\Delta r_{pq} \approx \frac{\mp 1}{N(k_p \mp 1)}[\theta_p(\theta_p - \theta_q^0) + \theta_p^0 X_p + \frac{(\theta_p - \theta_q^0)^2 + (\theta_p^0)^2\Upsilon_p}{2(k_p \mp 1)}], \tag{4.68}$$

with $X_p = \sum_{i=1}^{N} a_{ip}(\frac{w_i+z_i}{k_i^2})$ and $Y_p = \sum_{i=1}^{N} a_{ip}(\frac{1}{k_i^2})$. The result in Eq. (4.68) estimates the effect of a removal/addition of a link in the degree of synchrony by neglecting the terms further than first-neighbours in the spatial expansion of Eq. (4.67) and therefore it shares the same range of validity as the former. Eq. (4.68) is considerably faster than the spectral perturbative approach of Eq. (4.64) but it still misses a clear physical interpretation due to the complicate interaction among several variables.

In order to get more analytical insight from Eq. (4.68), we can approximate Δr_{pq} by assuming that the degrees of the nodes are large enough, such that $(k_p \mp 1) \approx k_p$. This implies that $z_p \approx 0$ (because the value $\langle \omega/k \rangle_p$ converges to zero as more neighbors the p-node has), and therefore $\theta_p \approx \theta_p^0$. Also, for large degree $k_p \gg 1$, the quantities X_p and Y_p will decay to zero faster than z_p and they can be neglected. After these simplifications, one obtains

$$\Delta r_{pq} \approx \mp \frac{1}{Nk_p}(\theta_p^0 \Delta\theta_{pq}^0 + \frac{(\Delta\theta_{pq}^0)^2}{2k_p}). \tag{4.69}$$

By considering the largest term in the right-hand side of Eq. (4.69), we explicitly obtain

$$\Delta r_{pq} \approx \mp \frac{1}{Nk_p}[\frac{\omega_p}{k_p}(\frac{\omega_p}{k_p} - \frac{\omega_q}{k_q})], \tag{4.70}$$

which is our main result for directed networks in the limit of sufficiently large degree and low clustering. We can make several interesting observations by directly inspecting Eq. (4.70). The absolute value $|\Delta r_{pq}|$ will be larger if the p-node has a high value of the ratio ω_q/k_q (large frequency or low degree) and the difference of phases (or ratios) between nodes (p,q) is large. In other words, the links that have more impact on the degree of synchrony are the ones that connect nodes that fall in the tails of the effective distribution $p(\omega/k)$. On the other hand, the links that will have the lowest impact on the synchrony are the ones connecting very similar nodes or if one of them falls in the center of $p(w/k)$.

To the best of our knowledge, these relations were only observed a posteriori, [118, 129, 130, 132, 232, 233] after performing a numerical optimization of the network to maximize its degree of synchrony or to measure its stability, and here we have provided a rigorous derivation of them from scratch.

Undirected links: We focus now on the problem of removing or adding an undirected link (p,q), this is a link both sent and received by p and q nodes. Under the local approximation of Eq. (4.61), the removal or addition of the link will affect only the phases of the (p,q)-nodes and the neighboring nodes that received an input from p or q, leaving all the rest of phases unchanged. After some algebra and again neglecting small terms, we finally obtain

$$\Delta r_{pq} \approx \mp \frac{1}{N}(\frac{w_p}{k_p} - \frac{w_q}{k_q})(\frac{w_p}{k_p^2} - \frac{w_q}{k_q^2}). \tag{4.71}$$

We note that Eq. (4.71) will be used in the following chapter. In Fig. 4.4 we confirm the accuracy of the approximations when applied to a random network.

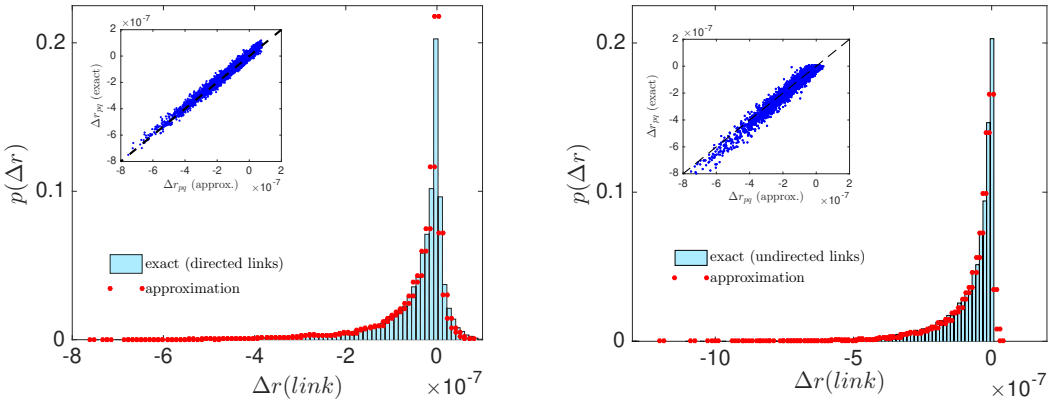

Figure 4.4: Numerical distribution of the impact of removed directed (left) and undirected (right) links in the overall synchronization for the exact Eq. (4.3) -blue boxes- and the directed (left) and undirected (right) approximations -red dots-. The network is an Erdös-Rényi with $N = 500$ and $\langle k \rangle = 20$, and the frequencies are Gaussian $g(\omega)$ with $\mathcal{N}(0,1)$. In the inset figure: scatter plot of the exact vs the approximation for the same network, where the straight line means zero error.

4.4.3 *Predicting Braess' Paradox*

Going one step further, we can predict which directed links will produce the counter-intuitive effect of increasing (decreasing) synchrony after its removal (addition). This effect, known as Braess Paradox in the context of road traffic [2], has been studied for oscillatory networks [111, 132, 233] although the identification of these particular links relied on numerical schemes or expressions in terms of the spectral decomposition of L. Also, while these works study if the perturbations break the stability of the current state, here we assume that the perturbations in the links drive the system towards a new steady-state. In our formalism, we can directly impose $\Delta r_{pq} > 0$ for a link removal to obtain the condition

$$\frac{\omega_p}{k_p}\left(\frac{\omega_p}{k_p} - \frac{\omega_q}{k_q}\right) < 0. \tag{4.72}$$

The condition in Eq. (4.72) describes two regions of the $(\omega_p/k_p, \omega_q/k_q)$-plane, namely the wedges $\omega_q/k_q > \omega_p/k_p$ for $\omega_p > 0$ and $\omega_q/k_q < \omega_p/k_p$ for $\omega_p < 0$. In terms of their area, these wedges describe a quarter of $(\omega_p/k_p, \omega_q/k_q)$ space. In Fig. (4.5) we plot the resulting change Δr_{pq} for each possible link removal in an Erdös-Rényi network of size $N = 500$ with mean degree $\langle k \rangle = 50$, color-coding the change so that positive (negative) changes are shaded more red (blue). We note that the positive changes fit well within the wedges predicted by our local theory, which are plotted in dashed black lines. In fact, approximately a quarter of directed links have the potential to increase synchronization after its removal as expected. While this phenomenon has been investigated in the context of identical oscillators [6, 234], here the frequencies of the oscillators play a critical role in determining which directed links are harmful or redundant, and we have shown that the local approximation is sufficient to capture this phenomenon.

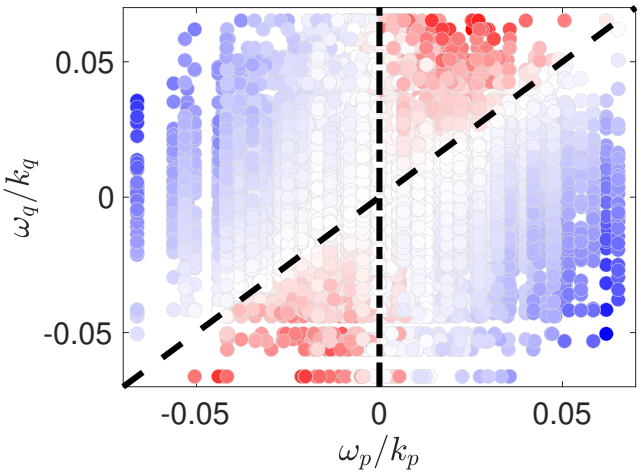

Figure 4.5: Distribution of removed directed links (p,q) in the phase-space $(\omega_p/k_p, \omega_q/k_q)$ for an Erdös-Rényi network with $N = 500$ and $\langle k \rangle = 50$, and Gaussian $g(\omega)$ with $\mathcal{N}(0,1)$. The color indicates whether if the removed link decreases (blue) or increases (red) the degree of synchrony, calculated exactly from Eq. (4.3). Straight lines bound the region predicted by Eq. (4.72) in the local approximation. Reprinted by permission of [231].

4.5 SUMMARY AND DISCUSSION

In this chapter, we have introduced a novel mathematical technique to analyze synchronization dynamics with a controllable amount of uncertainty on the network of interactions, gradually ranging from purely local to global information. In particular, in section 4.2 we have shown that the synchronized state can be written as a geometric –Taylor– series in contributions from increasingly further network neighborhoods and that these geometric series converge under relatively mild conditions on the network at hand, namely that the network has a primitive adjacency matrix (meaning that it is connected, aperiodic and not bipartite). We have also discussed the implications of our results in the problems of the previous chapter and related problems in the field. In section 4.3 we have provided a convergence analysis of the proposed expansions, showing that the truncated error is controlled by the spectra of the normalized adjacency matrix. After deriving exact results for uncertain frequency allocations, we have unveiled a connection between the convergence paths in the expansion and the decays of a classical damped harmonic oscillator. Using this analogy, structure and dynamics emerge as two faces of the same coin, meaning that the structural bounds determine the dynamical ones, and vice-versa. As a consequence, the range of behaviors and dynamical configurations that can be achieved from a given network can be understood by the spectral distribution and by the alignment of the frequencies with the extreme eigenvectors. Finally, in section 4.4, we have applied our results to derive a local approximation of synchrony, which is used to give analytical insight on the microscopic requirements of optimal synchrony and other relevant phenomena, including the local prediction of directed links that induce the counter-intuitive Braess' Paradox.

The results included in this chapter are key findings of this thesis. The geometric approach constructs the synchronized state from its local origin and provides a spatial basis

to unfold the oscillatory dynamics, in an alternative manner to standard spectral results found in the literature. This novel spatial approach facilitates the control, optimization and prediction of the system when having access only to decentralized information available at the nodes' scale. Under these uncertain conditions, the current theory can be used to tackle important practical problems such as network inference [164] and optimization [118, 129, 130], the prediction of phase-locking loss [44] and the effect of noisy frequencies or weights [165, 192], or the control of synchronized states by local weight tuning or structure modifications [69, 162], just to name a few. In fact, the geometric unfolding provides nodal constraints in the form ω_i/k_i that exploit both dynamical and structural information and could be directly applied to the mapping problem, improving the constraints proposed in section 3.4.2. However, the current constraints are derived from the linearized regime, and the study of the performance in the full mapping problem is left for further research.

There are also some limitations and improvements that await for further work. We have proposed, in section 4.2.1, a potential extension of our formalism beyond the linearized regime by means of the Collective Coordinates ansatz, but a detailed exploration of the geometric unfolding on the fully non-linear system is still missing. Also, the connection between the spectra and the possible ways to allocate the frequencies should be addressed within the emergent context of metadata-enriched networks [235, 236], the recent epidemic models considering homophily and behavioral effects [237–239] and also in exponential random graphs [240], with the possibility to provide spectral-based null-models for dynamical network measures such as assortativity and effective community structure. Lastly, the dichotomy between spectral and spatial unfolding of the synchronized state resembles the interesting uncertainty principle found for graphs, a result from the field of graph signal processing [227] that bounds the joint spectral and real representation of a signal in a graph, analogously to the classical uncertainty principle in harmonic analysis, that limits the joint representation of a function and its Fourier transform (thus in time and frequency domains). From the findings of this chapter, one might wonder to which extent these uncertainty bounds can be found when combining the spectral and spatial representations of the synchronized state.

It is time to move to the next chapter, where we give a final proof of the potential of this geometric formalism. In particular, we introduce the concept of synchronization bombs in a model that bridges the network optimization of synchrony under uncertainty (using local information and noise) to the emergence of explosive transitions [108], one of the most striking and relevant phenomenon in network synchronization and in the physics of phase transitions [6, 58, 143, 241].

5 ON THE EMERGENCE OF SYNCHRONIZATION BOMBS

5.1 INTRODUCTION

Uncertainty and noise play a decisive role in the evolution and adaption processes of many complex biological and ecological systems, as the wiring of neuronal circuits in the human brain or the course of interactions in a flock of birds. In these systems, individual units operate under noisy conditions and in a decentralized manner (exploiting only the local information that is available in their immediate surroundings) but they can abruptly display coherent collective behavior, which seem to require specific network configurations to be optimized for these specific global tasks. There is an ongoing consensus and increasing empirical evidence that abrupt synchronization plays a role in the malfunctioning of neuronal circuits during periods of epileptic seizures [242, 243], in the onset of anesthesic-induced unconsciousness [30, 244, 245] and in chronic pain diseases as fibromyalgia [246]. In infrastructural and power-grids networks, it is also key to detect and control small vulnerabilities that can lead to abrupt structural damages and global desynchronization blackouts [2, 247]. While the theoretical requirements for the emergence of abrupt phenomena are becoming more understood [143, 241], there is far less knowledge on the specific routes that empirical systems may follow to display these kinds of behaviors. It is natural to wonder which are the mechanisms or rules that the units obey in order to self-organize in a way that the collective –ordered– behavior can emerge.

In this chapter, we address this question from a theoretical perspective, in an attempt to explain the emergence of abrupt, explosive phenomena in the structural and dynamical properties of a networked-coupled system of oscillators using minimal self-organized principles. We do so within the framework of competitive link percolation –a process of network growth that is discussed in more detail in the following section–, and using the new mathematical machinery presented in the previous chapter –the local rule that maximizes the gain of global synchrony when connecting or disconnecting pairs of oscillators–. We will see that, when this local rule is applied during the percolation process, the system self-organizes towards network structures that display the well-known structural fingerprints of ES behavior and in fact induces abrupt transitions in the evolution of both structural and dynamical macroscopic properties. We are able to analytically predict the critical points using state-of-art model reduction techniques. We show that phenomena are robust to changes in the main parameters and also hold for chaotic oscillators, paving the way

for its implementation in the lab, and in a model of cardiac pacemaker cells, pointing to potential biological applications. Interestingly, noise turns out to be beneficial in the model because it improves the decentralized optimization of synchrony driven by the proposed local rule. Results presented in this chapter are based on the submitted work [248]:

- "Self-organized explosive synchronization in complex networks: Emergence of synchronization bombs", L. Arola-Fernández, S. Faci-Lázaro, P. S. Skardal, E. C. Boghiu, J. Gómez-Gardeñes and A. Arenas. In peer-review process (Comm. Phys. 2022)

where the naming of *synchronization bombs* is chosen to illustrate the idea that we can design networks of oscillators to be at the onset of total synchrony in which they show no dynamical coherence but, after applying a minimal wiring (just one or few links), display synchronization explosions. Before exploring our proposed model in depth in section 5.3, we employ section 5.2 to give some historical background on the key advances made about the study of explosive percolation and synchronization phenomena. A brief review of these pioneer results will allow us to better motivate our model and to highlight the open problems that can be addressed here.

5.2 PERCOLATION AND SYNCHRONIZATION: A MISSING EXPLOSIVE LINK

Network percolation studies the behavior of macroscopic structural properties –measured by the so-called order parameters– when links or nodes are added/removed into the network. The most used order parameter in percolation is the relative size of the giant component (SGC), which captures the proportion of the nodes that belong to the largest connected cluster. It is bounded between zero (a system of isolated, disconnected units) and one (a single connected component spanning the whole network). Accordingly, one important goal of percolation theory is to predict the behavior of the SGC under small changes in the density of links or nodes in the network, which play the role of the control parameter.

Percolation represents one of the simplest models in which macroscopic phase-transitions emerge, and its analysis finds several applications. The first results were introduced in the study of polymers growth in the 1940s [249, 250], and the problem was then addressed by the mathematical community, under the so-called bond-percolation framework [251] (considering the addition or removal of links or edges). Later on, more sophisticated frameworks were developed to study percolation in random, Erdös-Rényi graphs [81] and lattices of different dimensions, focusing on the prediction of the threshold and the classification of the transitions in different universality classes depending on the scaling of the order parameter near the transition point. We refer the reader to [252] for a careful review of these results. With the renewed advance of network theory and the increasing amount of available data in the current century, percolation theory gained even more popularity. Researchers have studied the robustness and resilience of systems like the power-grid or the Internet against structural failures and the fragility of ecological systems and food webs, to name a few examples [2, 57, 58, 87]. A milestone in percolation research was achieved in 2009 with the discovery of explosive percolation (EP), an

abrupt growth of the giant component of the network induced by the addition or removal of single links, that was found to occur when competitive rules (also known as Achlioptas processes, check Fig. 5.1 for more details) are applied on the choice of the links in a way that the formation of a giant cluster is delayed [253]. Discovering this abrupt structural transition, which was shown to be continuous (i.e. second-order) in the thermodynamic limit but with anomalous scaling properties [143], triggered further analyses to understand the mechanisms that can lead to the explosive behavior in the network growth. We refer the reader to detailed reviews [143, 241] but we remark the idea that allowing choices on the links that are selected in the percolation process is crucial to control the anticipation or delay of the percolation transition.

Advancing in parallel, abrupt transitions have been analyzed when a physical process is running among the units, as the spreading of a disease [195, 254], opinion diffusion [255] or traffic flow [256, 257], to name a few examples [143, 241]. Among the myriad of processes, the synchronization of heterogeneous coupled oscillators emerged as a particularly suitable framework to model the birth of explosive transitions [5, 6, 62, 258, 259]. For populations of globally coupled phase-oscillators, abrupt transitions in synchrony as the coupling parameter is increased and hysteresis were found to occur for particular frequency distributions as the bounded uniform [260] and the bimodal one [123]. However, the phenomena of explosive synchronization (ES) emerging from the interplay of structure and dynamics was firstly discovered for scale-free networks when one imposes positive correlations between the internal frequencies and the nodal degrees [108]. Further analyses showed that this is only one of the possible mechanisms that inhibit the emergence of a large synchronization cluster, and it was found that, by imposing frequency anti-correlations among connected units in the form of frequency gaps [109] or adaptive anti-Hebbian rules for the weights [261], explosive transitions occur as the coupling constant is tuned. Furthermore, they can appear in multilayer and dynamically coupled systems [142, 262] and they can be enhanced by the presence of noise in the frequencies [178] and higher-order -beyond pair-wise- interactions [125].

Research on ES and EP has focused on abrupt changes on macroscopic dynamical and structural properties, respectively, under small variations of the control parameter (the coupling strength or the density of links). In [263], it was found that a particular choice of frequency-dependent coupling (inducing again anti-correlations) produces ES process and the formation of synchronized clusters is delayed analogously to its percolation counterpart. These results unveil a first connection between both phenomena, but the choice on the coupling dependence is heuristic and the system produces the explosive behavior under changes in a global control parameter (the coupling strength), unlike the EP which is induced locally, by addition or removal of single links. Interestingly, in the previous chapter we have seen that the microscopic requirements for ES (namely frequency-degree correlations and frequency-frequency anti-correlations) naturally emerge from the optimization of the strongly synchronized, linearized, state [231]. Also, very recently, it has been found that these requirements can also be found by minimizing the threshold at which the

phase-locking state is lost, and when these constraints are imposed *ad-hoc* in the system, explosive transitions indeed emerge [264].

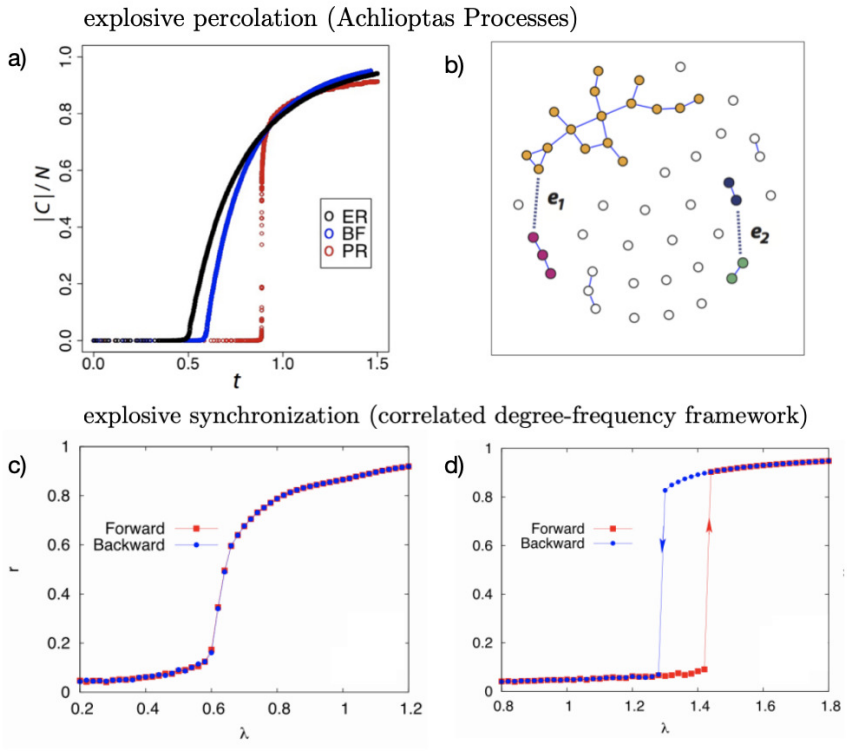

Figure 5.1: a) Evolution of the relative size of the giant component depending on link density for different percolation models. a) Black curve corresponds to the standard –random– percolation process in the ER model, blue corresponds to a Bohman-Frieze (BF) process, and the red one to the Product Rule (PR) process. Both BF and PR are considered Achlioptas Processes, i.e. competitive m-link percolation processes (with a fixed $m = 2$) but only the PR process induces an abrupt jump of the giant component at a critical density of links. The BF uses a bounded-size rule (in which connected components of size larger or equal than two are treated equally) to decide the selected link and the PR is based on an unbounded-size rule, that takes into account the actual size of the components merging the potential links. In b) we show a schematic representation of the PR process, where two links are randomly sampled but only the link for which the product of the size of the giant components connecting the links is larger, is selected (in this example e_1). Bottom: pioneer results on ES phenomena under the framework where the frequencies of the oscillators are correlated with the degrees of the nodes [108], i.e. $\omega_i \sim k_i$. c) corresponds to the evolution of the synchronization order parameter r depending on the coupling strength, here named K, for a fixed random ER network where the correlation does not induce the explosive phenomena and d) corresponds to the same process in a fixed SF network with exponent $\gamma = 3$. In the latter, we observe that the imposed correlation leads to an abrupt jump in the synchronization order parameter r and the appearance of a hysteresis cycle, where large synchronization values are sustained in the backward process (blue curve, decreasing K) below the forward transition (red curve, increasing K). The hysteresis cycle indicates bi-stability, meaning that, in this region of K there are two stable points of the order parameter depending on the initial conditions of the oscillators. Reprinted by permission of [108, 253].

By gathering all these previous results, we realize that our fundamental understanding of ES has significantly increased lately, but due to the analytical challenges faced when modeling synchronization dynamics on arbitrary complex networks, a rigorous framework

analogous to EP is still missing [143]. Apart from the theoretical interest, there is a strong empirical evidence that ES phenomena is behind the operation of biological switches and neural systems displaying abrupt responses to external perturbations [30, 242–246, 265, 266]. Evidence show that biological units operate with limited, decentralized information and are affected by noise [16, 155–157]. Thus, the ubiquity of ES cannot be driven by global and deterministic optimization routes, specific network and oscillator designs or global fine-tuning of coupling parameters, and it is still not very well understood how complex biological systems like the brain can self-organize to display the observed abrupt behavior [243, 265, 267].

5.3 THE MODEL

We return to the more controllable realm of theory to tackle the aforementioned empirical challenges by proposing and solving a minimal model of a self-organized dynamical network that behaves as a synchronization bomb, i.e. showing an abrupt synchronization transition in the course of a self-organized wiring process. Our model attempts to bridge the conceptual gap between ES and EP by imposing local structural perturbations instead of global ones and proposes a self-organized and stochastic route to ES by invoking a simple principle of synchrony maximization in a decentralized and noisy environment.

We begin, as always, with the standard Kuramoto model, and we extend it later on to other dynamics. We consider a large ensemble of N heterogeneous Kuramoto oscillators interacting on top of a network follows the equations of motion

$$\dot{\theta}_i = \omega_i + K \sum_{j=1}^{N} a_{ij} \sin(\theta_j - \theta_i), \ \forall \ i \in 1, \dots, N, \tag{5.1}$$

where, as usual θ_i is the phase and ω_i is the intrinsic frequency of the i-oscillator, a_{ij} are the entries of the adjacency matrix A, that capture the interactions among the units and K is a constant coupling strength. We will also consider here that the macroscopic behavior of the system is captured by the modulus of the Kuramoto order parameter $r(t) = (1/N) \left| \sum_{j=1}^{N} e^{i\theta_j(t)} \right|$, which measures the degree of phase synchronization and is bounded between zero and one. In the following, we will work only with temporal averages of the order parameter, i.e. $r = \langle r(t) \rangle$, neglecting fluctuations in time, and we initially consider unweighted ($a_{ij} = 0, 1$) and undirected networks ($a_{ij} = a_{ji}$), although results will also be extended to more general set-ups. Regarding the distribution of internal frequencies, we assume $g(\omega)$ with zero mean and fixed variance, giving special attention to the uniform distribution $g(\omega) \in [-\gamma, \gamma]$ for analytical convenience, but we will also show results for alternative, perhaps more realistic, choices of $g(\omega)$.

A first ingredient of our model that makes it deviate from most of previous works [143] is that we keep the coupling strength K constant during the percolation process, and it is the density of links or connections in the network, p, that acts as the control parameter, with the parameter p ranging from 0 (disconnected network) to 1 (fully-connected, all-to-all network). We initialize our system from scratch, with a completely disconnected network

$(p = 0)$ of oscillators with assigned random phases drawn from $(-\pi, \pi)$. We then run the percolation processes in the forward –construction– direction by adding undirected links (increasing p) in a sufficiently slow manner such that the system in Eq. (5.1) reaches the stationary state at each network step in the process (what is known as an adiabatic process). In the backward –destruction– process, we assume that the system has some sort of memory and choose to remove the links in the reversed order of the forward process, Numerical results show that the phenomena of this model also holds in a scenario with an alternative backward stochastic branch (therefore with a lack of memory), but its study is left for further research.

The second novel ingredient of the model is that the percolation rule that is used to select the added/removed link in the process is derived from a minimal self-organized principle, with the assumption that the system attempts to maximize the overall degree of synchrony using only local information available at the surroundings of the units. For this purpose, we use the geometric unfolding of the synchronized state, introduced with rigorous detail in the previous chapter, since is the mathematical tool that allow us to study networks of phase-oscillators in the scenario of decentralized information. Using this tool, in section 4.4.2 we obtained a local approximation of the degree of synchrony r and applied it to estimate the impact that adding or removing single directed and undirected links has on the global behavior. The calculation for the directed case was then used in 4.4.3 to successfully predict the counter-intuitive Braess Paradox effect in random networks.

Here, we initially consider the calculation obtained for the undirected case, given by Eq. (4.71), the formula that approximates the impact of adding or removing an undirected link using only local information. The key point here is that we use this result to optimize the synchrony of the system in a link percolation process that evolves under stochastic, noisy dynamics. The self-organized ingredient is precisely the fact the system exploits decentralized information in a competitive manner, since there is no global function that optimizes the growing structure. We rewrite here the approximation of Δr in Eq. (4.71) for the sake of clarity, which is given by

$$\Delta r_{ij} = \frac{\pm 1}{K^2 N} \left(\frac{\omega_i}{k_i} - \frac{\omega_j}{k_j} \right) \left(\frac{\omega_i}{k_i^2} - \frac{\omega_j}{k_j^2} \right), \tag{5.2}$$

referring the reader to section 4.4.2 for details on the derivation. We note that alternative lines of calculations, including both discrete (considering single link perturbations) and continuous (using derivatives with respect to the degrees) in the limit of large degrees $(k_i \gg 1)$ all lead to Eq. (5.2). It is important to remark that one could obtain more accurate rules for the maximization of r by using the exact result for the phases given by the SAF framework introduced in the previous chapter, or by including higher-order terms beyond the local approximation, although this increase of accuracy would require to use either spectral (thus global) information or to go beyond the local variables up to second-neighbors and so on. Interestingly, we note that a quadratic approximation of Eq. (5.2) as $\Delta r \sim (\omega_i/k_i - \omega_j/k_j)^2$ also induces the explosive phenomena via linear correlations of frequencies and degrees, and it may simplify the analytical treatment, but its study is left

for further research. Importantly, we use Eq. (5.2), a particular rule from a broader class of rules $p(k_i, k_j, \omega_i, \omega_j)$ because it is the one that satisfies our decentralized and self-organized assumptions.

The addition (removal) of a new link at each p-step is made in a competitive manner, by randomly sampling M pairs of oscillators and selecting the connection (i, j) that maximizes the decentralized gain (or minimizes the loss) of synchrony after its addition (removal) given by the rule in Eq. (5.2). The reader should note that the proposed model is stochastic in nature and belongs to the family of m-edge Achlioptas Process [143], becoming completely deterministic in the limit $M \to \infty$ and equivalent to a random percolation for $M = 1$. Importantly, the function o select the link among the M sampled ones does not depend only on structural properties as occurs in standard percolation cases, but also on dynamical information contained in the frequencies of the units, i.e. a feature-enriched percolation process [235].

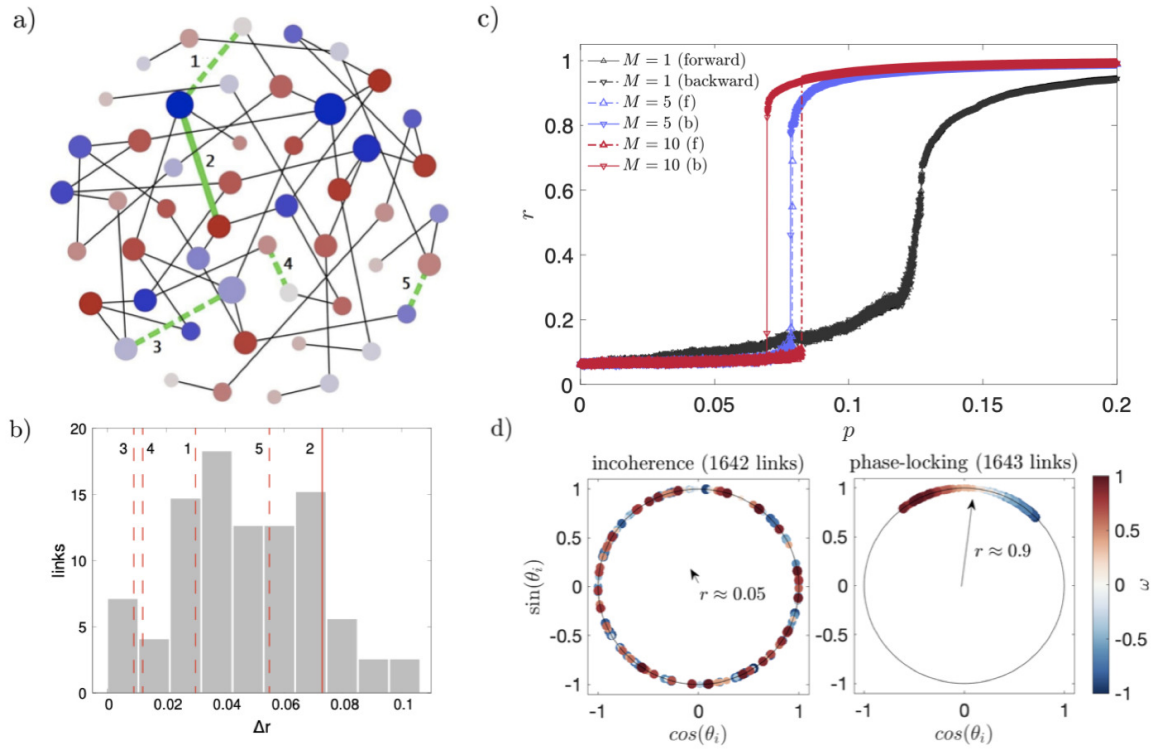

Figure 5.2: a) Illustrative network of $N = 50$ oscillators where the size of the node is proportional to its degree, the color is related to its natural frequency (blue for $\omega = -1$, gray for $\omega = 0$ and red for $\omega = 1$) and the black lines represent the links between the oscillators. Green lines mark the $M = 5$ potential links sampled in that p-step. The continuous line represents the chosen link and the dashed ones are the discarded ones. b) Histogram of the Δr values for the existing links of the network, where red lines correspond to the values of the five sampled links. c) Example of the typical synchronization transition in our bomb-like model, with the order parameter r depending on the fraction of links, p in a system of $N = 200$ Kuramoto oscillators for three values of noise M. Temporal averages of r are taken at each link change. In d), we represent the oscillators phases for the $M = 10$ case before (left) and after (right) the forward transition. Note that the jump in the Kuramoto order parameter from incoherence to complete phase–locking takes place just with the addition of one link. Reprinted by permission of [248].

We can already explore the basic mechanisms and phenomenology that our system displays. In the left panels of Fig. 5.2, we illustrate a schematic representation of the process when the number of sampled links at each p-step is fixed to $M = 5$. In the right panels of Fig. 5.2, we show the forward and backward synchronization curves $r(p)$ when different values of M are used. In Fig. 5.2.c), we observe both the abruptness of the jump and the region of hysteresis increase with M. In Fig. 5.2.d), we observe that the transition from incoherence ($r \approx 0.05$) to full phase-locking ($r \approx 0.9$) when a single link is added to the system, in the so-called synchronization bomb.

5.3.1 *Emergence of structural explosive fingerprints*

We focus on the evolution of network structural properties during the course of the percolation process when the rule of Eq. (5.2) is applied. This mechanism induces the emergence of several patterns that are usually associated with explosive transitions in the literature [143, 231]. In Fig. 5.3, depicted at the end of the section, we visualize a summary of these three findings.

Degree-frequency correlations and frequency-frequency anti-correlations. The competition between degrees and frequencies that occurs in the rule of Eq. (5.2) –since ω_i appears in the numerators and k_i in the denominators of the expression– produces a stationary degree distribution that scales with system density. The rule tends to connect oscillators with very different frequencies, which in turn increases their degree and reduces the chances of making new connections. The dynamical balance of both quantities tends to homogenize the values of Δr_{ij} among the new potential links and naturally induces a stationary positive correlation between frequencies and degrees. Since the scaling of the rule is given by $\Delta r \sim \omega^2/k^3$, we find that, in the deterministic (large M) regime and considering a uniform distribution with $\omega \in [-\gamma, \gamma]$ the correlation is given by

$$k_i \simeq \frac{5}{3} pN\gamma^{-2/3}|\omega_i|^{2/3}, \tag{5.3}$$

where the scaling factor that depends on p is obtained by imposing a normalization condition ensuring that the sum of degrees equals the number of links $\langle k \rangle = pN$. Eq. (5.3) becomes more accurate as noise is reduced in the system, as observed Fig. 5.3.a). In Fig. 5.3.b), we also see that, as a direct consequence of applying the percolation rule, frequency anti-correlations among connected nodes are also present in the system and increase as the rule becomes more deterministic (large M). These type of correlations are explicitly imposed in the majority of studied mechanisms that induce ES [143, 241], but interestingly here they emerge from a decentralized optimization of the synchronized state. We explain now, using the spectral properties of the network, how these dynamical anti-correlations translate into structural ones.

Spectral signatures: towards optimal and bipartite networks. We observe in the central panels of Fig. (5.3) that the network evolves towards maximizing the largest eigenvalue of the Laplacian matrix $L = D - A$ and the largest negative eigenvalue of the normalized Adjacency matrix $\hat{A} = D^{-\frac{1}{2}}AD^{-\frac{1}{2}}$. In the insets, we can see how the frequency vector ω tends to align with the entries of the associated extreme eigenvectors. These spectral signatures unveil that the system is evolving towards optimal and bipartite configurations.

First, it is well understood that optimal synchronization is reached by the alignment of the frequencies with the largest eigenvector of the Laplacian matrix and by increasing the magnitude of the associated eigenvalue $\mu_{max}(L)$ [118]. This concept is introduced in detail in previous chapters, specifically in chapter 2.3, where we discuss the main results in the context of the SAF framework. We also explored the connection between optimal synchronization and local correlations in chapter 4.3.3 where we explained how the alignment of the frequencies with the largest eigenvector of L induces anti-correlations among the neighbor frequencies of the nodes. Second, considering that the normalized Adjacency matrix, defined here as $\hat{A}$ is a stochastic row sum, its spectra is bounded in $\hat{\mu} \in [-1, 1]$, with the largest eigenvalue $\mu_{max}(\hat{A}) = 1$ if the network is connected. The remaining of the spectra follows Wigner's semicircle law for random networks, becoming narrower as the link density increases, and it deviates from the random case in the presence of modules (shifting towards positive eigenvalues) or bipartite-like structures (shifting towards negative eigenvalues), an effect that we already discussed in section 4.3.3 and in [231]. Accordingly, in Fig. 5.3.d) we observe that bipartite patterns arise as determinism is increased (larger M) and the trajectory of the extreme eigenvalues tuple follows a clear asymmetric path in the route towards the all-to-all ($p = 1$) limit. This effect clearly shows that the rule derived in Eq. (5.2) induces negative structural correlations (in terms of bipartite patterns) as a consequence of the negative dynamical correlations that emerge in terms of natural frequencies, and vice-versa.

Delayed percolation threshold. Now we wonder to which extent this synchrony-driven percolation process deviates from the natural one (when links are chosen at random) and what occurs to the critical threshold. To tackle these points, we measure the growth in size of the giant component (SGC) as we increase the control parameter p in our model, for different values of the noise parameter M and network sizes N. In Fig. 5.3.e) we observe how the proposed rule clearly delays the percolation threshold with respect the random case, producing in fact more abrupt transitions. The nature of the transition appears to be continuous (*i.e.* second order) even for large system sizes, although the proposed rule significantly delays the structural transition. We confirm this effect by studying more closely the effect of systems parameters in Fig. 5.3.f), where it is shown that increasing both the size of the system (large N) and the determinism in the rule (large M), percolation transitions become sharper and occur at higher p.

We can obtain a rough approximation for the critical density associated to the value of the percolation threshold by using the well-known Molloy and Reed criterion [268], a celebrated result that is derived in the context of random networks with arbitrary degree

distributions. This criterion involves a rather technical mathematical proof but relies on the simple idea that in order to have a connected component spanning the whole network, each node has to be connected, in average, to two neighbors (as it would occur in a one-dimensional chain). The Molloy-Reed criterion for random graphs predicts the critical density for a macroscopic giant component to exist when the condition

$$\langle k^2 \rangle = 2\langle k \rangle, \tag{5.4}$$

is satisfied. Eq. (5.4) has been used to predict the percolation threshold in random ER and SF networks [2], unveiling the interesting effect that networks with very heterogeneous degree distributions have a vanishing small random percolation threshold, making them very robust to random attacks to the nodes or links.

Here, we can use this criterion in the deterministic limit of our model (large M) and neglecting the negative structural correlations that the rule induces (the bipartite patterns). Then, by using the emergent correlation between frequencies and degrees explored in the previous lines, we can compute the moments of the degree distribution depending on the $g(\omega)$ and in terms of our control parameter, the density of the links p. For a uniform distribution $g(\omega) = 1/(2\gamma)$ with $\omega \in [-\gamma, \gamma]$, we have that the correlation is given by Eq. (5.3). Then, we can compute the moments as

$$\langle k \rangle = \frac{5}{3} pN\gamma^{-2/3} \langle |\omega|^{2/3} \rangle \tag{5.5}$$

$$\langle k^2 \rangle = \frac{25}{9} p^2 N^2 \gamma^{-4/3} \langle |\omega|^{4/3} \rangle. \tag{5.6}$$

The moments of the distribution of $|\omega|$ are computed by direct integration. After substituting in Eq. (5.4) the resulting expressions, we obtain

$$p_c^{rule} = \frac{42}{25} \cdot \frac{1}{N}. \tag{5.7}$$

For the random percolation case, it is well understood that the threshold occurs at $p_c = 1/N$ [2] and therefore, the new threshold induced by applying our percolation rule can be written as

$$p_c^{rule} = 1.68 \cdot p_c^{rand}, \tag{5.8}$$

which highlights that the rule delays the threshold with respect to the random case, as a consequence of having a broader degree distribution. In Fig. 5.3.e) we observe that Eq. (5.8) works well for sufficiently large M. The reader should note that a similar calculation could be done for other $g(\omega)$, but results would change because the distribution of frequencies affects the percolation threshold in our rule-dependent process. Importantly, the previous calculation, despite its remarkable success at predicting the percolation threshold, neglects important structural correlations in the underlying network. More sophisticated analytical tools, as the recently developed feature-enriched percolation framework [235], could improve the predictions under local rules, such as Eq. (5.2), that exploit information both from the degrees and the frequencies of the units.

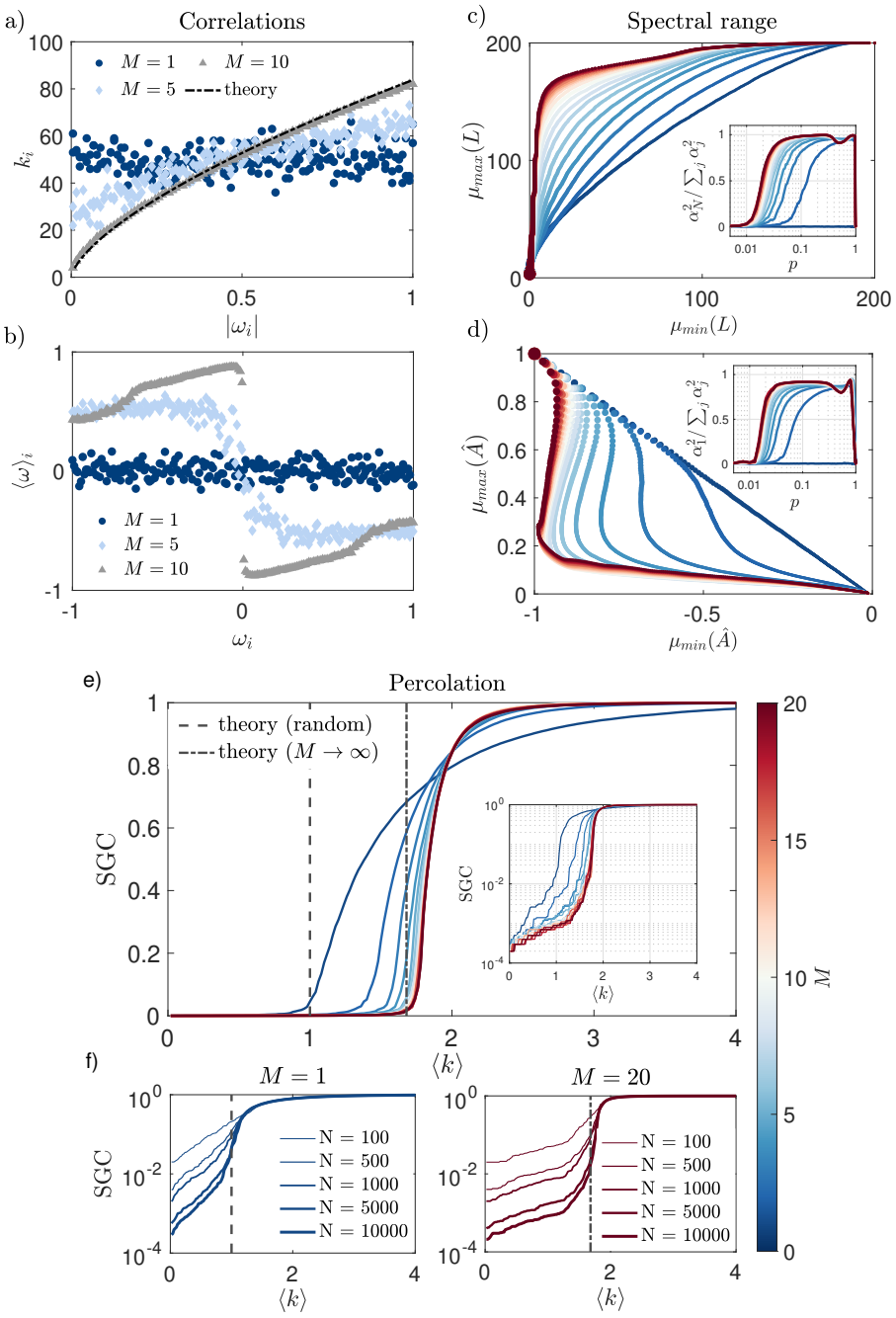

Figure 5.3: a) Scatter plot of the tuples $(|\omega_i|, k_i)$ and b) $(|\omega_i|, \langle\omega\rangle_i)$ -where $\langle\omega\rangle_i$ is the average frequency of the neighbors of the *ith*-node- for each oscillator at $p = 0.1$, in a single realization of the forward process, for three values of noise and $N = 200$, including in a) the deterministic prediction of Eq. (5.3). c) Scatter plot of the largest negative and positive eigenvalues of the Laplacian matrix and the normalized Adjacency matrix (d) at different p-steps of the forward process for different values of M. In the inset, we plot the relative correlation $\alpha_i = \langle\omega, v_i\rangle$ between the frequency vector and the eigenvector of L (or $\hat{A}$) associated with the largest (or minimum) eigenvalue. e) Evolution of the average size of giant component (SGC), for noise ranging from the random scenario of $(M = 1)$ to a more deterministic one with $(M = 20)$ in a network of size $N = 5000$. Results are averaged over 20 realizations of the process. Inset in e) shows a single realization in log scale. In f) we show the effect of network size on the percolation transition for the $M = 1$ (left) and $M = 20$ (right) scenarios. It is observed that larger and more deterministic networks under the rule of Eq. (5.2) experiment sharper transitions. Reprinted by permission of [248].

5.3.2 *Analytical characterization of the Kuramoto bomb*

It is time to focus on the dynamical aspects of our model, in particular on the interesting ES transitions induced by single link changes that we observed in Fig. 5.1. The main questions that we can address by solving the model here are related to the dependence of the main parameters, namely how the coupling strength K, the noise parameter M in the percolation process, the size of the network N and the choice of the frequencies via $g(\omega)$ affect the nature and location of the synchronization transitions. The main findings of this section are summarized in Fig. 5.4.

Backward predictions using the CC ansatz

To this date, one of the most precise approaches in the literature to capture the reduce the dimensionality in oscillator networks described by Eq. (5.1) and also to take into account the finite-size effects of the system is given by the model reduction technique based on Collective Coordinates, introduced first by Gottwald to mean-field systems [145] and extended to complex networks in [146]. We have already discussed this approach in section 2.4.2. The idea is that we can use this technique to estimate the values of the phases for the oscillators at any given p-step, the corresponding order parameter $r(p)$ in the backward branch and, additionally, we can calculate the backward synchronization threshold, that we define as p_c^b. As we explained, the key step of the method is to reduce the dimensionality of the system by considering, as an *ansatz*, that the phases of the oscillators in the phase-locking regime are in the form $\theta_i = q(t)\psi_i$ where ψ_i is the exact solution of the linearized dynamics of Eq. (5.1) [118], i.e. $\psi_i = K^{-1}L^{\dagger}\omega$. By minimizing the error made by the ansatz in the full system and after some manipulation [146], one ends up with only one differential equation for the evolution of the q coefficient, thus drastically reducing dimensionality, from N coupled differential equations to a single one. We rewrite here the reduced equation, that reads as

$$\dot{q} = 1 + \frac{1}{\psi^T L \psi} \sum_{i,j} \psi_i \sin(q(\psi_j - \psi_i)). \tag{5.9}$$

At a given p-step of the process, we compute the linearized solution ψ via the exact pseudo-inverse of the Laplacian matrix. Then, we numerically find the value of q that implicitly solves Eq. (5.9) for $\dot{q} = 0$ and finally compute the phases by applying the CC ansatz. This method allows estimating the whole stationary curve for the order parameter $r(p, K)$ in the backward direction, when the system is in the phase-locking regime (meaning that all of them rotate at the same frequency). This approach requires some a fast numerical computation and it just exploits static and global information of the system (from A and ω) meaning that we can use it *off-line*, without any need of integrating the full dynamics. It is worth mentioning here that one could exploit the truncated geometric unfolding of the synchronized state, introduced in detail in the previous chapter, and in particular the geometric version of Eq. (5.9) given by Eq. (4.32) to estimate the solution of the full non-linear system using only local information in terms of frequencies ω and degrees k_i and that this

approach may allow obtaining approximated closed form solutions for the evolution of $r(p)$ in the backward process of our model.

Furthermore, we employ an *explosive trick* to predict the appearance of the backward critical threshold (p_c, K_c) with the same technique. The trick relies on assuming beforehand that, in the explosive regime of our system, the backward process transits from full phase-locking to complete incoherence. With this idea in mind, we predict the backward threshold by looking at the last value of p_c for which Eq. (5.9) has a solution. Additionally, we need to check that the solution is stable, meaning that the system returns to the state after a small perturbation is applied. We apply here a standard linear stability analysis to check for stability, described as follows.

Our non-linear dynamics given by the system in Eq. (5.1) can be expressed as

$$\frac{d\theta}{dt} = F(\theta). \tag{5.10}$$

By applying a Taylor expansion around an equilibrium point θ^*, we get

$$F(\theta) \approx F(\theta^*) + \frac{\partial F}{\partial \theta}|_{\theta=\theta^*}(\theta - \theta^*). \tag{5.11}$$

The equilibrium θ^* is a fixed point of the system, meaning that $F(\theta^*) = 0$. Setting $\delta\theta = \theta - \theta^*$, we can write

$$\frac{d(\delta\theta)}{dt} = J(\theta^*). \tag{5.12}$$

The matrix J is known as the Jacobian matrix, a non-linear matrix that encapsulate all the partial derivatives of the non-linear system with respect to the system variables. Since the matrix is evaluated around a fixed point, θ^*, J is constant and independent of θ, and therefore the system of Eq. (5.12) can be solved exactly as a superposition of normal modes [116]. The general solution of Eq. (5.12) reads as

$$\theta(t) = \theta^* + \sum_{i=1}^{N} a_i v_i e^{K_i t}, \tag{5.13}$$

where K_i and v_i are the i-th eigenvalue and eigenvector of $J(\theta^*)$ and a_i are constants determined by initial conditions of the perturbation, $\theta(t=0)$. From Eq. (5.13) one can see that, for an arbitrary small perturbation, the system will relax towards the equilibrium θ^* if and only if all the eigenvalues of J are negative. For the particular case of the Kuramoto model, the entries of the Jacobian matrix evaluated at the equilibrium point $\theta^* = q^*\Psi$ are computed using $J_{ij} = \partial\dot{\theta}_i/\partial\theta_j$. It is straightforward to show [69, 146] that the Jacobian of our system reads as

$$\begin{aligned} J_{ij} &= a_{ij}\cos(q^*(\psi_j - \psi_i)),\ i \neq j \\ J_{ij} &= -\sum_k a_{ik}\cos(q^*(\psi_k - \psi_i)),\ i = j. \end{aligned} \tag{5.14}$$

As mentioned, the system is stable if all the eigenvalues of J are negative. Thus, the backward critical threshold occurs at the last value of the link density p_c (which appears impli-

citly in J via the adjacency matrix A) at which Eq. (5.9) admits a solution that is linearly stable. The explosive *trick* is particularly useful to simplify the calculation because, when considering transitions from full phase-locking to incoherence, we do not need to compute a partial synchronized solution involving clusters of smaller size than the whole network [146]. In other words, we predict the loss of stability of the full phase-locking state, which in the explosive regime of our system corresponds to the desired backward synchronization threshold. The agreement between this prediction based on collective coordinates and numerical simulations becomes evident in the backward synchronization diagrams shown in Fig. 5.4.a) for $K = 0.02$ and 0.04 ($M = 10$).

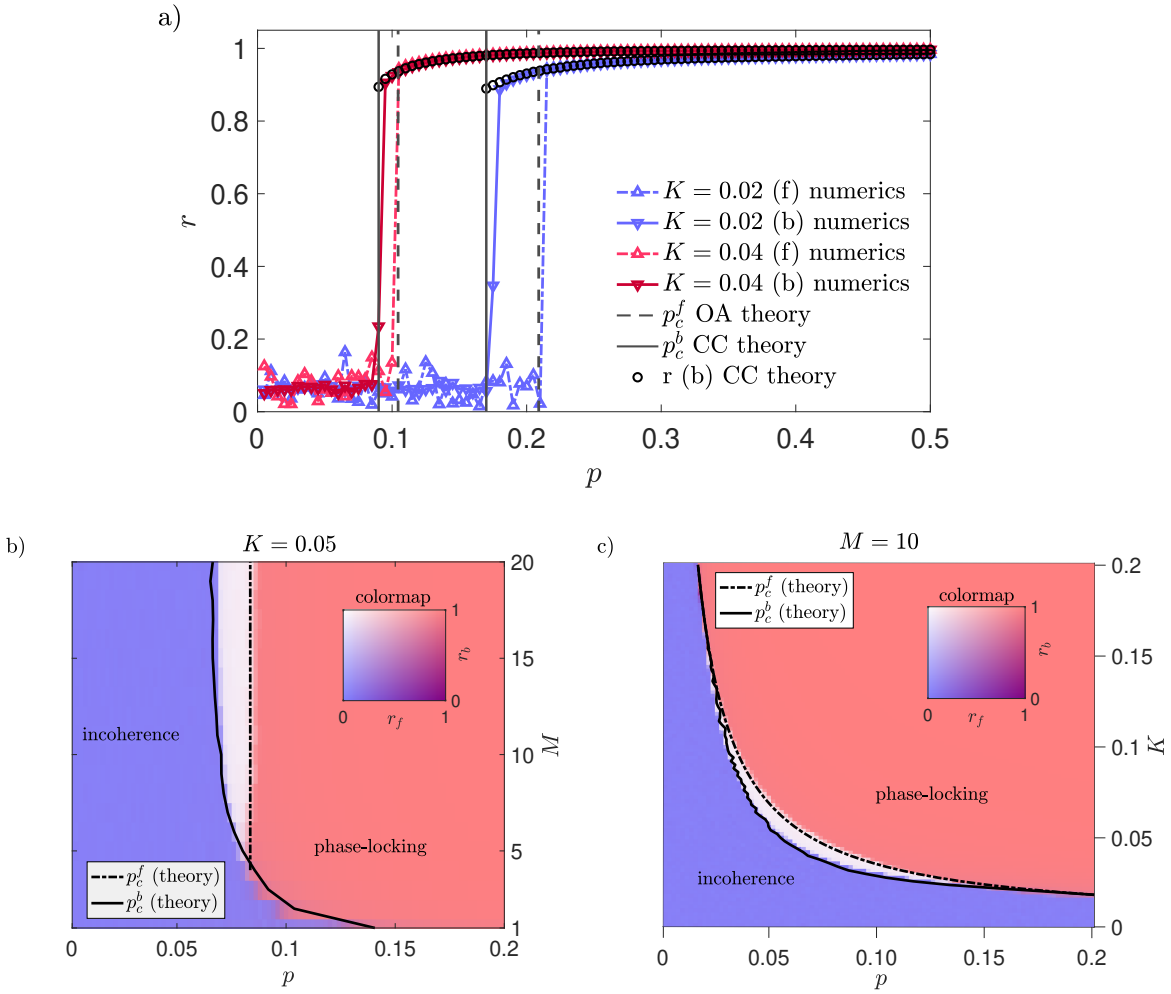

Figure 5.4: a) Examples of synchronization curves, $r(p)$ for a rule dependent ($M = 10$) case in a network of size $N = 200$ and fixed coupling to $K = 0.02$ and $K = 0.04$. Measurements here are taken every 40 links and results are obtained in a single realization of the process. b) Synchronization phase-space depending on M and p for a fixed $K = 0.05$. In the three panels, dashed (solid) lines correspond to the theoretical predictions of the forward (backward) synchronization thresholds, and circle markers in a) to the analytical prediction of the whole backward curve. c) Synchronization phase-space depending on K and p for a certain level of sampling noise $M = 10$, where the color-map indicates whether the system is in the incoherent, bistable or phase-locking regime. Results are averaged over 20 realizations. Reprinted by permission of [248].

Forward predictions with OA ansatz

Since our system departs from the incoherent state, in the forward direction we cannot use the CC approach anymore, because the ansatz $\theta_i = q(t)\psi_i$ is not valid. From numerical experiments, one sees that usually for $M > 1$, the incoherent state $r \approx 0$ remains stable beyond the backward critical transition, thus creating a bistable region and a delayed forward transition. To predict the forward critical threshold by analytical means, we take the limit of large size N and sampling/noise M (towards a deterministic rule applied in a large system). In practice, the results become valid even for quite small values like $N = 200$ and $M = 5$, but we remark that the theory is derived in the thermodynamic and deterministic limit. Our approach is based on the celebrated OA ansatz [122], introduced in section 2.4.1, which has been successfully used to deal with frequency and degree correlations [110, 126, 269]. Our calculations benefit from the recent development of [126], where the mean-field dynamics of Janus oscillators (a verstaile model of synchronization) are solved.

We begin by defining the local order parameter $R_i = \sum_j a_{ij} e^{i\theta_j}$ such that Eq. (5.1) can be written as

$$\dot{\theta}_i = \omega_i + Im[e^{i\theta_i} R_i] \ \forall \ i \in 1, \dots, N. \tag{5.15}$$

Following [126], we take a large ensemble of systems, which state is captured by the joint probability density $\rho(\theta, \omega, t)$, with $\theta = (\theta_i, \dots, \theta_N)$ and $\omega = (\omega_i, \dots, \omega_N)$. The evolution of the joint probability has to satisfy the continuity equation [122]

$$\frac{\partial \rho}{\partial t} + \sum_{i=0}^{N} \frac{\partial}{\partial \theta_i}(\rho \dot{\theta}_i) = 0. \tag{5.16}$$

where θ_i follows Eq. (5.15). One multiplies the density function ρ by $\prod_{j \neq i} d\omega_j d\theta_j$ and integrates to obtains the evolution for the marginal oscillator density, $\rho_i(\theta_i, \omega_i, t)$ as

$$\frac{\partial \rho_i}{\partial t} + \frac{\partial}{\partial \theta_i}(\rho_i \dot{\theta}_i) = 0. \tag{5.17}$$

Now, one can apply the OA ansatz by expanding ρ_i in a Fourier series and setting the coefficients of the expansion to $b_{i,n} = \alpha_i^n$ [122, 126], as explained in section 2.4.1. By inserting the Fourier series with the OA ansatz in Eq. (5.17), one obtains

$$\dot{\alpha}_i + i\alpha_i \omega_i + \frac{K}{2}(\alpha_i^2 R_i - R_i^*) = 0, \ \forall \ i \in 1, \dots, N \tag{5.18}$$

$$R_i = \sum_{j=1} a_{ij} \int_{-\infty}^{\infty} \alpha_j^*(\omega_j, t) g(\omega) d\omega_j, \ \forall \ i \in 1, \dots, N. \tag{5.19}$$

where R^* and α_j^* are the complex conjugate and i the imaginary unit. Now we invoke the large M assumption. In this limit, the underlying network is purely bipartite, separated between nodes with positive frequencies and nodes with negative ones (see previous Fig. 5.3.c)-d)). Also, the frequencies of the oscillators are completely controlled by their degrees. Then, we look for solutions $\alpha_i = \alpha_{k,\pm}$ [126], reducing the problem to find the

coefficients of degree classes in the two groups. The local order parameter in this setting is written as [126]

$$R_{k,\pm} = \frac{k}{\langle k \rangle} \sum_{k'} k' p_{k'} \alpha^*_{k',\pm}. \tag{5.20}$$

The frequencies of the degree classes in the two groups are driven by the percolation rule. For a wide p range, we have $\omega_{k,\pm} = \pm \left(\frac{k}{c}\right)^{3/2}$. The parameter c is a scaling constant given in Eq. (5.3). Then, the resulting system can be written as

$$\dot{\alpha}_{k,+} = -i \left(\frac{k}{c}\right)^{3/2} \alpha_{k,+} + \frac{Kk}{2\langle k \rangle} \left[\sum_{k'} k' p_{k'} \alpha_{k',-} - \alpha^2_{k',+} \sum_{k'} k' p_{k'} \alpha^*_{k',-} \right] \tag{5.21}$$

$$\dot{\alpha}_{k,-} = +i \left(\frac{k}{c}\right)^{3/2} \alpha_{k,-} + \frac{Kk}{2\langle k \rangle} \left[\sum_{k'} k' p_{k'} \alpha_{k',+} - \alpha^2_{k',-} \sum_{k'} k' p_{k'} \alpha^*_{k,+} \right]. \tag{5.22}$$

We aim at evaluating the stability of the incoherent state, here $\alpha_{k,\pm} = 0$. To do so, we linearize the system and evaluate it around $\alpha_{k,\pm} = \delta\alpha_{k,\pm} \ll 1$. After neglecting small terms of order $\delta\alpha^2$, and doing some algebra, the dependence on the complex conjugates vanish and one ends up with the following system for each degree class

$$\delta\dot{\alpha}_{k,+} = -i \left(\frac{k}{c}\right)^{3/2} \delta\alpha_{k,+} + \frac{Kk}{2\langle k \rangle} \sum_{k'} k' p_{k'} \delta\alpha_{k',-} \tag{5.23}$$

$$\delta\dot{\alpha}_{k,-} = +i \left(\frac{k}{c}\right)^{3/2} \delta\alpha_{k,-} + \frac{Kk}{2\langle k \rangle} \sum_{k'} k' p_{k'} \delta\alpha_{k',+}. \tag{5.24}$$

We define the variables $\delta x = \sum_{k'} k' p_{k'} \delta\alpha_{k',+}$ and $\delta y = \sum_{k'} k' p_{k'} \delta\alpha_{k',-}$, and sum over degree classes (taking into account the degree distribution), to be able to write

$$\sum_k k p_k \delta\dot{\alpha}_{k,+} = -i \sum_k \left(\frac{k}{c}\right)^{3/2} k p_k \delta\alpha_{k,+} + \sum_k \frac{Kk^2 p_k}{2\langle k \rangle} \delta y \tag{5.25}$$

$$\sum_k k p_k \delta\dot{\alpha}_{k,-} = +i \sum_k \left(\frac{k}{c}\right)^{3/2} k p_k \delta\alpha_{k,-} + \sum_k \frac{Kk^2 p_k}{2\langle k \rangle} \delta x. \tag{5.26}$$

Approximating $\sum_k k^{5/2} p_k \delta\alpha_{k,+} \approx \langle k^{3/2} \rangle \delta x$ and $\sum_k k^{5/2} p_k \delta\alpha_{k,-} \approx \langle k^{3/2} \rangle \delta y$, one arrives at a 2-dimensional variational system for the evolution of δx and δy that reads as

$$\delta\dot{x} = -\frac{i\langle k^{3/2} \rangle}{c^{3/2}} \delta x + \frac{K\langle k^2 \rangle}{2\langle k \rangle} \delta y \tag{5.27}$$

$$\delta\dot{y} = \frac{K\langle k^2 \rangle}{2\langle k \rangle} \delta x + + \frac{i\langle k^{3/2} \rangle}{c^{3/2}} \delta y \tag{5.28}$$

It is now straightforward to show that the critical condition for the stability of the incoherent state is

$$c^{3/2} K \langle k^2 \rangle = 2\langle k^{3/2} \rangle \langle k \rangle. \tag{5.29}$$

The eigenvalues of the Jacobian matrix change from being both imaginary to become both real as density increases in the system. The fully imaginary spectrum predicts the exist-

ence of a center attractor [179], indicating a marginal stability of the incoherent state. Accordingly, one may expect stationary oscillations of the order parameter [126]. Here these oscillations appear too small to be observed in the forward process, because the system is initialized with isolated units –in the incoherent state– and stays there as the network evolves adiabatically. Fortunately, the forward abrupt transition to phase-locking is still well predicted by the critical condition given by Eq. (5.29). When the eigenvalues become real (a pair of positive and negative values), the marginal stability of the incoherent state is lost via the appearance of what is known as an unstable saddle point, and the system transits from incoherence to full phase-locking.

Finally, invoking the deterministic limit, we have that $k_i = c|\omega_i|^{2/3}$, and for a general $g(\omega)$ the constant is given by $c = \langle k \rangle / \langle |\omega|^{2/3} \rangle$. Then, a closed form for the forward critical threshold p_c^f is finally obtained as

$$p_c^f = \frac{2\langle |\omega|^{2/3} \rangle^2 \langle |\omega| \rangle}{KN \langle |\omega|^{4/3} \rangle}. \tag{5.30}$$

For a uniform distribution $g(\omega) \in [-\gamma, \gamma]$, one can explicitly solve the integrals that give the expected moments and, after plugging these results in Eq. (5.30), one ends up with the simple formula

$$p_c^f = \frac{21\gamma}{25KN}. \tag{5.31}$$

The predicted value p_c^f is plotted in Fig. 5.4.a) showing again a remarkable agreement. This analytical estimation allows addressing the aforementioned issue about the relation between synchronization and percolation onsets by making use of Eq. (5.7) and Eq. (5.31). Combining both expressions, a simple relation for the percolation p_c and forward synchronization p_c^f thresholds is given by

$$p_c \approx 2Kp_c^f. \tag{5.32}$$

Eq. (5.32) is probably the most remarkable analytical result of the chapter. It illustrates the natural connection between the structural and dynamical aspects of our model, proving by analytical means that EP and ES transitions can emerge under the same mechanistic framework, i.e. in a competitive percolation process.

We close our analysis by looking at the synchronization diagram in the (p, M)-plane, shown in Fig. 5.4.b), and in the (p, K)-plane, shown Fig. 5.4.c). In Fig. 5.4.b), we observe that, fixing $K = 0.05$, a saddle-node bifurcation collides/appears with a pitchfork bifurcation and bistability emerges [125], i.e. the collision of the theoretical backward curve and the approximated forward threshold successfully predicts the codimension-two point. This critical point for which ES shows up takes place around $M \approx 5$. In Fig. 5.4.c), we see that K, the coupling parameter that does not play a role in the percolation process, it is crucial to synchronization dynamics. The precise location of the synchronization thresholds can be controlled from occurring simultaneously with the percolation one for large values of K, to occur much later for smaller values of K and to finally disappear for sufficiently small K.

Interestingly, the system transits more sharply for large K (low p), but has a wider region of hysteresis for low K (large p).

In the remaining of this section, we explore the dynamics of the model for different system sizes and values of the sampling noise, unveiling an interesting effect. We also show that the phenomenology is robust to changes in the distribution of intrinsic frequencies, and that our results also hold for directed networks. To round off proving the generality of these findings, in the following section we will also extend the model to more realistic biological and engineering contexts.

5.3.3 *Finite-size and noise effects*

First, we jointly consider the effect of size N and noise (via sampling parameter M). We corroborate that the abruptness of the transitions occurring at single link changes holds for increasing size, such that Δr in a single step does not vanish as size grows [143]. We observe in Fig. 5.5.a) and Fig. 5.6.a) that the mean maximum jump value increases with size (towards red colors) and induces a macroscopic jump in r at single link changes, even at large system sizes. The same effect occurs for the hysteresis area (which is normalized by size N for proper comparison), which increases for large system sizes, as observed in Fig. 5.5.b) and Fig. 5.6.b). Interestingly, the dependence on noise, via the sampling parameter M, is non-monotonous, showing a peak around $M \approx 50$, maximized again at the largest studied size.

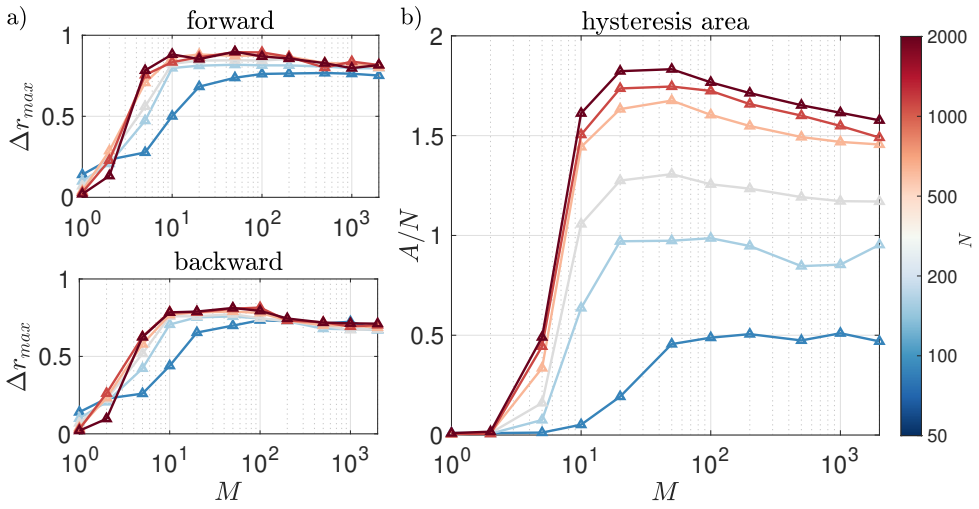

Figure 5.5: a) We plot the maximum difference of the average r between two consecutive link changes in the forward (top) and backward (bottom) directions for different values of M in log scale and for different sizes (from blue to red colors). b) We plot the normalized hysteresis area A/N (sum of differences between r backward and r forward) for increasing M and different sizes. We observe the monotonous dependence with N and the non-monotonous dependence with M. Results are averaged over 10 realizations of the process. Each percolation process is run in both directions from $p = 0$ to $p = 20/N$, corresponding to a maximum mean degree $\langle k \rangle = 20$, using Heun's method, with $dt = 0.05$ and 10^3 steps, discarding the first half for averaging r. Coupling strength is set to $K = 0.05$ and $g(\omega) \in [-1, 1]$. Reprinted by permission of [248].

We explain the counter–intuitive effect of the local rule better sustaining synchrony as noise is widely present with the following argument: The rule is derived using local information, such that higher-order effects are neglected by assumption. However, applying the rule itself makes higher-order effects more important (inducing structural and dynamical anti–correlations). Therefore, the local prediction of Δr deviates from the exact one as we advance in the percolation process, producing negative feedback that penalizes the maximization of Δr as the M-sampling increases. In this context, a precise value of sampling (noise) leads to the optimal performance. Luckily, we can still find the optimal value of M in a particular setting without running the dynamics. Due to the proven goodness of the CC ansatz in the explosive regime, finding the M that maximizes synchrony in the linearized regime (which can be directly computed via the aforementioned pseudo-inverse Laplacian) will turn out to be the M that maximizes ES behvior. However, the reader should note that the proposed model is intrinsically noisy, and the location of the synchronization transitions may vary between different realizations of the process. Alternative –deterministic– methods to build synchronization bombs may be interesting to remove this uncertainty, but the current mechanism is intentionally designed in the presence of noise. The noisy aspect turns out to be crucial to the optimal performance of our synchronization bomb.

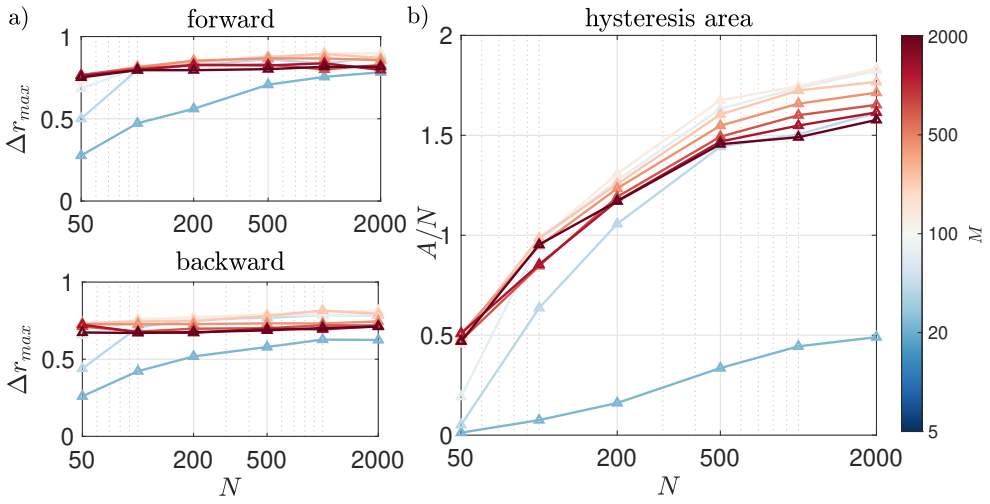

Figure 5.6: a) We plot the maximum difference of the average order parameter between two consecutive link changes in the forward (top) and backward (bottom) directions for increasing size N in log scale and for different sampling/noise M (from blue to red colors). b) We plot the normalized hysteresis area A/N (sum of differences between the values in the backward and forward curves) for increasing values of N and for different samplings M. We observe, from a complementary perspective, the monotonous dependence with N and the non-monotonous one with M shown in Fig. 5.5. Parametrization is the same as in the previous figure. Reprinted by permission of [248].

5.3.4 *Robustness to varying parameters*

Here we extend our results considering a more general parametrization of the model. In particular, we analyze the output of the model for different distributions of internal frequencies and considering also the case of directed (non-symmetric) interactions.

Effect of the frequency distribution

Here we consider that $g(\omega)$ is drawn from a normal distribution and a bounded bimodal one, generated with a $Beta(0.1, 0.1)$ distribution, a family of continuous probability distributions defined on the interval [0,1], fixing the mean to zero and the variance to $\sigma^2 = 1/3$, in order to compare against the uniform case in [-1,1] used in all the other experiments, which has the aforementioned variance. From Fig. 5.7, one can observe that a clear bistable

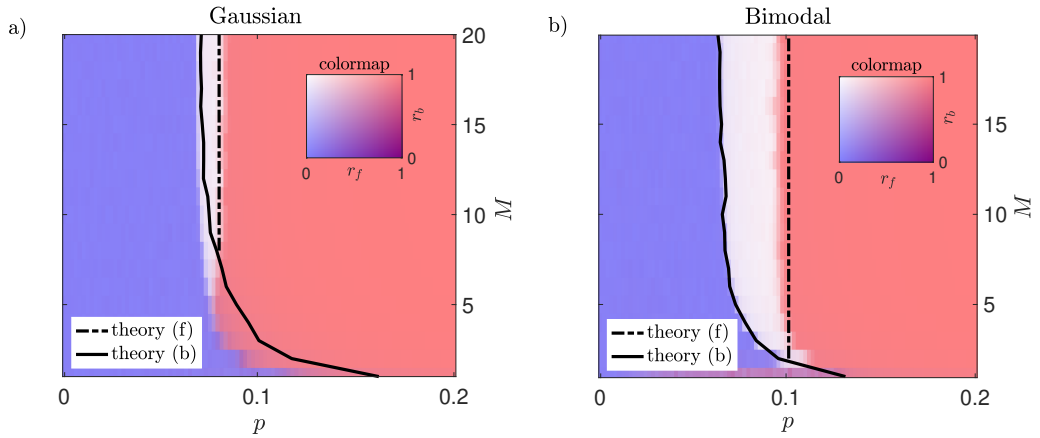

Figure 5.7: We plot the synchronization phase-space depending on M and p for a fixed $K = 0.05$ for a) Gaussian a) and b) bimodal distribution of frequencies with mean zero, $\langle\omega\rangle = 0$ and variance $\sigma^2 = 1/3$. Dashed (solid) lines correspond to the theoretical predictions of the forward (backward) synchronization thresholds, and the colorbar shows the legend for both r_b (backward) and r_f (forward). Reprinted by permission of [248].

region in the plane (p, M) is present for these choices of $g(\omega)$. The bistable region is larger for the bimodal distribution than for the Gaussian one, which means that having a more polarized distribution of frequencies enhances the explosivity of the system, a result that one could expect from the construction of the model. In the Gaussian case (less polarized than the uniform one), the bistable region is much narrower, as can be observed in Fig. 5.7.a). In the latter case, the prediction of the backward synchronization threshold (solid line) is less accurate than in other scenarios for low M. This source of error can be explained by noting that the CC method [145, 146] used in our model is based on an *explosive trick*. The trick assumes that the whole system is in the phase-locking state before the (backward) transition. This assumption does not hold for a Gaussian distribution of $g(\omega)$. It seems that the global phase-locking state is not supported by the overall network (but by a large fraction of the oscillators), and the value at which the full phase-locking state loses the stability does not coincide with the backward synchronization threshold. Nevertheless, this theory can be still used by finding the largest synchronized cluster of a

given size smaller than N, although this improvement would require larger computational costs [146]. The forward prediction (dashed line), based on the OA ansatz [122], does not suffer from this issue and captures well the critical threshold even for high values of noise (low sampling M).

Extension to directed networks

We close this section by shifting from undirected networks to a more general setting by allowing directed, asymmetric connections. We can leverage the results presented in [231] and in section 4.4.2, and use a modified version of our percolation rule, Eq. (5.2), that accounts for the directionality of links and predicts the change of synchrony with local information. The directed rule given by Eq. (4.70) can be written as

$$\Delta r_{ij} = \pm \frac{1}{N k_i} \left[\frac{\omega_i}{k_i} \left(\frac{\omega_j}{k_j} - \frac{\omega_j}{k_j} \right) \right], \tag{5.33}$$

where Δr_{ij} accounts for the change in r after adding (or removing) a directed link coming from j to i, and $k_i = \sum_j a_{ij}$ is the in-degree of the i-node.

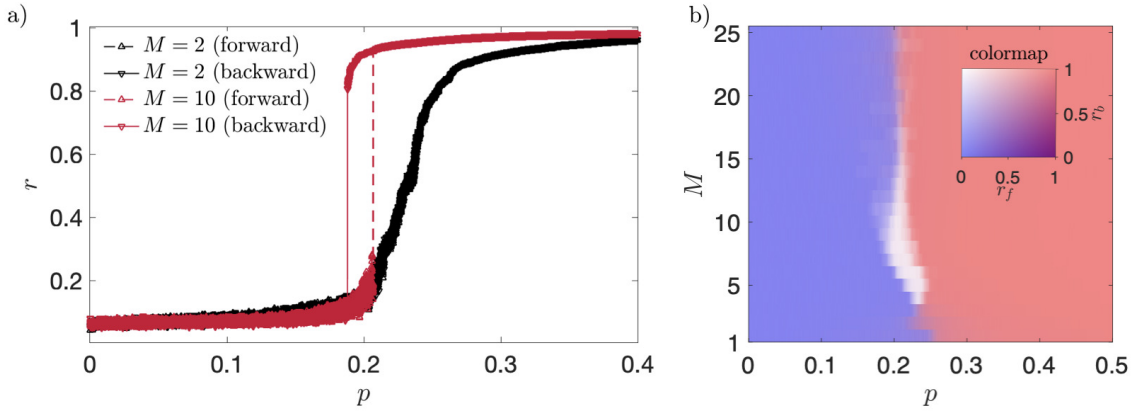

Figure 5.8: a) We plot the synchronization curves depending on p for two values of sampling/noise, $M = 2$ (black) and $M = 10$ (red). Measurements are taken at every single link. Parametrization is the same as in previous figures, and coupling strength is set to $K = 0.025$. b) Numerical diagram in the (p, M)-plain. Colormap shows the corresponding values of r in the forward and backward directions. Results are averaged over 25 realizations of the process. Reprinted by permission of [248]

We wonder to which extent the ES found in our model remain present in the directed scenario. The answer is affirmative: we numerically found that the bomb-like transitions occur at single directed link changes when the rule of Eq. (5.33) is applied. In Fig. 5.8.a), we show two examples of the synchronization curves in the forward and backward directions, observing an abrupt synchronization diagram, with its associated hysteresis, that occurs for a sampling parameter $M = 10$, but it is completely absent for a much lower value $M = 2$. In Fig. 5.8.b) we plot the phase-space depending on both the density p and sampling/noise M. Interestingly, for the coupling value $K = 0.025$, the hysteresis window

is quite small, and it is only present for $M \in [5, 20]$. Nevertheless, the phenomenology is qualitatively similar to the undirected case (see Fig. 5.4 for a proper comparison). We expect the region of hysteresis to be enhanced by an increase in the coupling strength (up to some value), as occurs in the undirected case.

The previous results confirm that the synchronization bomb can be extended to directed networks, which perhaps represent a more realistic scenario, at least in biological systems like the brain, where synaptic interactions are directional [15]. A more detailed analysis of the directed synchronization bomb, including the results on the structural properties such as the percolation threshold and microscopic correlations and its extension to other dynamical processes, is left for further work. However, these preliminary results confirm that the results are robust to changes in model assumptions, such as link directionality. Furthermore, the already known appearance of Braess' Paradox in directed networks [231], studied in more detail in section 4.4.3, unveils the counter–intuitive possibility of designing *reversed* synchronization bombs, meaning that the transition from incoherence to global synchrony (or vice-versa) can be induced by the removal (or addition) of a single directed link. Up to now, the *reversed* design of the synchronization bomb is a mere conjecture, but hopefully it will be proven true in the future.

5.4 SYNCHRONIZATION BOMBS BEYOND PHASE MODELS

Here we show our final results. We extend the results for our bomb-like model beyond the dynamics of idealized coupled phase-oscillators. We go beyond the Kuramoto model and consider a coupled Rössler system of chaotic units and a standard model of cardiac pacemaker cells. In both cases, we confirm, by numerical means, the existence of abrupt transitions induced by single link perturbations in a competitive percolation process driven by the local rule of Eq. (5.2).

5.4.1 *Chaotic oscillators*

Synchronization phenomena observed when coupling chaotic systems [6] is a quite counter–intuitive phenomenon. This type of synchronization process achieves a perfect dynamical coherence between systems that, when isolated, display deterministic chaos, i.e. exponential divergence of nearby trajectories. We consider the Rössler system, a paradigmatic model for the emergence of chaotic dynamics [50], to show the robustness of our bomb-like model in this context.

We choose to work with a large ensemble of diffusively coupled heterogeneous chaotic oscillators [270–272], a modified, piece-wise linear Rössler system [50], which evolves in a 3-dimensional space following the equations of motion

$$\begin{aligned} \dot{x}_i &= -f_i \left[\tau \left(x_i - K \textstyle\sum_{j=1}^{N} a_{ij}(x_j - x_i) \right) + \beta y_i + \delta z_i \right], \\ \dot{y}_i &= -f_i \left(-x_i + \nu y_i \right), \\ \dot{z}_i &- f_i \left(-g(x_i) + z_i \right), \end{aligned} \tag{5.34}$$

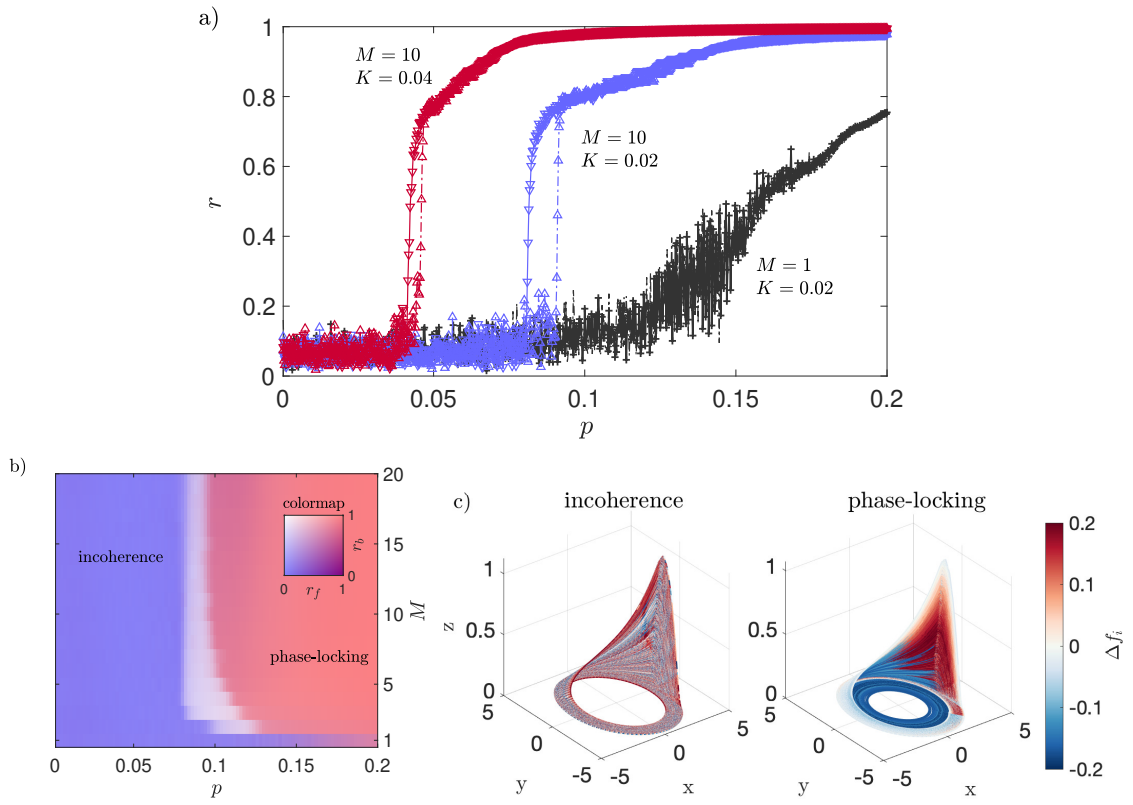

Figure 5.9: a) Examples of synchronization curves for several values of M and K. As observed, hysteresis cycle appears when $M > 1$ and lower (higher) values of K translate into wider (narrower) cycles and less (more) abrupt transitions. b) Synchronization phase-space in the (p, M)-plain, for a fixed strength $K = 0.02$. Results are qualitatively similar to the ones found in Fig. 5.4.b)), although here the transitions are blurrier than in the Kuramoto case, and the birth of hysteresis occurs for higher noise (lower M). c) Evolution of the oscillators trajectories in the Rössler attractor for $M = 10$ and $K = 0.02$ at two different p-steps, before (left) and after (right) the forward synchronization transition. The color bar captures the frequency of the oscillator relative to the mean. Eq. (5.34) is numerically integrated using Heun's method, with $dt = 0.05$, 10^3 time-steps and temporal averages of r are taken at every 5 link changes. Reprinted by permission of [248]

where the non-linear function inducing the chaotic behavior is defined as $g(x) = 0$ if $x \leq 3$ and $g(x) = \mu(x - 3)$ if $x > 3$. The other parameters are set following [271, 272], with $\tau = 0.05$, $\beta = 0.5$, $\delta = 1$, $\nu = 0.02 - 100/R$. The parameter $R = 100$ ensures a phase-coherent regime (even in the uncoupled case) [270–272], where a phase can be defined after projecting onto the xy-plane, i.e. $\theta_i = arctan(y_i/x_i)$, such that the synchronization order parameter r can be measured by the standard Kuramoto order parameter r. In Fig. 5.9.c), we plot a 3D representation of the trajectories of the chaotic, phase-coherent, oscillators at two different p-steps of the forward process, where the notion of phase from the projection into the xy-plane becomes evident. As in Eq. (5.1), K is the (fixed) coupling strength and the entries a_{ij} of the adjacency matrix A capture the presence of undirected and symmetric interactions between the oscillators, evolving under the rule of Eq. (5.2). The instantaneous velocity of the units is determined by f_i, which we assign proportional to the frequency, $f_i = 10 + 0.2\omega_i$, drawn again from a uniform distribution $g(\omega)$ in $[-1, 1]$.

Figure 5.9.a) displays three examples of synchronization transitions $r(p)$ for a system of $N = 200$ and different choices of K and M. Similarly to the Kuramoto case, in the construction process, for noise values of $M > 1$, the order parameter r experiments abrupt jumps from incoherence ($r \sim 0.1$) to a more coherent state ($r > 0.7$), that continues to grow to stronger synchronization ($r \sim 0.9$) as the density of links, p, increases. For the backward transition, the jump from phase-locking to incoherence happens at a lower value of p, resulting in a small hysteresis cycle. In panel 5.9.c) we visualize the diagram in the (p, M)-plane, unveiling that the bistable region appears even for very small values of M.

The presented success of the chaotic synchronization bomb is supported by some available results that exploits optimal [272] and ES properties [271] of Kuramoto oscillators on the diffusively coupled Rössler system. However, as numerical results in Fig. 5.9.a)-b) indicate, the bomb is slightly noisier than in the KM. The fine-tuning of more parameters and the chaotic behavior may difficult its control and design from scratch. In any case, from a more practical standpoint, these results predict that synchronization bombs can be implemented in the lab, at least by means of electronic circuits of Rössler chips [271].

5.4.2 *Cardiac pacemaker cells*

In our final application, we consider as a biologically-plausible extension of our results, a model of cardiac pacemaker cells –the collection of cells responsible for generating a strong, coherent pulse that propagates through the entire heart and initiates each contraction [273]–. We consider a standard system of network-coupled pacemaker cells consisting of, for each pacemaker, a two-variable system describing the dimensionless transmembrane voltage v and gating variable h which summarizes ionic concentrations. For more details on the model, we refer the reader to the reference [273]. For a system of N pacemakers, the equations of motion are given by

$$\begin{aligned} \dot{v}_i &= \tau_i^{-1} f(v_i, h_i) + K_v \sum_{j=1}^{N} a_{ij}(v_j - v_i), \\ \dot{h}_i &= \tau_i^{-1} g(v_i, h_i) + K_h \sum_{j=1}^{N} a_{ij}(h_j - h_i). \end{aligned} \tag{5.35}$$

The local dynamics of each v_i and h_i are described by

$$f(v,h) = \frac{h(v+0.2)^2(1-v)}{0.3} - \frac{v}{6}, \tag{5.36}$$

$$g(v,h) = \frac{1}{150} + (8.333 \times 10^{-4})[1 - \mathrm{sgn}(v - 0.13)] \times \{0.5[1 - \mathrm{sgn}(v - 0.13)] - h\}. \tag{5.37}$$

In this model, the timescales τ_i capture local heterogeneity between the different pacemakers, scaling the period of each isolated cell, which is equivalent to having an effective natural frequency for each pacemaker proportional to τ_i^{-1}. Using a system of $N = 200$ pacemakers with τ_i^{-1} randomly distributed in $[0.4, 1.6]$ and coupling strengths $K_v = 0.009$ and $K_h = 0.0044$ (imposing a stronger coupling via the voltage diffusion compared to ionic

diffusion [273]) we implement the already familiar competitive percolation process driven by our proposed local rule.

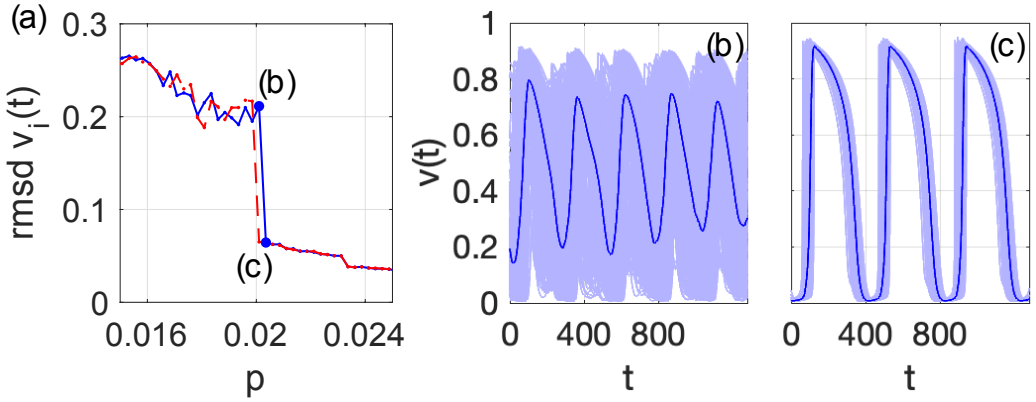

Figure 5.10: a) We plot the voltage error (captured by the standard deviation) as a function of the percolation parameter p, under percolation dynamics in the forward and backward processes, plotted in dot-dashed and solid lines respectively. b) and c) Right before and after the explosive transition observed in a), we show the individual voltage (light blue) time series $v_i(t)$ and the mean (dark blue). Reprinted by permission of [248].

Instead of using the standard order parameter computed from the phases, here we measure the collective synchrony by considering the error in the voltage variable, in terms of its overall standard deviation. We compute temporal means of the error as the percolation process evolves in both directions, and plot the voltage error in Fig. 5.10.a). Note that at around $p \approx 0.02$ the system displays ES, jumping from considerably large to small errors, indicating an abrupt synchronization transition. In Figs. 5.10.b-c) we visualize the actual voltage dynamics just before and after the transition. Individual voltage time series $v_i(t)$ are plotted in light blue color, and the overall (average) voltage is plotted in dark blue.

Note that the physiological features of the pacemakers dynamics, more complex than the ones of Kuramoto phase-oscillators, still allow to reproduce the key phenomenology of the synchronization bomb. These experiments illustrate the fact that our bomb-like model can be extended to many types of oscillator networks. The dynamics of cardiac pacemaker cells describe one of many plausible scenarios of biological units (synchronized heart pulses) and the reader should note that the system described in Eq. (5.35) is mechanistically similar to other type of relaxation oscillators with membrane potentials, including the well-known Van der Pol and FitzHugh-Nagumo models [46, 47, 274], which are used to capture the dynamics of neuronal circuits. We expect our results to be relevant in these neuronal-inspired models, but the current work already proves the potential design of synchronization bombs in systems of biological units, beyond phase oscillators with sinusoidal periods.

5.5 SUMMARY AND DISCUSSION

The main findings introduced in this chapter are three-fold. First, we have proposed a model that serves as a proof of concept to validate the theoretical machinery developed

in this thesis. In this sense, we have successfully applied several mathematical tools that were introduced in the previous chapters, allowing us to characterize the behavior of the synchronization bombs and to explain the dependence of the main parameters by analytical and numerical means. Second, with our model we have bridged the decentralized and noisy optimization of synchrony with the emergence of explosive behavior, showing that a minimal self-organized mechanism of network growth can be used to understand and control ES in adaptive biological systems like the brain or the heart and engineered ones like power-grids or electronic circuits. And third, and focusing more on the theoretical challenges of the problem, the emergence of synchronization explosions and bi-stability induced by localized structural perturbations –without any fine-tuning of global parameters– has allowed us to join explosive synchronization and percolation under the same mechanistic framework [143, 263].

The nuances of the self-organized synchronization bomb unveiled several interesting phenomena. Besides the birth of ES due to single link perturbations, the effects of the proposed local rules include a delayed percolation threshold and a non-monotonous dependence of the bistable region with noise (in terms of a sampling parameter), meaning that a significantly large amount of noise produces the optimal synchronization bomb. This finding highlights the fact that noise is a necessary feature of decentralized optimization processes, here in the context of a self-organized network growth driven by the gain of synchrony. Furthermore, we have seen the persistence of our results in the extensions to directed networks and in models beyond phase-oscillators, as the Rössler system of chaotic units or a model of cardiac pacemaker cells, pointing to potential implementations and applications in empirical settings. It is worth mentioning that, alternative, deterministic approaches could lead to a better optimization of the explosive behavior and a more precise control of the location of the transitions in empirical networked systems. This deterministic approach is still missing. From a theoretical perspective, our results unveils a mechanistic origin of ES in phase models that aligns well with the recent framework of self-organized bistability [275] and make a step towards the missing explanation for the birth of abrupt synchronization in pair-wise networks via a universal route [276]. By switching on a single additional parameter (the amount of sampling in a percolation process), we have seen how an oscillator network can self-organize towards a high-dimensional correlated state where explosive behavior spontaneously emerges.

The design of synchronization bombs is almost the final result of this thesis. Uncertainty has also played an important role here, controlling the pace of a decentralized and noisy percolation process. Before concluding our dissertation, we take a loop of time from the most recent results in our field back to the origins of synchronization theory, and leverage this loop to pave further lines of research.

6

ON THE LOOP OF TIME

What is a matrix? Werner Heisenberg (1925)
What is the matrix? Keanu Reeves (1999)

Andreas Wirzba

6.1 INTRODUCTION

This chapter is a bit of an outlier, self-consistent on its own, but somehow related to the previous chapters and to future work to come.

Very recently, L. Muller and colleagues [147] have proposed an algebraic approach to study a particular complex-valued extension of the Kuramoto model (KM), which admits an analytical solution in closed form. The dynamics of the linear model is different from the Kuramoto one, as explained in [150]. However, the striking resemblance between both allows to predict and control different synchronization regimes [147, 150, 151], including equilibrium solutions in the non-linear dynamics for a system of identical oscillators and chimeras or twisted states as shown in Fig 1.8.a) of the introduction of this thesis. Interestingly, this complex linear model, with an additional damping parameter that bounds the amplitude of the oscillators, was already studied in detail by D. Roberts in 2008 [277]. Roberts found a phase-transition from incoherence to full phase-locking at a critical value of the coupling strength, instead of going through a partial phase-locking state, as occurs in the KM. This research line was not continued in depth, and we indeed discovered this paper from the recent work of Muller et al. [147].

In this chapter, we show that the derivation of the results in [147] is actually the reverse way that Kuramoto followed in his short report of 1975 to introduce his model for the first time, starting from a system of non-linear Stuart-Landau oscillators in the weakly coupling limit [4]. This ironic time loop raises whether Kuramoto was not aware of the potential advantages of solving the linear system of coupled complex oscillators, or he was not particularly interested on it. He was looking for macroscopic phase transitions [3], and that is exactly what he found using the self-consistent analysis in the phase model. In any case, the story deserves a mention and the explicit connection between both models appears to be a promising line for further work.

In fact, we will make a first step in this direction here by realizing that the phase transition in the linear system can be linked to the onset of synchronization in the KM on top of complex networks. This connection allows us to exactly recover the mean-field ap-

proximation of [102] from the solution of a spectral problem in linear algebra, using the configuration model (a rank-one network approximation) and assuming a random allocation of frequencies. We will discuss how these findings already sketch a more general method to estimate the onset of synchronization in arbitrary networks with any kind of correlations and frequency distributions, a quest that we will tackle in the very near future. We close the chapter by noting that the analytical solution of the complex linear system is analogous to the solution of the linearized phase system in terms of the Laplacian eigenmodes, and it also provides an alternative view of diffusion geometry [119] and a novel origin to network communicability [230], a well-known metric in the field. We argue that these recent observations seem to align surprisingly well with the research lines followed during the course of this thesis.

6.2 A REVIEW OF THE NOVEL ALGEBRAIC APPROACH

Let us begin by summarizing the recent result of [147]. The derivation starts with a variation of the KM, with an additional imaginary component in the interaction term

$$\dot{\theta}_n = \omega_n + \gamma \sum_{j=1}^{N} a_{nj}[\sin(\theta_j - \theta_n) - i\cos(\theta_j - \theta_n)], \forall\ n \in 1, \ldots, N, \tag{6.1}$$

where $\theta_n \in \mathbb{C}$ is now a complex-valued variable. Multiplying both sides by the imaginary unit i and using Euler's formula, Eq. (6.1) transforms into

$$i\dot{\theta}_n = i\omega_n + \gamma e^{-i\theta_n} \sum_{j=1}^{N} a_{nj} e^{i\theta_j}, \tag{6.2}$$

or in matrix form

$$\dot{\theta} = \omega + \frac{\gamma}{i} diag[e^{-i\theta}] A e^{i\theta}. \tag{6.3}$$

Multiplying both sides by the matrix $diag[e^{i\theta}]$ and using the derivative relation

$$diag[e^{i\theta}]\dot{\theta} = \frac{1}{i}\frac{d}{dt}e^{i\theta}. \tag{6.4}$$

one ends up with the linear autonomous system given by

$$\dot{x} = \hat{H}(\gamma, A, \omega)x, \tag{6.5}$$

where $x = e^{i\theta}$ is a complex-valued vector and its argument $arg(x)$ is a vector of real-valued phases (here we take the first argument, i.e. $\theta \in [-\pi, \pi]$ without loss of generality). The operator $\hat{H}(\gamma, A, \omega) = iW + \gamma A$ (with W a diagonal matrix with entries $w_{ij} = \delta_{ij}\omega_i$) is a time independent matrix, and non-hermitian if the frequencies are heterogeneous (i.e. $\omega \neq 0$). The general solution of Eq. (6.5) is given by

$$x(t) = e^{t\hat{H}(\gamma, A, \omega)}x(0), \tag{6.6}$$

with $x(0)$ being the initial condition $x(0) = e^{i\theta_0}$. The matrix exponential can be expressed in the basis of eigenvectors of $\hat{H}$, diagonalizing the matrix using the decomposition $\hat{H} = V\Lambda V^{-1}$, where Λ is a diagonal matrix with the eigenvalues and V is the matrix of eigenvectors in columns. Finally, the solution can be written as

$$x(t) = Ve^{t\Lambda}V^{-1}x(0). \tag{6.7}$$

In terms of the eigenmodes of $\hat{H}$, Eq. (6.7) is explicitly given by

$$x(t) = \sum_{j=n}^{N} \alpha_n e^{t\lambda_n} v_n, \tag{6.8}$$

where the coefficients are given by the alignment between the initial condition and the eigenvectors, i.e. the inner product $\alpha_n = \langle x(0), v_n \rangle$. Also note that the eigenvalues can be complex-valued in general, due to the non-hermiticity of $\hat{H}$. Using that the vector $\theta \in \mathbb{C}$, decomposing it in real and imaginary parts $\theta = \theta_{re} + i\theta_{im}$ and plugging it in $x = e^{i\theta}$, one finds that

$$x(t) = e^{\theta_{im}(t)} e^{i\theta_{re}(t)}, \tag{6.9}$$

thus the argument of the complex variable is related to the imaginary part of θ as $|x_n| = e^{(\theta_n)_{im}}$. Taking the time derivative of Eq. (6.9) and separating real and imaginary parts, one obtains [150, 277]

$$(\dot{\theta_n})_{re} = \omega_n + \gamma \sum_{j=1}^{N} a_{jn} \frac{|x_n|}{|x_n|} \sin\left((\theta_j)_{re} - (\theta_n)_{re}\right), \tag{6.10}$$

$$(\dot{\theta_n})_{im} = \gamma \sum_{j=1}^{N} \frac{|x_j|}{|x_i|} \cos\left((\theta_n)_{re} - (\theta_j)_{re}\right). \tag{6.11}$$

The KM is given by the first equation assuming that the amplitudes are constant and of equal value, and neglecting the imaginary equation. This means that the linear system of Eq. (6.5) is not equivalent to the Kuramoto one, although they share some properties that deserve more exploration.

This line was initiated, almost fifteen years ago by Roberts [277], who found a critical point in the case of heterogeneous frequencies, as we will see later on, and he also derived an asymmetric coupling scheme in an all-to-all network that maps exactly to the KM. More recently, the authors in [150, 151], following the work of [147] have considered the situation where $\omega = 0$, i.e. identical oscillators. Then, the operator $\hat{H}$ reduces to γA, and equilibrium solutions of the non-linear model can be obtained from the eigenvectors of A. They put special focus on ring networks where the spectra of the adjacency matrix is known, and to explain the origin of several synchronization phenomena (as partial synchro, chimeras or waves) from the geometry of the adjacency spectra. Before moving further, let us take a step back in time.

6.3 CLOSING THE LOOP

Now we show that an alternative, much shorter derivation of Eq. (6.7) can be obtained by going back to the inception of the KM, and we discuss some immediate consequences of this finding. In his seminal paper of 1975 [4], Y. Kuramoto considered, as the starting point, a coupled system of heterogeneous Stuart-Landau oscillators, the simplest non-trivial model for a temporally organized system of macroscopic self-sustained oscillations in two dimensions. The system is modeled by a set of coupled differential equations for the complex-valued vector Q, with entries $Q_n = \rho_n e^{i\phi_n}$ where ρ_n is the amplitude and ϕ the angle, or equivalently the modulus and phase of a complex variable. The system evolves following

$$\dot{Q}_n = (i\omega_n + \alpha)Q_n - \beta|Q_n|^2 Q_n + k\sum_{j=1}^{N} a_{nj}Q_j, \forall\ n \in 1,\dots,N. \tag{6.12}$$

In order to simplify this model, Kuramoto made the following assumptions: *i)* the system is globally coupled, meaning $a_{nj} = 1\ \forall\ n \neq j$, *ii)* the system is in the thermodynamic limit, $N \to \infty$ and *iii)*, the oscillators are weakly coupled, meaning that parameters $\alpha, \beta \to \infty$ while the ratio α/β remains finite. This last assumption is equivalent to say that there are two different time-scales, a very fast one where oscillators evolve towards a fixed limit-cycle with constant amplitude, and a slow scale where oscillators interact with the rest without leaving the limit cycle. The previous argument can be understood by plugging $Q_n = \rho_n e^{i\phi_n}$ into Eq. (6.12). Using assumption *iii)* to set the amplitude of the limit-cylce to a constant value, given by

$$\rho = \sqrt{\alpha/\beta}, \tag{6.13}$$

then the terms αQ_n and $\beta|Q_n|^2 Q_n$ in Eq. (6.12) cancel each other because $\alpha\rho e^{i\phi_n} = \beta\rho^3 e^{i\phi_n}$. Note that this procedure is exactly the same as setting $\alpha = \beta = 0$ in the model (thus considering only the evolution in the slow timescale of the system). After using the weakly-coupled trick, Eq. (6.12) reduces to

$$\dot{Q}_n = i\omega_n Q_n + k\sum_{j=1}^{N} a_{nj}Q_j, \forall\ n \in 1,\dots,N, \tag{6.14}$$

or in matrix form

$$\dot{Q} = [iW + kA]Q. \tag{6.15}$$

Eq. (6.15) is nothing but Eq. (6.5) with $Q = x$ and $\hat{H} = [iW + kA]$. The fun part is that Kuramoto used the exact same procedure of Muller and co. in [147] introduced before, but in the reverse direction, to arrive to the sinusoidal form of Eq. (6.1) and then he solved the model in the thermodynamic limit by finding the phase transition of the order parameter! Note that in this derivation, the KM is a limit, and the full complex-valued linear system never shows up. The KM can be reached by less heuristic means using a phase-reduction technique from Eq. (6.12) up to a first-order approximation [38, 78]. In any case, the linear problem of Eq. (6.15) is not the KM (even if $arg(x)$ approaches the phases of KM for short time windows [150]). This does not mean that the similarity cannot be further exploited.

We focus here on the onset of synchronization in complex networks, where we unveil a spectral shortcut that provides an accurate estimate of the threshold without requiring self-consistent arguments as in the usual cases [102–104, 179].

6.4 SPECTRAL SHORTCUT TO THE SYNCHRONIZATION ONSET

As noted by Roberts [277], the continuum limit of the linear model in Eq. (6.5) (in the noise-free/damping-free scenario) has the same form as the equation describing a fundamental mode in the stability analysis of Strogatz and Mirollo in the KM, see for instance [3, 179]. This mode describes the evolution of a perturbation to the incoherent state in the mean-field case, and its growth determines the birth of synchronization in the KM. The two equations are equivalent if $\gamma = k/2$, with k being the usual coupling in the KM. In other words, the linear model has two times the same *effective* coupling than the equation of the fundamental mode that is used to find the change of stability of the incoherent state at the critical point in the KM [179]. This way, Roberts was able to show that his linear model also had a phase transition, although from incoherence to full phase-locking. At a critical $\gamma_c = 1/(\pi g(0))$ in the all-to-all, infinitely large network, an eigenvalue of the infinite dimensional operator equivalent to our matrix $H = [iW + \gamma A]$ separates from the imaginary axis and becomes real. Exactly as occurs with the growth of a perturbation in [179], thus predicting the synchronization onset in the KM at the threshold

$$k_c = 2\gamma_c. \tag{6.16}$$

In Fig. 6.1 we illustrate the differences between the models in terms of the order parameter, in an all-to-all network with normal frequency distribution. After the appropriate scaling of the coupling given by Eq. (6.16), one can see the match in the transition point.

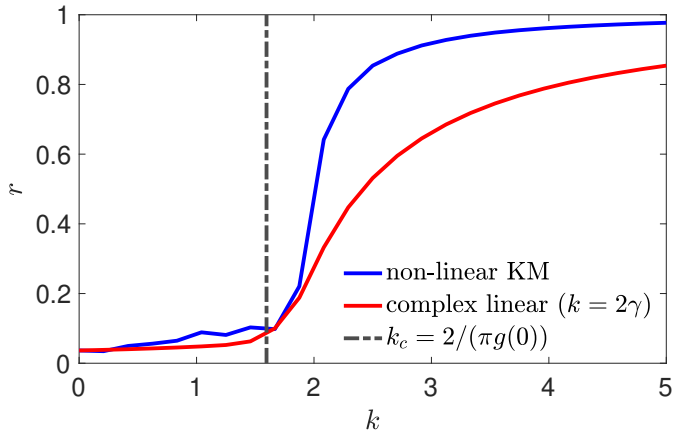

Figure 6.1: Average order parameter r depending on coupling k in a simulation of the non-linear KM in a network of $N = 10^3$ (blue), against the exact solution of the complex linear model (with coupling $\gamma = 2k$) (red). The distribution $g(\omega)$ is Gaussian with unit variance. The vertical line predicts the onset of synchronization in the mean-field KM and also the transition in the linear system with half the coupling.

Here we tackle the problem of finding the synchronization onset in the KM on top of complex networks, thus beyond the all-to-all case, by leveraging the previous results but from a different angle. We remark that we aim at determining the γ where the real part of the largest eigenvalue of $\hat{H} = [iW + \gamma A]$ becomes positive, i.e. $Re(\lambda_* > 0)$. Inspired by the work of [278] and by a recurrent assumption in this thesis –the lack of information–, we work with a rank reduction of the adjacency matrix A. In particular, the configuration model is the rank-one representation with $A' = kk^T$ and entries $A' = k_i k_j/(N\langle k\rangle)$, where only the information on the degree sequence is used [2, 94]. The eigenvalues of $\hat{H}$ are given by the roots of the characteristic equation

$$det(\hat{H} - \lambda I) = 0. \tag{6.17}$$

Using the rank-one reduction $A \approx kk^T$, we can write

$$det(iW - \lambda I + \gamma kk^T) = 0. \tag{6.18}$$

We apply the matrix determinant lemma $det(A + uv^T) = (1 + uA^{-1}v^T)det(A)$ to get

$$det(1 + \gamma k[iW - \lambda I]^{-1}k^T)\prod_j (i\omega_j - \lambda) = 0. \tag{6.19}$$

To proceed further, let us invoke a few assumptions. We consider a random allocation, i.e. the frequencies are uncorrelated from the degrees, such that we can write

$$\left[1 + \frac{\gamma\langle k^2\rangle}{N\langle k\rangle}\sum_j (i\omega_j - \lambda)^{-1}\right]\prod_j (i\omega_j - \lambda) = 0. \tag{6.20}$$

We take the continuum (infinite size) limit where $\sum_j (i\omega_j - \lambda)^{-1} = \int_{-\infty}^{\infty} g(w)dw/(i\omega - \lambda)$. We also assume that the roots are in the left-hand factor of the product (since the right factor will never vanish in the continuum limit), and therefore we end up with the equation

$$1 + \frac{\gamma\langle k^2\rangle}{N\langle k\rangle}\int_{-\infty}^{\infty}\frac{g(w)d\omega}{(i\omega - \lambda)} = 0, \tag{6.21}$$

where $g(\omega)$ is the distribution of frequencies. By multiplying the numerator and denominator in the integral by $i\omega + \lambda$, we have

$$\frac{\gamma\langle k^2\rangle}{N\langle k\rangle}\int_{-\infty}^{\infty}\frac{(i\omega + \lambda)g(w)d\omega}{(\omega^2 + \lambda^2)} = 1. \tag{6.22}$$

Here, we consider a symmetric and unimodal distribution of $g(\omega)$ as in the original KM and in the classical approximations to the onset in complex networks [102, 103], discussed in section 2.2. Since we are interested in finding the value of γ at which $Re(\lambda) > 0$, we can focus on the real part of the integral

$$\frac{\gamma\langle k^2\rangle}{N\langle k\rangle}\int_{-\infty}^{\infty}\frac{\lambda g(w)d\omega}{(\omega^2 + \lambda^2)} = 1. \tag{6.23}$$

Since $\int_{-\infty}^{\infty} \lambda d\omega/(\omega^2+\lambda^2) = \pi$ for any λ, as explained in [179], in the limit $\lambda \to 0^+$, the integral in Eq. (6.23) approaches $\pi g(0)$. After isolating the coupling strength, normalizing it by N as usual, and using Eq. (6.16), we obtain

$$k_c = \frac{2\langle k \rangle}{\langle k^2 \rangle \pi g(0)}. \tag{6.24}$$

Eq. (6.24) corresponds to the well-known mean-field approximation to the onset of synchronization in complex networks, introduced in section 2.2 and discussed throughout the thesis. Here we have arrived at the same result using a linear algebraic approach, finding the spectra of a certain non-hermitian matrix under a rank-one approximation of the network model, without requiring any self-consistent equation for an order parameter.

The previous result confirms the validity of the approach connecting the onset of synchronization in the KM and the onset of phase-locking in the complex-valued linear model. Remarkably, a spectral transition emerges from the interplay between an imaginary matrix and a real one. This mechanism captures the essence of synchronization, the competition between the internal rhythms and the interactions with the group. Using our matrix framework, it is natural to wonder several things. For instance, if these spectral transitions can capture the transitions between other macroscopic regimes observed in network synchronization (as the synchronization bomb introduced in the previous chapter), and if the previous mathematical analysis can be extended to higher-rank network models [278] and other configurations, including negative weights, directed or higher-order interactions, etc. Also, by numerical means, it should be possible to estimate the onset of sync in arbitrary networks with frequency correlations of any kind. We have validated that some of these conjectures are correct, and we are planning to present these results in future work [279]. Overall, here we attempted to provide a first step in this line, and before closing the chapter, we give a few last comments on the potential of exploiting the analogy between both models beyond the synchronization onset.

6.5 GEOMETRIC UNFOLDING IN THE COMPLEX PLANE

First, we note that the system of the complex-valued vector x in Eq. (6.5) has the same structure as a system of identical oscillators in the linearized regime (thus for sufficiently large coupling k), where the evolution of the real phases $\theta \in \mathbb{R}^N$ is given by

$$\dot{\theta} = -kL\theta, \tag{6.25}$$

with $L = D - A$ the Laplacian matrix of the network. This system converges to the trivial solution $\theta = 0$ for any $K > 0$ if the network is connected. Accordingly, the smallest eigenvalue of L (besides the zero eigenvalue associated to a constant eigenvector) $\lambda_2 > 0$ and thus, the solution of Eq. (6.25) $\theta(t) = Ve^{kt\Lambda'}V^{-1}\theta(0)$ converges regardless of the initial conditions, where the matrix Λ' now contains the eigenvalues of L. This idea was used in the seminal work of [116] to unveil the topological (hierarchical) scales of complex networks by relating the synchronization times of the different communities with the eigenvalues of

L, and the nodes in the communities with the components of the eigenvectors. This finding was key to understand the tight relation between the spectra of networks, synchronization and the concept of communities. The new insight is that the linear, complex-valued model can provide more information about dynamical communities and diffusion geometry [119] emerging from the interplay of the structure and purely oscillatory dynamics.

In the same line, the solution of the system in Eq. (6.6) shows that the matrix $e^{t\hat{H}}$ is nothing but the propagator, i.e. a Green function acting on the initial state [222]. In the case where $\omega = 0$, $\hat{H} = \gamma A$, the propagator is just the exponential of the adjacency matrix, times γ, and the solution of the system can be written as a power series in the form

$$x(t) = \sum_{n=0}^{\infty} \frac{(t\gamma A)^n}{n!} x(0), \tag{6.26}$$

thus, expressed in terms of powers of the adjacency matrix A, meaning that the solution can be expressed in an infinite series of increasing neighborhoods of the nodes. This idea aligns well with some of our previous results, and also shows that the particular basis of the exponential adjacency matrix naturally emerges from the linear dynamics in the complex plane, similarly to how the geometric unfolding introduced in chapter 4 naturally emerged from the linearized forced system (i.e. from the strongly synchronized regime). Also, let us bring here the notion of the communicability matrix, a quite well-known measure in complex networks introduced by Estrada and Hatano [230] in 2008 to quantify diffusion distances in a network, among other things. The communicability matrix was built following a heuristic argument, with a measure that counted the number of random walks between nodes, and the exponential of the adjacency matrix turned out to be the most appropriate choice. Here, our results recover the communicability matrix from a temporal snapshot of the propagator (when $\gamma t = 1$), directly from the linear, complex-valued system of identical oscillators. This finding provides an alternative explanation for the success of the communicability object in different problems of diffusive nature [66, 119].

The results of this chapter illustrate that a linear model in the complex plane can explain many features of network synchronization. This reminds the findings obtained using the linearized regime of the original KM in terms of the Laplacian spectra, that we used in this thesis to optimize synchronization with higher-order interactions (in section 3.3 of chapter 3), to find exact geometric expansions (in chapter 4) and to derive local optimal rules that can induce explosive phenomena (in chapter 5). The current findings allow extending these ideas to another linear system connected to the KM, which can inform us more about properties of the synchronization onset and the non-linear regime, against the Laplacian system that is more useful to study phase-locking properties. We recall that, in this chapter, the persistent concept of uncertainty has been introduced in terms of a rank reduction of the adjacency matrix and assuming a random allocation to arrive at a closed form for the critical threshold. Our final result of Eq. (6.24) obtained by spectral means was precisely the formula that we used at the beginning of the thesis, in chapter 3, to estimate the critical range under noisy weights. Thus here we are closing the time loop again. With this last observation, we feel ready to dive into the final conclusions of this thesis.

7

CONCLUSIONS

You tell me of an invisible planetary system in which electrons gravitate around a nucleus. You explain this world to me with an image. I realize that you have been reduced to poetry. So that science that was to teach me everything ends up in a hypothesis, that lucidity founders in metaphor, that uncertainty is resolved in a work of art.

Albert Camus[1]

This thesis proposed a theoretical study of synchronization phenomena emerging from the dynamics of network-coupled oscillators. Throughout this document, we have provided strong evidence that analytical approaches based on a minimal description of the physical process, in terms of the celebrated Kuramoto model in complex networks, and the usage of partial, incomplete information from the system at hand are relevant in at least two quests. First, to find clear and interpretable mechanistic insights of the interplay between structure and dynamics that were hidden inside spectral and numerical black-boxes and second, to provide suitable tools to predict, optimize and control the functionality of oscillator networks from a decentralized perspective and under conditions of imperfect measurements.

In chapter 3, we raised a broad question that has persisted during the length of this work. How do network constraints limit the range of synchronization behaviors? We started by providing partial answers in three specific problems, leveraging different sources of uncertainty in the coupling weights between the oscillators. In the first one, we applied error propagation techniques to show how small quenched noise in the microscopic weights propagates in a non-linear way towards the prediction of the global synchronization onset. Our results give analytical confidence bars for critical predictions depending on the heterogeneity of the structure and show that particular structures, such as scale-free networks with an exponent of three, are able to maximize the critical range, suggesting intriguing implications in adaptive and noisy systems. In the second problem, we explored the effect that balancing pair-wise and higher-order interactions has in the ranges of phase synchrony using a composite Laplacian framework, unveiling that three-way interactions increase the dynamical range and improve optimal properties in spatially-embbeded networks, a finding that is consistent with the ubiquity of higher-order interaction patterns in self-regulatory systems like the brain. In the third one, we attempted a functional mapping between pairs of networks, by tuning the weights in one network in a way that the

1 In “An Absurd Reasoning", The Myth of Sisyphus and Other Essays (1955), translated by Justin O’Brien.

synchronization behavior remains invariant in both. We proposed an information-theoretic approach under extended mean-field constraints to heuristically solve this weight-tuning optimization in uncorrelated networks, and we found that the mapping is reachable although limited by structural constraints posed by network hubs, especially around the critical point. These results called for further work and suggested descriptions of the oscillator network in terms of increasing neighborhoods as useful tools for prediction and control purposes.

In chapter 4, the previous conjecture was confirmed, by proving that the solution of the synchronized state in an arbitrary complex network can be written as a particular geometric series of increasing neighborhoods when assuming that the network is connected and not purely bipartite. This method facilitates the analysis of several synchronization properties using limited information, providing an alternative, geometric view of the system with respect to standard spectral approaches, which exploit global information that may not be available at the operative level. The convergence analysis of the geometric expansions showed spectral scalings of the truncation error and revealed a novel way of describing network and frequency arrangements, and their associated range of synchrony, in terms of the solutions of a classical damped harmonic oscillator. From a more practical standpoint, we derived a local approximation of synchrony to explain the microscopic mechanisms that optimize the system (observed before from the outcome of numerical optimizations) and to predict the existence of the Braess Paradox effect in directed networks. In a final proof of concept for this decentralized, geometric approach, in chapter 5 we built a minimal model of competitive link percolation based on a decentralized optimization of synchrony driven by a local rule. With this model, we showed that explosive, abrupt transitions and bistable behavior can emerge during the course of a self-organized network growth, and explosive transitions can occur at single link changes. We chose the name "synchronization bomb" to illustrate this phenomenon. An analytical characterization of the Kuramoto bomb was obtained using recent dimensionality reduction techniques and the robustness of the phenomena was tested under different conditions and beyond phase oscillators, in models of chaotic systems and cardiac pacemaker cells. These results suggest that synchronization bombs can be designed in the lab and propose a mechanistic and solvable route to explain the evidence of self-organized bistable and explosive phenomena in biological networks.

Lastly, in chapter 6, we deviated a bit from the previous line to clarify the explicit connection between a recent algebraic approach to the study of the Kuramoto model and a complex-valued linear system that shows up in the original derivation of Kuramoto from the weakly-coupled limit of a mean-field population of phase and amplitude oscillators. This connection allowed us to recover the prediction of the synchronization onset in complex networks in the "mean-field" approximation, studied in detail in previous chapters, from a different perspective. In particular, we found that a purely linear algebra approach combined with a one-rank reduction of the network (the configuration model) provides a fast shortcut to the problem. This result confirms once again the benefit of dealing with network representations under limited information and suggests that the approach can be extended to analyze and classify different type transitions and collective behaviors like

incoherence, partial or explosive transitions, chaos or travelling waves, from a direct estimation of the spectra of a certain non-hermitian matrix. We expect that this line will continue in further work by considering higher-rank reductions of network models and more realistic network conditions, as directed, negative or higher-order interactions and structural-dynamical correlations, which are known to produce even richer phenomena in oscillator networks.

Overall, this dissertation provides analytical solutions to several key open questions dealing with the interplay structure-dynamics in oscillator networks. The development of robust methods to manage uncertainty and partial information has led to theoretical discoveries in different aspects of synchronization dynamics. We have revealed the crucial role of prevalent network features like heterogeneity, moludar and bipartite patterns or higher-order interactions in the range-amplification and control of collective behaviors and critical points. A global finding of this thesis is a geometric and mechanistic theoretical framework that successfully quantifies how the constraints posed by a complex network determine the accessible synchronization behaviors and critical transitions, i.e. the range of collective *sounds* that an oscillator network can play.

Our approach relates microscopic configurations with macroscopic behaviors and also bridges the decentralized, geometric description of the system with the global, spectral view. The results and methods may find application in technical problems of neuroscience and engineering, but more importantly, we advance the quest of a general mathematical framework to classify and predict the whole palette of synchronization behaviors from the microscopic details, at least in the flexible context of the Kuramoto model in complex networks. This view aligns well with other recent theoretical lines that look for missing principles in oscillator networks and in non-linear physics and complex systems more broadly. Some of these works include the exact low-dimensional reductions of mean-field populations of oscillators like the Ott-Antonsen technique and its extensions [7, 122, 127], the successful analysis of complex phenomena from minimal features in ecological and genetic landscapes [87, 280, 281] and in coupled dynamics of epidemics and human behavior [142, 237–239, 282]. We expect that the mechanistic and geometric insights obtained here will become particularly relevant when combined with the recent elegant classifications of network models [278], non-hermitian hamiltonians [86], and random matrices [84, 283], and also with the promising versatility of novel artificial neural nets inspired by state-of-art neuroscience and physical systems [284].

We should also note that the community of network dynamics is gradually moving towards more applied contexts, ranging from data-driven modeling of epidemics and neuronal systems to detailed control of large engineering networks, motivated by the urgent needs of current times and access to large datasets. In most of these works, the management of uncertainty is usually treated with statistical methods and inference algorithms, since the main goal is to improve quantitative predictions. Accordingly, our results may receive more immediate attetion in the smaller theoretical realm. We believe that our mechanistic view and the uncertainty-driven methods open a novel and promising path at the fundamental level, a route connecting the geometry of synchronization with the spectra

of complex networks. In fact, a broad strength of this work is that we have connected tools, ideas and phenomenology from different fields, in the form of solid mathematical results and physical predictions that balance a moderate technical and computational complexity with high mechanistic insight and accuracy. A limitation may be precisely that we found these answers in theoretical scenarios, sometimes under strong approximations and assumptions, which might complicate a direct translation into more realistic cases. Nevertheless, the path followed in this thesis has led us to analytically solve some general problems in the field that called for clear explanations, and from a personal view, this research has rewarded me with a global view of synchronization dynamics and diffusion processes on top of complex networks, and with a diverse set of tools and concepts suitable to explore novel theoretical lines and to deal with more concrete empirical scenarios in the future.

This thesis ends with a last personal thought. During these years, I have had the chance to enjoy thinking about a beautiful problem that falls in a sweet spot of mathematics and physics, with implications that pervade almost all fields of science and even arts. It is fascinating to look back and realize how much I have learned from the brilliant people that have thought about this problem before and alongside me, and also how all these concepts have changed my view of the world. At the same time, the more I learned, the more I realized how little I was aware of, ending this path with more open questions than definitive answers. A well-known quote ascribed to A. Einstein on the idea of the perimeter of ignorance says that learning is akin to the light of a candle: “as our circle of knowledge expands, so does the circumference of darkness surrounding it." This metaphor appears to hide the sad truth, as chaos theory once did, that we will never be able to predict or know everything around us, although there is still much to discover. In complex systems, deep learning black-boxes are doing quite a remarkable job in solving key aspects of the tricky interplay of structure-dynamics, and theoreticians might want to hurry if they aim to preserve their historical relevance in science. There might be some hope in current multidisciplinary approaches driven by solid physical principles and mathematical models, synchronization in complex networks being one of the most successful paradigms. When one thinks on this problem for a while, it is likely to get a feeling that, in a near future, different branches of human knowledge will be linked and apparently distant concepts will become synchronized, in this liquid brain of collective thought [285]. Will we witness a burst of synchrony in complex systems that will eventually shed light on a big picture emerging from minimal principles? If that happens, I am quite confident that the picture will still be blurred by some kind of uncertainty.

APPENDIX: KURAMOTO'S SPEECH

In this appendix we include the full transcription of the speech given by Y. Kuramoto, in a video message[1] to the international conference "Dynamics of coupled oscillators: 40 years of the Kuramoto model", organized by A. Pikovsky, A. Politi and M. Rosenblum, and held at Max Planck Institute of Complex System, Dresden, Germany, on 27th July 2015.

> Hello everyone, I'm Kuramoto, I'm sending a message from Tokyo. This workshop, especially its title, makes me realize how far I have come and how old I'm getting.
>
> I want to take advantage of this message to tell you something from my old memories and I focus on what motivated me to develop my model of coupled oscillators forty years ago and also why I was nevertheless so reluctant to write a decent paper of this work for relatively long time. I remember that it was around 1974, that I first came across with Art Winfree famous paper which was published seven years before, entitled "Biological rhythms and the behavior of populations of coupled oscillators". I was instantly fascinated by the first few paragraphs of the introductory section of the paper, and specially my interest was stimulated when he spoke about the analogy between the synchronization transition and the phase transition of ferroelectrics, because my earlier research theme was the theory of second order phase transitions, specially in ferromagnets, and actually there is a striking similarity between synchronization phase transition and magnetic phase transition. Despite such analogy, there was one thing that made me feel a little uncomfortable: the problem of mutual coupling. Mutual coupling between two magnets or spins and mutual coupling between oscillators is quite different. For magnetic spins, the interaction energy is given by the scalar product of the two spin vectors, which means that for the particular case of planar spins, the coupling function is given by the sinusoidal coupling of phase differences. In contrast, Winfree assumed that the coupling of phase oscillators is given by the product of two period functions of the respective phases, each called stimulus function and sensitivity function, and it seemed that this product was the main problem to mathematical analysis.
>
> I didn't care much about this fact, however, because my main interest was to find a solvable model. I knew that product form coupling is more natural and realistic, but I preferred the sinusoidal form of coupling because my interest

1 From https://www.youtube.com/watch?v=lac4TxWyBOg.

was to find a solvable model. So, I looked for some plausible reason on why the sinusoidal coupling is not so unreasonable. In connection with this, the complex Ginzburg-Landau (GL) equation, which I was already familiar with, helped me. I modified the complex GL equation in such a way that the continuous oscillator field was replaced by a discrete population of oscillators, the local diffusive coupling was replaced by an all-to-all diffusion coupling, and random frequency distribution was introduced in the model. If all these assumptions are put together, it was very easy to derive my model of coupled oscillators with sinusoidal coupling and all-to-all coupling. I was sure that, like spin systems with global coupling, a self-consistent equation for a suitable defined order parameter could be derived, also for the oscillator system, but there was one subtle problem which is: how to deal with the subgroup of these oscillators that cannot synchronize with the collective oscillation?. My intuition was that those oscillators would form a stationary phase distribution in a co-rotating frame, and if that is true, then those oscillators would not contribute to the order parameter at all, for this particular model of sine coupling. In this way, I succeeded in finding that there is a critical coupling strength above which a new branch of solution corresponding to collective oscillation is obtained. Although, my argument was so crude that it involved a number of unjustified logical jumps.

Despite my success, I didn't write a paper except for a very short report for the proceeding of the International Symposium entitled "Mathematical foundations of theoretical physics" which was held in 1975 in Kyoto. I published a short report, of just two pages long, plus a few lines, typewriting with a lot of spacing, so I knew that such a brief report would be so unkind to the readers, but I was reluctant to write a paper, why? maybe I was simply lazy, but possibly there was another reason that is that I couldn't evaluate my own work partly because I was just a beginner in non-linear sciences those days, so I needed advices from experienced statistical physicists and I visited several such people to have them hear what I had done and to ask for their opinions. But unfortunately, their reactions were not so encouraging. They showed little interest in my work, and they were even critical by saying in some cases that "what you have done doesn't seem new at all, there might be a lot of similar works in the fields of mechanical and electrical engineering, you should search those fields for relevant works". I was discouraged, of course, but I still had a little hope. My hope was that there might still be some positive reactions to my fifteen minutes talk in the symposium of Kyoto. So, I presented my model and its analysis in that symposium. There was just one question from the audience. The question came from one physicist, a solid state physicist, a rather famous man[2]. His question was a rather conventional one: what is your relevance of

2 A comment to the speech on YouTube mentions that it was Brian Greene. This would be an ironic occurrence, since Greene is known for his work on string theory (a theory that is quite hard to prove empirically) and also because Greene gave a very positive criticism to the book of synchronization by Strogatz [3].

your work to real world phenomena? uhmmm. . . well, being poor of my English, I replied just one word[3]: "circadian rhythms" and virtually nothing more. His face looked puzzled, he gazed at me, dubiety. I sat down, without saying one word, and the chairman called the next speaker.

Well, again, this experience wasn't so encouraging to me. So, for the next five years or so, the model I have developed, and its analysis, was a matter of little concern to me. So, I concentrated myself to other problems of reaction-diffusion systems, and it was a big surprise when I received a letter from Art Winfree, one day in 1980 I suppose, in which he admired my short report which appeared five years before. I don't know how he could search out my short article, but I later learned that about that time, Winfree was just finishing his manuscript for the monograph about geometry of biological time, so it seems that just before the list of references for the book was completed, that my short article got his attention. And fortunately, my short article was included in the bibliography of that book and moreover he spent a few paragraphs for the discussion of my model in the book. So, I think it was the turning point of my model, in the fate of my model. Well, in the same letter, Winfree raised a very important question. He asked, "how about the stability of the particular solution you have discovered? Is there any change of stability between the coherent and the incoherent solution across the critical point?" Well, naturally I didn't have one word to answer, but I know that several years later, a number of brilliant scientists worked around this problem, and it seemed that a mathematical complete solution was almost at hand.

3 Actually two words.

BIBLIOGRAPHY

1. Anderson, P. W. More Is Different. *Science* **177,** 393–396 (1972).
2. Newman, M. *Networks: An Introduction* (Oxford University Press, Inc., New York, NY, USA, 2010).
3. Strogatz, S. H. *Sync: The Emerging Science of Spontaneous Order* (Hyperion, New York, 2003).
4. Kuramoto, Y. *Self-entrainment of a population of coupled nonlinear oscillators* in *International Symposium on Mathematical Problems in Theoretical Physics, Lecture Notes in Physics, Vol. 39,* (Springer, 1975), 420–422.
5. Acebrón, J. A., Bonilla, L. L., Pérez Vicente, C. J., Ritort, F. & Spigler, R. The Kuramoto model: A simple paradigm for synchronization phenomena. *Rev. Mod. Phys.* **77,** 137–185 (2005).
6. Arenas, A, Díaz-Guilera, A., Kurths, J., Moreno, Y & Zhou, C. Synchronization in complex networks. *Phys. Rep.* **469,** 93–153 (2008).
7. Bick, C., Goodfellow, M., Laing, C. R. & A., M. E. Understanding the dynamics of biological and neural oscillator networks through exact mean-field reductions: a review. *The Journal of Mathematical Neuroscience* **10** (2020).
8. Feynman, R. P., Leighton, R. B. & Sands, M. *The Feynman lectures on physics; New millennium ed.* (Basic Books, New York, NY, 2010).
9. Tononi, G. & Koch, C. Consciousness: Here, There and Everywhere? *Philosophical transactions of the Royal Society of London. Series B, Biological sciences* **370** (2015).
10. Bassett, D. & Sporns, O. Network neuroscience. *Nature Neuroscience* **20,** 353–364 (2017).
11. Fried, I. Neurons as will and representation. *Nature Neuroscience* **23,** 104–114 (2022).
12. Ramón y Cajal, S. *Histology of the Nervous System of Man and Vertebrates* (Oxford University Press, Oxford, 1995).
13. Hodgkin, A. & Huxley, A. A quantitative description of membrane current and its application to conduction and excitation in nerve. *Journal of Physiology* **117,** 500–544 (1952).
14. Meunier, D., Lambiotte, R. & Bullmore, E. Modular and Hierarchically Modular Organization of Brain Networks. *Frontiers in neuroscience* **4,** 200 (2010).
15. Chialvo, D. R. Emergent complex neural dynamics. *Nature Physics* **6,** 744–750 (2010).
16. Orlandi, J. G., Soriano, J., Alvarez-Lacalle, E., Teller, S. & Casademunt, J. Noise focusing and the emergence of coherent activity in neuronal cultures. *Nature Physics* **9,** 582–590 (2013).
17. Quian, R., Reddy, L., Kreiman, G., Koch, C. & Fried, I. Invariant Visual Representation by Single Neurons in the Human Brain. *Nature* **435,** 1102–7 (2005).
18. Teller, S., Estévez-Priego, E., Granell, C., Tornero, D., Andilla, J., Olarte, O., Loza-Alvarez, P., Arenas, A. & Soriano, J. Spontaneous Functional Recovery after Focal Damage in Neuronal Cultures. *eneuro* **7,** ENEURO.0254–19.2019 (2019).
19. Bialek, W., Rieke, F., Steveninck, R & Warland, D. Reading a Neural Code. *Science (New York, N.Y.)* **252,** 1854–7 (1991).
20. Hebb, D. O. *The Organization of Behavior: A Neuropsychological Theory* (John Wiley, New York, USA, 1949).
21. Martin, S., Grimwood, P. & Morris, R. Synaptic Plasticity and Memory: An Evaluation of the Hypothesis. *Annual review of neuroscience* **23,** 649–711 (2000).
22. Citri, A. & Malenka, R. Synaptic Plasticity: Multiple Forms, Functions, and Mechanisms. *Neuropsychopharmacology : official publication of the American College of Neuropsychopharmacology* **33,** 18–41 (2008).
23. Ramirez, S., Liu, X., Lin, P.-A., Suh, J., Pignatelli, M., Redondo, R., Ryan, T. & Tonegawa, S. Creating a False Memory in the Hippocampus. *Science (New York, N.Y.)* **341,** 387–91 (2013).
24. Rosenblatt, F. The perceptron: A probabilistic model for information storage and organization in the brain. *Psychological Review* **65,** 386–408 (1958).
25. Schmidhuber, J. Deep Learning in Neural Networks: An Overview. *Neural Networks* **61** (2014).
26. Silver, D. *et al.* A general reinforcement learning algorithm that masters chess, shogi, and Go through self-play. *Science* **362,** 1140–1144 (2018).

27. Brown, N. & Sandholm, T. Superhuman AI for multiplayer poker. *Science* **365,** 885–890 (2019).

28. Tunyasuvunakool, K. *et al.* Highly accurate protein structure prediction for the human proteome. *Nature* **596,** 1–9 (2021).

29. Huang, K. *Statistical Mechanics: 2nd Edition* (John Wiley, New York, USA, 1987).

30. Kim, M., Mashour, G. A., Moraes, S.-B., Vanini, G., Tarnal, V., Janke, E., Hudetz, A. G. & Lee, U. Functional and topological conditions for explosive synchronization develop in human brain networks with the onset of anesthetic-induced unconsciousness. *Frontiers in computational neuroscience* **10,** 1 (2016).

31. Schnitzler, A. & Gross, J. Normal and pathological oscillatory communication in the brain. *Nature reviews. Neuroscience* **6,** 285–96 (2005).

32. Jaynes, E. T. Information Theory and Statistical Mechanics. *Phys. Rev.* **106** (1957).

33. Onsager, L. Crystal Statistics. I. A Two-Dimensional Model with an Order-Disorder Transition. *Phys. Rev.* **65,** 117–149 (1944).

34. Sherrington, D. & Kirkpatrick, S. Solvable Model of a Spin-Glass. *Phys. Rev. Lett.* **35,** 1792–1796 (1975).

35. J.Baxter, R. in *Integrable Systems in Statistical Mechanics* 5–63 (1982).

36. Mezard, M, Parisi, G & Virasoro, M. *Spin Glass Theory and Beyond* (World Scientific, 1986).

37. Hopfield, J. J. Neural networks and physical systems with emergent collective computational abilities. *Proceedings of the National Academy of Sciences* **79,** 2554–2558 (1982).

38. Kuramoto, Y. *Chemical Oscillations, Waves, and Turbulence* (Dover Publications, 2003).

39. Arenas, A., Cota, W., Gómez-Gardeñes, J., Gómez, S., Granell, C., Matamalas, J. T., Soriano-Paños, D. & Steinegger, B. Modeling the Spatiotemporal Epidemic Spreading of COVID-19 and the Impact of Mobility and Social Distancing Interventions. *Phys. Rev. X* **10,** 041055 (2020).

40. Pastor-Satorras, R., Castellano, C., Van Mieghem, P. & Vespignani, A. Epidemic processes in complex networks. *Rev. Mod. Phys.* **87,** 925–979 (2015).

41. Matamalas, J., Arenas, A. & Gómez, S. Effective approach to epidemic containment using link equations in complex networks. *Science Advances* **4,** eaau4212 (2018).

42. De Domenico, M. & Biamonte, J. Spectral entropies as information-theoretic tools for complex network comparison. *Phys. Rev. X.* **6,** 041062 (2016).

43. May, R. M. Will a large complex system be stable? *Nature* **238,** 413–414 (1972).

44. Dörfler, F., Chertkov, M. & Bullo, F. Synchronization in complex oscillator networks and smart grids. *Proceedings of the National Academy of Sciences* **110,** 2005–2010 (2013).

45. Rohden, M., Sorge, A., Timme, M. & Witthaut, D. Self-Organized Synchronization in Decentralized Power Grids. *Phys. Rev. Lett.* **109,** 064101 (2012).

46. FitzHugh, R. Mathematical models of threshold phenomena in the nerve membrane. *The bulletin of Mathematical Biophysics* **17,** 257–278 (1955).

47. Nagumo, J., Arimoto, S. & Yoshizawa, S. An active pulse transmission line simulating nerve axon. *Proc. IRE* **50,** 2061–2070 (1962).

48. Cvitanović, P., Artuso, R., Mainieri, R., Tanner, G. & Vattay, G. *Chaos: Classical and Quantum* (Niels Bohr Inst., Copenhagen, Denmark, 2016).

49. Lorenz, E. N. Deterministic Nonperiodic Flow. *Journal of Atmospheric Sciences* **20,** 130–148 (1963).

50. Rössler, O. An equation for continuos chaos. *Phys. Lett. A* **57,** 397 (1976).

51. May, R. Simple Mathematical Models With Very Complicated Dynamics. *Nature* **26,** 457 (1976).

52. Ott, E., Grebogi, C. & Yorke, J. A. Controlling chaos. *Phys. Rev. Lett.* **64,** 1196–1199 (1990).

53. Pecora, L. M. & Carroll, T. L. Synchronization in chaotic systems. *Phys. Rev. Lett.* **64,** 821–824 (1990).

54. Watts, D. J. & Strogatz, S. H. Collective dynamics of 'small-world' networks. *Nature* **393,** 440–442 (1998).

55. Barabasi, A.-L & Albert, R. Emergence of scaling in random networks. *Science* **286,** 509–512 (1999).

56. Strogatz, S. H. Exploring complex networks. *Nature* **410,** 268–276 (2001).

57. Boccaletti, S., Latora, V., Moreno, Y., Chavez, M. & Hwang, D. U. Complex networks: Structure and dynamics. *Phys. Rep.* **424,** 175–308 (2006).

58. Dorogovtsev, S. N., Goltsev, A. V. & Mendes, J. F. F. Critical phenomena in complex networks. *Rev. Mod. Phys.* **80,** 1275–1335 (2008).

59. Parker, B. *Good Vibrations: The Physics of Music* (Johns Hopkins University Press, Baltimore, Maryland, USA, 2009).

60. Peskin, C. S. *Mathematical Aspects of Heart Physiology* (Courant Institute of Mathematical Sciences, New York University, New York, NY, USA, 2009).

61. Buck, J. & Buck, E. Mechanism of Rhythmic Synchronous Flashing of Fireflies. *Science* **159,** 1319–1327 (1968).

62. Rodrigues, F. A., Peron, T. K., Ji, P. & Kurths, J. The Kuramoto model in complex networks. *Phys. Rep.* **610,** 1–98 (2016).

63. Fell, J. & Axmacher, N. The role of phase synchronization in memory processes. *Nature reviews. Neuroscience* **12,** 105–18 (2011).

64. Unsworth, C. & Cumin, D. Generalising the Kuramoto Model for the study of Neuronal Synchronisation in the Brain. *http://www.esc.auckland.ac.nz/research/tech/esc-tr-638.pdf* **226** (2007).

65. Politi, A. & Rosenblum, M. Equivalence of phase-oscillator and integrate-and-fire models. *Phys. Rev. E* **91,** 042916 (2015).

66. Estrada, E. *The structure of complex networks: theory and applications* (Oxford University Press, Inc., New York, NY, USA, 2012).

67. Spielman, D. A. Spectral graph theory and its applications. *Proc. 48th Annual IEEE Symposium on Foundations of Computer Science,* 29–38 (2007).

68. Mieghem, P. V. *Graph Spectra for Complex Networks* (Cambridge University Press, Cambridge, UK, 2011).

69. Skardal, P. S. & Arenas, A. Control of coupled oscillator networks with application to microgrid technologies. *Sci. Adv.* **1,** e1500339 (2015).

70. Wiener, N. *Nonlinear Problems in Random Theory* (MIT Press, Cambridge, MA, USA, 1958).

71. Winfree, A. Biological rhythms and the behavior of populations of coupled oscillators. *Journal of Theoretical Biology* **16,** 15–42 (1967).

72. Arenas, A. & Pérez Vicente, C. J. Exact long-time behavior of a network of phase oscillators under random fields. *Phys. Rev. E* **50,** 949–956 (1994).

73. Daido, H. Quasientrainment and slow relaxation in a population of oscillators with random and frustrated interactions. *Phys. Rev. Lett.* **68,** 1073–1076 (1992).

74. Vicente, C. J. P., Arenas, A. & Bonilla, L. L. On the short-time dynamics of networks of Hebbian coupled oscillators. *Journal of Physics A* (1996).

75. Mirollo, R. & Strogatz, S. H. Synchronization of pulse-coupled biological oscillators. *Siam Journal on Applied Mathematics* **50,** 1645–1662 (1990).

76. Ariaratnam, J. T. & Strogatz, S. H. Phase Diagram for the Winfree Model of Coupled Nonlinear Oscillators. *Phys. Rev. Lett.* **86,** 4278–4281 (2001).

77. P. Ashwin, A. R. Hopf normal form with S_N symmetry and reduction to systems of nonlinearly coupled phase oscillators. *Physica D* **325,** 14 (2016).

78. León, I. & Pazó, D. Phase reduction beyond the first order: The case of the mean-field complex Ginzburg-Landau equation. *Phys. Rev. E* **100,** 012211 (2019).

79. Skardal, P. S., Arola-Fernández, L., Taylor, D. & Arenas, A. Higher-order interactions can better optimize network synchronization. *Phys. Rev. Research* **3,** 043193 (2021).

80. Motter, A. E., Zhou, C. & Kurths, J. Network synchronization, diffusion, and the paradox of heterogeneity. *Phys. Rev. E* **71,** 1–10 (2005).

81. Erdös, P & Rényi, A. On Random Graphs I. *Publicationes Mathematicae Debrecen* **6,** 290–297 (1959).

82. P. Erdös, A. R. On the evolution of random graphs. *Publ. Math. Inst. Hung. Acad. Sci.* **5,** 1761 (1960).

83. Brouwer, A. & Haemers, W. *Spectra of Graphs* (2012).

84. Mehta, M. L. *Random matrices* (Elsevier Academic Press, 2004).

85. Wigner, E. Characteristic vectors of bordered matrices with infinite dimensions. *Annals of Mathematics* **62,** 548–564 (1955).

86. Gong, Z., Ashida, Y., Kawabata, K., Takasan, K., Higashikawa, S. & Ueda, M. Topological Phases of Non-Hermitian Systems. *Phys. Rev. X* **8,** 031079 (2018).

87. Allesina, S. & Tang, S. Stability Criteria for Complex Ecosystems. *Nature* **483,** 205–8 (2012).

88. Fiedler, M. Algebraic Connectivity of Graphs. *Czechoslovak Mathematical Journal* **23,** 298–305 (1973).

89. Milgram, S. The small world problem. *Psychology Today* **1,** 61–67 (1967).

90. Albert, R. & Barabási, A.-L. Statistical mechanics of complex networks. *Rev. Mod. Phys.* **74,** 47–97 (2002).

91. Dorogovtsev, S. N., Mendes, J. F. F. & Samukhin, A. N. Structure of Growing Networks with Preferential Linking. *Phys. Rev. Lett.* **85,** 4633–4636 (2000).

92. Holme, P. & Kim, B. Growing Scale-Free Networks with Tunable Clustering. *Physical review. E, Statistical, nonlinear, and soft matter physics* **65,** 026107 (2002).

93. Caldarelli, G., Capocci, A., De Los Rios, P. & Muñoz, M. A. Scale-Free Networks from Varying Vertex Intrinsic Fitness. *Phys. Rev. Lett.* **89,** 258702 (2002).

94. Newman, M. E. J., Strogatz, S. H. & Watts, D. J. Random graphs with arbitrary degree distributions and their applications. *Phys. Rev. E* **64,** 026118 (2001).

95. Park, J. & Newman, M. E. J. Statistical mechanics of networks. *Phys. Rev. E* **70,** 1–13 (2004).

96. Peixoto, T. Inferring the mesoscale structure of layered, edge-valued, and time-varying networks. *Phys. Rev. E.* **92,** 042807 (2015).

97. Danon, L., Duch, J., Diaz-Guilera, A. & Arenas, A. Comparing community structure identification. *Journal of Statistical Mechanics: Theory and Experiment* **2005** (2005).

98. Newman, M. E. J. Spectral methods for community detection and graph partitioning. *Phys. Rev. E* **88,** 042822 (2013).

99. Castellano, C., Fortunato, S. & Loreto, V. Statistical physics of social dynamics. *Rev. Mod. Phys.* **81,** 591–646 (2009).

100. Barahona, M. & Pecora, L. M. Synchronization in Small-World Systems. *Phys. Rev. Lett.* **89,** 054101 (2002).

101. Gómez-Gardeñes, J., Moreno, Y. & Arenas, A. Paths to synchronization on complex networks. *Phys. Rev. Lett.* **98,** 1–4 (2007).

102. Ichinomiya, T. Frequency synchronization in a random oscillator network. *Phys. Rev. E* **70,** 026116 (2004).

103. Restrepo, J. G., Ott, E. & Hunt, B. R. Onset of synchronization in large networks of coupled oscillators. *Phys. Rev. E* **71,** 036151 (2005).

104. Restrepo, J. G., Ott, E. & Hunt, B. Synchronization in large directed networks of coupled phase oscillators. **16,** 015107 (2006).

105. Kuramoto, Y. & Battogtokh, D. Coexistence of Coherence and Incoherence in Nonlocally Coupled Phase Oscillators: A Soluble Case. *J. Nonlin. Phenom. Complex Syst.* **5** (2002).

106. Panaggio, M. J. & Abrams, D. M. Chimera states: coexistence of coherence and incoherence in networks of coupled oscillators. *Nonlinearity* **28,** R67–R87 (2015).

107. Nicosia, V., Valencia, M., Chavez, M., Díaz-Guilera, A. & Latora, V. Remote Synchronization Reveals Network Symmetries and Functional Modules. *Phys. Rev. Lett.* **110,** 174102 (2013).

108. Gómez-Gardeñes, J., Gómez, S., Arenas, A. & Moreno, Y. Explosive Synchronization Transitions in Scale-Free Networks. *Phys. Rev. Lett.* **106,** 128701 (2011).

109. Leyva, I., Navas, A., Sendiña-Nadal, I., Almendral, J, Buldu, J., Zanin, M., Papo, D. & Boccaletti, S. Explosive transitions to synchronization in networks of phase oscillators. *Scientific reports* **3,** 1281 (2013).

110. Skardal, P. S., Restrepo, J. G. & Ott, E. Frequency assortativity can induce chaos in oscillator networks. *Phys. Rev. E* **91,** 060902 (2015).

111. Motter, A. E. & Timme, M. Antagonistic Phenomena in Network Dynamics. *Ann. Rev. Cond. Matt. Phys.* **9,** 463–484 (2018).

112. Chavez, M., Hwang, D. U., Amann, A., Hentschel, H. G. E. & Boccaletti, S. Synchronization is enhanced in weighted complex networks. *Phys. Rev. Lett.* **94,** 1–4 (2005).

113. Donetti, L., Hurtado, P. I. & Muñoz, M. A. Entangled Networks, Synchronization, and Optimal Network Topology. *Phys. Rev. Lett.* **95,** 188701 (2005).

114. Tanaka, T. & Aoyagi, T. Optimal weighted networks of phase oscillators for synchronization. *Phys. Rev. E* **78,** 046210 (2008).

115. Nicolaou, Z. G., Sebek, M., Kiss, I. Z. & Motter, A. E. Coherent Dynamics Enhanced by Uncorrelated Noise. *Phys. Rev. Lett.* **125,** 094101 (2020).

116. Arenas, A., Díaz-Guilera, A. & Pérez-Vicente, C. J. Synchronization reveals topological scales in complex networks. *Phys. Rev. Lett.* **96,** 114102 (2006).

117. McGraw, P. N. & Menzinger, M. Analysis of nonlinear synchronization dynamics of oscillator networks by Laplacian spectral methods. *Phys. Rev. E* **75,** 027104 (2007).

118. Skardal, P. S., Taylor, D. & Sun, J. Optimal Synchronization of Complex Networks. *Phys. Rev. Lett.* **113,** 144101 (2014).

119. De Domenico, M. Diffusion geometry unravels the emergence of functional clusters in collective phenomena. *Phys. Rev. Lett.* **118,** 168301 (2017).

120. Gfeller, D. & De Los Rios, P. Spectral Coarse Graining of Complex Networks. *Phys. Rev. Lett.* **99,** 038701 (2007).

121. Gómez-Gardeñes, J. & Moreno, Y. From scale-free to Erdos-Rényi networks. *Phys. Rev. E* **73,** 1–7 (2006).

122. Ott, E. & Antonsen, T. Low Dimensional Behavior of Large Systems of Globally Coupled Oscillators. *Chaos (Woodbury, N.Y.)* **18,** 037113 (2008).

123. Martens, E. A., Barreto, E., Strogatz, S. H., Ott, E., So, P. & Antonsen, T. M. Exact results for the Kuramoto model with a bimodal frequency distribution. *Phys. Rev. E* **79,** 026204 (2009).

124. Skardal, P. S. Low-dimensional dynamics of the Kuramoto model with rational frequency distributions. *Phys. Rev. E* **98,** 022207 (2018).

125. Skardal, P. S. & Arenas, A. Abrupt Desynchronization and Extensive Multistability in Globally Coupled Oscillator Simplexes. *Phys. Rev. Lett.* **122,** 248301 (2019).

126. Peron, T., Eroglu, D., Rodrigues, F. & Moreno, Y. Collective dynamics of random Janus oscillator networks. *Physical Review Research* **2** (2020).

127. Lipton, M., Mirollo, R. & Strogatz, S. H. The Kuramoto model on a sphere: Explaining its low-dimensional dynamics with group theory and hyperbolic geometry. *Chaos* **31,** 093113 (2021).

128. Hannay, K. M., Forger, D. B. & Booth, V. Macroscopic models for networks of coupled biological oscillators. *Science Advances* **4,** e1701047 (2018).

129. Skardal, P. S., Taylor, D. & Sun, J. Optimal synchronization of directed complex networks. *Chaos: An Interdisciplinary Journal of Nonlinear Science* **26,** 094807 (2016).

130. Taylor, D., Skardal, P. S. & Sun, J. Synchronization of heterogeneous oscillators under network modifications: perturbation and optimization of the synchrony alignment function. *SIAM J. Appl. Math.* **76,** 1984–2008 (2016).

131. Liu, Y.-Y. & Barabasi, A.-L. Control principles of complex systems. *Reviews of Modern Physics* **88** (2016).

132. Coletta, T. & Jacquod, P. Linear stability and the Braess paradox in coupled-oscillator networks and electric power grids. *Phys. Rev. E* **93,** 032222 (2016).

133. Manik, D., Rohden, M., Ronellenfitsch H.and Zhang, X., Hallerberg, S., Witthaut, D. & Timme, M. Network susceptibilities: Theory and applications. *Phys. Rev. E* **95,** 012319 (2017).

134. Yan, G., Vértes, P., Towlson, E., Chew, Y. L., Walker, D., Schafer, W. & Barabási, A.-L. Network control principles predict neuron function in the Caenorhabditis elegans connectome. *Nature* **550** (2017).

135. Menara, T., Baggio, G., Bassett, D. & Pasqualetti, F. Functional Control of Oscillator Networks. *arXiv:2102.08566* (2021).

136. Kivelä, M., Arenas, A., Barthelemy, M., Gleeson, J. P., Moreno, Y. & Porter, M. A. Multilayer networks. *Journal of Complex Networks* **2,** 203–271 (2014).

137. Tanaka, T. & Aoyagi, T. Multistable Attractors in a Network of Phase Oscillators with Three-Body Interactions. *Phys. Rev. Lett.* **106,** 224101 (2011).

138. Giusti, C, Ghrist, R. & Bassett, D. S. Two's company, three (or more) is a simplex. *J. Comput. Neurosci.* **41,** 1 (2016).

139. Battiston, F., Cencetti, G., Iacopini, I., Latora, V., Lucas, M., Patania, A., Young, J.-G. & Petri, G. Networks beyond pairwise interactions: Structure and dynamics. *Phys. Rep.* **874,** 1 (2020).

140. P. S. Skardal, A. A. Higher-order interactions in complex networks of phase oscillators promote abrupt synchronization switching. *Comm. Physics* **3,** 218 (2020).

141. Nicosia, V., Skardal, P. S., Arenas, A. & Latora, V. Collective Phenomena Emerging from the Interactions between Dynamical Processes in Multiplex Networks. *Phys. Rev. Lett.* **118,** 138302 (2017).

142. Soriano-Paños, D., Guo, Q., Latora, V. & Gómez-Gardeñes, J. Explosive transitions induced by interdependent contagion-consensus dynamics in multiplex networks. *Phys. Rev. E* **99,** 062311 (2019).

143. D'Souza, R. M., Gómez-Gardeñes, J., Nagler, J. & Arenas, A. Explosive phenomena in complex networks. *Advances in Physics* **68,** 123–223 (2019).

144. Nicolaou, Z. G., Eroglu, D. & Motter, A. E. Multifaceted Dynamics of Janus Oscillator Networks. *Phys. Rev. X* **9,** 011017 (2019).

145. Gottwald, G. Model reduction for networks of coupled oscillators. *Chaos* **25** (2015).

146. Hancock, E. & Gottwald, G. Model reduction for Kuramoto models with complex topologies. *Physical Review E* **98** (2018).

147. Muller, L., Minác, J. & Nguyen, T. T. Algebraic approach to the Kuramoto model. *Phys. Rev. E* **104,** L022201 (2021).

148. Lohe, M. Non-Abelian Kuramoto models and synchronization. *Journal of Physics A: Mathematical and Theoretical* **42,** 395101 (2009).

149. Zhang, Y. & Strogatz, S. H. Basins with Tentacles. *Phys. Rev. Lett.* **127,** 194101 (2021).

150. Budzinski, R., Nguyen, T., Doan, J., Minac, J., Sejnowski, T. & Muller, L. A simple geometry unites synchrony, chimeras, and waves in nonlinear oscillator networks. *arXiv:2111.02560* (2021).

151. Nguyen, T., Budzinski, R., Doan, J., Pasini, F., Minac, J. & Muller, L. Equilibria in Kuramoto oscillator networks: An algebraic approach. *arXiv:2111.02568* (2021).

152. Bronski, J. C., He, Y., Li, X., Liu, Y., Sponseller, D. R. & Wolbert, S. The stability of fixed points for a Kuramoto model with Hebbian interactions. *arXiv:2111.02201* (2021).

153. Witthaut, D., Wimberger, S., Burioni, R. & Timme, M. Classical synchronization indicates persistent entanglement in isolated quantum systems. *Nature Communications* **8,** 14829 (2017).

154. Rohn, J., Schmidt, K. P & Genes, C. Phase synchronization in dissipative non-Hermitian coupled quantum systems. *arXiv:2111.02201* (2021).

155. Ishida, Y. *The immune system as a prototype of autonomous decentralized systems: an overview* in *Proceedings of the Third International Symposium on Autonomous Decentralized Systems. ISADS 97* (1997), 85–92.

156. Izhikevich, E. M. Simple model of spiking neurons. *IEEE Transactions on neural networks* **14,** 1569–1572 (2003).

157. Zhang, W.-H., Chen, A., Rasch, M. J. & Wu, S. Decentralized multisensory information integration in neural systems. *Journal of Neuroscience* **36,** 532–547 (2016).

158. Iatsenko, D, McClintock, P. V. E. & Stefanovska, A. Glassy states and super-relaxation in populations of coupled phase oscillators. *Nature communications* **5,** 4118 (2014).

159. Ronellenfitsch, H., Dunkel, J. & Wilczek, M. Optimal Noise-Canceling Networks. *Phys. Rev. Lett.* **121,** 208301 (2018).

160. Sonnenschein, B. & Schimansky-Geier, L. Approximate solution to the stochastic Kuramoto model. *Phys. Rev. E* **88,** 052111 (2013).

161. Zhou, C., Motter, A. E. & Kurths, J. Universality in the synchronization of weighted random networks. *Phys. Rev. Lett.* **96,** 1–5 (2006).

162. Arola-Fernández, L., Díaz-Guilera, A. & Arenas, A. Synchronization invariance under network structural transformations. *Phys. Rev. E* **97,** 060301 (2018).

163. Pietras, B., Deschle, N. & Daffertshofer, A. Equivalence of coupled networks and networks with multimodal frequency distributions: Conditions for the bimodal and trimodal case. *Phys. Rev. E* **94,** 052211 (2016).

164. Timme, M. Revealing Network Connectivity from Response Dynamics. *Phys. Rev. Lett.* **98,** 224101 (2007).

165. Skardal, P., Taylor, D. & Sun, J. Synchronization of Network-Coupled Oscillators with Uncertain Dynamics. *SIAM Journal on Applied Mathematics* **79,** 2409–2433 (2019).

166. Delabays, R., Tyloo, M. & Jacquod, P. Rate of change of frequency under line contingencies in high voltage electric power networks with uncertainties. *Chaos: An Interdisciplinary Journal of Nonlinear Science* **29,** 103130 (2019).

167. Shannon, C. & Weaver, W. *The Mathematical Theory of Communication* (University of Illinois Press., 1949).

168. Peixoto, T. P. Network Reconstruction and Community Detection from Dynamics. *Phys. Rev. Lett.* **123,** 128301 (2019).

169. Young, J.-G., Cantwell, G. & Newman, M. Bayesian inference of network structure from unreliable data. *Journal of Complex Networks* **8** (2021).

170. Hoffmann, T., Peel, L., Lambiotte, R. & Jones, N. S. Community detection in networks with unobserved edges. *arXiv:1808.06079* (2018).

171. Anand, K. & Bianconi, G. Entropy measures for networks: Toward an information theory of complex topologies. *Phy. Rev. E* **80,** 1–4 (2009).

172. Anand, K., Bianconi, G. & Severini, S. Shannon and von Neumann entropy of random networks with heterogeneous expected degree. *Phys. Rev. E* **83,** 036109 (2011).

173. Sonnenschein, B. & Schimansky-Geier, L. Onset of synchronization in complex networks of noisy oscillators. *Phys. Rev. E* **85,** 051116 (2012).

174. Prignano, L. & Díaz-Guilera, A. Extracting topological features from dynamical measures in networks of Kuramoto oscillators. *Phys. Rev. E* **85,** 036112 (2012).

175. Nitzan, M., Casadiego, J. & Timme, M. Revealing physical interaction networks from statistics of collective dynamics. *Sci. Adv.* **3** (2017).

176. Zhang, X., Hallerberg, S., Matthiae, M., Witthaut, D. & Timme, M. Fluctuation-induced distributed resonances in oscillatory networks. *Science Advances* **5,** eaav1027 (2019).

177. Eguíluz, V. M., Pérez, T., Borge-Holthoefer, J. & Arenas, A. Structural and functional networks in complex systems with delay. *Phys. Rev. E* **83,** 056113 (2011).

178. Skardal, P. S. & Arenas, A. Disorder induces explosive synchronization. *Physical Review E* **89,** 062811 (2014).

179. Strogatz, S. H. From Kuramoto to Crawford: exploring the onset of synchronization in populations of coupled oscillators. *Physica D: Nonlinear Phenomena* **143,** 1 –20 (2000).

180. Peron, T., Messias F. de Resende, B., Mata, A. S., Rodrigues, F. A. & Moreno, Y. Onset of synchronization of Kuramoto oscillators in scale-free networks. *Phys. Rev. E* **100,** 042302 (2019).

181. Ben-Israel, A. & Greville, T. *Generalized Inverses: Theory and Applications* (Wiley, New York, 1974).

182. Van Mieghem, P., Devriendt, K. & Cetinay, H. Pseudoinverse of the Laplacian and best spreader node in a network. *Phys. Rev. E* **96,** 032311 (2017).

183. Kinouchi, O. & Copelli, M. Optimal dynamical range of excitable networks at criticality. *Nature Physics* **2,** 348–351 (2006).

184. Chen, B., Hall, D. & Chklovskii, D. Wiring optimization can relate neuronal structure and function. *Proceedings of the National Academy of Sciences of the United States of America* **103,** 4723–8 (2006).

185. Ashton, D. J., Jarrett, T. C. & Johnson, N. F. Effect of Congestion Costs on Shortest Paths Through Complex Networks. *Phys. Rev. Lett.* **94,** 058701 (2005).

186. Li, G., Reis, S. D. S., Moreira, A. A., Havlin, S., Stanley, H. E. & Andrade, J. S. Towards Design Principles for Optimal Transport Networks. *Phys. Rev. Lett.* **104,** 018701 (2010).

187. Solé-Ribalta, A., Gomez, S. & Arenas, A. A model to identify urban traffic congestion hotspots in complex networks. *Royal Society open science* **3** (2016).

188. Kadanoff, L. & Baym, G. *Quantum Statistical Mechanics* (W.A. Benjamin Inc., New York, 1962).

189. Mahan, G. D. *Condensed Matter in a Nutshell* (Princeton University Press, 2010).

190. Zuckerman, D. *Statistical Physics of Biomolecules: An Introduction* 1–325 (2010).

191. Barrat, A., Barthlemy, M. & Vespignani, A. *Dynamical Processes on Complex Networks* 1st (Cambridge University Press, New York, NY, USA, 2008).

192. Arola-Fernández, L., Mosquera-Doñate, G., Steinegger, B. & Arenas, A. Uncertainty propagation in complex networks: From noisy links to critical properties. *Chaos* **30,** 023129 (2020).

193. Castellano, C. & Pastor-Satorras, R. Thresholds for Epidemic Spreading in Networks. *Phys. Rev. Lett.* **105,** 218701 (2010).

194. Gómez, S., Arenas, A., Borge-Holthoefer, J., Meloni, S. & Moreno, Y. Discrete-time Markov chain approach to contact-based disease spreading in complex networks. *EPL (Europhysics Letters)* **89,** 38009 (2010).

195. De Domenico, M., Granell, C., Porter, M. A. & Arenas, A. The physics of spreading processes in multilayer networks. *Nature Physics* **12,** 901–906 (2016).

196. Clauset, A., Moore, C. & Newman, M. E. Hierarchical structure and the prediction of missing links in networks. *Nature* **453,** 98 (2008).

197. Guimerà, R. & Sales-Pardo, M. Missing and spurious interactions and the reconstruction of complex networks. *PNAS* **106,** 22073–20078 (2009).

198. Hric, D., Peixoto, T. P. & Fortunato, S. Network structure, metadata, and the prediction of missing nodes and annotations. *Physical Review X* **6,** 031038 (2016).

199. Barrat, A., Barthélemy, M., Pastor-Satorras, R. & Vespignani, A. The architecture of complex weighted networks. *Proceedings of the National Academy of Sciences* **101,** 3747–3752 (2004).

200. Chung, F., Lu, L. & Vu, V. Spectra of random graphs with given expected degrees. *Proceedings of the National Academy of Sciences* **100,** 6313–6318 (2003).

201. Restrepo, J. G., Ott, E. & Hunt, B. R. Approximating the largest eigenvalue of network adjacency matrices. *Phys. Rev. E* **76,** 056119 (2007).

202. Mana, G. & Pennecchi, F. Uncertainty propagation in non-linear measurement equations. *Metrologia* **44,** 246 (2007).

203. Sarkar, C. & Jalan, S. Spectral properties of complex networks. *Chaos: An Interdisciplinary Journal of Nonlinear Science* **28,** 102101 (2018).

204. Hong, H. & Strogatz, S. H. Kuramoto Model of Coupled Oscillators with Positive and Negative Coupling Parameters: An Example of Conformist and Contrarian Oscillators. *Phys. Rev. Lett.* **106,** 054102 (2011).

205. Dwivedi, S. K. & Jalan, S. Extreme-value statistics of networks with inhibitory and excitatory couplings. *Phys. Rev. E* **87,** 042714 (2013).

206. Yu, S., Yang, H., Nakahara, H., Santos, G. S., Nikolić, D. & Plenz, D. Higher-order interactions characterized in cortical activity. *J. Neurosci.* **31,** 17514–16 (2011).

207. Reimann, M. W. a. a. Cliques of neurons bound into cavities provide a missing link between structure and function. *Frontiers in Comp. Neuro.* **11,** 48 (2011).

208. D. Horak S. Maletić, M. R. Persistent homology of complex networks. *J. of Stat. Mech.* **3,** P03034 (2009).

209. V. Salnikov D. Cassese, R. L. Simplicial complexes and complex systems. *Eur. J. Phys.* **40,** 014001 (2019).

210. C. Bick P. Ashwin, A. R. Chaos in generically coupled phase oscillator networks with nonpairwise interactions. *Chaos* **26,** 09814 (2016).

211. Millán, A. P., Torres, J. J. & Bianconi, G. Explosive Higher-Order Kuramoto Dynamics on Simplicial Complexes. *Phys. Rev. Lett.* **124,** 218301 (2020).

212. Kahle, M. Topology of random clique complexes. *Discrete Math.* **309,** 1658 (2009).

213. Napoletani, D. & Sauer, T. Reconstructing the topology of sparsely connected dynamical networks. *Phys. Rev. E* **77** (2008).

214. Barzel, B. & Biham, O. Quantifying the connectivity of a network: The network correlation function method. *Phys. Rev. E* **80,** 046104 (2009).

215. Serrano, M. Á. & Boguñá, M. Weighted configuration model. *AIP Conference Proceedings* **776,** 101–107 (2005).

216. Baronchelli, A. & Pastor-Satorras, R. Mean-field diffusive dynamics on weighted networks. *Phys. Rev. E* **82,** 1–8 (2010).

217. Gleeson, J. P., Melnik, S., Ward, J. A., Porter, M. A. & Mucha, P. J. Accuracy of mean-field theory for dynamics on real-world networks. *Phys. Rev. E* **85,** 026106 (2012).

218. Valverde, S., Ferrer-i Cancho, R. & Sole, R. V. Scale-Free Networks from Optimal Design. *EPL (Europhysics Letters)* **60,** 512–517 (2002).

219. Larremore, D. B., Shew, W. L. & Restrepo, J. G. Predicting Criticality and Dynamic Range in Complex Networks: Effects of Topology. *Phys. Rev. Lett.* **106,** 058101 (2011).

220. Corominas-Murtra, B., Goñi, J., Solé, R. V. & Rodríguez-Caso, C. On the origins of hierarchy in complex networks. *Proceedings of the National Academy of Sciences* **110,** 13316–13321 (2013).

221. Muñoz, M. A. Colloquium: Criticality and dynamical scaling in living systems. *Rev. Mod. Phys.* **90,** 031001 (2018).

222. Chung, F. & Yau, S. T. Discrete Green's functions. *J. of Comb. Theory (A)* **91,** 191–214 (2000).

223. Jalan, S. & Bandyopdhyay, J. Random matrix analysis of complex networks. *Phys. Rev. E* **76,** 046107 (2007).

224. Neri, I. & Metz, F. L. Spectral theory for the stability of dynamical systems on large oriented locally tree-like graphs. *arXiv:1908.07092* (2019).

225. Cencetti, G., Clusella, P. & Fanelli, D. Pattern invariance for reaction-diffusion systems on complex networks. *Scientific Reports* **8,** 16226 (2018).

226. Forrow, A., Woodhouse, F. G. & Dunkel, J. Functional Control of Network Dynamics Using Designed Laplacian Spectra. *Phys. Rev. X* **8,** 041043 (2018).

227. Shuman, D. I., Narang, S. K., Frossard, P., Ortega, A. & Vandergheynst, P. The emerging field of signal processing on graphs: Extending high-dimensional data analysis to networks and other irregular domains. *IEEE Signal Processing Magazine* **30,** 83–98 (2013).

228. Masuda, N., Porter, M. A. & Lambiotte, R. Random walks and diffusion on networks. *Physics Reports* **716-717,** 1 –58 (2017).

229. Newman, M. E. J. Spectra of networks containing short loops. *Phys. Rev. E* **100,** 012314 (2019).

230. Estrada, E. & Hatano, N. Communicability in complex networks. *Phys. Rev. E* **77,** 036111 (2008).

231. Arola-Fernández, L., Skardal, P. S. & Arenas, A. Geometric unfolding of synchronization dynamics on networks. *Chaos* **31,** 061105 (2021).

232. Skardal, P. S., Sun, J., Taylor, D. & Restrepo, J. G. Effects of degree-frequency correlations on network synchronization: Universality and full phase-locking. *Europhys. Lett.)* **101,** 20001 (2013).

233. Witthaut, D. & Timme, M. Braesss paradox in oscillator networks, desynchronization and power outage. *New J. Phys.* **14,** 083036 (2012).

234. Nishikawa, T. & Motter, A. Synchronization is optimal in nondiagonalizable networks. *Phys. Rev. E* **73,** 065106 (2006).

235. Artime, O. & De Domenico, M. Percolation on feature-enriched interconnected systems. *Nature Communications* **12,** 2478 (2021).

236. Cinelli, M., Peel, L., Iovanella, A. & Delvenne, J.-C. Network constraints on the mixing patterns of binary node metadata. *Phys. Rev. E* **102,** 062310 (2020).

237. Burgio, G., Steinegger, B., Rapisardi, G. & Arenas, A. Homophily in the adoption of digital proximity tracing apps shapes the evolution of epidemics. *Phys. Rev. Research* **3,** 033128 (2021).

238. Steinegger, B., Arenas, A., Gómez-Gardeñes, J. & Granell, C. Pulsating campaigns of human prophylaxis driven by risk perception palliate oscillations of direct contact transmitted diseases. *Phys. Rev. Research* **2,** 023181 (2020).

239. Steinegger, B., Arola-Fernández, L., Granell, C., Gómez-Gardeñes, J. & Arenas, A. Behavioural response to heterogeneous severity of COVID-19 explains temporal variation of cases among different age groups. *Philosophical Transactions of the Royal Society A: Mathematical, Physical and Engineering Sciences* **380,** 20210119 (2022).

240. Newman, M. E. J. Analysis of weighted networks. *Phys. Rev. E* **70,** 056131 (2004).

241. Boccaletti, S., Almendral, J., Guan, S., Leyva, I., Liu, Z., Sendiña-Nadal, I., Wang, Z. & Zou, Y. Explosive transitions in complex networks' structure and dynamics: Percolation and synchronization. *Physics Reports* **660,** 1–94 (2016).

242. Wang, C.-Q., Pumir, A., Garnier, N. B. & Liu, Z.-H. Explosive synchronization enhances selectivity: Example of the cochlea. *Frontiers of Physics* **12,** 1–9 (2017).

243. Wang, Z., Tian, C., Dhamala, M. & Liu, Z. A small change in neuronal network topology can induce explosive synchronization transition and activity propagation in the entire network. *Scientific reports* **7,** 1–10 (2017).

244. Joiner, W. J., Friedman, E. B., Hung, H.-T., Koh, K., Sowcik, M., Sehgal, A. & Kelz, M. B. Genetic and anatomical basis of the barrier separating wakefulness and anesthetic-induced unresponsiveness. *PLoS genetics* **9,** e1003605 (2013).

245. Kim, M., Kim, S., Mashour, G. A. & Lee, U. Relationship of topology, multiscale phase synchronization, and state transitions in human brain networks. *Frontiers in computational neuroscience* **11,** 55 (2017).

246. Lee, U., Kim, M., Lee, K., Kaplan, C. M., Clauw, D. J., Kim, S., Mashour, G. A. & Harris, R. E. Functional brain network mechanism of hypersensitivity in chronic pain. *Scientific reports* **8,** 1–11 (2018).

247. Dobson, I., Carreras, B., Lynch, V. & Newman, D. Complex systems analysis of series of blackouts: Cascading failure, critical points, and self-organization. *Chaos: An Interdisciplinary Journal of Nonlinear Science* **17,** 026103 (2007).

248. Arola-Fernández, L., Faci-Lázaro, S., Skardal, P., Boghiu, E., Gómez-Gardenes, J & Arenas, A. Self-organized explosive synchronization in complex networks: Emergence of synchronization bombs. *to be published* (2022).

249. Flory, P. J. Molecular Size Distribution in Three Dimensional Polymers. I. Gelation. *Journal of the American Chemical Society* **63,** 3083–3090 (1941).

250. Stockmayer, W. H. Theory of Molecular Size Distribution and Gel Formation in Branched Polymers II. General Cross Linking. *Journal of Chemical Physics* **12,** 125–131 (1944).

251. Broadbent, S. R. & Hammersley, J. M. Percolation processes: I. Crystals and mazes. *Mathematical Proceedings of the Cambridge Philosophical Society* **53,** 629–641 (1957).

252. Sahini, M. & Sahimi, M. *Applications of Percolation Theory* (CRC Press, New York, NY, USA, 1994).

253. Achlioptas, D., D'Souza, R. M. & Spencer, J. Explosive Percolation in Random Networks. *Science* **323,** 1453–1455 (2009).

254. Böttcher, L., Woolley Meza, O., Araujo, N., Herrmann, H. & Helbing, D. Disease-induced resource constraints can trigger explosive epidemics. *Scientific reports* **5** (2015).

255. Gómez-Gardeñes, J., Lotero-Vélez, L., Taraskin, S. & Pérez-Reche, F. Explosive Contagion in Networks. *Scientific Reports* **6,** 19767 (2016).

256. Echenique, P., Gómez-Gardeñes, J. & Moreno, Y. Dynamics of jamming transitions in complex networks. *Europhys. Lett.* **71,** 325–331 (2005).

257. Lampo, A., Borge-Holthoefer, J., Gómez, S. & Solé-Ribalta, A. Multiple abrupt phase transitions in urban transport congestion. *Phys. Rev. Research* **3,** 013267 (2021).

258. Pikovsky, A., Rosenblum, M. G. & Kurths, J. *Synchronization, A Universal Concept in Nonlinear Sciences* (Cambridge University Press, 2001).

259. Arenas, A., Díaz-Guilera, A. & Pérez-Vicente, C. J. Synchronization processes in complex networks. *Physica D* **224,** 27–34 (2006).

260. Pazó, D. Thermodynamic limit of the first-order phase transition in the Kuramoto model. *Phys. Rev. E* **72,** 046211 (2005).

261. Avalos-Gaytán, V., Almendral, J. A., Leyva, I., Battiston, F., Nicosia, V., Latora, V. & Boccaletti, S. Emergent explosive synchronization in adaptive complex networks. *Phys. Rev. E* **97,** 042301 (2018).

262. Zhang, X., Boccaletti, S., Guan, S. & Liu, Z. Explosive Synchronization in Adaptive and Multilayer Networks. *Phys. Rev. Lett.* **114,** 038701 (2015).

263. Zhang, X., Zou, Y., Boccaletti, S. & Liu, Z. Explosive synchronization as a process of explosive percolation in dynamical phase space. *Scientific reports* **4,** 5200 (2014).

264. Chen, W., Wang, S., Lan, Y., Liu, W. & Xiao, J. Explosive synchronization caused by optimizing synchrony of coupled phase oscillators on complex networks. *Eur. Phys J. B* **94,** eabe3824 (2021).

265. Chatterjee, A., Kaznessis, Y. N. & Hu, W.-S. Tweaking biological switches through a better understanding of bistability behavior. *Current Opinion in Biotechnology* **19,** 475–481 (2008).

266. Myung, J., Schmal, C., Hong, S., Tsukizawa, Y., Rose, P., Zhang, Y., Holtzman, M. J., De Schutter, E., Herzel, H., Bordyugov, G. *et al.* The choroid plexus is an important circadian clock component. *Nature communications* **9,** 1–13 (2018).

267. Scarpetta, S., Apicella, I., Minati, L. & de Candia, A. Hysteresis, neural avalanches, and critical behavior near a first-order transition of a spiking neural network. *Physical Review E* **97,** 062305 (2018).

268. Molloy, M. & Reed, B. A critical point for random graphs with a given degree sequence. *Random Structures & Algorithms* **6,** 161–180 (1995).

269. Restrepo, J. & Ott, E. Mean field theory of assortative networks of phase oscillators. *EPL (Europhysics Letters)* **107** (2014).

270. Rosenblum, M., Pikovsky, A. & Kurths, J. Phase Synchronization of Chaotic Oscillators. *Physical Review Letters* **76,** 1804–1807 (1996).

271. Leyva, I., Sevilla-Escoboza, R., Buldu, J., Sendiña-Nadal, I., Gómez-Gardeñes, J., Arenas, A., Moreno, Y., Gomez, S., Jaimes-Reategui, R. & Boccaletti, S. Explosive First-Order Transition to Synchrony in Networked Chaotic Oscillators. *Phys. Rev. Lett.* **108,** 168702 (2012).

272. Skardal, P., Sevilla-Escoboza, V., Vera-Ávila, V. & Buldú, J. Optimal phase synchronization in networks of phase-coherent chaotic oscillators. *Chaos* **27,** 013111 (2017).

273. Djabella, K., Landau, M. & Sorine, M. *A two-variable model of cardiac action potential with controlled pacemaker activity and ionic current interpretation* in *2007 46th IEEE Conference on Decision and Control* (2007), 5186–5191.

274. Der Pol, B. V. On relaxation-oscillators. *The London, Edinburgh and Dublin Phil. Mag. and J. of Sci.* **2,** 987–992 (1927).

275. Buendía, V., di Santo, S., Villegas, P., Burioni, R. & Muñoz, M. A. Self-organized bistability and its possible relevance for brain dynamics. *Phys. Rev. Research* **2,** 013318 (2020).

276. Kuehn, C. & Bick, C. A universal route to explosive phenomena. *Science Advances* **7,** eabe3824 (2021).

277. Roberts, D. A linear reformulation of the Kuramoto model of self-synchronizing oscillators. *Physical review. E, Statistical, nonlinear, and soft matter physics* **77,** 031114 (2008).

278. Valdano, E. & Arenas, A. Exact Rank Reduction of Network Models. *Phys. Rev. X* **9,** 031050 (2019).

279. Arola-Fernández, L., Steinegger, B. & Arenas, A. Spectral shortcut to the onset of synchronization in networks. *to be published* (2022).

280. Barbier, M., Arnoldi, J.-F., Bunin, G. & Loreau, M. Generic assembly patterns in complex ecological communities. *Proceedings of the National Academy of Sciences* **115** (2018).

281. Aguadé-Gorgorió, G. & Solé, R. Genetic instability as a driver for immune surveillance. *Journal for ImmunoTherapy of Cancer* **7,** 345 (2019).

282. Steinegger, B., Arenas, A., Gómez-Gardeñes, J. & Granell, C. Pulsating campaigns of human prophylaxis driven by risk perception palliate oscillations of direct contact transmitted diseases. *Phys. Rev. Research* **2,** 023181 (2020).

283. Bernard, D. & LeClair, A. in *Statistical Field Theories: A Classification of Non-Hermitian Random Matrices* 207–214 (Springer Netherlands, Dordrecht, 2002).

284. Ito, T., Yang, G., Laurent, P., Schultz, D. & Cole, M. Constructing neural network models from brain data reveals representational transformations linked to adaptive behavior. *Nature Communications* **13** (2022).

285. Piñero, J. & Solé, R. Statistical physics of liquid brains. *Philosophical Transactions of the Royal Society B: Biological Sciences* **374,** 20180376 (2019).

UNIVERSITAT ROVIRA I VIRGILI
SYNCHRONIZATION IN COMPLEX NETWORKS UNDER UNCERTAINTY
Lluís Arola Fernández

UNIVERSITAT
ROVIRA i VIRGILI